frontiers | Research Topics

Molecular crosstalk between oilseed crops and pathogens

Edited by
Qi Peng, Cunmin Qu and Huajian Zhang

Published in
Frontiers in Plant Science

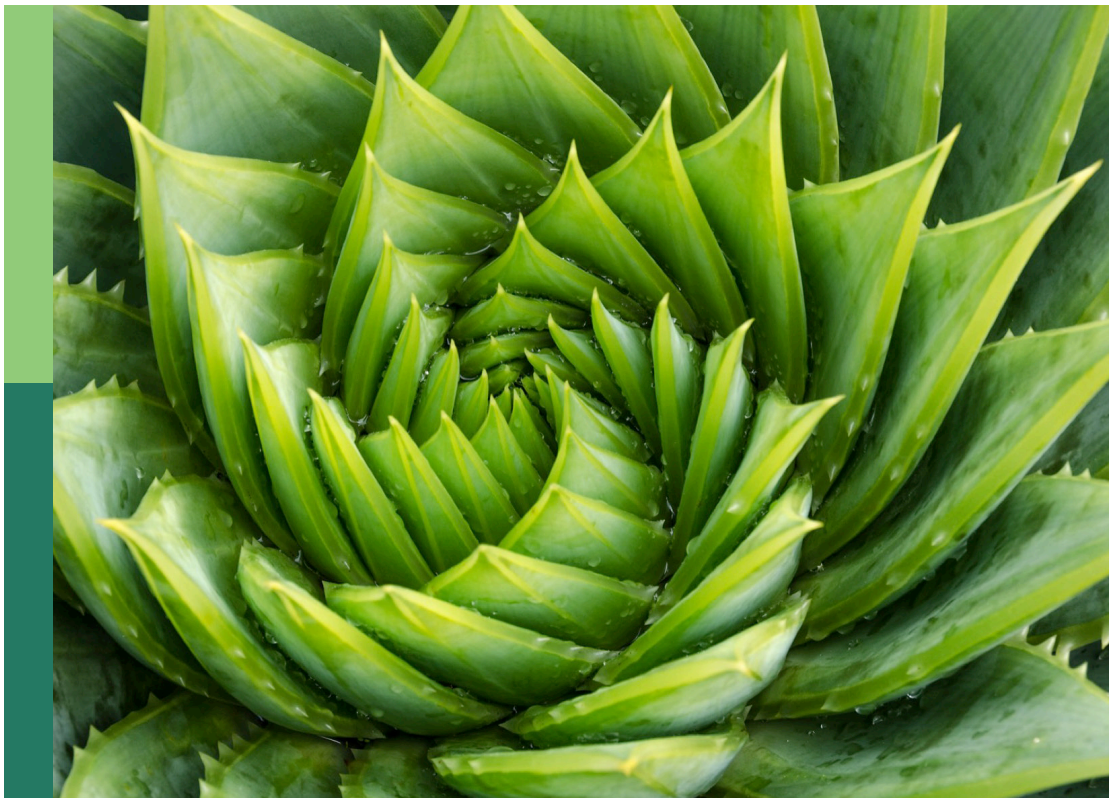

ISSN 1664-8714
ISBN 978-2-8325-3188-4
DOI 10.3389/978-2-8325-3188-4

About Frontiers

Frontiers is more than just an open access publisher of scholarly articles: it is a pioneering approach to the world of academia, radically improving the way scholarly research is managed. The grand vision of Frontiers is a world where all people have an equal opportunity to seek, share and generate knowledge. Frontiers provides immediate and permanent online open access to all its publications, but this alone is not enough to realize our grand goals.

Frontiers journal series

The Frontiers journal series is a multi-tier and interdisciplinary set of open-access, online journals, promising a paradigm shift from the current review, selection and dissemination processes in academic publishing. All Frontiers journals are driven by researchers for researchers; therefore, they constitute a service to the scholarly community. At the same time, the *Frontiers journal series* operates on a revolutionary invention, the tiered publishing system, initially addressing specific communities of scholars, and gradually climbing up to broader public understanding, thus serving the interests of the lay society, too.

Dedication to quality

Each Frontiers article is a landmark of the highest quality, thanks to genuinely collaborative interactions between authors and review editors, who include some of the world's best academicians. Research must be certified by peers before entering a stream of knowledge that may eventually reach the public - and shape society; therefore, Frontiers only applies the most rigorous and unbiased reviews. Frontiers revolutionizes research publishing by freely delivering the most outstanding research, evaluated with no bias from both the academic and social point of view. By applying the most advanced information technologies, Frontiers is catapulting scholarly publishing into a new generation.

What are Frontiers Research Topics?

Frontiers Research Topics are very popular trademarks of the *Frontiers journals series*: they are collections of at least ten articles, all centered on a particular subject. With their unique mix of varied contributions from Original Research to Review Articles, Frontiers Research Topics unify the most influential researchers, the latest key findings and historical advances in a hot research area.

Find out more on how to host your own Frontiers Research Topic or contribute to one as an author by contacting the Frontiers editorial office: frontiersin.org/about/contact

Molecular crosstalk between oilseed crops and pathogens

Topic editors

Qi Peng — Jiangsu Academy of Agricultural Sciences (JAAS), China
Cunmin Qu — Southwest University, China
Huajian Zhang — Anhui Agricultural University, China

Citation

Peng, Q., Qu, C., Zhang, H., eds. (2023). *Molecular crosstalk between oilseed crops and pathogens*. Lausanne: Frontiers Media SA. doi: 10.3389/978-2-8325-3188-4

Table of contents

frontiers | Frontiers in Plant Science

TYPE Original Research
PUBLISHED 01 August 2022
DOI 10.3389/fpls.2022.983786

OPEN ACCESS

EDITED BY
Cunmin Qu,
Southwest University, China

REVIEWED BY
Jinpeng Wang,
Institute of Botany (CAS), China
Zongxiang Zhan,
Shenyang Agricultural University, China
Xiaodong Wang,
Jiangsu Academy of Agricultural Sciences (JAAS), China

*CORRESPONDENCE
Yuanyuan Zhang
zhangyy@caas.cn

†These authors have contributed equally to this work and share first authorship

SPECIALTY SECTION
This article was submitted to Plant Pathogen Interactions, a section of the journal Frontiers in Plant Science

RECEIVED 01 July 2022
ACCEPTED 11 July 2022
PUBLISHED 01 August 2022

CITATION
He Y, Li Y, Bai Z, Xie M, Zuo R, Liu J, Xia J, Cheng X, Liu Y, Tong C, Zhang Y and Liu S (2022) Genome-wide identification and functional analysis of cupin_1 domain-containing members involved in the responses to *Sclerotinia sclerotiorum* and abiotic stress in *Brassica napus*. *Front. Plant Sci.* 13:983786. doi: 10.3389/fpls.2022.983786

Genome-wide identification and functional analysis of cupin_1 domain-containing members involved in the responses to *Sclerotinia sclerotiorum* and abiotic stress in *Brassica napus*

Yizhou He[1†], Yan Li[2,3†], Zetao Bai[1], Meili Xie[1], Rong Zuo[1], Jie Liu[1], Jing Xia[1], Xiaohui Cheng[1], Yueying Liu[1], Chaobo Tong[1], Yuanyuan Zhang[1*] and Shengyi Liu[1,3]

[1]The Key Laboratory of Biology and Genetic Improvement of Oil Crops, The Ministry of Agriculture and Rural Affairs of the PRC, Oil Crops Research Institute of the Chinese Academy of Agricultural Sciences, Wuhan, China, [2]State Key Laboratory of Biocatalysis and Enzyme Engineering, School of Life Sciences, Hubei University, Wuhan, China, [3]Hubei Collaborative Innovation Center for Green Transformation of Bio-Resources, School of Life Sciences, Hubei University, Wuhan, China

Cupin_1 domain-containing proteins (CDPs) are ubiquitously present in higher plants, which are known to play essential roles in various biological processes. In this study, we carried out genome-wide characterization and systematic investigation of the *CDP* genes in *Brassica napus*. A total of 96 BnCDPs, including 71 germin-like proteins (GLPs; proteins with a single cupin_1 domain) and 25 CDP bicupins (proteins with two cupin_1 domains), were identified and clustered into six distinct subfamilies (I–VI) based on the phylogenic analysis, gene structure and motif distribution. Further analysis indicated that whole-genome duplication (WGD) and segmental duplication are main contributors to the species-specific expansion of the *BnCDP* gene family, and all the duplicated genes subsequently underwent strong purification selection. The promoter region of *BnCDPs* showed enrichment of *cis*-regulatory elements associated with development, hormone and stress, as well as transcription factor binding sites, which validates the prediction that *BnCDPs* are widely involved in plant growth and biotic and abiotic stress responses. The *BnCDPs* in different subfamilies exhibited obvious differences in expression among 30 developmental tissues/stages of *B. napus*, implying that *BnCDP*s may be involved in tissue- and stage-specific developmental processes. Similar trends in expression of most *BnCDPs* were observed under *Sclerotinia sclerotiorum* inoculation and four abiotic stresses (dehydration, cold, ABA and salinity), particularly the *BnGLPs* in subfamily I and III with single cupin_1 domain, revealing that *BnCDPs* are of great importance in the environmental adaption of *B. napus*. We then performed a genome-wide association study (GWAS) of 274 *B. napus* core germplasms on *S. sclerotiorum* resistance and identified four significantly associated loci harboring five

BnGLPs. The expression levels of two candidate genes, *BnGLP1.A08* and *BnGLP1.C08*, were significantly correlated with *S. sclerotiorum* resistance. Their functional responses to multiple stages of *S. sclerotiorum* inoculation and four abiotic stresses were further examined through qPCR. Overall, this study provides rich resources for research on the function and evolutionary playground of *CDP* genes.

KEYWORDS

cupin_1 domain, germin-like protein, *Sclerotinia sclerotiorum* resistance, abiotic stress, GWAS, *Brassica napus*

Introduction

Adverse environmental conditions including biotic and abiotic stresses pose serious threats to crop productivity in agriculture and food security (Zhu, 2016; Zhao et al., 2022). How plants adapt to adverse environments is a critical issue of biological studies and global agricultural production. It is critical to tune the expression of stress-responsive genes for resistance and adaptation to various biotic and abiotic stresses. The cupin_1 domain-containing protein (CDP) coding genes such as *GLP* members tend to be induced by pathogen attack and abiotic stress, and play important roles in response to a number of biotic and abiotic stresses to improve the development and environmental adaption of plants (Dunwell et al., 2004). Cupin superfamily proteins, which were named based on a conserved β-barrel fold, were first discovered using a conserved motif found within germin and germin-like proteins from higher plants (Dunwell et al., 2000, 2004). To date, the cupin superfamily has been considered as one of the most functionally diverse super-gene families in plants (Dunwell et al., 2004; Brunetti et al., 2022). This superfamily contains 69 gene families according to the Pfam database (accessed on 1st, June 2022), including the cupin_1 domain-containing family (Mistry et al., 2021). The cupin superfamily can be divided to monocupin (one single cupin domain), bicupin (a duplicated cupin structure) and multicupin (>two cupin domains; Dunwell et al., 2004). Germin and germin-like protein (GLP), which contain a single cupin_1 domain and belong to monocupin (Dunwell et al., 2000, 2004), have been widely deciphered in various plants, while the duplicated cupin_1 domain protein (CDP bicupin) has been rarely characterized. GLPs are defined by their sequence homology to germin, which was initially identified as a germination-specific marker in wheat embryos (Thompson and Lane, 1980; Dunwell et al., 2008; Rietz et al., 2012). Both germin and GLP display extremely high resistance to proteasome activity, heating, extreme pH, and detergents (Woo et al., 2000). Due to the conserved sequences and similarity in structural characteristics, it is difficult to classify GLPs and germins (Agarwal et al., 2009). In general, germins belong to a well-conserved homogeneous group and can be uniquely found within cereal plant species, including barley (*Hordeum*), maize (*Zea*), oat (*Avena*), rice (*Oryza*), rye (*Secale*) and wheat (*Triticum*) (Lane, 2002). In contrast, the GLP proteins have a wider taxonomic distribution and are generally present in other land plants besides cereals (Dunwell et al., 2008). Despite similarities in sequence among the members of GLPs, they have undergone significant functional diversification, and this family comprises numerous classes of important enzymes such as superoxide dismutase (SOD) that converts superoxide to H_2O_2 and O_2 (Gucciardo et al., 2007; Guevara-Olvera et al., 2012), oxalate oxidase (OXO) that degrades oxalic acid to H_2O_2 and CO_2 (Sakamoto et al., 2015), and polyphenol oxidase, dioxygenases, isomerases, epimerases, synthases and decarboxylases (Davidson et al., 2010; Cheng et al., 2014).

The *CDP* genes have different spatial and temporal expression characteristics during development in a variety of plants, and their expression also varies greatly among different tissues such as roots, stems, leaves, flowers, seeds and embryos and various developmental processes of the same plant (Lu et al., 2010; Wang et al., 2013; Li L. et al., 2016). Among the 69 identified cupin genes in soybean, 35 were found to be expressed in at least one tissue, and most of them displayed distinct tissue-specific expression patterns (Wang et al., 2014). Expression profiling of *GLPs* in rice and *Arabidopsis thaliana* has demonstrated that many of the members are only expressed in certain tissues or developmental stages (Li L. et al., 2016). For example, *OsGLP3-3* and *OsGLP8-2* are specifically expressed in developing seeds and *OsGLP8-14* is preferentially expressed in developing panicles in rice (Li L. et al., 2016). These tissue specifically expressed *GLPs* may have essential functions in plant growth and development. For example, *OsGLP2-1*, which is specifically expressed in seed scutellum, positively regulates the dormancy of developing seeds through the abscisic acid and gibberellic acid signaling pathways (Wang et al., 2020); while *OsGLP1* is predominantly expressed in green vegetative tissues and down-regulation of its expression in transgenic rice resulted in a semi-dwarfism phenotype (Banerjee and Maiti, 2010). *GbGLP2* is mainly expressed in

elongating fiber at 10 days post anthesis and negatively regulates fiber elongation in cotton (Sun et al., 2020). All these studies have demonstrated that *GLPs* play various roles in many tissues and organs or certain vital developmental stages of plants.

The *CDP* genes have long been considered be associated with responses to various biotic and abiotic stresses in different plant species (Thompson et al., 1995; Liu et al., 2004; Zou et al., 2007; Dong et al., 2008). Some GLP members with inherent OXO or SOD enzymatic activity can confer tolerance to biotic stress by hyper-accumulation of H_2O_2 and enhancement of cross-link between cell wall components during pathogen infection (Banerjee et al., 2010; Gangadhar et al., 2021). Riezt et al. identified 14 *BnGLP* genes in *Brassica napus* and demonstrated that both *BnGLP3* and *BnGLP12* have SOD activity, whose early induction is involved in the oxidative burst, and play a pivotal role in defense against *Sclerotinia sclerotiorum* (Rietz et al., 2012). *GmGLP10* positively regulates the resistance to *S. sclerotiorum*, and transgenic tobacco overexpressing *GmGLP10* from soybean showed significantly enhanced tolerance to oxalate acid and *S. sclerotiorum* infection (Zhang et al., 2018). Similarly, *A. thaliana* plants expressing sunflower *HaGLP1* exhibited higher reactive oxygen species accumulation and resistance against *S. sclerotiorum* and *Rhizoctonia solani* (Beracochea et al., 2015). Overexpression in *A. thaliana* of a novel *GLP* gene *GhABP19* from *Gossypium hirsutum* resulted in enhanced resistance to *Verticillium dahliae* and *Fusarium oxysporum* infection through its SOD activity and activation of the Jasmonic acid (JA) pathway (Pei et al., 2019). Moreover, *GLPs* also widely participate in defense against some other fungal pathogens such as *Blumeria graminis* (Yuan et al., 2021), *Verticillium longisporum* (Knecht et al., 2010), *Magnaporthe oryzae* (Liu et al., 2016) and *Aspergillus flavus* (Wang et al., 2013), as well as responses to viruses, bacteria, and even insect herbivores (Dunwell et al., 2008). Apart from biotic stress, the *CDP* genes are also widely involved in defense against abiotic stress in plants. For instance, *A. thaliana* with ectopic overexpression of soybean *GmGLP7* exhibited obviously enhanced tolerance to drought, salt and oxidative stress, and was hypersensitive to exogenous ABA treatment (Li Y. et al., 2016). Similarly, *A. thaliana* overexpressing *AhGLP2* or *AhGLP3* from peanut showed higher tolerance to salt stress (Wang et al., 2013). Knockout of *OsGLP1* by CRISPR/Cas9 resulted in higher sensitivity of rice plants to UV-B, suggesting that *OsGLP1* is involved in the acclimation to UV-B radiation (He et al., 2021). In addition, overexpression of *StGLP* in potato plants increased the H_2O_2 level, triggered the scavenging signaling pathways of reactive oxygen species and induced the expression of heat stress-responsive genes to enhance the tolerance to heat stress (Gangadhar et al., 2021). Besides, the *GLP* genes are also responsive to other abiotic stresses such as drought (Anum et al., 2022), heavy metal (Cheng et al., 2018) and wound (Wang et al., 2013).

Brassica napus (2n = 4x = 38, AACC) is an important source of vegetable oil and stock feed in the world, which is cultivated in an area of more than 36 million hectares with an annual seed yield of 72 million tons (FAO STAT[1]). In actual production, the yield of *B. napus* is threatened by various biotic (insect pest and disease) and environmental/abiotic (salinity, acidity, alkalinity, drought, heat and water-logging) stresses (Liu et al., 2022). Therefore, it is urgent to explore genes with durable disease resistance and tolerance to diverse abiotic stresses in crop breeding. Considering the important roles of *CDP* genes in resistance and adaptation of plants to various biotic and abiotic stresses, it is reasonable to speculate that *CDPs* may also function in the environmental adaptation of *B. napus*. However, there has been no genome-wide identification and systematic investigation of the *CDP* family represented by monocupion *GLPs* in *B. napus* to date. In this study, we identified a total of 96 *CDP* genes (including 71 *BnGLPs* and 25 CDP *bicupins*) in the *B. napus* genome through genome-wide analysis. In addition, we comprehensively analyzed their evolutionary relationships, gene structures, conserved motifs, *cis*-regulatory elements and transcription factor binding sites (TFBSs). Expression profiling in 30 *B. napus* tissues/stages demonstrated that *BnCDPs* are involved in tissue- and stage-specific developmental processes. Expression analysis under biotic (*S. sclerotiorum* infection) and abiotic (dehydration, cold, ABA and salinity) stress treatments together with GWAS on *S. sclerotiorum* resistance demonstrated that two *BnGLPs* are commonly responsive to multiple biotic and abiotic stresses. The findings provide important insights into the role of *BnCDPs* in resistance to biotic and abiotic stresses and lay a foundation for future functional study of the *CDP* genes.

Results

Identification of *BnCDP* gene family members in *Brassica napus*

A total of 96 *BnCDP* genes with the cupin_1 domain were identified in *B. napus* through HMMsearch by using PF00190 as the query and subsequent domain verification. Among these genes, 50 genes were located in the A_n subgenome, while the remaining 46 genes were found in the C_n subgenome. The overall distribution of *BnCDP* genes was uneven across chromosomes (**Supplementary Figure 1**). Chromosome A02 (seven genes), A06 (eight genes), A07 (eight genes), A09 (six genes) and C08 (11 genes) had the most *BnCDP* genes; while A04 and C02 only contained two and one *BnCDP* gene, respectively; and A05 chromosome even had no *BnCDP*. The length of BnCDP proteins ranged from

1 https://www.fao.org/faostat/

175 aa (BnaC08g43590D) to 652 aa (BnaC03g48460D), with an average length of 286 aa. The exon number of each *BnCDP* gene ranged from 1 to 7 (only *BnaA06g25170D*), with most of the members (74%) having no more than three exons. The predicted theoretical pI values varied from 4.77 to 9.77 and the MW values were between 19.45 and 78.20 kDa. Moreover, the GRAVY (grand average of hydrophobicity) index values ranged from −1.300 to 0.545. According to the predicted subcellular location, the BnCDP proteins showed a wide subcellular distribution pattern and were mainly located in extracellular (41/96) and plasma membrane (18/96), and the remaining proteins were specifically located in the chloroplast (11), cytoplasmic region (11), nuclear (7), endoplasmic reticulum (5) and mitochondrion (3) (**Supplementary Table 1**).

Phylogenetic analysis of *BnCDPs*

To further characterize and classify the *BnCDP* family members, we constructed a phylogenetic tree using all the 96 BnCDP proteins from *B. napus* and 42 AtCDP proteins from *A. thaliana*. Previous studies have reported 32 *AtGLP* genes in *A. thaliana* (Li L. et al., 2016). In this research, we identified ten new *AtCDP* genes including two monocupin coding genes (*AT4G36700* and *AT5G44120*) and eight bicupin coding

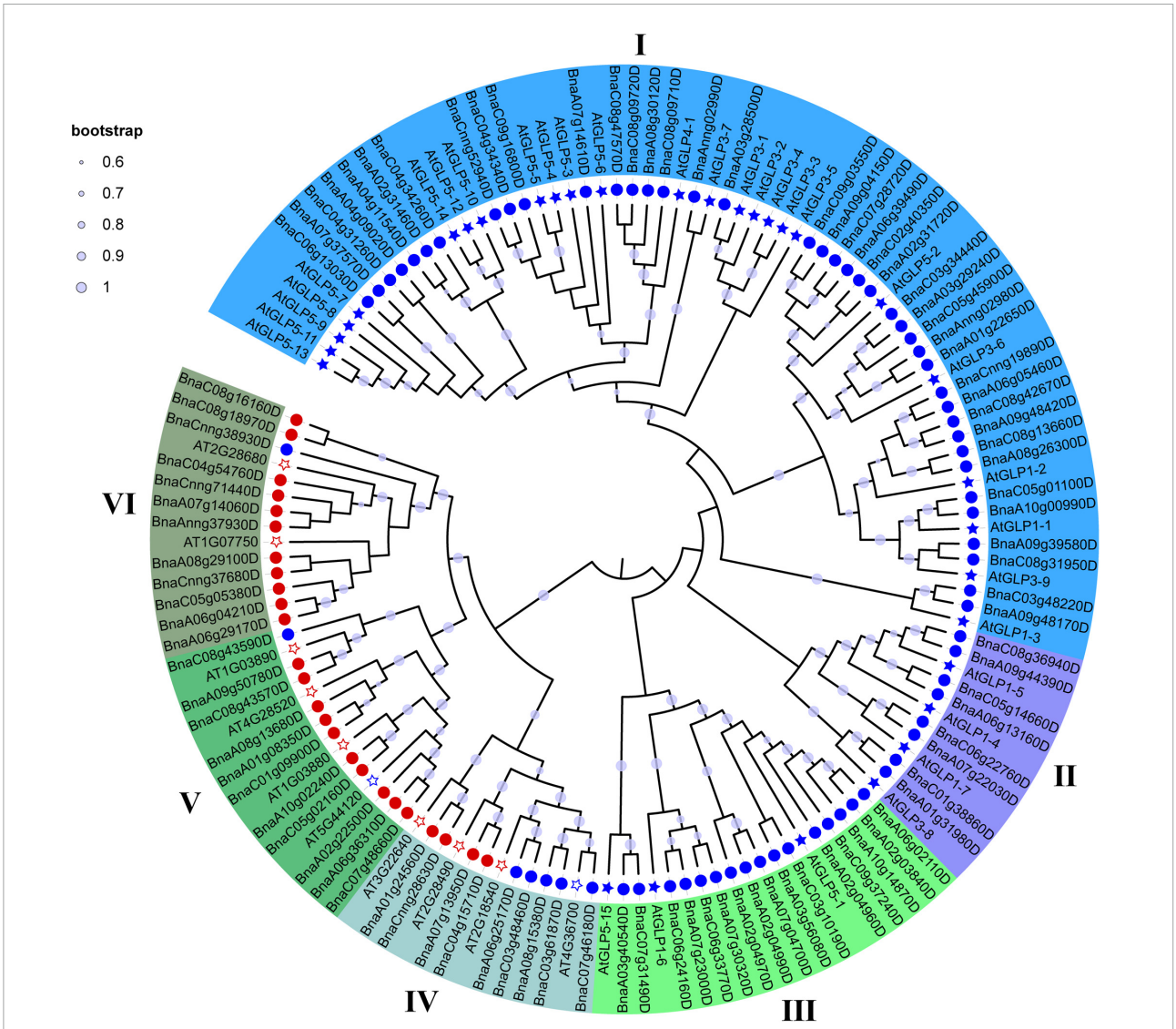

FIGURE 1
A neighbor-joining (NJ) phylogenetic tree of CDP proteins in *Arabidopsis thaliana* (At) and *Brassica napus* (Bn). All CDP proteins were clustered into six subfamilies, and each subfamily was represented by a different color. Light purple dot on a branch in the figure indicates that the bootstrap support is greater than 60%. Circles refer to BnCDPs, while filled stars refer to AtGLPs identified previously and empty stars refer to AtCDPs identified in this research; Blue and Red refer to CDPs with single or duplicated cupin_1 domain, respectively.

genes (*AT2G28490*, *AT3G22640*, *AT1G03880*, *AT1G03890*, *AT4G28520*, *AT1G07750*, *AT2G28680* and *AT2G18540*) in *A. thaliana* (**Supplementary Table 2**). Finally, these CDP proteins were assigned to I–VI subfamilies based on the topology of the phylogenetic tree, in which the members in subfamily I–III were all monocupins; the members in subfamily V (except for AT5G44120 and BnaC08g43590D) and VI (except for BnaCnng38930D) are almost all bicupins; while subfamily IV was a mixture of monocupins (six) and bicupins (seven; **Figure 1** and **Supplementary Table 2**). The number of *BnCDP* genes varied significantly among the six subfamilies, with subfamily I including approximately half of all the *BnCDP* genes (40), while the subfamily II–VI only comprised 8, 16, 9, 11 and 12 *BnCDP* members, respectively. Except for four genes (*AtGLP1-4*, *AtGLP1-5*, *AtGLP1-7* and *AtGLP3-8*) clustered in subfamily II and three genes (*AtGLP5-1*, *AtGLP1-6* and *AtGLP5-15*) clustered in subfamily III, the remaining previously reported *AtGLP* genes (Li L. et al., 2016) all fell into subfamily I, and all the ten newly identified *AtCDP* members were scattered in subfamily IV (four members), V (four members) and VI (two members). These results indicated that the *CDP* genes were present in the common ancestors of *A. thaliana* and *B. napus*, and some of them might have undergone species-specific expansion and subsequently significant divergence.

Duplication events of the *BnCDP* genes were detected based on BLAST and MCScan X. Briefly, all 96 *BnCDPs* were derived from duplication, among which 72 genes (75.0%) were generated from whole-genome duplication (WGD) or segmental duplication, and 18 genes (18.75%) resulted from dispersed duplication (**Supplementary Table 1**). Moreover, three tandem and three proximal gene duplication types were detected. There were 191 paralogous gene pairs with high identities (identity > 75%, and alignment length > 75%) in *B. napus*, with 56 gene pairs in the A_n subgenome, 32 gene pairs in the C_n subgenome, and the remaining 103 duplication events occurring between the two subgenomes (**Figure 2** and **Supplementary Table 3**). To estimate the selection pressure on *BnCDP* genes in *B. napus*, the ratio of non-synonymous substitution to synonymous substitution (K_a/K_s) for the 191 paralogous gene pairs was calculated. The results showed that the K_a/K_s ratio for all paralogous gene pairs varied from 0 to 0.52 and lower than 1, suggesting that the *BnCDP* genes have undergone purification selection during evolution (**Supplementary Table 3**).

Gene structure and conserved motif analysis of the *BnCDP* family in *Brassica napus*

The exon-intron structure of all the *BnCDP* genes in six subfamilies was displayed based on their phylogenetic relationships (**Figures 3A,B**). As shown in **Figure 3B**, 36 members contained both 5′ and 3′ UTRs; 33 members exhibited no UTR; while the remaining 27 members possessed either a 5′ or 3′ UTR. Furthermore, the gene structure seemed to vary remarkably among different subfamilies, but were relatively conserved within the subfamily. For example, most *BnCDPs* in subfamily I had two exons, and all members in subfamily II and nearly all members in subfamily III were intronless. Most of members in subfamily VI had three exons, while members in subfamily IV had the maximum number of exons and introns.

We also analyzed the distribution of conserved motifs in the *BnCDP* family. In total, 20 distinct conserved motifs were identified (**Figure 3C** and **Supplementary Table 4**). In subfamily I–III, the motifs were well conserved. Most genes in these subfamilies simultaneously contained motif 1, 2, 3, 4, 7. However, motif 9 was specifically identified in members in subfamily I except for two genes in subfamily III (*BnaC07g31490D* and *BnaA03g40540D*). Members in subfamily III specifically contained motif 20 but were lack of motif 5 prevalently present in other five subfamilies. Motif 10, 12 and 19 were only found in subfamily VI, and motif 11 was present in nearly all members in subfamily IV–VI. The specificity of motifs was conformed to the observed evolutionary characteristics of *BnCDP* genes, implying that the specifically conserved motifs in different *BnCDP* subfamilies are associated with their functions.

Analysis of *cis*-regulatory elements in the promoter region of *BnCDPs*

The regulatory elements in the promoter region are often relatively conserved in sequence and function throughout evolution, particularly in tolerance to biotic and abiotic stresses (Oudelaar and Higgs, 2021). To explore the potential roles of *BnCDP* genes, we analyzed the *cis*-regulatory elements in the 2-kb promoter regions of *BnCDPs* based on the PlantCARE database. As a result, the *cis*-acting regulatory elements associated with development, hormone and stress were enriched in these promoters (**Figure 4**, **Supplementary Figure 2**, and **Supplementary Tables 5, 6**). These *cis*-regulatory elements included development related elements such as the circadian element (involved in circadian control), the GT1-motif, Sp1, ACE, G-box and GT1 motif (involved in light responsiveness); hormone responsive elements such as ABRE (involved in the abscisic acid response), AuxRR-core and TGA-element (involved in auxin response), GARE-motif and TATC-box (involved in gibberellin response), CGTCA-motif and TGACG-motif (involved in MeJA response) and the TCA-element (involved in salicylic acid response); stress-responsive elements such as ARE elements (essential for anaerobic induction), TC-rich repeats (involved in defense and stress responsiveness), AT-rich sequence (element for maximal elicitor-mediated activation), LTR (involved in low-temperature

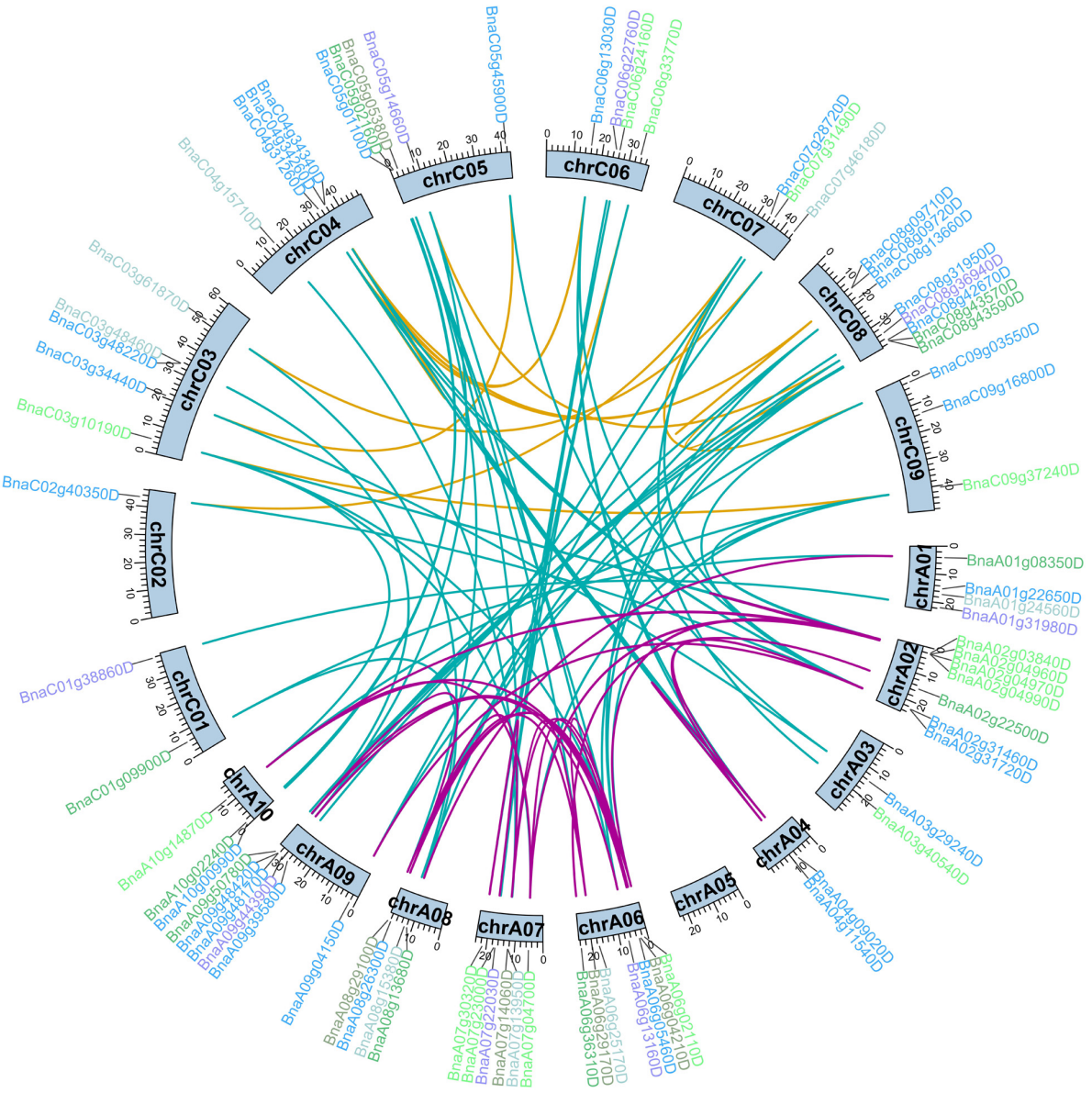

FIGURE 2
Duplication analysis of *BnCDP* genes in *Brassica napus*. The gene names are marked outward of the corresponding chromosomes. The different colors indicate different subfamilies of the *BnCDP* genes. The duplicated gene pairs are highlighted with connecting lines colored according to the subgenomes, purple indicates that both genes in the gene pair are from the A_n subgenome, yellow represents that both genes in the gene pair are from the C_n subgenome, while the blue shows that two genes in the gene pair come from different subgenomes.

responsiveness), MBS (MYB binding site involved in drought-inducibility), MBSI (involved in flavonoid biosynthesis) and WUN-motif (involved in wound response). There were many MeJA-related *cis*-acting regulatory elements in the promoters of *BnCDP* genes: the CGTCA-motif was identified in 71 of the 96 *BnCDP* gene promoters (2.13 on average for each promoter), and the ABRE elements were present in 75 *BnCDP* promoters (with 3.39 on average for each promoter). Besides, 65 TC-rich repeats associated with defense and stress response were unevenly scattered in 45 *BnCDP* gene promoters, which were the most enriched in cluster III (10/16) and VI (8/12), but were rare in cluster V (2/11), while 83 low-temperature response (LTR) elements showed relatively unbiased distribution in subfamily I–VI. Moreover, ARE (84/96, 87.50%) and MBS (49/96, 51.04%) elements were also common in the promoters of *BnCDP* genes. These results implied that members of the *BnCDP* family are potentially involved in biotic and abiotic stress response during plant growth and development.

The spatiotemporal expression patterns of the genes playing essential roles in plant development and stress responses tend to

10.3389/fpls.2022.983786

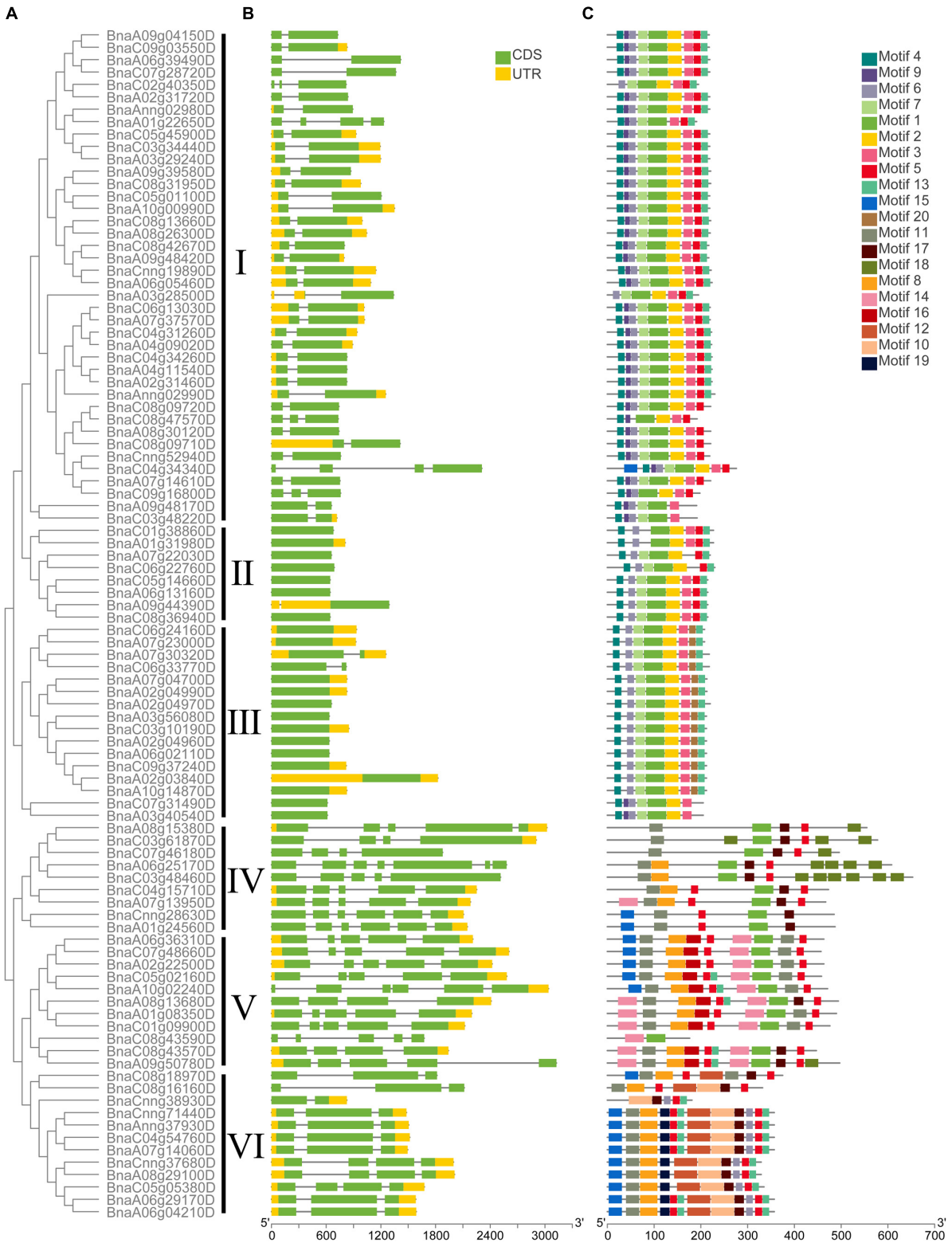

FIGURE 3
The phylogenetic relationship, exon-intron architecture, and conserved motifs of 96 BnCDP in *Brassica napus*. **(A)** The phylogenetic relationships of BnCDP proteins based on the NJ method. **(B)** Gene structures of *BnCDP* genes. Yellow boxes represent the untranslated region (UTR), green boxes represent exons and the gray lines represent introns. **(C)** The conserved motif composition of BnCDP proteins. Scale bars represent gene length (bp) and protein sequence length (aa).

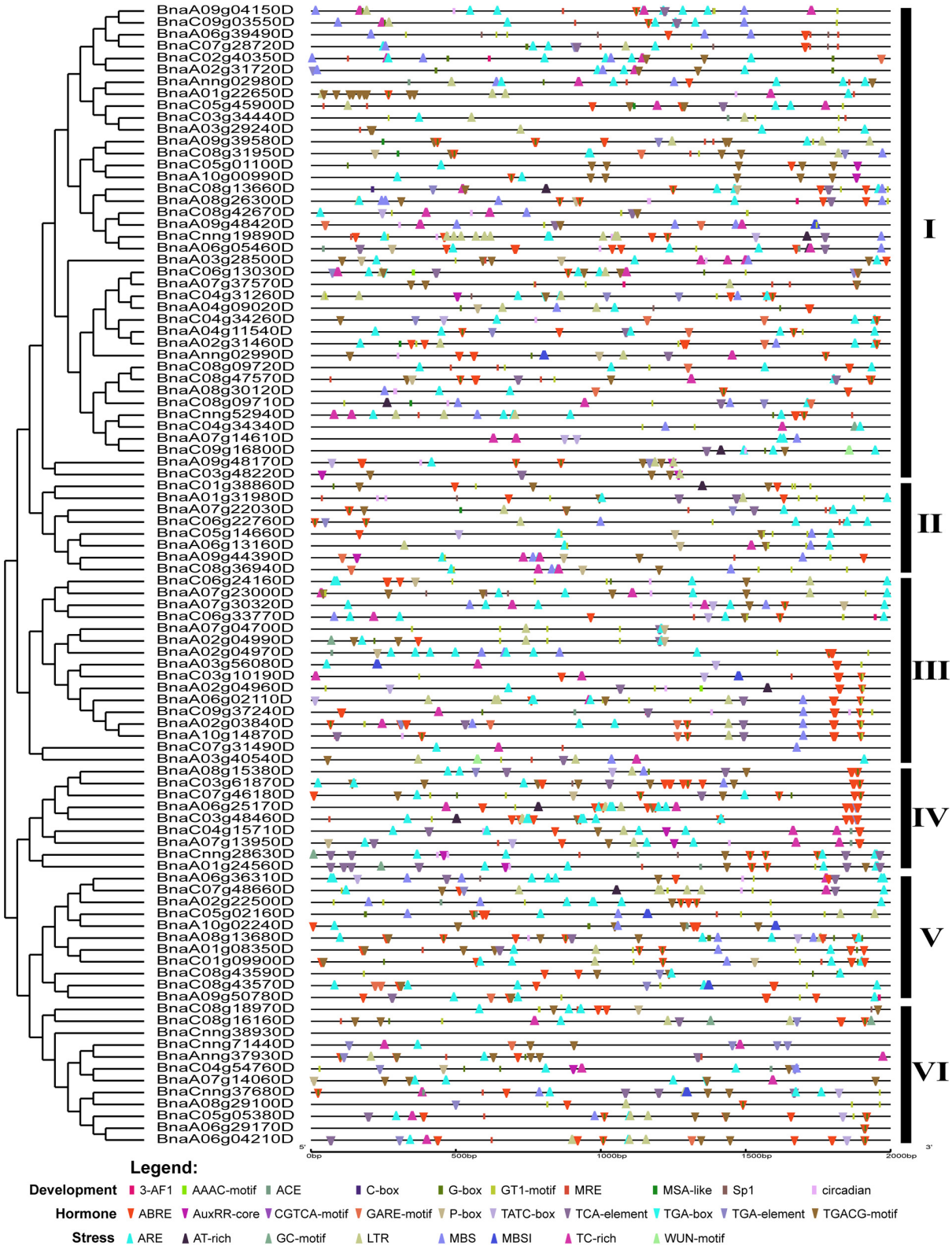

FIGURE 4
Cis-acting regulatory elements identified in promoters of *BnCDP* genes in *Brassica napus*. Boxes indicate development-related elements, down-wedges indicate hormone-related elements, and up-wedges indicate stress-related elements. Different colors indicate different elements.

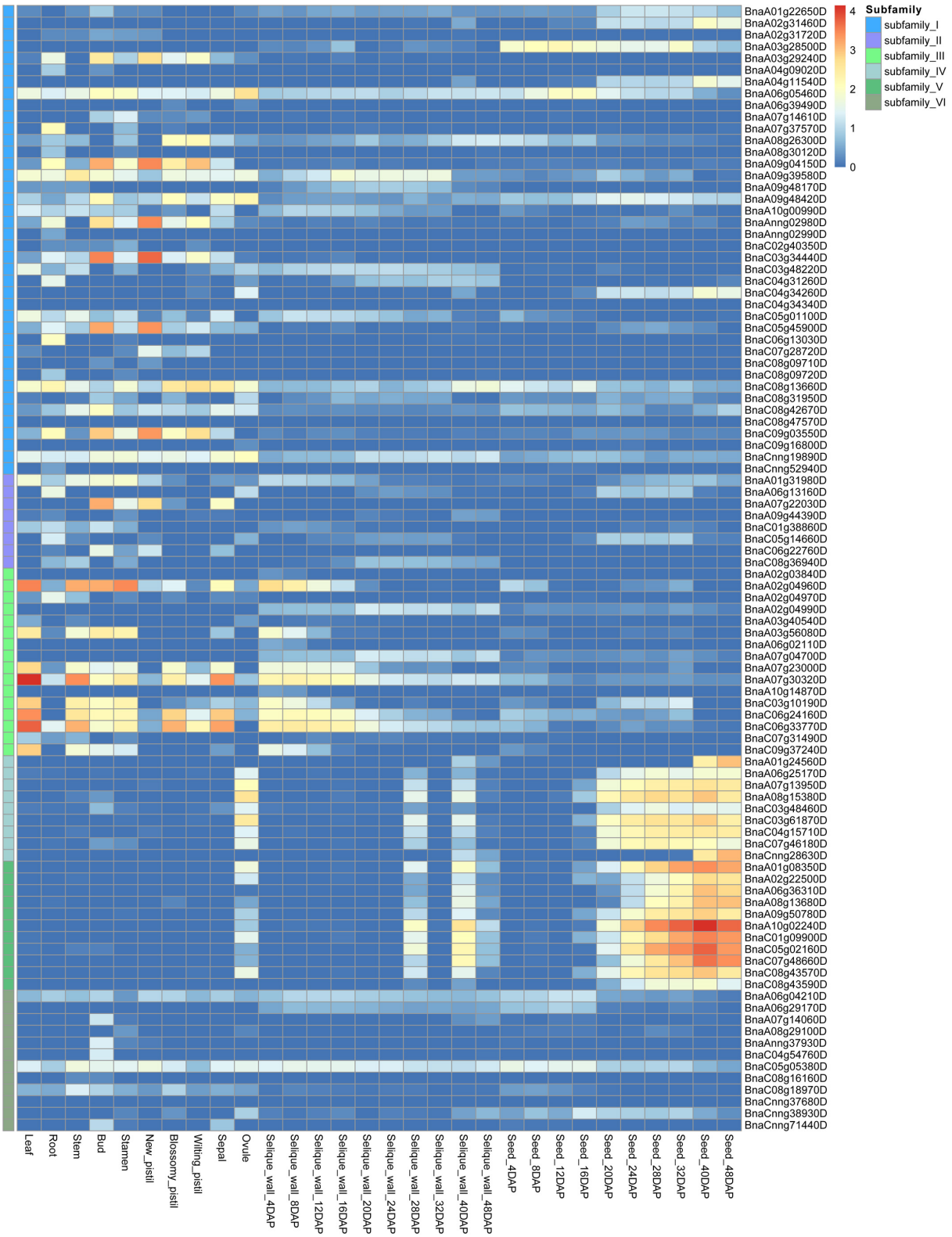

FIGURE 5
Expression patterns of 96 *BnCDP* genes in 30 tissues of *Brassica napus* ZS11 variety. The expression data were processed with the $\log_{10}$ normalization of fragments per kilobase million (FPKM). The color scale represents relative expression levels from low (blue color) to high (red color).

be regulated by their corresponding transcription factors (TFs) (Jin et al., 2014). Hence, we analyzed the transcription factor binding sites (TFBSs) in the promoter regions of all 96 *BnCDP* genes, and found that 64 of the promoters contain TFBSs, which correspond to 21 TF families (**Supplementary Table 7**). These TFs included Dof, B3, AP2, MIKC_MADS, MYB, MYB_related, GATA, ERF, C2H2, LBD, GRAS, Nin-like, BBR-BPC, SRS, NAC, E2F/DP, bZIP, ARF, bHLH, SBP, and Trihelix. Among the 64 promoters, 22 and 42 potentially bind to single and multiple TFs, respectively (**Supplementary Table 7**).

Expression patterns of *BnCDP* genes in multiple tissues of the whole growth period

To comprehensively explore the potential function of *BnCDP* genes, we investigated the expression patterns of all 96 *BnCDP* members in 30 tissues/stages, including the leaf, root, stem, bud, stamen, new pistil, blossomy pistil, wilted pistil, sepal, ovule and ten time-course seeds and silique walls [from 4 to 48 days after pollination (DAP)] based on our previously published transcriptome data (**Figure 5** and **Supplementary Table 8**; He et al., 2022). Overall, 89 genes were expressed (FPKM > 1) in at least one tissue or stage, with 48 genes showing high expression (FPKM > 50), 24 genes exhibiting intermediate expression (FPKM > 10) and three genes being lowly expressed (FPKM < 10). Generally, most of the *BnCDP* genes showed highly tissue-specific expression patterns, and only three genes (*BnaC08g13660D*, *BnaCnng19890D* and *BnaC05g05380D*) were expressed in all the 30 tissues or stages (**Figure 5**). Members in subfamily IV and subfamily V displayed nearly identical expression patterns, which were highly expressed in the ovule and silique wall (28 and 40 DAP), and had extremely high expression in the seed at the intermediate to late stages, implying their essential roles in the successful reproduction of *B. napus*. The genes in subfamily I and subfamily II showed great differences in expression and some of them were highly expressed in the root, bud and pistil. Overall, members in subfamily III showed high expression levels, such as in the leaf, stem and early stages of silique wall development, particularly *BnaA02g04960D*, *BnaA07g23000D*, *BnaA07g30320D*, *BnaC06g24160D* and *BnaC06g33770D*; while the members in subfamily VI exhibited relatively low expression levels. These differences in expression pattern among subfamilies implied that the *BnCDP* genes may be involved in tissue- or stage-specific developmental processes.

Expression patterns of *BnCDP* genes under biotic and abiotic stresses

As sessile organisms, the growth and development of plants are constantly challenged by various stresses. *S. sclerotiorum* is an ascomycete plant pathogen causing Sclerotinia stem rot in *B. napus* and severely affecting its seed yield and quality. To analyze the role of *BnCDPs* in the response to biotic stress, we investigated the expression profiles of 96 *BnCDPs* in the leaves of tolerant variety ZY821 of *B. napus* at 0 and 24 h after inoculation with *S. sclerotiorum* (Girard et al., 2017). Interestingly, just a part of *BnCDP* members were responsive to *S. sclerotiorum* inoculation, as many of them were inactive in the leaves of ZY821, such as all members in subfamily IV and V, which had no transcript accumulation at all (**Figure 6**). Among the 18 expressed *BnCDP* genes (FPKM > 1), 13 exhibited remarkable expression changes at 24 h post-inoculation (hpi), with eight genes (*BnaA08g26300D*, *BnaA09g48420D*, *BnaC06g13030D*, *BnaC08g13660D* from subfamily I; *BnaA09g44390D* from subfamily II; and *BnaA07g30320D*, *BnaC06g24160D*, *BnaC06g33770D* from subfamily III) being up-regulated and five genes (*BnaA02g31720D*, *BnaA07g37570D*, *BnaAnng02990D* from subfamily I; and *BnaA06g04210D*, *BnaC05g05380D* from subfamily VI) being down-regulated. Particularly, *BnaA08g26300D* and *BnaC08g13660D* in subfamily I exhibited high expression (FPKM > 500) and heavily induced by *S. sclerotiorum* inoculation in ZY821 (**Figure 6** and **Supplementary Table 9**).

To identify the potential functions of *BnCDP* genes in response to different abiotic stresses, we analyzed the RNA-seq data from samples under dehydration, cold, ABA and salinity treatment, respectively (Zhang et al., 2019). By taking two-fold change as the threshold value, we identified and compared the differentially expressed genes under each of the above-mentioned stresses (**Figure 6** and **Supplementary Table 10**). Under dehydration treatment, 25 out of the 29 expressed *BnCDP* genes (FPKM > 1) were significantly responsive at 1 h and/or 8 h of treatment, and most of upregulated genes (9/12) were from subfamily I, while the downregulated genes (8/12) were mainly from subfamily III. Besides, one gene (*BnaA01g31980D*) in subfamily II displayed an opposite pattern, which was downregulated at 1 h of treatment, but subsequently upregulated at 8 h. Under cold treatment, 29 *BnCDPs* showed differential expression, and more than two-thirds (21/29) of them belong to subfamily I and III. A total of 20 *BnCDP* genes were significantly responsive to ABA treatment and almost all down-regulated genes (8/9) belonged to subfamily III. Twenty-four *BnCDP* genes showed significant fold changes in response to NaCl treatment, and 90% of the responsive genes (9/10) in subfamily I were upregulated except for *BnaC03g48220D*, while all ten responsive members in subfamily III were downregulated. The transcript levels of genes from subfamily VI almost showed no fluctuation during ABA and NaCl treatment. Overall, the *BnCDP* family showed highly similar expression patterns in response to the above four abiotic stresses, and mainly the members in subfamily I and subfamily III were responsive to the treatments: The former tended to be induced while the latter was usually down-regulated in response to these stresses. Besides, we found that 13 *BnCDPs*

10.3389/fpls.2022.983786

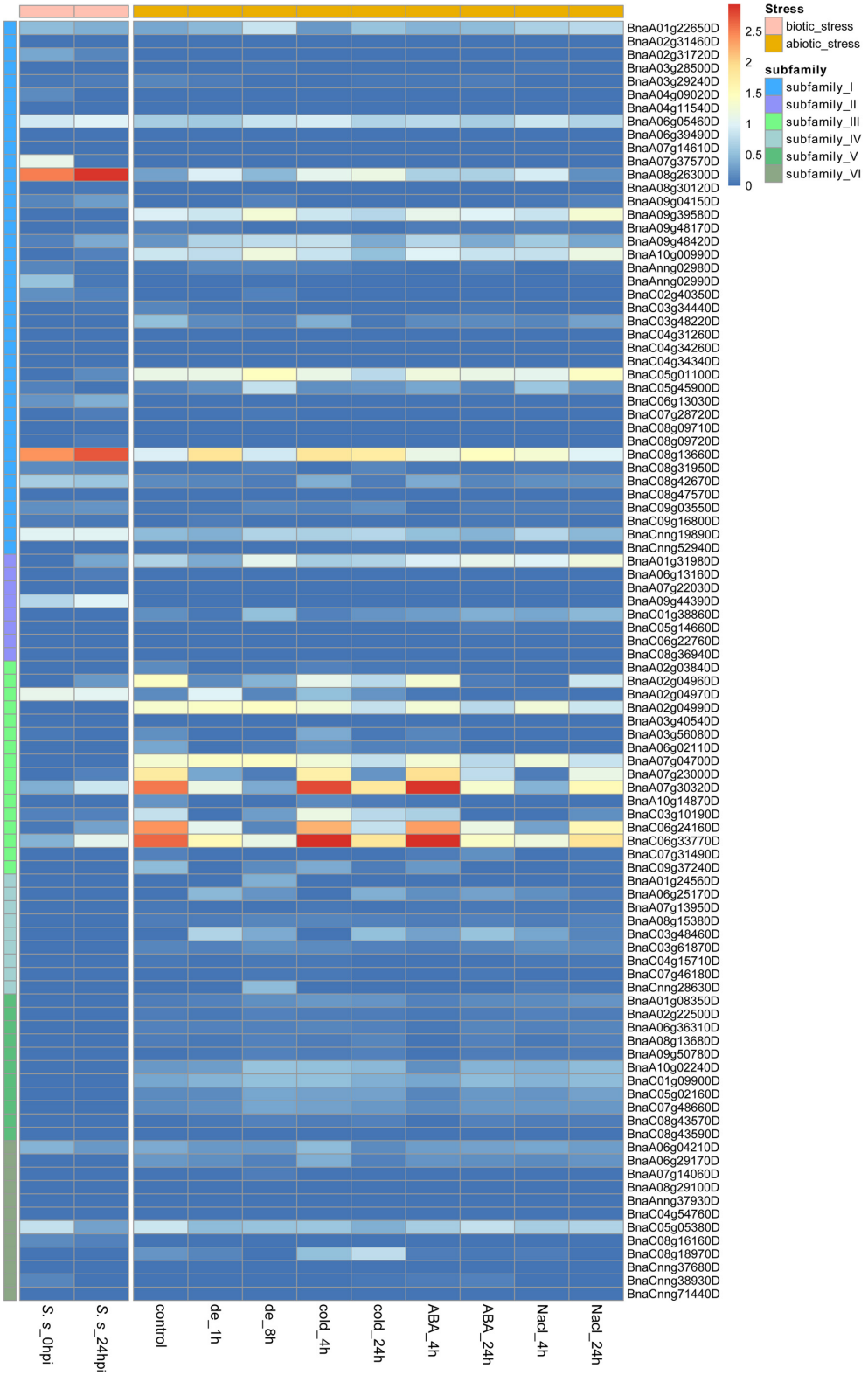

FIGURE 6
Expression profiles of 96 *BnCDP* genes under biotic (left) and abiotic (right) stress conditions. The left panel shows the expression level of *BnCDP* genes in ZY821 at 0 and 24 h after *Sclerotinia sclerotiorum* inoculation; The left panel shows the expression level of *BnCDP* genes under different abiotic stress conditions (dehydration, cold, ABA and salinity). The expression data were processed with the $\log_{10}$ normalization of fragments per kilobase million (FPKM). The color scale represents relative expression levels from low (blue color) to high (red color).

were significantly responsive to all the four abiotic stresses, among which six members (*BnaA07g23000D*, *BnaA07g30320D*, *BnaA08g26300D*, *BnaC06g24160D*, *BnaC06g33770D* and *BnaC08g13660D*) were involved in response to *S. sclerotiorum* inoculation (**Supplementary Figure 3**). These genes are common stress-responsive genes shared by multiple biotic and abiotic stresses and may be used for the breeding of varieties with multiple stress resistance in *B. napus*.

Genome wide association study on *Sclerotinia sclerotiorum* resistance and functional candidate gene *BnGLPs* analysis

To further examine the potential effects of *BnCDP* genes in *S. sclerotiorum* resistance, we used more than 2.38 million SNPs with MAF > 0.05 across 274 worldwide collected accessions to perform a GWAS based on disease index using the FarmCPU model. As shown in **Figure 7A**, the frequency distribution of disease index approximates to normal distribution, indicating that this population was suitable for association analysis. Then, the SNP GWAS was conducted and the significant SNPs associated with *S. sclerotiorum* resistance were displayed on Manhattan plot (**Figure 7B**) and QQ plot (**Figure 7C**). A total of 24 significant SNP loci ($P < 4.199 \times 10^{-7}$; Bonferroni-adjusted significance threshold $1/n$, n = 2,381,566; **Figure 7B**) associated with *S. sclerotiorum* resistance were detected, which constituted 10 QTL distributed on ten chromosomes including A01, A02, A03, A04, A08, A10, C03, C03, C04 and C08 of *B. napus*. Among them, four QTL containing five *BnGLPs* (*BnaA04g11540D*, *BnaA08g26300D*, *BnaC04g34260D*, *BnaC04g34340D* and *BnaC08g13660D*) were identified. Furthermore, *BnaA08g26300D* and *BnaC08g13660D* are WGD genes (ortholog of *AT1G09560/AtGLP1-2*), while *BnaA04g11540D* and *BnaC04g34260D* are WGD genes (ortholog of *AT5G39130/AtGLP5-10*). Considering that *BnaA08g26300D* and *BnaC08g13660D* (named as *BnGLP1.A08* and *BnGLP1.C08*, respectively) gene pairs are both common responsive genes for biotic and abiotic (dehydration, cold, ABA and salinity treatment) stresses, we took the two genes as candidates for further haplotype analysis. Our results revealed that each of *BnGLP1.A08* and *BnGLP1.C08* had two major haplotypes associated with *S. sclerotiorum* resistance (**Figures 7D,E**).

To confirm that *BnGLP1.A08* and *BnGLP1.C08* are involved in adaptive stress response, we determined their expression levels of *B. napus* seedlings under *S. sclerotiorum* infection

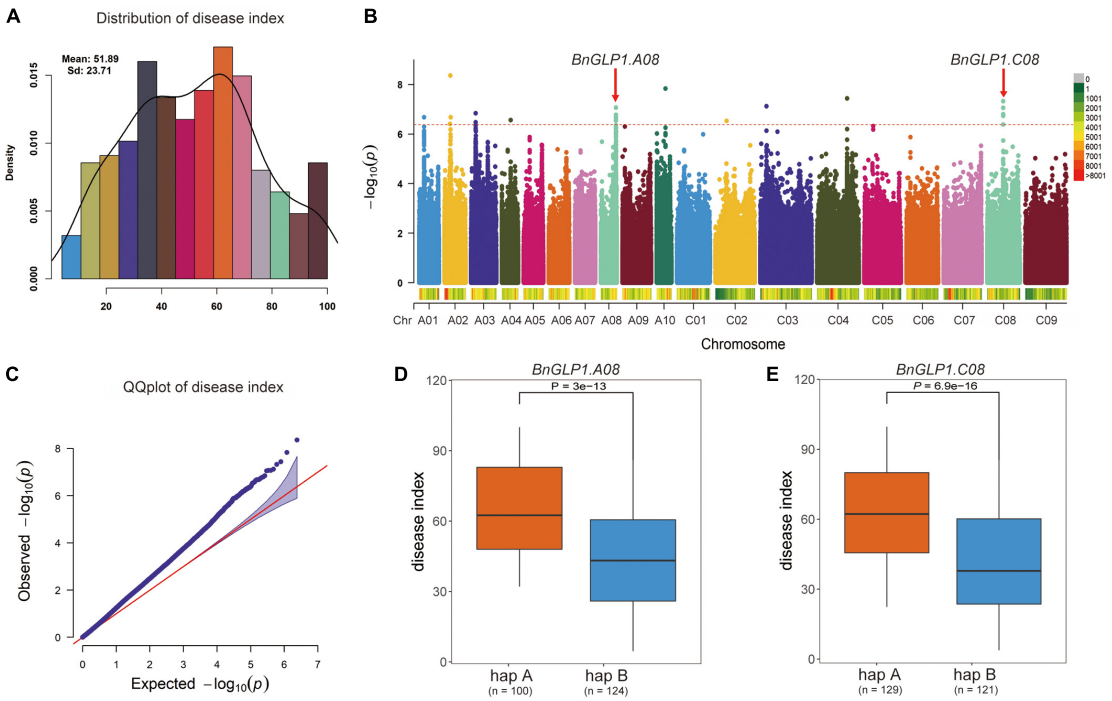

FIGURE 7
Both *BnGLP1.A08* and *BnGLP1.C08* are associated with *Sclerotinia sclerotiorum* resistance in *Brassica napus*. **(A)** Frequency distribution of disease index of 274 *B. napus* accessions. **(B)** Manhattan plot of the disease index from association analyses by FarmCPU model. Each point represents a SNP, and the SNP that exceeds the threshold (red dotted line) $-\log_{10}(1/n) = 6.377$ is significant. **(C)** QQ plot for the disease index from association analyses. **(D,E)** Boxplots for disease index based on the two haplotypes of *BnaGLP1.A08* **(D)** and *BnaGLP1.C08* **(E)**. The phenotypic differences between groups were tested using a two-tailed *t*-test ($P < 0.01$).

and different abiotic stress treatments (dehydration, cold, ABA and salinity) by quantitative real-time PCR (qRT-PCR). The leaves at four time points (12 h, 24 h, 36 h and 48 h) after *S. sclerotiorum* inoculation were collected to explore the dynamic gene expression changes (**Figure 8**). The results demonstrated that the expression pattern of *BnGLP1.A08* and *BnGLP1.C08* after *S. sclerotiorum* inoculation was very similar, which stayed relatively consistent during the first 24 h and was then upregulated to a peak (**Figure 8**). For abiotic stress responses, the expression level of both *BnGLP1.A08* and *BnGLP1.C08* genes showed significantly increased expression under dehydration, cold, ABA or salinity treatment, and displayed more sensitive to ABA treatment, leading to more accumulation in transcripts (**Figure 8**). Taking together, the qRT-PCR analysis verified the reliability of the RNA-seq data and revealed that both *BnGLP1.A08* and *BnGLP1.C08* gene pairs are common responsive genes shared by multiple stresses.

Discussion

Environmental stresses such as pathogen infection or drought, salinity, heat and cold cause devastating impacts on plant growth and extensive losses in the crop yield (Suzuki et al., 2014). Sclerotinia stem rot caused by *S. sclerotiorum* is a devastating disease leading to significant yield and economic losses in many crop and vegetable plants, particularly *Brassica* crops (Liu et al., 2021). Moreover, drought and salt stresses are important limiting factors affecting about 26% and 20% of the agricultural land, respectively (Raza et al., 2021). Therefore, it is urgent to identify more effective loci with durable disease resistance or diverse abiotic stress tolerance in plants, especially in important agricultural crops, to develop biotic and abiotic stress-tolerant genotypes. Single cupin_1 domain GLPs play essential roles in regulating plant development and biotic/abiotic stress resistance (Dunwell et al., 2004). However, the prevalence and functional diversity of the *CDP* gene family in *B. napus* have not been thoroughly investigated. In this study, we performed a comprehensive analysis of the *BnCDP* family in *B. napus*. The features of *BnCDP* genes, including their chromosomal distribution, phylogenetic classification, gene structures, conserved motifs, *cis*-regulatory elements, expression profiles, and responses to various stresses were explored. The results will provide insights into this gene family and offer valid information for predicting their potential functions in plant growth and stress response.

To date, the *GLP* genes (encoding single cupin_1 domain protein) have been genome-wide identified in numerous plant species, such as *A. thaliana* (Li L. et al., 2016), rice (Li L. et al., 2016), soybean (Lu et al., 2010), *Vitis vinifera* (Ilyas et al., 2022), cucumber (Liao et al., 2021), potato (Zaynab et al., 2021), peanut (Wang et al., 2013) and *Physcomitrella patens* (Nakata et al., 2004). However, the genes encoding duplicated cupin_1 domain protein were till rarely characterized. In this study, 96 *BnCDPs* in *B. napus* and 42 *AtCDPs* (including 32 previously identified *AtGLPs*) were systematically identified. Gene duplication might

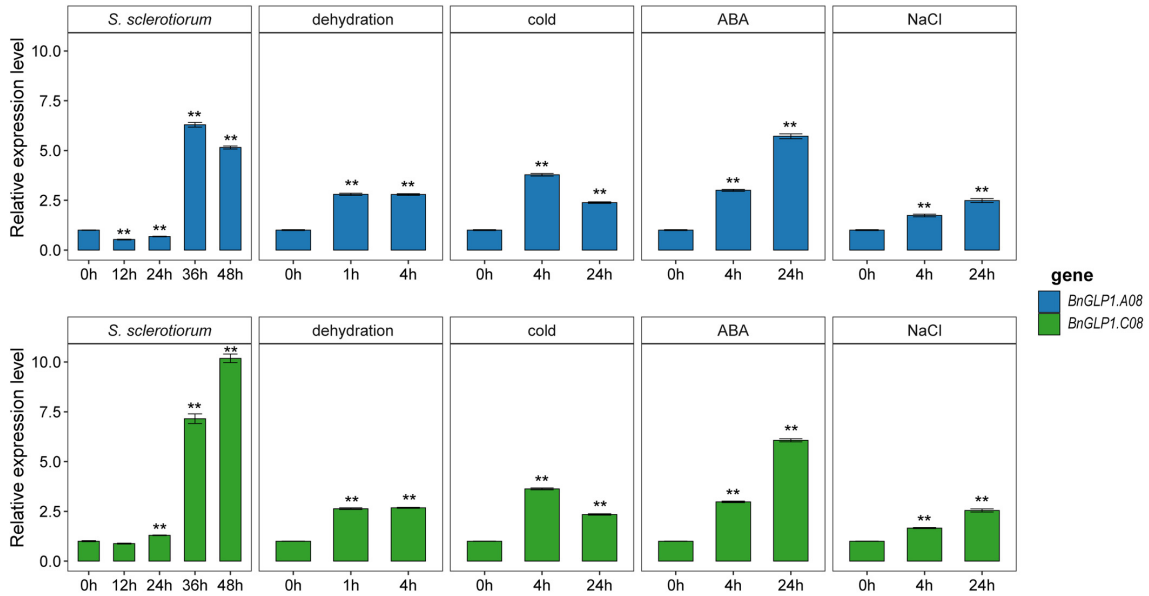

FIGURE 8
The expression validation of candidate *BnGLP1.A08* and *BnGLP.C08* genes in response to *Sclerotinia sclerotiorum* infection and four abiotic stress treatments (dehydration, cold, ABA and salinity) by qRT-PCR. The time points under the x-axis represent hours (h) after corresponding biotic and abiotic treatments. The error bars show the standard error of three replicates. Student's *t*-test was used for statistical analysis, ** indicates significant differences at $P < 0.01$, all compared to the treatment at 0 h.

account for the differences in the number of *CDP* family members between *B. napus* and *A. thaliana*. In our results, 75.0% of *BnCDPs* (72 *BnCDP* genes) were originated from WGD or segmental duplication, which is consistent with the conclusion that WGD and segmental duplication are the main contributors to the expansion of gene families in other researches (Ma et al., 2017; Wu et al., 2018; Xie et al., 2022). Since *B. napus* was formed by the interspecific hybridization between *B. rapa* and *B. oleracea* about 7,500 years ago, both of which had undergone a genome triplication event after divergence from *A. thaliana* lineage, six homologs for each *A. thaliana* gene are expected to be present in *B. napus* (Allender and King, 2010). However, the number of identified *BnCDPs* was much smaller than expected (less than threefold of *AtCDPs*), which may be ascribed to the occurrence of gene loss during the diploidization process (Albalat and Canestro, 2016). Despite the uneven distribution of *BnCDP* genes at the chromosome level, the total number of genes was roughly similar in the A_n (50 members) and C_n subgenome (46 members) ($\chi^2 = 0.167 < 3.84$). Based on the K_a/K_s ratio of paralogous gene pairs (**Supplementary Table 3**), it can be speculated that purification selection plays a significant role in the evolution of *BnCDP* genes in *B. napus*.

A phylogenetic analysis of the CDP members from *B. napus* and *A. thaliana* revealed that these CDPs could be divided into six subfamilies (I–VI). All members in subfamily I–III are GLPs, while those in subfamily IV–VI tend to be bicupins, and their monocupin members showed closer evolutionary relationship with bicupins than with other GLPs (**Figure 1**). Dunwell et al. predicted that bicupins probably evolved from the duplication and then fusion of a single domain ancestor (Dunwell et al., 2004). Our phylogenetic analysis indicated that the fused duplicated domain protein (bicupin) might also lose a domain during the subsequent evolution to produce a new monocupin with higher similarities in sequence and gene structure to its bicupin ancestor. Furthermore, *BnCDPs* within the same subfamily have high similarities in gene structure and motif distribution (**Figure 3**), implying that the members in the same subfamily have similar functions.

Spatio-temporal expression pattern can reflect the potential function of a gene to a certain extent. In the present study, we analyzed the expression patterns of all 96 *BnCDP* members in 30 tissues/stages (He et al., 2022). As shown in **Figure 5**, most of the *BnCDP* genes showed preferential expression in specific tissues/stages, which is consistent with the previous findings in cucumber, rice and *A. thaliana* (Li L. et al., 2016; Liao et al., 2021). For example, almost all members in subfamily IV and subfamily V were predominantly expressed in seeds at the intermediate to the late stage; *BnaA09g04150D*, *BnaAnng02980D* and *BnaC03g34440D* from subfamily I were predominantly expressed in the bud and pistil; *BnaA07g22030D* from subfamily II was highly expressed in the pistil; *BnaA07g30320D* and *BnaC06g33770D* from subfamily III showed high accumulation of transcripts in the leaf. These results indicate that they play essential roles in these tissues/stages. Besides, three genes (*BnaC08g13660D*, *BnaCnng19890D*, *BnaC05g05380D*) were expressed in all the 30 tissues/stages (**Figure 5**), suggesting their possible essential roles in the entire growth and development stages.

Plant *GLP* genes also play vital roles in regulating biotic and abiotic stress responses. Numerous studies have demonstrated that the *GLPs* are widely involved in resistance to diverse pathogens such as *S. sclerotiorum* (Rietz et al., 2012; Zhang et al., 2018), *Rhizoctonia solani* (Beracochea et al., 2015), *Blumeria graminis* (Yuan et al., 2021), *Magnaporthe oryzae* (Liu et al., 2016), *Aspergillus flavus* (Wang et al., 2013), and response to UV-B radiation (He et al., 2021), heat (Gangadhar et al., 2021; Zaynab et al., 2021), drought (Wang et al., 2013; Anum et al., 2022), heavy metal (Cheng et al., 2018) and wound (Wang et al., 2013). To further explore the possible function of *BnCDPs* in stress resistance, the analysis of *cis*-acting regulatory elements in the promoter regions was conducted in this study. The results revealed the enrichment of elements associated with development, hormone and stress (**Figure 4**, **Supplementary Figure 2** and **Supplementary Table 5**), implying that the members of the *BnCDP* family are potentially involved in biotic and abiotic stress responses during plant growth and development. Consistently, many members in the *BnCDP* family were significantly responsive to one or more stresses according to the transcriptome data under one biotic stress (*S. sclerotiorum* infection) and four abiotic stresses (dehydration, cold, ABA and salinity). Furthermore, six *BnCDP* genes were commonly regulated by *S. sclerotiorum* infection and all the four abiotic stresses, which belong to multiple biotic and abiotic stress-responsive genes. Similar results were previously obtained that several members in both barley *HvGER* family (Zimmermann et al., 2006) and Peanut *AhGLP* family (Wang et al., 2013) appeared to participate in multiple biotic and abiotic stress responses. Notably, the *bicupins* from subfamily IV–VI are also responsive to multiple stresses, such as *BnaCnng28630D* in subfamily IV responsive to dehydration treatment, *BnaA10g02240D* in subfamily V responsive to dehydration, cold and ABA treatments, *BnaC05g05380D* in subfamily VI responsive to dehydration, cold treatments and *S. sclerotiorum* infection. These results suggested that some other *BnCDP* genes apart from *BnGLPs* may also have important functions in environmental adaption, and some of them were promising broad-spectrum stress resistance candidates with tremendous potential in improving crop resistance to different stresses. To further examine the potential roles of *BnCDP* genes in *S. sclerotiorum* resistance, we performed a GWAS analysis. The results showed that five *BnGLPs* are located in the significant associated regions, including a duplicate gene pair *BnGLP1.A08* and *BnGLP1.C08*, whose response patterns to different biotic and abiotic stresses were validated by qPCR experiment. The results support the conclusion that the *BnCDP* family members are widely involved in environmental adaption

of *B. napus*. This study provides a useful resource for future research on the biological function and evolutionary history of the *BnCDP* gene family.

Conclusion

In this study, the cupin_1 domain protein (CDP) gene family in *B. napus* was genome widely characterized and systematically investigated. In total, 96 *BnCDP* genes were identified and clustered into six distinct subfamilies (I–VI) based on their evolutionary relationships. Genes from the same subfamily have similar gene structure and motif distribution, which are more conserved in subfamily I–III (BnGLP) than in subfamily IV–VI. To better understand their potential functional roles, we analyzed the *cis*-regulatory elements and TFBSs in the promoters of *BnCDP*s, as well as their expression patterns in diverse tissues/stages and under various biotic and abiotic stresses. The results demonstrated that the *BnCDP* family members play important roles in plant development and stress tolerance, particularly the six genes commonly regulated by *S. sclerotiorum* infection and four abiotic stresses, which may serve as promising broad-spectrum stress tolerance candidates. GWAS on *S. sclerotiorum* resistance revealed that two (*BnGLP1.A08* and *BnGLP.C08*) of the six common stress response candidate genes were located in significant associated regions, and their expression patterns under different biotic and abiotic stress treatments were further validated by qPCR analysis. In summary, this study provides detailed information about *BnCDP*s in *B. napus*, and will facilitate the functional studies and genetic improvement to deal with different stresses.

Materials and methods

Identification of *BnCDP* gene family in *Brassica napus*

The genome (v4.1) and annotation (v5) information of the *B. napus* cultivar "*Darmor-bzh*" (Chalhoub et al., 2014) was obtained from the Brassicaceae Database (BRAD[2]). To identify BnCDPs in *B. napus*, PF00190 from the Pfam database[3] (Mistry et al., 2021) was used as a query to search in the entire protein database of *B. napus* using HMMER 3.3.2[4] (Mistry et al., 2013; the e-value was set to 1×10^{-5}). Then, all putative BnCDPs identified were subjected to the NCBI Conserved Domain Database[5] (Lu et al., 2020) and the SMART database[6] (Letunic et al., 2021) to verify the presence of cupin_1 domain. Moreover, the peptide length, molecular weight (MW), isoelectric point (pI), instability index, gravy of each BnCDP proteins were calculated using ProtParam[7] (Wilkins et al., 1999), an online software of SWISS-PROT. Subcellular location prediction for these BnCDP proteins was conducted using CELLO v2.5[8] (Yu et al., 2006). The physical locations on the chromosomes and the exon number of the *BnCDP* genes were obtained from the GFF3 annotation file of the *B. napus* genome using a custom shell script.

Phylogenetic analysis

To gain insights into the evolutionary relationships of *BnCDP* genes in *B. napus*, the amino acid sequences of all 96 BnCDPs identified in this study, combined with 32 previously identified *A. thaliana* GLPs (Li L. et al., 2016) and 10 newly identified cupins, were subjected to multiple sequence alignment using ClustalW2 program (Larkin et al., 2007) with default parameters. Then, MEGA 11 (Tamura et al., 2021) software was used to generate the phylogenetic tree using the neighbor-joining (NJ) method with 1,000 bootstrap replicates. The final phylogenetic tree was visualized using iTOL v6.[9] The *BnCDP* genes were further categorized into different subfamilies based on the topology of the phylogenetic tree.

Chromosomal distribution and gene duplication analysis of *BnCDP* genes

To identify gene duplication events, BLASTP with the e-value of 1e−10 was used to align the sequence, and MCScanX (Wang et al., 2012) was used to detect the duplication patterns including segmental and tandem duplication. Chromosomal locations and duplication events were visualized using the TBtools software (Chen et al., 2020). To determine the evolutionary pressure on duplicated genes, the ratio of non-synonymous substitution to synonymous substitution (K_a/K_s) of duplicate gene pairs was calculated using TBtools (Chen et al., 2020).

Gene structure, conserved motif, and *cis*-regulatory element analysis

The conserved motif analysis of BnCDPs was conducted using the online motif finding tool, MEME (Multiple

2 http://brassicadb.cn/
3 http://pfam.xfam.org
4 http://www.hmmer.org/
5 https://www.ncbi.nlm.nih.gov/
6 http://smart.embl.de/
7 https://web.expasy.org/protparam/
8 http://cello.life.nctu.edu.tw/
9 https://itol.embl.de/

Expectation Maximization for Motif Elicitation, v5.4.1[10]; Bailey et al., 2015) with 20 motif numbers, and the remaining parameters were set to default values. The identified motifs were annotated by using the Interpro database.[11] The TBtools (Chen et al., 2020) software was used to display the gene structures and conserved motifs in BnCDP proteins. To identify the *cis*-regulatory elements of *BnCDP* genes, the promoters (2-kb upstream sequences from initiation codon) of *BnCDPs* were extracted and predicted by PlantCARE[12] (Lescot et al., 2002). The location and type of each selected *cis*-regulatory element were displayed by Gene Structure Display Server (GSDS 2.0; Hu et al., 2015). Besides, the transcription factor binding sites (TFBSs) in the promoter region of *BnCDP* genes were predicted using PlantRegMap/PlantTFDB v5.0[13] and the threshold *p*-value was set to 1e-7.

Expression analysis of *BnCDP* genes in *Brassica napus*

To explore the spatial-temporal expression patterns of *BnCDPs*, transcriptome data from 30 tissues/stages which include leaf, root, stem, bud, stamen, new pistil, blossomy pistil, wilted pistil, sepal, ovule and ten time-course seeds and silique walls (4, 8, 12, 16, 20, 24, 28, 32, 40, 48 days after pollination) of ZS11 were used in this study (He et al., 2022). Furthermore, in order to detect the expression patterns of *BnCDP* genes under biotic and abiotic stresses, RNA-seq data from tolerant *B. napus* cultivar ZY821 under the induction of *S. sclerotiorum* fungi and different abiotic stress conditions (dehydration, cold, ABA and salt) of *B. napus* cultivar ZS11 were also used in this study (Girard et al., 2017; Zhang et al., 2019). Then, the RNA-seq reads from each sample were aligned to the reference genome of *Darmor-bzh* (v4.1) using Hisat2 (Kim et al., 2015). Subsequently, the expression levels of *BnCDP* genes were calculated with Stringtie (Pertea et al., 2015) and displayed by Pheatmap in R.

Ribonucleic acid isolation and quantitative real-time PCR analysis of *BnCDP* genes

For *S. sclerotiorum* inoculation, the seedlings of ZY821 were kept growing in greenhouse at 22°C with a 16-h light and 8-h dark photoperiod for 6 weeks. *S. sclerotiorum* isolate obtained from Wuhan field was cultured on potato dextrose agar (PDA) medium and sub-cultured twice before inoculation at 22°C in darkness. Mycelial agar plug (7 mm in diameter) punched from the margin of a 2-day-old culture of *S. sclerotiorum* grown on PDA was carefully upended onto the adaxial surface of the latest or penultimate fully extended leaves with similar size. The inoculated plants were placed in a humidification chamber with high relative humidity (>85%) and samples were taken every 12 h. For abiotic stress treatments, the seeds of ZS11 were sterilized in 75% ethanol for 1 min, in 3.1% NaOCl for 10 min, and then rinsed six times with sterile water. Next, the seeds were sowed on Murashige and Skoog (MS) medium (MS, 1% sucrose, 0.7% agar, pH 5.8) in plates. The plates were placed vertically in the growth chamber with the temperature of 22°C and photoperiod of 16 h/8 h day/night. Two-week-old uniform plants/seedlings were removed from MS medium and subjected to dehydration, low temperature (4°C), ABA (25 uM), and salt (200 mM) stress treatment according to previously described methods (Zhang et al., 2019). Whole seedlings were collected at 1 h and 4 h after dehydration while 4 h and 24 h of low temperature, ABA, and salt treatment. All the samples mentioned above were flash frozen in liquid nitrogen and store at –80°C. Total RNA was extracted using the TRIZOL reagent (Invitrogen) according to the manufacturer's protocol and subjected to reverse transcription with the PrimeScript RT Reagent Kit with genomic DNA Eraser (Takara). Quantitative Real-time PCR (qRT-PCR) was performed by using SYBR Green Real-time PCR Master Mix (Bio-Rad) in 20 ml reaction mixture and run on CFX96 Real-time PCR system (Bio-Rad). β-actin gene was used as internal control. All the results were obtained with three biological replications, and each with three technical replications. The results were analyzed using the $2^{-\Delta\Delta CT}$ method as described previously (Livak and Schmittgen, 2001). The list of all the primers used in this study is included in **Supplementary Table 11**.

Genome wide association study on *Sclerotinia sclerotiorum* resistance

We selected 274 *B. napus* core germplasm accessions from all over the world to form a natural population. The genotypic data were obtained by 7 × re-sequencing and referring to the genome of 'Darmor-*bzh*' (Ding et al., 2020). SNPs were tested using the Broad Institute's opensource Genome Analysis Toolkit.[14] Then, the sites with SNP deletion of more than 0.9 or with minor allele frequency (MAF) less than 0.05 were filtered using VCFtools (Danecek et al., 2011), and finally 2,381,566 SNPs were obtained for GWAS. The phenotypic data were collected by investigating the disease index of mature rapeseeds grown at the Yangluo test base (Wuhan, China) from 2015 to 2018 (Ding et al., 2020). GWAS was

10 https://meme-suite.org/meme/

11 https://www.ebi.ac.uk/interpro/search/sequence/

12 https://bioinformatics.psb.ugent.be/webtools/plantcare/html/

13 http://plantregmap.gao-lab.org/binding_site_prediction.php

14 https://software.broadinstitute.org/gatk/

performed for *S. sclerotiorum* resistance using Fixed and random model Circulating Probability Unification (FarmCPU) model (Yin et al., 2021), and the significance threshold was set to $p < 4.199 \times 10^{-7}$.

Data availability statement

The original contributions presented in this study are included in the article/**Supplementary material**, further inquiries can be directed to the corresponding author.

Author contributions

YH, YL, and YZ designed the research. SL supervised the research. YH, YL, RZ, and JL performed the experiments. YH, YL, ZB, and MX analyzed the data. CT collected the data. XC and YYL provided the plant materials. YH and YL wrote the manuscript. YZ revised the manuscript. All authors have read and approved the current version of the manuscript.

Funding

This research was funded by the National Key Research and Development Program of China (2018YFE0108000), the Central Public-interest Scientific Institution Basal Research Fund (No. Y2020YJ03), the Agricultural Science and Technology Innovation Program of the Chinese Academy of Agricultural Sciences (CAAS-ZDRW202105 and CAAS-ASTIP-2013-OCRI), the Young Top-notch Talent Cultivation Program of Hubei Province, and the National Natural Science Foundation of China (31770250).

Acknowledgments

We thank all the laboratory members for investigating the phenotype of *Brassica napus* population. We also thank Minqiang Tang at the college of forestry of Hainan university for analyzing the SNP data. The numerical calculations in this manuscript have been done on the supercomputing system in the Supercomputing Center of Oil Crops Research Institute, Chinese Academy of Agricultural Sciences.

Conflict of interest

The authors declare that the research was conducted in the absence of any commercial or financial relationships that could be construed as a potential conflict of interest.

Publisher's note

All claims expressed in this article are solely those of the authors and do not necessarily represent those of their affiliated organizations, or those of the publisher, the editors and the reviewers. Any product that may be evaluated in this article, or claim that may be made by its manufacturer, is not guaranteed or endorsed by the publisher.

Supplementary material

The Supplementary Material for this article can be found online at: https://www.frontiersin.org/articles/10.3389/fpls.2022.983786/full#supplementary-material

SUPPLEMENTARY FIGURE 1
Chromosomal (chr) localization of 96 *BnCDP* genes on *Brassica napus* chromosomes and contigs. The different colors in chromosomes represent gene density, and *BnCDP* genes from different subfamilies are represented in different colors.

SUPPLEMENTARY FIGURE 2
Number of *cis*-acting regulatory elements in promoters of *BnCDP* genes in *Brassica napus*. The color scale represents amounts from low (blue color) to high (red color).

SUPPLEMENTARY FIGURE 3
Venn diagrams analysis of the stress-responsive *BnCDP* genes under different treatments. **(A)** Venn diagram shows overlapping responsive genes in *BnCDP* family among different abiotic stresses. **(B)** Venn diagram shows overlapping responsive genes in *BnCDP* family under *S. sclerotiorum* inoculation and four abiotic stress treatments.

References

Agarwal, G., Rajavel, M., Gopal, B., and Srinivasan, N. (2009). Structure-based phylogeny as a diagnostic for functional characterization of proteins with a cupin fold. *PLoS One* 4:e5736. doi: 10.1371/journal.pone.0005736

Albalat, R., and Canestro, C. (2016). Evolution by gene loss. *Nat. Rev. Genet.* 17, 379–391. doi: 10.1038/nrg.2016.39

Allender, C. J., and King, G. J. (2010). Origins of the amphiploid species *Brassica napus* L. investigated by chloroplast and nuclear molecular markers. *BMC Plant Biol.* 10:54. doi: 10.1186/1471-2229-10-54

Anum, J., O'Shea, C., Zeeshan Hyder, M., Farrukh, S., Skriver, K., Malik, S. I., et al. (2022). Germin like protein genes exhibit modular expression during salt and drought stress in elite rice cultivars. *Mol. Biol. Rep.* 49, 293–302. doi: 10.1007/s11033-021-06871-3

Bailey, T. L., Johnson, J., Grant, C. E., and Noble, W. S. (2015). The MEME suite. *Nucleic Acids Res.* 43, W39–W49. doi: 10.1093/nar/gkv416

Banerjee, J., and Maiti, M. K. (2010). Functional role of rice germin-like protein1 in regulation of plant height and disease resistance. *Biochem. Biophys. Res. Commun.* 394, 178–183. doi: 10.1016/j.bbrc.2010.02.142

Banerjee, J., Das, N., Dey, P., and Maiti, M. K. (2010). Transgenically expressed rice germin-like protein1 in tobacco causes hyper-accumulation of H_2O_2 and reinforcement of the cell wall components. *Biochem. Biophys. Res. Commun.* 402, 637–643. doi: 10.1016/j.bbrc.2010.10.073

Beracochea, V. C., Almasia, N. I., Peluffo, L., Nahirñak, V., Hopp, E. H., Paniego, N., et al. (2015). Sunflower germin-like protein HaGLP1 promotes ROS accumulation and enhances protection against fungal pathogens in transgenic *Arabidopsis thaliana*. *Plant Cell Rep.* 34, 1717–1733. doi: 10.1007/s00299-015-1819-4

Brunetti, S. C., Arseneault, M., and Gulick, P. J. (2022). Characterization and expression of the *Pirin* gene family in *Triticum aestivum*. *Genome* doi: 10.1139/gen-2021-0094 [Epub ahead of print].

Chalhoub, B., Denoeud, F., Liu, S., Parkin, I. A., Tang, H., Wang, X., et al. (2014). Plant genetics. Early allopolyploid evolution in the post-Neolithic *Brassica napus* oilseed genome. *Science* 345, 950–953. doi: 10.1126/science.1253435

Chen, C., Chen, H., Zhang, Y., Thomas, H. R., Frank, M. H., He, Y., et al. (2020). TBtools: an integrative toolkit developed for interactive analyses of big biological data. *Mol. Plant*. 13, 1194–1202. doi: 10.1016/j.molp.2020.06.009

Cheng, D., Tan, M., Yu, H., Li, L., Zhu, D., Chen, Y., et al. (2018). Comparative analysis of Cd-responsive maize and rice transcriptomes highlights Cd co-modulated orthologs. *BMC Genomics* 19:709. doi: 10.1186/s12864-018-5109-8

Cheng, X., Huang, X., Liu, S., Tang, M., Hu, W., and Pan, S. (2014). Characterization of germin-like protein with polyphenol oxidase activity from *Satsuma mandarine*. *Biochem. Biophys. Res. Commun.* 449, 313–318. doi: 10.1016/j.bbrc.2014.05.027

Danecek, P., Auton, A., Abecasis, G., Albers, C. A., Banks, E., DePristo, M. A., et al. (2011). The variant call format and VCFtools. *Bioinformatics* 27, 2156–2158. doi: 10.1093/bioinformatics/btr330

Davidson, R. M., Manosalva, P. M., Snelling, J., Bruce, M., Leung, H., and Leach, J. E. (2010). Rice germin-like proteins: allelic diversity and relationships to early stress responses. *Rice* 3, 43–55. doi: 10.1007/s12284-010-9038-7

Ding, L. N., Li, M., Guo, X. J., Tang, M. Q., Cao, J., Wang, Z., et al. (2020). *Arabidopsis* GDSL1 overexpression enhances rapeseed *Sclerotinia sclerotiorum* resistance and the functional identification of its homolog in *Brassica napus*. Plant Biotechnol. J. 18, 1255–1270. doi: 10.1111/pbi.13289

Dong, X., Ji, R., Guo, X., Foster, S. J., Chen, H., Dong, C., et al. (2008). Expressing a gene encoding wheat oxalate oxidase enhances resistance to *Sclerotinia sclerotiorum* in oilseed rape (*Brassica napus*). *Planta* 228, 331–340. doi: 10.1007/s00425-008-0740-2

Dunwell, J. M., Gibbings, J. G., Mahmood, T., and Saqlan Naqvi, S. M. (2008). Germin and germin-like proteins: evolution, structure, and function. *Crit. Rev. Plant Sci.* 27, 342–375. doi: 10.1080/07352680802333938

Dunwell, J. M., Khuri, S., and Gane, P. J. (2000). Microbial relatives of the seed storage proteins of higher plants: conservation of structure and diversification of function during evolution of the cupin superfamily. *Microbiol. Mol. Biol. Rev.* 64, 153–179. doi: 10.1128/MMBR.64.1.153-179.2000

Dunwell, J. M., Purvis, A., and Khuri, S. (2004). Cupins: the most functionally diverse protein superfamily? *Phytochemistry* 65, 7–17. doi: 10.1016/j.phytochem.2003.08.016

Gangadhar, B. H., Mishra, R. K., Kappachery, S., Baskar, V., Venkatesh, J., Nookaraju, A., et al. (2021). Enhanced thermo-tolerance in transgenic potato (*Solanum tuberosum* L.) overexpressing hydrogen peroxide-producing germin-like protein (GLP). *Genomics* 113, 3224–3234. doi: 10.1016/j.ygeno.2021.07.013

Girard, I. J., Tong, C., Becker, M. G., Mao, X., Huang, J., de Kievit, T., et al. (2017). RNA sequencing of *Brassica napus* reveals cellular redox control of *Sclerotinia* infection. *J. Exp. Bot.* 68, 5079–5091. doi: 10.1093/jxb/erx338

Gucciardo, S., Wisniewski, J. P., Brewin, N. J., and Bornemann, S. (2007). A germin-like protein with superoxide dismutase activity in pea nodules with high protein sequence identity to a putative rhicadhesin receptor. *J. Exp. Bot.* 58, 1161–1171. doi: 10.1093/jxb/erl282

Guevara-Olvera, L., Ruíz-Nito, M. L., Rangel-Cano, R. M., Torres-Pacheco, I., Rivera-Bustamante, R. F., Muñoz-Sánchez, C. I., et al. (2012). Expression of a germin-like protein gene (*CchGLP*) from a geminivirus-resistant pepper (*Capsicum chinense* Jacq.) enhances tolerance to geminivirus infection in transgenic tobacco. *Physiol. Mol. Plant P.* 78, 45–50. doi: 10.1016/j.pmpp.2012.01.005

He, Y., Yang, Z., Tang, M., Yang, Q. Y., Zhang, Y., and Liu, S. (2022). Enhancing canola breeding by editing a glucosinolate transporter gene lacking natural variation. *Plant Physiol.* 188, 1848–1851. doi: 10.1093/plphys/kiac021

He, Z. D., Tao, M. L., Leung, D., Yan, X. Y., Chen, L., Peng, X. X., et al. (2021). The rice germin-like protein OsGLP1 participates in acclimation to UV-B radiation. *Plant Physiol.* 186, 1254–1268. doi: 10.1093/plphys/kiab125

Hu, B., Jin, J., Guo, A. Y., Zhang, H., Luo, J., and Gao, G. (2015). GSDS 2.0: an upgraded gene feature visualization server. *Bioinformatics* 31, 1296–1297. doi: 10.1093/bioinformatics/btu817

Ilyas, M., Rahman, A., Khan, N. H., Haroon, M., Hussain, H., Rehman, L., et al. (2022). Analysis of germin-like protein genes family in *Vitis vinifera* (*VvGLPs*) using various in silico approaches. *Braz. J. Biol.* 84:e256732. doi: 10.1590/1519-6984.256732

Jin, J., Zhang, H., Kong, L., Gao, G., and Luo, J. (2014). PlantTFDB 3.0: a portal for the functional and evolutionary study of plant transcription factors. *Nucleic Acids Res.* 42, D1182–D1187. doi: 10.1093/nar/gkt1016

Kim, D., Langmead, B., and Salzberg, S. L. (2015). HISAT: a fast spliced aligner with low memory requirements. *Nat. Methods* 12, 357–360. doi: 10.1038/nmeth.3317

Knecht, K., Seyffarth, M., Desel, C., Thurau, T., Sherameti, I., Lou, B., et al. (2010). Expression of *BvGLP-1* encoding a germin-like protein from sugar beet in *Arabidopsis thaliana* leads to resistance against *phytopathogenic* fungi. *Mol. Plant Microbe Interact.* 23, 446–457. doi: 10.1094/MPMI-23-4-0446

Lane, B. G. (2002). Oxalate, germins, and higher-plant pathogens. *IUBMB Life* 53, 67–75. doi: 10.1080/15216540211474

Larkin, M. A., Blackshields, G., Brown, N. P., Chenna, R., McGettigan, P. A., McWilliam, H., et al. (2007). Clustal W and Clustal X version 2.0. *Bioinformatics* 23, 2947–2948. doi: 10.1093/bioinformatics/btm404

Lescot, M., Déhais, P., Thijs, G., Marchal, K., Moreau, Y., Van de Peer, Y., et al. (2002). PlantCARE, a database of plant *cis*-acting regulatory elements and a portal to tools for in silico analysis of promoter sequences. *Nucleic Acids Res.* 30, 325–327. doi: 10.1093/nar/30.1.325

Letunic, I., Khedkar, S., and Bork, P. (2021). SMART: recent updates, new developments and status in 2020. *Nucleic Acids Res.* 49, D458–D460. doi: 10.1093/nar/gkaa937

Li, L., Xu, X., Chen, C., and Shen, Z. (2016). Genome-Wide characterization and expression analysis of the germin-like protein family in rice and *Arabidopsis*. *Int. J. Mol. Sci.* 17:1622. doi: 10.3390/ijms17101622

Li, Y., Zhang, D., Li, W., Mallano, A. I., Zhang, Y., Wang, T., et al. (2016). Expression study of soybean germin-like gene family reveals a role of *GLP7* gene in various abiotic stress tolerances. *Can. J. Plant Sci.* 96, 296–304. doi: 10.1139/cjps-2015-0213

Liao, L., Hu, Z., Liu, S., Yang, Y., and Zhou, Y. (2021). Characterization of germin-like proteins (GLPs) and their expression in response to abiotic and biotic stresses in cucumber. *Horticulturae* 7:412. doi: 10.3390/horticulturae7100412

Liu, D., Wu, J., Lin, L., Li, P., Li, S., Wang, Y., et al. (2021). Overexpression of Cinnamoyl-CoA Reductase 2 in *Brassica napus* increases resistance to *Sclerotinia sclerotiorum* by affecting lignin biosynthesis. *Front. Plant Sci.* 12:732733. doi: 10.3389/fpls.2021.732733

Liu, Q., Yang, J., Yan, S., Zhang, S., Zhao, J., Wang, W., et al. (2016). The germin-like protein OsGLP2-1 enhances resistance to fungal blast and bacterial blight in rice. *Plant Mol. Biol.* 92, 411–423. doi: 10.1007/s11103-016-0521-4

Liu, S., Fitt, B. L., Liu, R., Evans, N., Dong, C., and Huang, Y. (2004). Cloning of plant defensin and oxalic acid oxidase genes and expressions of these genes induced by pathogens and chemicals in *Brassica napus*. *Chin. J. Oil Crop Sci.* 26:3.

Liu, S., Raman, H., Xiang, Y., Zhao, C., Huang, J., and Zhang, Y. (2022). De novo design of future rapeseed crops: challenges and opportunities. *Crop J.* 10, 587–596. doi: 10.1016/j.cj.2022.05.003

Livak, K. J., and Schmittgen, T. D. (2001). Analysis of relative gene expression data using real-time quantitative PCR and the 2(−Delta Delta C(T)) Method. *Methods* 25, 402–408. doi: 10.1006/meth.2001.1262

Lu, M., Han, Y. P., Gao, J. G., Wang, X. J., and Li, W. B. (2010). Identification and analysis of the germin-like gene family in soybean. *BMC Genomics* 11:620. doi: 10.1186/1471-2164-11-620

Lu, S., Wang, J., Chitsaz, F., Derbyshire, M. K., Geer, R. C., Gonzales, N. R., et al. (2020). CDD/SPARCLE: the conserved domain database in 2020. *Nucleic Acids Res.* 48, D265–D268. doi: 10.1093/nar/gkz991

Ma, J. Q., Jian, H. J., Yang, B., Lu, K., Zhang, A. X., Liu, P., et al. (2017). Genome-wide analysis and expression profiling of the *GRF* gene family in oilseed rape (*Brassica napus* L.). *Gene* 620, 36–45. doi: 10.1016/j.gene.2017.03.030

Mistry, J., Chuguransky, S., Williams, L., Qureshi, M., Salazar, G. A., Sonnhammer, E. L. L., et al. (2021). Pfam: the protein families database in 2021. *Nucleic Acids Res.* 49, D412–D419. doi: 10.1093/nar/gkaa913

Mistry, J., Finn, R. D., Eddy, S. R., Bateman, A., and Punta, M. (2013). Challenges in homology search: HMMER3 and convergent evolution of coiled-coil regions. *Nucleic Acids Res.* 41:e121. doi: 10.1093/nar/gkt263

Nakata, M., Watanabe, Y., Sakurai, Y., Hashimoto, Y., Matsuzaki, M., Takahashi, Y., et al. (2004). Germin-like protein gene family of a moss, *Physcomitrella patens*, phylogenetically falls into two characteristic new clades. *Plant Mol. Biol.* 56, 381–395. doi: 10.1007/s11103-004-3475-x

Oudelaar, A. M., and Higgs, D. R. (2021). The relationship between genome structure and function. *Nat. Rev. Genet.* 22, 154–168. doi: 10.1038/s41576-020-00303-x

Pei, Y., Li, X., Zhu, Y., Ge, X., Sun, Y., Liu, N., et al. (2019). GhABP19, a novel germin-like protein from *Gossypium hirsutum*, plays an important role in the regulation of resistance to *Verticillium* and *Fusarium* wilt pathogens. *Front. Plant Sci.* 10:583. doi: 10.3389/fpls.2019.00583

Pertea, M., Pertea, G. M., Antonescu, C. M., Chang, T. C., Mendell, J. T., and Salzberg, S. L. (2015). StringTie enables improved reconstruction of a transcriptome from RNA-seq reads. *Nat. Biotechnol.* 33, 290–295. doi: 10.1038/nbt.3122

Raza, A., Razzaq, A., Mehmood, S. S., Hussain, M. A., Wei, S., He, H., et al. (2021). Omics: the way forward to enhance abiotic stress tolerance in *Brassica napus* L. *GM Crops Food* 12, 251–281. doi: 10.1080/21645698.2020.1859898

Rietz, S., Bernsdorff, F. E., and Cai, D. (2012). Members of the germin-like protein family in *Brassica napus* are candidates for the initiation of an oxidative burst that impedes pathogenesis of *Sclerotinia sclerotiorum*. *J. Exp. Bot.* 63, 5507–5519. doi: 10.1093/jxb/ers203

Sakamoto, A., Nishimura, T., Miyaki, Y. I., Watanabe, S., Takagi, H., Izumi, S., et al. (2015). In vitro and in vivo evidence for oxalate oxidase activity of a germin-like protein from azalea. *Biochem. Biophys. Res. Commun.* 458, 536–542. doi: 10.1016/j.bbrc.2015.02.002

Sun, M., Ye, Z., Tan, J., Chen, S., Zhang, X., and Tu, L. (2020). A cotton germin-like protein GbGLP2 controls fiber length via regulating genes involved in secondary cell wall synthesis. *Mol. Breed.* 40:98. doi: 10.1007/s11032-020-01177-x

Suzuki, N., Rivero, R. M., Shulaev, V., Blumwald, E., and Mittler, R. (2014). Abiotic and biotic stress combinations. *New Phytol.* 203, 32–43. doi: 10.1111/nph.12797

Tamura, K., Stecher, G., and Kumar, S. (2021). MEGA11: molecular evolutionary genetics analysis version 11. *Mol. Biol. Evol.* 38, 3022–3027. doi: 10.1093/molbev/msab120

Thompson, C., Dunwell, J. M., Johnstone, C. E., Lay, V., Ray, J., Schmitt, M., et al. (1995). Degradation of oxalic acid by transgenic oilseed rape plants expressing oxalate oxidase. *Euphytica* 85, 169–172. doi: 10.1007/BF00023945

Thompson, E. W., and Lane, B. G. (1980). Relation of protein synthesis in imbibing wheat embryos to the cell-free translational capacities of bulk mRNA from dry and imbibing embryos. *J. Biol. Chem.* 255, 5965–5970. doi: 10.1016/s0021-9258(19)70725-x

Wang, H., Zhang, Y., Xiao, N., Zhang, G., Wang, F., Chen, X., et al. (2020). Rice *GERMIN-LIKE PROTEIN 2-1* functions in seed dormancy under the control of abscisic acid and gibberellic acid signaling pathways. *Plant Physiol.* 183, 1157–1170. doi: 10.1104/pp.20.00253

Wang, T., Chen, X., Zhu, F., Li, H., Li, L., Yang, Q., et al. (2013). Characterization of peanut germin-like proteins, AhGLPs in plant development and defense. *PLoS One* 8:e61722. doi: 10.1371/journal.pone.0061722

Wang, X., Zhang, H., Gao, Y., Sun, G., Zhang, W., and Qiu, L. (2014). A comprehensive analysis of the Cupin gene family in soybean (*Glycine max*). *PLoS One* 9:e110092. doi: 10.1371/journal.pone.0110092

Wang, Y., Tang, H., Debarry, J. D., Tan, X., Li, J., Wang, X., et al. (2012). MCScanX: a toolkit for detection and evolutionary analysis of gene synteny and collinearity. *Nucleic Acids Res.* 40:e49. doi: 10.1093/nar/gkr1293

Wilkins, M. R., Gasteiger, E., Bairoch, A., Sanchez, J. C., Williams, K. L., Appel, R. D., et al. (1999). Protein identification and analysis tools in the ExPASy server. *Methods Mol. Biol.* 112, 531–552. doi: 10.1385/1-59259-584-7

Woo, E. J., Dunwell, J. M., Goodenough, P. W., Marvier, A. C., and Pickersgill, R. W. (2000). Germin is a manganese containing homohexamer with oxalate oxidase and superoxide dismutase activities. *Nat. Struct. Biol.* 7, 1036–1040. doi: 10.1038/80954

Wu, Y., Ke, Y., Wen, J., Guo, P., Ran, F., Wang, M., et al. (2018). Evolution and expression analyses of the MADS-box gene family in *Brassica napus*. *PLoS One* 13:e0200762. doi: 10.1371/journal.pone.0200762

Xie, M., Zuo, R., Bai, Z., Yang, L., Zhao, C., Gao, F., et al. (2022). Genome-wide characterization of serine/arginine-rich gene family and its genetic effects on agronomic traits of *Brassica napus*. *Front. Plant Sci.* 13:829668. doi: 10.3389/fpls.2022.829668

Yin, L., Zhang, H., Tang, Z., Xu, J., Yin, D., Zhang, Z., et al. (2021). RMVP: a memory-efficient, visualization-enhanced, and parallel-accelerated tool for genome-wide association study. *Genom. Proteom. Bioinf.* 19, 619–628. doi: 10.1016/j.gpb.2020.10.007

Yu, C. S., Chen, Y. C., Lu, C. H., and Hwang, J. K. (2006). Prediction of protein subcellular localization. *Proteins* 64, 643–651. doi: 10.1002/prot.21018

Yuan, B., Yang, Y., Fan, P., Liu, J., Xing, H., Liu, Y., et al. (2021). Genome-wide identification and characterization of germin and germin-like proteins (GLPs) and their response under powdery mildew stress in wheat (*Triticum aestivum* L.). *Plant Mol. Biol. Rep.* 39, 821–832. doi: 10.1007/s11105-021-01291-w

Zaynab, M., Peng, J., Sharif, Y., Fatima, M., Albaqami, M., Al-Yahyai, R., et al. (2021). Genome-wide identification and expression profiling of germin-like proteins reveal their role in regulating abiotic stress response in potato. *Front. Plant Sci.* 12:831140. doi: 10.3389/fpls.2021.831140

Zhang, Y., Ali, U., Zhang, G., Yu, L., Fang, S., Iqbal, S., et al. (2019). Transcriptome analysis reveals genes commonly responding to multiple abiotic stresses in rapeseed. *Mol. Breed.* 39:158. doi: 10.1007/s11032-019-1052-x

Zhang, Y., Wang, X., Chang, X., Sun, M., Zhang, Y., Li, W., et al. (2018). Overexpression of germin-like protein *GmGLP10* enhances resistance to *Sclerotinia sclerotiorum* in transgenic tobacco. *Biochem. Biophys. Res. Commun.* 497, 160–166. doi: 10.1016/j.bbrc.2018.02.046

Zhao, Y., Zhu, X., Chen, X., and Zhou, J. M. (2022). From plant immunity to crop disease resistance. *J. Genet. Genomics* doi: 10.1016/j.jgg.2022.06.003 [Epub ahead of print].

Zhu, J. K. (2016). Abiotic stress signaling and responses in plants. *Cell* 167, 313–324. doi: 10.1016/j.cell.2016.08.029

Zimmermann, G., Baumlein, H., Mock, H. P., Himmelbach, A., and Schweizer, P. (2006). The multigene family encoding germin-like proteins of barley. Regulation and function in Basal host resistance. *Plant Physiol.* 142, 181–192. doi: 10.1104/pp.106.083824

Zou, Q. J., Liu, S. Y., Dong, X. Y., Bi, Y. H., Cao, Y. C., Xu, Q., et al. (2007). *In vivo* measurements of changes in pH triggered by oxalic acid in leaf tissue of transgenic oilseed rape. *Phytochem. Anal.* 18, 341–346. doi: 10.1002/pca.988

frontiers | Frontiers in Plant Science

TYPE Original Research
PUBLISHED 12 August 2022
DOI 10.3389/fpls.2022.986635

OPEN ACCESS

EDITED BY
Huajian Zhang,
Anhui Agricultural University, China

REVIEWED BY
Maoteng Li,
Huazhong University of Science and Technology, China
Daojie Wang,
Henan University, China
Qiong Hu,
Oil Crops Research Institute (CAAS), China

*CORRESPONDENCE
Youping Wang
wangyp@yzu.edu.cn

SPECIALTY SECTION
This article was submitted to Plant Pathogen Interactions, a section of the journal Frontiers in Plant Science

RECEIVED 05 July 2022
ACCEPTED 27 July 2022
PUBLISHED 12 August 2022

CITATION
Sun Q, Xi Y, Lu P, Lu Y, Wang Y and Wang Y (2022) Genome-wide analysis of the G-box regulating factors protein family reveals its roles in response to *Sclerotinia sclerotiorum* infection in rapeseed (*Brassica napus* L.). *Front. Plant Sci.* 13:986635. doi: 10.3389/fpls.2022.986635

Genome-wide analysis of the G-box regulating factors protein family reveals its roles in response to *Sclerotinia sclerotiorum* infection in rapeseed (*Brassica napus* L.)

Qinfu Sun, Ying Xi, Panpan Lu, Yingying Lu, Yue Wang and Youping Wang*

Jiangsu Provincial Key Laboratory of Crop Genetics and Physiology, Yangzhou University, Yangzhou, China

The G-box regulating factors (GRFs) are involved in a wide array of signal transduction pathway and play important roles in plant physiological and developmental processes and stress responses. The GRF proteins have previously been described in several plant species, but not in rapeseed (*Brassica napus* L.). In this study, we carried out genome-wide analysis of *GRFs* in *B. napus* based on the available genome sequence information, and analyzed their expression in different tissues under different hormone treatments and after inoculation with *Sclerotinia sclerotiorum*. We identified 46 putative *BnaGRF* genes in rapeseed, unevenly distributed on 18 chromosomes. Like the 14-3-3 proteins in other plant species, the 46 putative BnaGRFs could be classified into two major evolutionary branches: epsilon (ε) group and non-epsilon (non-ε) group. Evolutionary analysis indicated that the *BnaGRF* gene family expanded in both groups much before speciation. We discovered an expansion of the *14-3-3* gene family that likely occurred during a recent gene duplication event. Collinearity analysis revealed that most of the *BnaGRF* genes shared syntenic relationships. Global gene expression profiling of *BnaGRFs* by RNA-seq analysis showed 41.3% (19/46) response to *S. sclerotiorum* infection, and this response was probably mediated through jasmonic acid (JA) and salicylic acid (SA) signaling pathways. These results provide key insights into the role of 14-3-3s in the biotic stress response and enhance our understanding of their multiple functions in *B. napus*.

KEYWORDS

14-3-3, GF14, GRF, general regulatory factor, *Brassica napus*, *Sclerotinia sclerotiorum*, rapeseed, G-box regulating factors

Introduction

The 14-3-3 proteins were named in 1967 during an extensive study on bovine brain proteins, which were given numerical designations based on the results of column fractionation and electrophoretic mobility assays (Rosenquist et al., 2001). The 14-3-3 proteins are present in all eukaryotic organisms and are expressed in virtually all tissue types (DeLille et al., 2001). Initially, an *Arabidopsis thaliana* isoform was identified as part of a protein/G-box complex, and therefore named "G box factor 14-3-3" (GF14), and the 14-3-3 isoforms in plants were named G-box regulating factors (GRFs) (Rosenquist et al., 2001). The 14-3-3 proteins participate in several peculiar functions, such as the regulation of primary metabolism, ion transport, cellular trafficking, chloroplast, and mitochondrial enzyme activities (Camoni et al., 2018). Based on gene structure, the encoded plant 14-3-3 proteins are divided into two distinct groups, namely, epsilon (ε) and non-epsilon (non-ε) (Ferl et al., 2002).

An increasing body of evidence suggests that 14-3-3 proteins play an important role in different aspects of plant hormone physiology (Camoni et al., 2018). Research results show that 14-3-3 proteins interact with brassinosteroid (BR) receptor Brassinosteroid-Insensitive1 (BRI1), BRI1 Kinase Inhibitor (BKI1), BRI1 Suppressor phosphatase (BSU1), and the transcription factors BRI1-EMS-Suppressor1 (BES1), and Brassinazole-Resistant1 (BZR1), which act both as negative and positive regulators of BR signaling pathways (Chang et al., 2009; Ryu et al., 2010; Wang et al., 2011). The 14-3-3 proteins function as members of the transcriptional complexes of abscisic acid (ABA)-regulated genes. In embryonic barley roots, 14-3-3 proteins function in the ABA-regulated transcriptional cascade by interacting with bZIP transcription factors ABI1-3 and ABI5 (Schoonheim et al., 2007, 2009). Additionally, 14-3-3 proteins have been reported to regulate the cell expansion by stimulating the H^+-ATPase-dependent proton extrusion into the cell wall, which was IAA-dependent regulatory processes. In Arabidopsis, IAA promotes Thr^{947} phosphorylation and subsequent 14-3-3 binding to H^+-ATPase, and is responsible for its activation (Takahashi et al., 2012). 14-3-3 proteins interacted with components of the signaling pathways of gibberellic acid (GA) (Ito et al., 2014), jasmonic acid (JA) (Holtman et al., 2000), salicylic acid (SA) (Yang et al., 2009), and other plant hormones (Jaspert et al., 2011; Yoon and Kieber, 2013; Camoni et al., 2018) as well.

The 14-3-3 proteins participate in many physiological processes of plants, including flowering and chloroplast, stomatal, and root development. In rice, 14-3-3 proteins interact with the FT homolog Hd3a and the OsFD1 transcription factor in the apical cells of shoots to induce the transcription of *OsMADS15*, leading to flowering (Taoka et al., 2011; Kaneko-Suzuki et al., 2018), while in Arabidopsis, the 14-3-3 ν and μ proteins affect photoperiodic flowering by interacting with CONSTANS, a central regulator of the photoperiod pathway (Mayfield et al., 2007), and regulate root growth and chloroplast development as components of the photosensory system (Mayfield et al., 2012).

Whole-genome studies and reverse genetics approaches revealed that 14-3-3 proteins are involved in plant stress resistance. Genome-wide analysis of 14-3-3 proteins in rice (Chen et al., 2006), soybean (Wang et al., 2019), wheat (Shao et al., 2021), grape (Cheng et al., 2018), and other crops showed that the expression of some 14-3-3 family members is induced, while that of others is repressed by stresses. Overexpression of a wild soybean (*Glycine soja*) 14-3-3 gene, *GsGF14o*, in Arabidopsis caused deficits in root hair formation and development, thereby reducing the water intake capacity of the root system (Sun et al., 2014). Heterologous expression of Arabidopsis 14-3-3 gene *AtGF14*λ in cotton improved stress tolerance under moderate drought conditions by regulating the stomatal aperture of transgenic plants (Yan et al., 2004). In another study, AtGFψ interacted with different ACC SYNTHASE (ACS) isoforms and decreased their stability, functioning as a negative regulator of constitutive freezing tolerance and cold acclimation in Arabidopsis (Catala et al., 2014).

A number of 14-3-3 family members have been reported in different plant species; for example, 13 in Arabidopsis (Rosenquist et al., 2001), 8 in rice (Chen et al., 2006), 16 in soybean (Wang et al., 2019), 17 in tobacco (Konagaya et al., 2004), 12 in *Populus* (Tian et al., 2015), 8 in sweet orange, 15 in cassava (Chang et al., 2020), 11 in grape (Cheng et al., 2018), 17 in wheat (Shao et al., 2021), 10 in *Medicago truncatula* (Qin et al., 2016), 16 in mango (Xia et al., 2022), 18 in apple (Zuo et al., 2021), 25 in banana (Li et al., 2016), 9 in *Citrus sinensis* (Lyu et al., 2021), and 21 in *Brassica rapa* (Chandna et al., 2016). Despite the documentation of 14-3-3 genes in many plant species and their investigation under different stress conditions, little is known about this gene family in rapeseed (*Brassica napus*) and its diploid progenitor *Brassica oleracea*. Only four 14-3-3 genes have been identified in *B. napus* to date (Zhan et al., 2010). Rapeseed is the second most important oilseed crop in the world, and Sclerotinia stem rot (SSR), which is caused by *Sclerotinia sclerotiorum*, is a serious problem in the rapeseed industry(Wu et al., 2016). In this study, taking advantage of the completion of the newly assembled rapeseed genome sequence (Song et al., 2020), we systemically identified members of the 14-3-3 gene family in the *B. napus* genome, performed a comprehensive sequence analysis of these genes, and investigated their function in *S. sclerotiorum* resistance. Our results demonstrate that the oilseed rape genome contains the highest number of *14-3-3s* (46 *BnaGRFs*) among all plant species investigated to date, and 19 of these genes are likely involved in disease resistance, probably through the SA signaling pathway.

Materials and methods

Sequence search and annotation of *14-3-3* genes

Genome sequence and gene annotations of oilseed rape (*B. napus* L.) cultivar 'Zhongshuang11' (ZS11) were downloaded from the *B. napus* pan-genome information resource database (BnPIR[1]). The Hidden Markov Model (HMM) profiles of 14-3-3 domains (PF00244) were obtained from the Protein family database (Pfam[2]), and was employed as a query to identify all possible BnaGRFs using the HMMER software (V3.0) (Finn et al., 2011). Then, the motif of the candidate protein was confirmed using the online tools SMART,[3] CCD,[4] and MOTIF Search.[5] The length, isoelectric point (pI), and molecular weight (MW) of 14-3-3 proteins were calculated using the online ExPASy program,[6] and their subcellular localization was predicted using the online tool WOLFPSORT.[7]

The genome sequence of *B. oleracea* was downloaded from Ensembl Plants,[8] and *B. oleracea* 14-3-3 proteins (BolGRFs) were identified using the approaches mentioned above. Additionally, 21 14-3-3 proteins (BraGRFs) in *B. rapa* were obtained from (Chandna et al., 2016).

Genomic organization and synteny of *BnaGRFs* in *B. napus*

To visualize the location of *BnaGRFs* in the genome and identify syntenic gene pairs, the locations of *BnaGRFs* were extracted from the gff files of the *B. napus* genome.[9] All protein sequences of *B. napus* were compared against themselves using the MCScanX tool of the TBtools software (*E*-value $<$ 1e$-$10, number of hits $\leq$5) (Chen et al., 2020), and the duplicated gene groups and tandem duplicates were as described previously (Pi et al., 2021). The chromosomal locations and duplication events of *BnaGRFs* were visualized using the Circos package of the TBtools software. The ratios of non-synonymous to synonymous substitutions (Ka/Ks) in duplicate gene pairs were used to evaluate the selection pressure (Wang et al., 2010).

1 http://cbi.hzau.edu.cn/bnapus/index.php, accessed on 10 February 2021.

2 http://pfam.xfam.org/

3 https://smart.embl-heidelberg.de/

4 https://www.ncbi.nlm.nih.gov/Structure/cdd/cdd.shtml

5 https://www.genome.jp/tools/motif/

6 https://www.expasy.org/

7 https://wolfpsort.hgc.jp/

8 http://plants.ensembl.org/info/data/ftp/index.html

9 http://cbi.hzau.edu.cn/cgi-bin/rape/download_ext

Phylogenetic analysis of *14-3-3* genes

To gain insights into the evolutionary relationships among *14-3-3* family members, the structure of *BnaGRFs* and *A. thaliana 14-3-3s* (*AtGRFs*) was visualized using TBtools, based on the information in gff files. The conserved motifs of BnaGRFs and AtGRFs were analyzed using Multiple Expectation Maximization for Motif Elicitation (MEME) (Bailey et al., 2015), and the results were visualized with TBtools.

Amino acid sequences of the 14-3-3 proteins of *B. rapa*, *B. oleracea*, *B. napus*, and *A. thaliana* were aligned using MAFFT v7.505 with default parameters (Nakamura et al., 2018). Maximum-likelihood phylogenetic trees were generated in the MEGA 11 program using the Neighbor-Joining (NJ) method with 1,000 bootstrap replications. Additionally, phylogenetic analysis of BnaGRFs and AtGRFs was performed for investigating gene structure, while that of only BnaGRFs was performed for visualizing gene expression.

Expression profiling of *BnaGRFs*

A highly comprehensive time-series analysis of the transcriptome in different tissues, and gene expression pattern under adverse conditions and following different hormone treatments was reported in *B. napus* cultivar ZS11 (Liu et al., 2021). These data were used in this research. To predict the potential functions of *BnaGRFs*, the expression patterns were illustrated using HeatMap in TBtools (Chen et al., 2020). The heatmap was constructed by taking Log2 values of the transcripts per kilobase of exon model per million mapped reads (TPM) generated from RNA-seq data. The bars of *BnaGRFs* on heatmap represent the expressional change after different treatments.

Plant material, hormone treatments, and *S. sclerotiorum* inoculation

To probe the potential roles of *BnaGRFs* in resistance to *S. sclerotiorum*, the expression of *BnaGRFs* was inspected by RNA-seq in leaves treated with SA, ethylene (ET), hydrogen peroxide (H_2O_2), and oxalic acid (OA) or inoculated with *S. sclerotiorum*. Seed germination and seedling cultivation of *B. napus* cultivar 'J9712' were conducted in a greenhouse at 24°C under 16 h light/8 h dark photoperiod. Leaves of 6-week-old plants were sprayed with hormones (1 mM SA, 1 mM ET, or 100 mM H_2O_2), a chemical (1 mM OA), the toxin secreted by the pathogen *S. sclerotiorum*, or the solvent for the above compounds (0.01% ethanol; control), and collected at 0, 3, and 6 h after treatment. All samples were immediately frozen in liquid nitrogen and stored at $-$80°C until needed for RNA extraction (Rahman et al., 2016).

TABLE 1 Information on rapeseed 14-3-3 genes.

Gene ID	Gene name	Location	Exon number	Size (aa)	MW (Da)	pI	Duplication type	Subcellular localization prediction
BnaA01G0224300ZS	BnaGRF1	ChrA01:14566057:14567144(+)	3	185	20,992.32	9.52	Dispersed	Cytosol
BnaA02G0231200ZS	BnaGRF2	ChrA02:14989506:14990918(+)	4	260	29,284.76	4.61	WGD or segmental	Plasma membrane
BnaA03G0040300ZS	BnaGRF3	ChrA03:1854228:1855164(−)	2	250	28,017.69	4.83	WGD or segmental	Nucleus membrane
BnaA03G0207200ZS	BnaGRF4	ChrA03:10808510:10810092(−)	6	272	30,608.46	4.8	WGD or segmental	Nucleus membrane
BnaA03G0288100ZS	BnaGRF5	ChrA03:15284066:15285120(−)	4	261	29,439.1	4.69	WGD or segmental	Chloroplast
BnaA04G0101600ZS	BnaGRF6	ChrA04:11985269:11986295(+)	4	257	28,877.5	4.72	WGD or segmental	Nucleus membrane
BnaA05G0316100ZS	BnaGRF7	ChrA05:31427849:31428915(−)	3	263	29,670.25	4.8	WGD or segmental	Nucleus membrane
BnaA05G0489800ZS	BnaGRF8	ChrA05:44320262:44321341(+)	4	261	29,465.05	4.7	WGD or segmental	Plasma membrane
BnaA05G0493100ZS	BnaGRF9	ChrA05:44440809:44441890(−)	4	261	29,449.06	4.7	WGD or segmental	Plasma membrane
BnaA07G0108700ZS	BnaGRF10	ChrA07:15374454:15375753(−)	6	245	27,976.12	4.72	WGD or segmental	Nucleus
BnaA07G0123200ZS	BnaGRF11	ChrA07:16439637:16440852(−)	4	260	29,156.83	4.7	WGD or segmental	Plasma membrane
BnaA07G0123900ZS	BnaGRF12	ChrA07:16484239:16485700(+)	6	253	28,752.22	4.76	WGD or segmental	Nucleus
BnaA07G0167800ZS	BnaGRF13	ChrA07:19568278:19569285(+)	4	258	28,964.53	4.74	WGD or segmental	Nucleus membrane
BnaA07G0235600ZS	BnaGRF14	ChrA07:23323067:23324443(−)	4	260	29,198.71	4.65	WGD or segmental	Plasma membrane
BnaA07G0373400ZS	BnaGRF15	ChrA07:31468756:31469982(−)	5	212	24,186.73	6.65	WGD or segmental	Cytosol
BnaA07G0374100ZS	BnaGRF16	ChrA07:31504845:31506571(+)	3	299	33,657.87	4.92	WGD or segmental	Chloroplast
BnaA08G0230100ZS	BnaGRF17	ChrA08:24101625:24103213(−)	7	328	37,702.26	4.89	WGD or segmental	Golgi apparatus
BnaA09G0091600ZS	BnaGRF18	ChrA09:5340343:5341619(−)	3	249	28,066.8	4.82	WGD or segmental	Nucleus membrane
BnaA09G0375500ZS	BnaGRF19	ChrA09:43270421:43271551(−)	4	261	29,793.4	4.75	WGD or segmental	Chloroplast
BnaA09G0441400ZS	BnaGRF20	ChrA09:49887816:49889023(−)	6	269	30,599.21	4.77	WGD or segmental	Nucleus membrane
BnaA09G0462600ZS	BnaGRF21	ChrA09:51319481:51321117(+)	6	253	28,752.21	4.74	WGD or segmental	Mitochondrion
BnaA10G0242300ZS	BnaGRF22	ChrA10:23807919:23808830(+)	2	248	27,991.74	4.72	WGD or segmental	Chloroplast
BnaC01G0287900ZS	BnaGRF23	ChrC01:25148028:25151640(+)	14	581	65,584.35	7.01	WGD or segmental	Nucleus
BnaC02G0311500ZS	BnaGRF24	ChrC02:30481661:30483110(+)	4	260	29,284.76	4.61	WGD or segmental	Plasma membrane
BnaC03G0244000ZS	BnaGRF25	ChrC03:14931129:14932753(−)	6	271	30,495.34	4.77	WGD or segmental	Nucleus membrane
BnaC03G0346100ZS	BnaGRF26	ChrC03:23526445:23527500(−)	4	261	29,409.07	4.7	WGD or segmental	Plasma membrane
BnaC03G0626500ZS	BnaGRF27	ChrC03:60205248:60206819(+)	7	328	37,691.27	4.89	WGD or segmental	Golgi apparatus
BnaC04G0029800ZS	BnaGRF28	ChrC04:2882891:2883539(+)	2	182	20,530.78	4.62	Dispersed	mitochondrion
BnaC04G0380200ZS	BnaGRF29	ChrC04:50440648:50441711(−)	4	257	28,847.51	4.74	WGD or segmental	Chloroplast
BnaC05G0194000ZS	BnaGRF30	ChrC05:13641970:13643756(−)	6	253	28,780.22	4.74	WGD or segmental	Mitochondrion
BnaC05G0221900ZS	BnaGRF31	ChrC05:16739710:16740903(+)	6	270	30,708.38	4.81	WGD or segmental	Nucleus membrane
BnaC05G0329400ZS	BnaGRF32	ChrC05:35401996:35403560(−)	4	265	30,023.66	4.76	WGD or segmental	Plasma membrane
BnaC06G0098700ZS	BnaGRF33	ChrC06:17625723:17627380(+)	7	394	45,018.09	5.61	Dispersed	Cytosol
BnaC06G0157000ZS	BnaGRF34	ChrC06:25447602:25448659(+)	4	257	28,891.48	4.74	WGD or segmental	Nucleus membrane
BnaC06G0256100ZS	BnaGRF35	ChrC06:36385398:36386709(−)	4	260	29,198.71	4.65	WGD or segmental	Plasma membrane
BnaC06G0439100ZS	BnaGRF36	ChrC06:51346480:51347852(−)	5	241	27,385.18	5.31	WGD or segmental	Cytosol
BnaC06G0440000ZS	BnaGRF37	ChrC06:51399614:51401340(+)	4	260	29,226.72	4.64	WGD or segmental	Plasma membrane
BnaC07G0163800ZS	BnaGRF38	ChrC07:29220090:29221461(−)	7	267	30,723.14	4.75	WGD or segmental	Nucleus
BnaC07G0181300ZS	BnaGRF39	ChrC07:31130202:31131472(−)	4	260	29,142.85	4.74	WGD or segmental	Plasma membrane
BnaC07G0181600ZS	BnaGRF40	ChrC07:31157168:31158438(−)	4	260	29,142.85	4.74	Proximal	Plasma membrane
BnaC07G0182400ZS	BnaGRF41	ChrC07:31284178:31285716(+)	7	253	28,779.25	4.76	WGD or segmental	Nucleus
BnaC08G0272000ZS	BnaGRF42	ChrC08:35792611:35793759(−)	5	269	30,756.99	5.23	WGD or segmental	Golgi apparatus
BnaC08G0272400ZS	BnaGRF43	ChrC08:35866753:35867833(+)	4	259	29,002.58	4.63	WGD or segmental	Chloroplast
BnaC09G0088500ZS	BnaGRF44	ChrC09:5828367:5830224(−)	3	249	28,048.77	4.82	WGD or segmental	Chloroplast
BnaC09G0404100ZS	BnaGRF45	ChrC09:51468318:51470346(−)	4	197	22,690.4	9.66	Dispersed	Chloroplast
BnaC09G0553200ZS	BnaGRF46	ChrC09:64088276:64093727(+)	3	228	25,371.85	4.81	WGD or segmental	Nucleus membrane

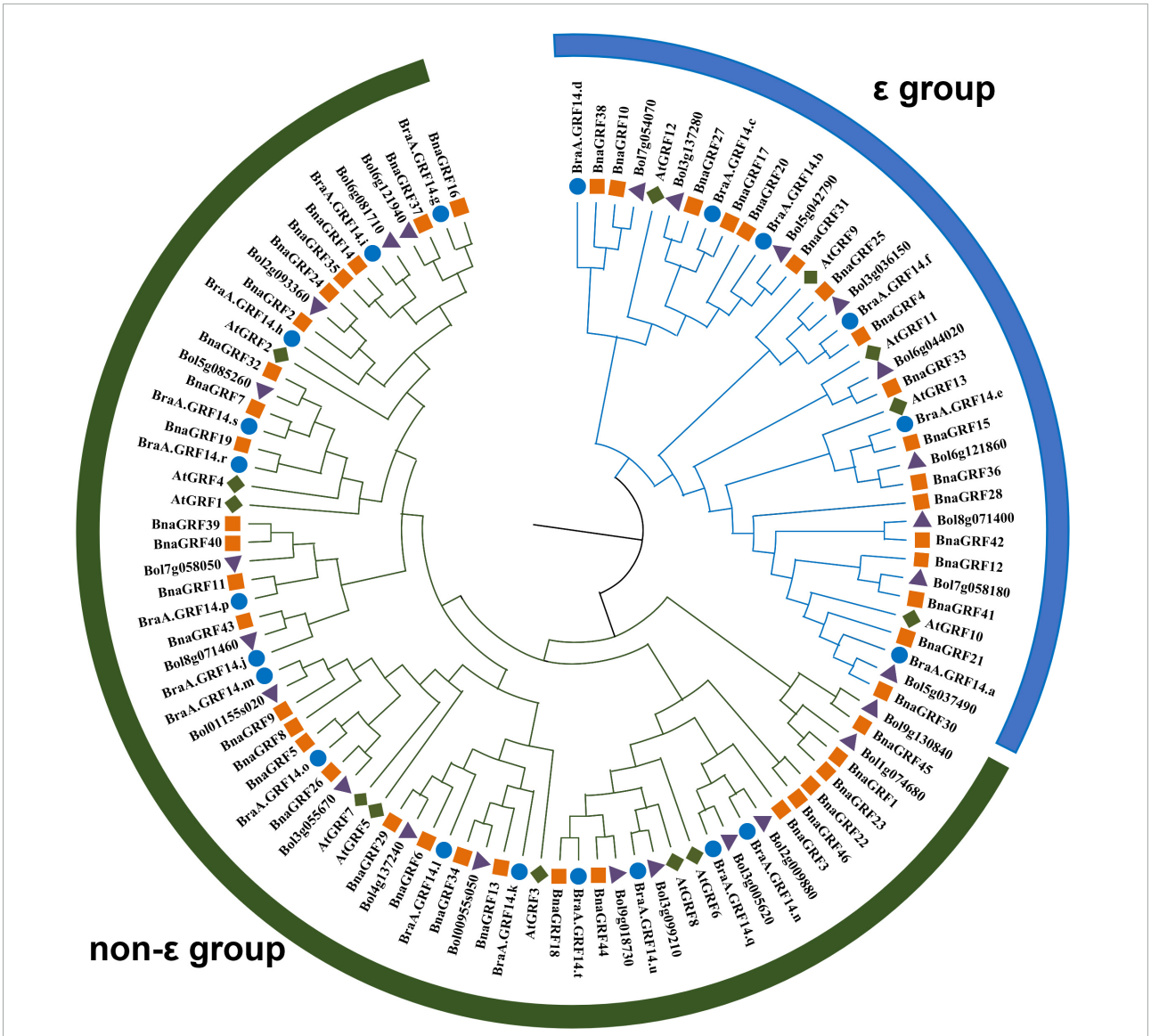

FIGURE 1
Phylogenetic analysis of the 14-3-3 protein family in *Brassica* species (*B. rapa*, *B. oleracea*, and *B. napus*) and *Arabidopsis thaliana*. A total of 46 14-3-3s were divided into two subgroups (ε and non-ε group), according to the evolutionary distance. Blue circles represent the 21 BraGRFs in *B. rapa*; purple triangles represent the 25 BolGRFs in *B. oleracea*; orange squares represent the 46 BnaGRFs in *B. napus*; and green diamonds represent the 13 AtGRFs in Arabidopsis.

To conduct pathogen inoculation, the leaves of 6-week-old plants were treated with agar disks containing the hyphae of *S. sclerotiorum*, as described previously (Wu et al., 2013). Briefly, the latest or penultimate fully extended leaves of similar size were excised from 6-week-old plants grown in the field. Nine leaves were collected and placed in a plastic tray (56 cm × 38 cm × 15 cm) with wet-gauze at the bottom of the tray. The mycelial agar plug was inoculated on the middle of each leaf. The inoculated leaves were further sprayed with a fine mist of water, and the plastic tray was covered with plastic film to maintain a high level of relative humidity. The plastic trays with inoculated leaves were kept at 22 ± 2°C in darkness. The leaves were sampled at 0, 6, 12, 24, and 36 h after inoculation.

RNA isolation and gene expression analysis

Leaves were collected at 0, 12, 24, and 36 h post-inoculation, with three biological replicates at each time point. Total RNA was extracted from the leaf samples using the RNA Purification Kit (TransGen, China), according to the manufacturer's instructions. The quality of RNA was evaluated by agarose gel

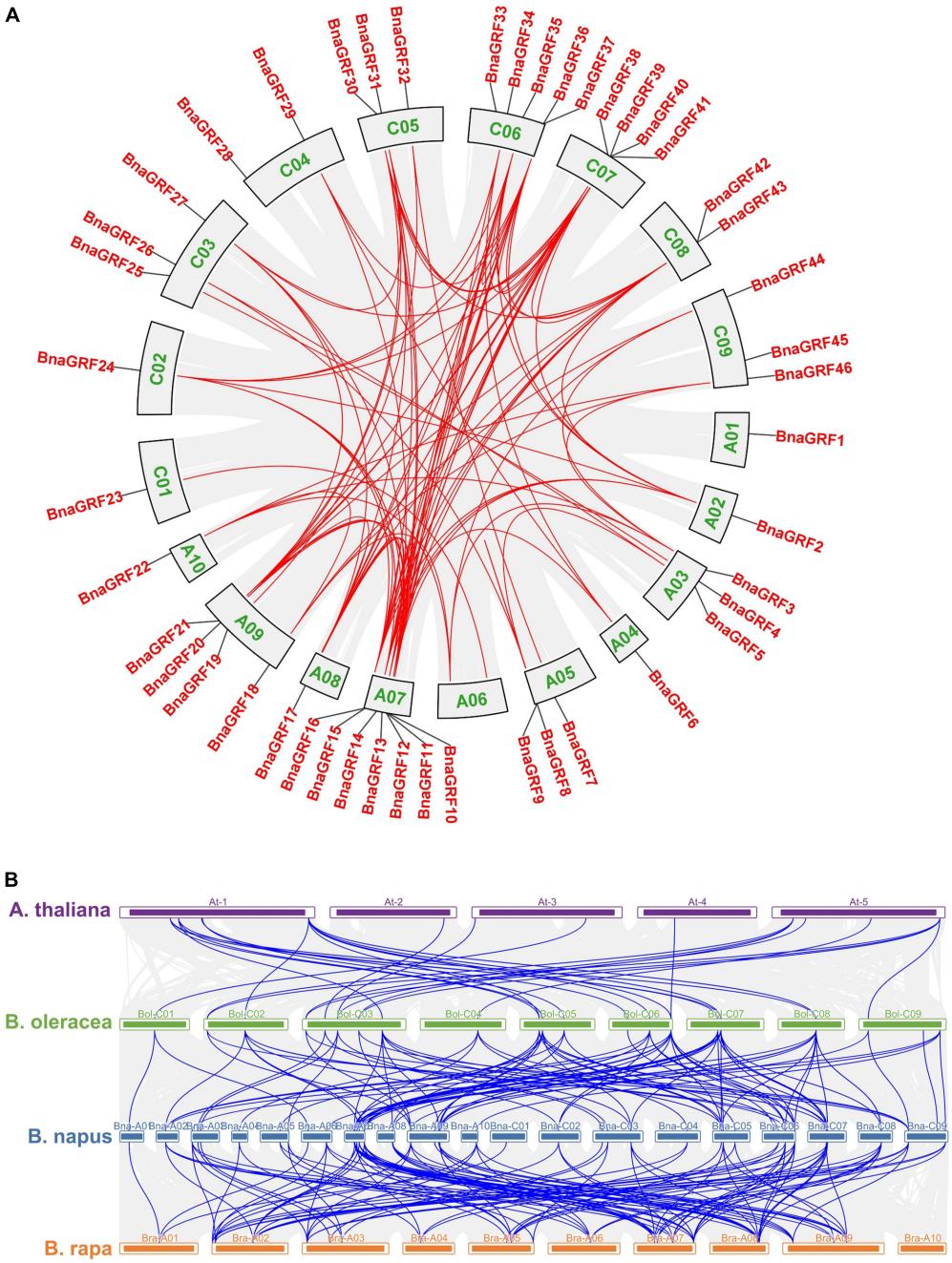

FIGURE 2
Circular illustrations of the chromosomal dispersal and inter-chromosomal associations of BnaGRFs, and synteny analysis of *14-3-3* genes in *B. rapa*, *B. oleracea*, *B. napus*, and Arabidopsis. **(A)** Analysis of syntenic relationships among BnaGRF homologs. Red lines inside the schematic view denote the duplicated pairs of BnaGRFs. **(B)** Analysis of syntenic relationships among BraGRFs, BolGRFs, BnaGRFs, and AtGRFs. Gray line represents the syntenic block in plant genomes, and blue line represents the collinear *14-3-3* gene pair.

electrophoresis and with a UV spectrophotometer. High-quality RNA was outsourced to Majorbio company (Shanghai, China) for library construction, RNA-seq, and the identification and analysis of differentially expressed genes (DEGs). The RNA-seq was performed based on Illumina platform. The raw data was filtered with SeqPrep and Sickle, and the clean data were mapped onto the *B. napus* genomes (AACC[10]) (Chalhoub et al., 2014) by using TopHat2 software. The expression profiles of DEGs between the treated and control samples were determined by

10 http://www.genoscope.cns.fr/brassicanapus/data/

edgeR (Robinson et al., 2010) program based on their relative quantities. Genes with a *P*-value $\leq$ 0.01 were recognized as significantly DEGs between the two samples. Transcript levels of *BnaGRFs* were extracted from the RNA-seq data and shown by HeatMap in TBtools. The heatmap was generated by taking Log2 values of the transcript per million fragments mapped (FPKM) generated from RNA-seq data. The bars of *BnaGRFs* on heatmap represent the expressional change after different treatments.

Results

Genome-wide identification and characterization of 14-3-3 proteins in rapeseed

The genome of *B. napus* cultivar 'ZS11' was used for the identification of rapeseed *14-3-3* genes. Based on a genome-wide investigation, a total of 46 *14-3-3* gene candidates were discovered (**Table 1**). Each gene was named *BnaGRF*, followed by a number (e.g., *BnaGRF1*, *BnaGRF2*, and *BnaGRF3*), based on its location on chromosomes A01 to C09. The details of all 46 *BnaGRFs* are summarized in **Table 1**. The BnaGRF proteins varied in length from 182 amino acids (aa; BnaGRF28) to 581 aa (BnaGRF23), with an average length of 266.23 aa, the length of 86.95% (40/46) *BnaGRFs* distribute in 200–300 aa. The MW of BnaGRFs ranged from 20.53 to 65.58 kDa. The pI was less than 7.0 for all BnaGRFs, except BnaGRF1, BnaGRF23, and BnaGRF45, whose pI was 7.01, 9.52, and 9.66, respectively. Subcellular localization prediction analysis showed that BnaGRFs localized to different subcellular compartments, including plasma membrane (12 BnaGRFs), nuclear membrane (11), chloroplast (8), nucleus (5), cytosol (4), Golgi apparatus (3), and mitochondrion (3).

To better understand the *14-3-3* family composition in the tetraploid *B. napus*, the *14-3-3* genes in its progenitor species *B. rapa* (*BraGRFs*) and *B. oleracea* (*BolGRFs*) were identified; *BolGRFs* were identified using approaches similar to those used for *BnaGRF* identification, while *BraGRFs* were identified based on the literature reported by Chandna (Chandna et al., 2016). The results showed that the *14-3-3* gene family composition was similar in the two *Brassica* species, with 21 members in *B. rapa* and 25 in *B. oleracea* (**Supplementary Table 1**). Comparative analysis indicated that the *B. napus* genome possessed the total copies of *14-3-3s* in its two progenitor species, but the A and C subgenomes possessed 22 and 24 *BnaGRFs*, respectively.

Phylogenetic and gene structure analyses of *14-3-3* genes

To determine the evolutionary relationships among *14-3-3s*, a phylogenetic tree was constructed using the NJ method, based on the full-length amino acid sequence alignment of GRFs of *B. rapa*, *B. oleracea*, *B. napus*, and *A. thaliana* (**Figure 1**). All 46 BnaGRFs clustered into two groups (ε and non-ε), with strong bootstrap support. Twenty-nine BnaGRFs clustered into the non-ε group, together with 8 AtGRFs, 15 BraGRFs, and 16 *B. oleracea* GRFs (BolGRFs), while the remaining 17 BnaGRFs members clustered into the ε group. *B. napus* inherited most copies of *14-3-3s* from its two progenitors, *B. rapa* and *B. oleracea*. Some BnaGRFs were highly homologous to BolGRFs; e.g., both BnaGRF12 and BnaGRF41. However, other BnaGRFs, such as BnaGRF22 and BnaGRF46, showed no high-level homology to GRFs in *B. rapa* and *B. oleracea*. Thus, this phylogenetic tree revealed that members of the *14-3-3* gene family in *B. napus* were not fully inherited from its diploid ancestors.

The intron-exon structure of *14-3-3s* provided potential insight into the functional diversification of BnaGRFs during evolution (**Table 1** and **Figure 2A**). Genes within the same group showed a similar number of introns and exons: 2–4 exons in the non-ε group [with 20 out of 28 genes (68.96%) containing 4 exons] and 5–7 exons in the ε group. The only exceptions were *BnaGRF23* in the non-ε group (14 exons) and *BnaGRF28* in the ε group (2 exons).

Ten conserved motifs were identified in 46 BnaGRFs and 13 AtGRFs (**Figure 2B**). The majority of BnaGRFs contained motif2, motif3, and motif4, except BnaGRF1, BnaGRF28, BnaGRF45 (which lacked motif2 and motif4), BnaGRF23 (lacked motif2), BnaGRF42 (lacked motif3), and BnaGRF46 (lacked motif4). Most BnaGRFs (40/46) contained motif1, except BnaGRF3, BnaGRF22, and BnaGRF46, all of which clustered in the non-ε group. Motif5 was found in most non-ε group members (21/29), whereas motif8 and motif9 were found in ε group members only. By contrast, AtGRFs showed a more consistent motif distribution than BnaGRFs, with all AtGRFs containing motif1, motif2, motif3, and motif4. Compared with all BnaGRFs, the non-ε group members BnaGRF1, BnaGRF3, BnaGRF22, BnaGRF23, BnaGRF45, and BnaGRF46 as well as the ε group member BnaGRF28 showed considerable differences in intron-exon structure, motif distribution, MW, and pI (**Table 1**). This variation in gene structure and motif composition among BnaGRFs suggests functional differentiation within and between the two BnaGRFs groups.

Chromosomal distribution and gene duplication of *BnaGRFs*

The 46 *BnaGRF* genes were unevenly distributed on 18 of the 19 chromosomes (**Figure 3**). In total, 22 *BnaGRFs* (15 non-ε group and 7 ε group) and 24 *BnaGRFs* (14 non-ε group and 10 ε group) were located in the A and C subgenomes, respectively. Chromosome A07 harbored the most *BnaGRF* genes (seven),

10.3389/fpls.2022.986635

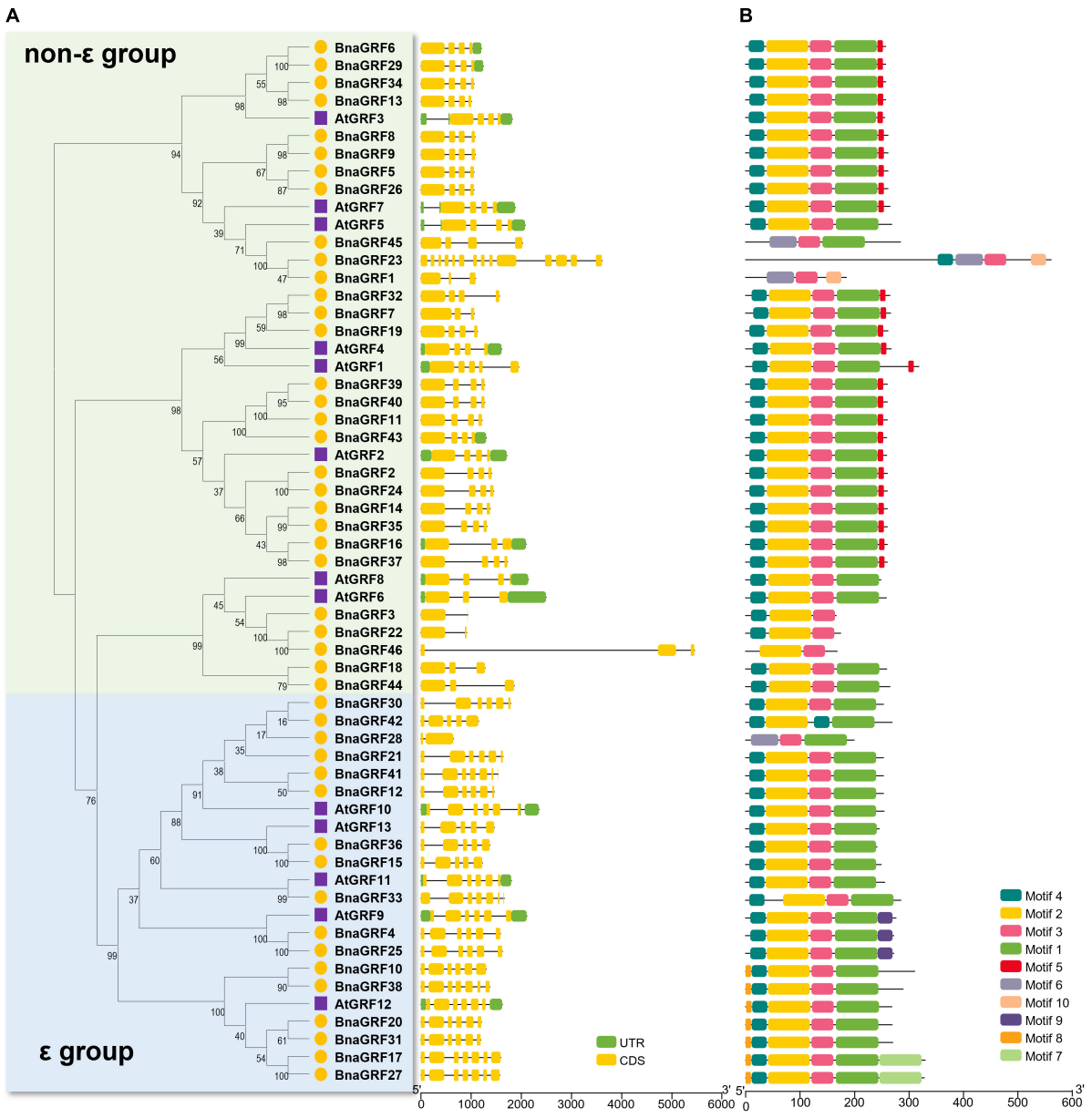

FIGURE 3
Gene structure and motif analysis of *14-3-3* family genes in *B. napus* and Arabidopsis. **(A)** Gene structure of *BnaGRFs* and *AtGRFs*. Green color indicates the untranslated regions (UTRs); yellow color represents the coding sequence (CDS) or exons; and black horizontal lines indicate the introns. **(B)** Conserved domain structures identified in *BnaGRFs* and *AtGRFs*. Boxes with different colors indicate different motifs.

while chromosomes A01, A02, A04, A08, A10, C01, and C02 contained only one *BnaGRF* gene each. No *BnaGRF* gene was located on chromosome A06.

Gene duplication reflects the expansion of the gene family. According to BLAST and MCScanX searches, gene duplication events of *BnaGRFs* were detected in *B. napus*. Briefly, all 46 *BnaGRF* genes were derived by different types of duplication events: 41 (89.13%) by whole-genome duplication (WGD) or segmental duplication; 4 by dispersed duplication; and 1 by proximal duplication. Moreover, we identified 101 paralogous gene pairs (Figure 2A and Supplementary Table 2), 24 of which originated in the A subgenome, 18 in the C subgenome, and the remaining 59 arose by duplication events between the A and C subgenomes. To estimate the selection mode of *BnaGRFs*, the Ka/Ks ratio of paralogous gene pairs was calculated. Generally, Ka/Ks $>$ 1 implies positive selection; Ka/Ks = 1 indicates neutral selection; and Ka/Ks $<$ 1 represents purifying selection. In this study, the Ka/Ks ratio of all paralogous gene pairs

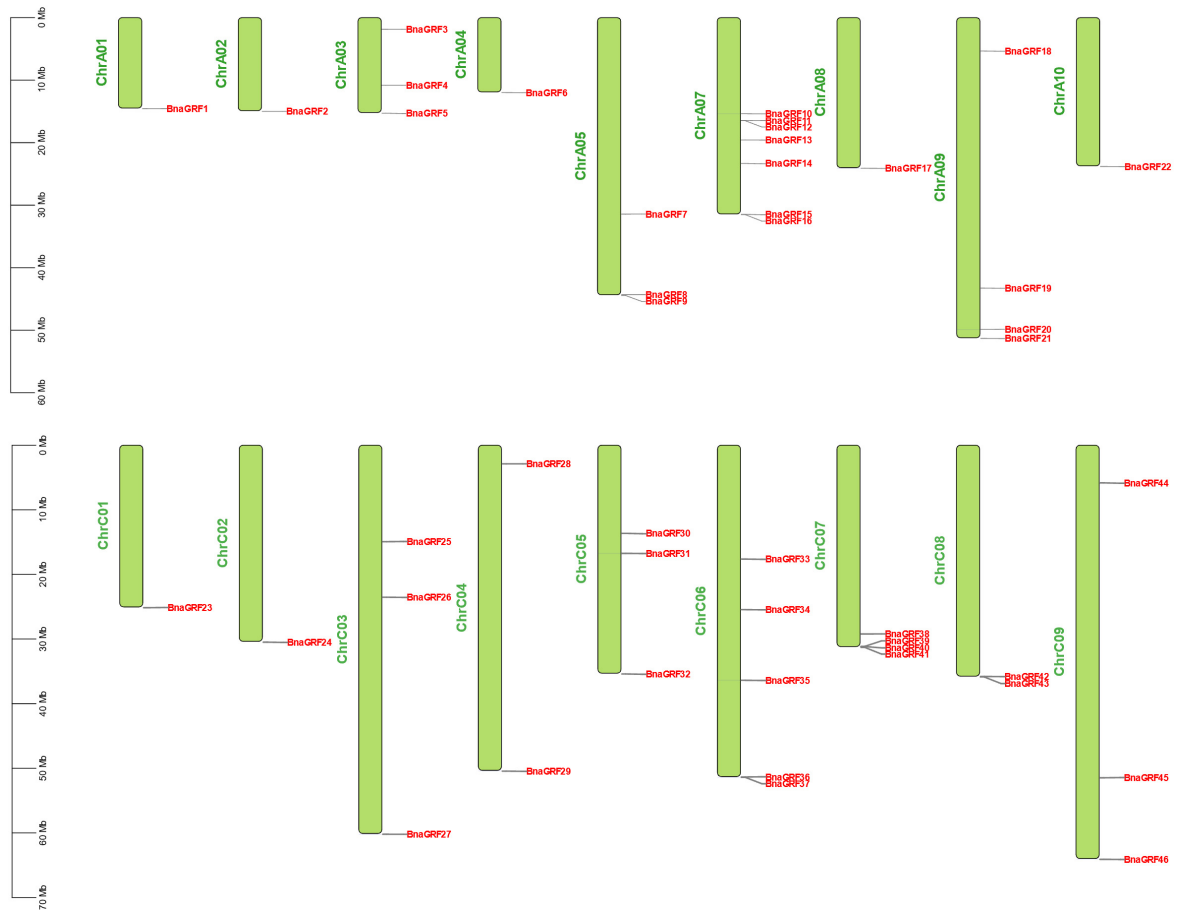

FIGURE 4
Chromosomal mapping of 46 *BnaGRFs*. The length of chromosomes is represented in Mb. The chromosome number is presented on the left side of each chromosome. *BnaGRFs* are marked in red.

(except three gene pairs for which the Ka/Ks ratio could not be calculated, because of high sequence divergence) was less than 1 (**Supplementary Table 2**), indicating that *BnaGRFs* are under purifying selection.

Prediction of *Cis*-acting elements in *BnaGRF* gene promoters

Cis-elements in promoter regions play a critical role in determining gene expression patterns. To obtain preliminary clues on how the *BnaGRF* genes respond to stress stimuli, we identified stress-related *cis*-elements in the promoters of *BnaGRF* genes (**Figure 5**). A total of 18 stress response-related *cis*-acting elements were detected in 2.0-kb sequence upstream of the ATG of each *BnaGRF* gene. These *cis*-acting elements could be divided into three classes: hormone-sensitive regulatory elements involved in biotic or abiotic stress responses, including ABA-responsive element (ABRE), indole-3-acetic acid (IAA)-responsive elements (AuxRRP-core and TGA-element), GA-responsive elements (GARE-motif, P-box, and TATC-box), JA responsive (TGACG-motif and box S), and SA-responsive element (TCA-element); MYB, MYC, and WRKY transcription factor-binding sites; and biotic or abiotic stress-responsive elements, including DRE core, LTR, G-box, ARE, TC-rich repeats, and WUN-motif. MYB-binding elements were detected in all 46 *BnaGRFs*, with a total number of 284. Other motifs identified in the majority of *BnaGRFs* included ABRE (41/46, 89.1%), MYC-binding (44/46, 95.7%), G-box (41/46, 89.1%), and ARE (43/46, 93.5%). More than half of *BnaGRFs* promoters contained methyl jasmonate (MeJA)-responsive elements [TGACG-motif (30/46, 65.2%) and TC-rich repeats (25/46, 54.3%)], WRKY-binding site (W box, 24/46, 52.2%) and low-temperature responsive (LTR) elements (24/46, 52.2%). Moreover, TGA-element (16/46, 34.8%), GARE-motif (13/46, 28.3%), TCA-element (14/46, 30.4%), DRE core (18/46, 39.1%), and WUN-motif (15/46, 32.6%) were identified in many promoters. The total number of elements in each gene varied from 14 (*BnaGRF2*) to 46 (*BnaGRF21*), and no significant difference was detected in the number or distribution

of elements between non-ε and ε groups. These findings suggest that BnaGRFs play an important role in the biotic and abiotic stress response in *B. napus*.

Expression profiling of *BnaGRF* genes in various *B. napus* tissues

To investigate the functions of *BnaGRF* genes, we analyzed their expression profiles in different tissues or organs based on the data available in the *Brassica napus* Transcriptome Information Resource (BnTIR) database[11] (Liu et al., 2021). Different *BnaGRF* genes exhibited distinct expression patterns; however, no transcriptome data were available for BnaGRF1 and BnaGRF33 (**Figure 6A**).

Most *BnaGRFs* were widely expressed in the *B. napus* plant at different developmental stages. However, some *BnaGRFs*, including *BnaGRF15*, *BnaGRF23*, *BnaGRF28*, *BnaGRF36*, *BnaGRF42*, *BnaGRF45*, and *BnaGRF46*, showed no expression in most of the tissues and organs; three of these genes belonged to the non-ε group, while four of them belonged to the ε group. *BnaGRF8* and *BnaGRF9* were highly expressed in the silique wall at 60 days after flowering (DAF), suggesting that both these genes play specific roles in silique dehiscence in *B. napus*. Additionally, *BnaGRF10*, *BnaGRF17*, *BnaGRF20*, *BnaGRF27*, and *BnaGRF38*, all of which belonged to the ε group, were expressed only in the filament and 2-DAF silique. Interestingly, many *BnaGRFs* were expressed to significantly lower levels in siliques at 2 DAF than in siliques at other developmental stages. These results suggest that *BnaGRFs* play important roles in the growth and development of *B. napus*.

Responses of *BnaGRFs* to phytohormones, abiotic stress, and *S. sclerotiorum* challenge

The expression profiles of *BnaGRFs* were analyzed in different tissues after treatment with various hormones [IAA, 1-aminocyclopropane-1-carboxylic acid (ACC), GA, ABA, trans-Zeatin (TZ), JA, and BL] and abiotic stresses (salt, drought, freezing, cold, heat, and osmotic), based on the data available in BnTIR (**Figures 6B,C**).

Heatmap analysis showed that the *BnaGRF* genes were downregulated upon most hormone treatments (**Figure 6B**), and were upregulated only in a few instances; however, six genes (*BnaGRF15*, *BnaGRF17*, *BnaGRF27*, *BnaGRF36*, *BnaGRF45*, and *BnaGRF46*) were either not expressed or expressed to very low levels in all hormone treatments. Most *BnaGRFs* were downregulated after ABA and JA treatments; the expression of a few genes either increased or did not change significantly. *BnaGRFs* showed different expression patterns in roots and leaves. For instance, *BnaGRF10* and *BnaGRF38* were down- or upregulated significantly under all of the hormone treatments in the root; however, their expression changed only at a few time points. In contrast to leaves, the expression levels of *BnaGRFs* changed more dramatically in roots. These results indicate *BnaGRFs* play important roles in the response to various stresses in the root. Members of the non-ε and ε groups showed different expression patterns. Most of the non-ε group members were downregulated upon hormone treatments, except BnaGRF23, which was upregulated by all phytohormones at some point in time. By contrast, the expression levels of ε group members, including *BnaGRF10*, *BnaGRF28*, *BnaGRF31*, and *BnaGRF38* changed more dramatically. In the root, the transcript level of *BnaGRF10* decreased by 32-fold at 6 h after the ACC treatment, while that of *BnaGRF31* decreased by 42-fold at 6 h post-ABA treatment. The ε group members were more frequently upregulated than the non-ε group members. For example, the transcript level of *BnaGRF28* was increased in the root at one or more sampling points after all hormone treatments; *BnaGRF10*, *BnaGRF31,* and *BnaGRF38* were significantly upregulated at some sampling points after treatment with IAA, ACC, GA, TZ, and BL. Additionally, paralogous gene pairs, such as *BnaGRF2*/*BnaGRF24*, *BnaGRF18*/*BnaGRF44*, and *BnaGRF4*/*BnaGRF25*, showed similar expression patterns.

Under abiotic stress conditions, most of the *BnaGRFs* showed relatively low expression levels, particularly in roots. All BnaGRFs were downregulated in roots under salt and drought stress, except *BnaGRF10*, *BnaGRF20*, *BnaGRF28*, and *BnaGRF42*, which were upregulated. Members of both non-ε and ε groups showed similar expression patterns under abiotic stresses ass under hormone treatments. Compared with the ε group members, the non-ε group members showed a smooth transition in expression levels from pre-treatment to post-treatment conditions, except *BnaGRF23*, which was downregulated by 31.00-fold in leaves at 12 h after under the cold stress treatment; *BnaGRF38*, which was significantly upregulated by 47-fold in roots at 1 h after the heat treatment; and *BnaGRF31*, which was upregulated by 43-fold and downregulated by 32-fold at 12 h after cold treatment and 6 h after osmotic stress treatment, respectively. These results indicate that *BnaGRFs* perform biologically relevant functions during plant development and are potentially involved in abiotic stress responses.

Next, to investigate the role of *BnaGRFs* in the disease resistance response, the expression levels of these genes were determined by RNA-seq analysis of leaves treated with SA, H_2O_2, and OA or inoculated with *S. sclerotiorum*. The DEGs were identified after treatments at different time points (**Supplementary Figure 1**). SA and H_2O_2 are important signaling molecules, and OA is a main pathogenic factor secreted by *S. sclerotiorum*. Our results showed that no

11 http://yanglab.hzau.edu.cn/BnTIR/eFP

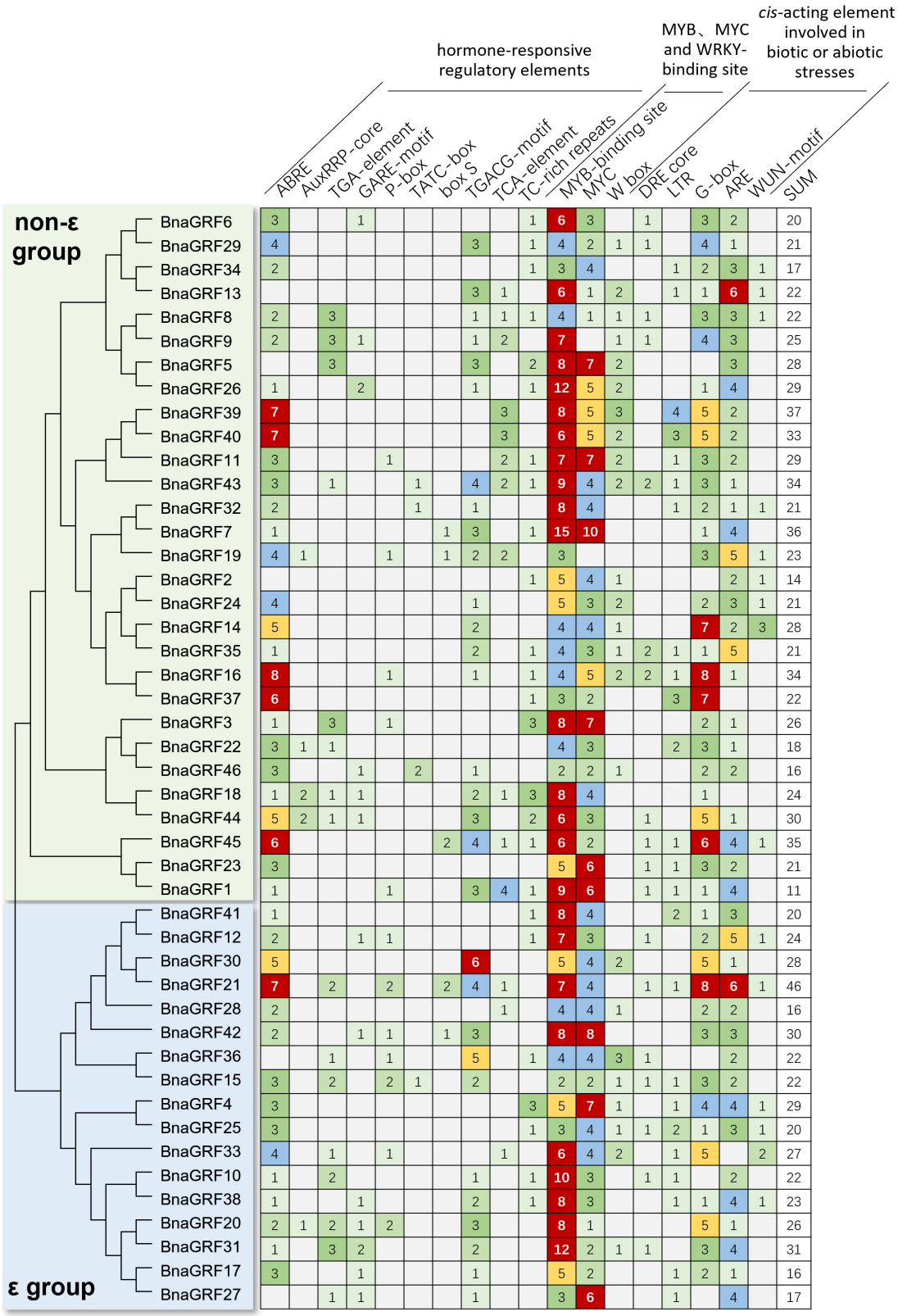

FIGURE 5
Number of hormone- and stress-responsive *cis*-elements in the promoters of the *BnaGRFs*.

10.3389/fpls.2022.986635

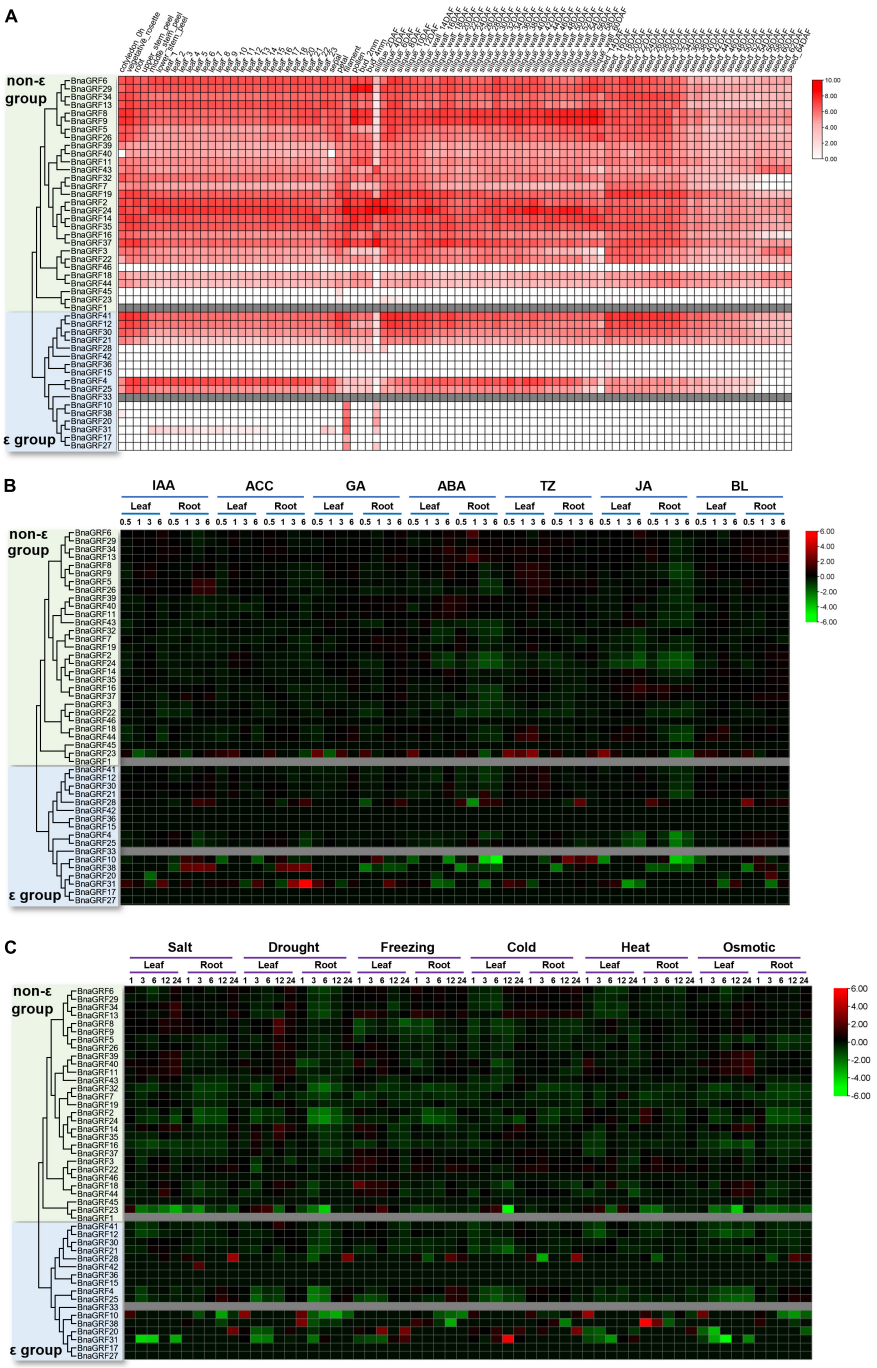

FIGURE 6

Expression analysis of *BnaGRFs* in various tissues and under various hormone and abiotic stress treatments. **(A)** Expression profiling in different tissues and organs. The scale bar represents the Log2 normalized expression. In the expression bar, white color indicates no expression, and gray color indicates the absence of data in the BnTIR database (*BnaGRF1* and *BnaGRF33*). **(B)** Expression profiles of *BnaGRFs* after treatment with various hormones, including indole-3-acetic acid (IAA), 1-aminocyclopropane-1-carboxylic acid (ACC), gibberellin (GA), ABA, trans-Zeatin (TZ), jasmonate (JA), and brassinolide (BL). The heatmap was constructed by taking Log2 values of the transcripts per kilobase of exon model per million mapped reads (TPM) generated from RNA-seq data. The bars of *BnaGRFs* on heatmap represent the expression change folds after treatments. **(C)** Expression profiles of *BnaGRFs* under abiotic stresses, including salt (200 mM NaCl), drought, freezing (−4°C), cold (4°C), heat (38°C), and osmotic stress (300 mM mannitol). In panels **(B,C)**, red and green colors indicate up- and downregulated *BnaGRFs*, respectively, and gray color indicates unavailability of data in the database (*BnaGRF1* and *BnaGRF33*). The heatmap was constructed by taking Log2 values of the transcripts per kilobase of exon model per million mapped reads (TPM) generated from RNA-seq data. The bars of *BnaGRFs* on heatmap represent the expression change folds after treatments.

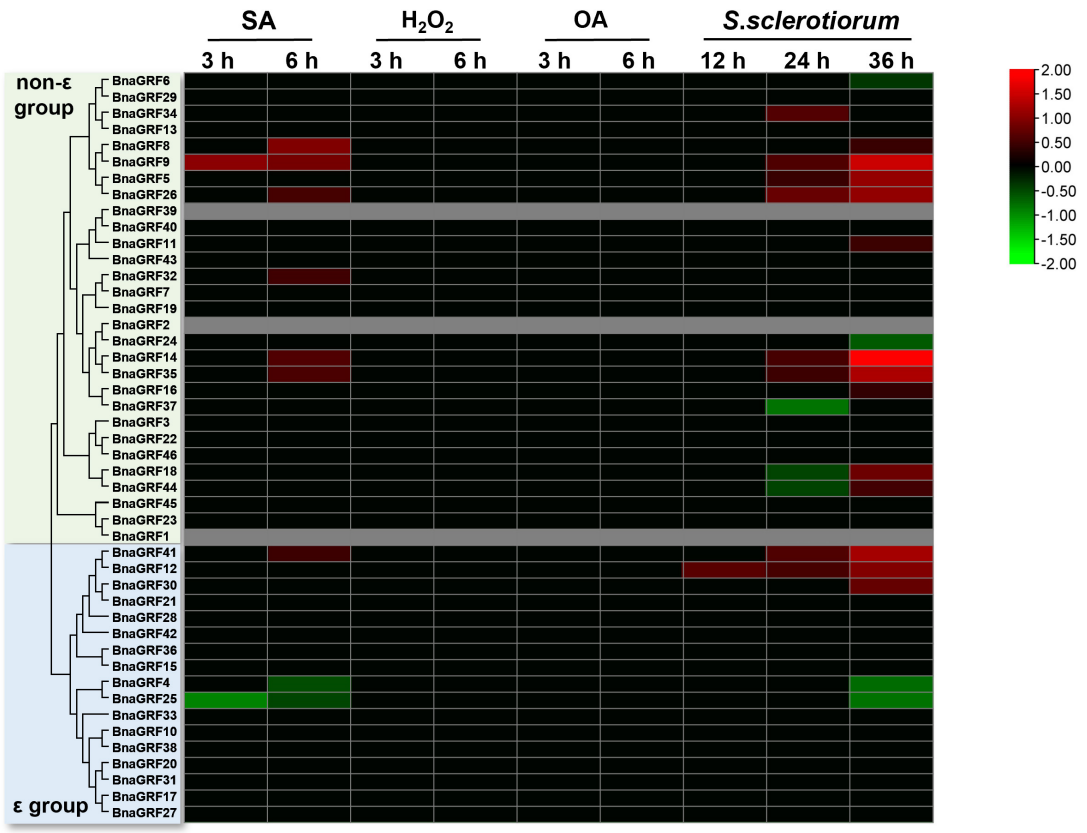

FIGURE 7
Relative expression levels of *BnaGRFs* under salicylic acid (SA), hydrogen peroxide (H_2O_2), and oxalic acid (OA) treatments and *Sclerotinia sclerotiorum* inoculation. No significant change in expression ($p > 0.01$) is shown as 0. Red and green colors indicate significantly up- and downregulated genes, respectively, and gray color represents no expression data. The heatmap was constructed by taking Log2 values of the transcript per million fragments mapped (FPKM) generated from RNA-seq data. The bars of *BnaGRFs* on heatmap represent the expression change folds after treatments.

BnaGRFs were induced or repressed by H_2O_2 and OA (**Figure 7**). In the SA treatment, seven *BnaGRF* genes (*BnaGRF8*, *BnaGRF9*, *BnaGRF26*, *BnaGRF32*, *BnaGRF35*, *BnaGRF41*, and *BnaGRF14*) were upregulated, and two *BnaGRFs* (*BnaGRF4* and *BnaGRF25*) were downregulated significantly. All of these genes were induced or depressed at a late time point (6 h post-treatment). Interestingly, all of these nine *BnaGRFs* showed the same expression patterns after *S. sclerotiorum* inoculation, except *BnaGFR32*, which was upregulated by SA but showed no significant expression variation after *S. sclerotiorum* inoculation. Nineteen *BnaGRFs* were differentially expressed by *S. sclerotiorum* inoculation at different time points. Among these 19 genes, 12 *BnaGRFs* and 5 *BnaGRFs* were up- and downregulated, respectively, and 2 *BnaGRFs* (*BnaGRF18* and *BnaGRF44*) were downregulated at 24 h post-inoculation (hpi) but upregulated at 36 hpi.

Overall, the expression profiles of *BnaGRFs* in response to phytohormones, abiotic stresses, and *S. sclerotiorum* inoculation suggest that these genes perform diverse or conserved biological functions during plant–environment and plant–microbe interactions.

Discussion

The 14-3-3 family has been found in all eukaryotes screened to date, and usually consists of multiple proteins and protein isoforms (DeLille et al., 2001). The 14-3-3 proteins exist as homo- and heterodimers in cells (Jones et al., 1995), and function as phosphor-binding regulators in signal transduction pathways by interacting with phosphorylated targets (Camoni et al., 2018). Because 14-3-3s exist as multiple isoforms, these proteins participate in various physiological processes. To the best of our knowledge, the largest *14-3-3* gene family reported to date in plants was identified in both banana and cotton, with each containing 25 *14-3-3s* (Sun et al., 2011; Li et al., 2016). However, in this research, we identified 46 *BnaGRF* genes in the *B. napus* genome; this number is almost twice that in banana and cotton. The lengths of BnaGRF isoforms varied

from 182 to 581 aa, and their pI ranged from 4.61 to 5.61, except BnaGRF1 (9.52), BnaGRF15 (6.65), BnaGRF23 (7.01) and BnaGRF45 (9.66) (**Table 1**). Overall, the data on gene structure, amino acid number, motif type and number, and pI indicated that BnaGRF1, BnaGRF23, and BnaGRF45 are much different from the standard 14-3-3 isoforms, and there are no orthologous genes in Arabidopsis (**Figure 1**), indicating that BnaGRFs have undergone neofunctionalization in *B. napus*.

Phylogenetic analysis showed that *BnaGRFs* could be classified into two groups (ε and non-ε) (**Figure 1**), consistent with the 14-3-3 family in other plant species (Ferl et al., 2002). The ε and non-ε group members showed considerable differences in intron-exon structure and motif distribution. For instance, *BnaGRFs* in the ε group contained 5–7 exons, whereas those in the non-ε group contained 2–4 exons, except *BnaGRF28* and *BnaGRF23*, which contained 2 and 14 exons, respectively. The expression patterns of *BnaGRF28* and *BnaGRF23* under hormone treatments differed from those of other *BnaGRFs* (**Figure 6**). Similar results have been reported in other plant species (Cheng et al., 2018; Wang et al., 2019; Shao et al., 2021), which imply evolutionary conservation within the 14-3-3 family.

Tandem duplication, segmental duplication, and WGD events were identified to evaluate the expansion of the *BnaGRF* gene family. Our results showed that 41 *BnaGRFs* were generated by WGD or segmental duplication; four *BnaGRFs* (*BnaGRF28*, *BnaGRF23*, *BnaGRF28,* and *BnaGRF23*) were a result of dispersed duplication; *BnaGRF40*, which is separated from *BnaGRF39* by only a few genes, originated by proximal duplication; and no *BnaGRFs* were caused by tandemly duplication (**Table 1** and **Figure 4**). These results indicate that WGD and segmental duplications were the key factors responsible for the expansion of the *14-3-3* gene family, which is consistent with previous studies (Xie et al., 2022).

BnaGRF genes in the A and C subgenomes of *B. napus* are closely related to *14-3-3* genes in *B. rapa* and *B. oleracea*, respectively. The number of *14-3-3* genes in *B. napus* is exactly equal to the sum of *14-3-3* genes in *B. rapa* and *B. oleracea*; however, the *14-3-3* genes in *B. napus* do not show a one-to-one correspondence with those in *B. rapa* and *B. oleracea*. We identified 22 and 24 *BnaGRFs* in the A and C subgenomes, respectively, of *B. napus*, and 21 *BraGRFs* and 25 *BolGRFs* in *B. rapa* and *B. oleracea* genomes, respectively. *BnaGRF8* (BnaA05G0489800ZS) is located on chromosome A05 and was identified as an ortholog of Bol01155s020; however, no orthologs of Bol3g099210 and Bol3g005620 were identified in the *B. napus* genome, even though both *BolGRFs* are highly homologous to *BnaGRF44* (BnaC09G0088500ZS). These results suggest that gene loss events likely occurred in the *14-3-3* gene family in *B. napus* after hybridization.

Cis-regulatory elements play an important role in the regulation of plant gene expression. The *cis*-acting element and expression pattern analysis showed that 14-3-3s were involved in hormone and abiotic stress responses in plants (Lyu et al., 2021; Xia et al., 2022; Xie et al., 2022). In this study, we analyzed the stress response-related *cis*-acting elements in the promoters of *BnaGRFs*. The 25 *cis*-regulatory elements were found in the majority of promoters (**Figure 5**), which implies that the corresponding genes are involved in the stress response.

Expression patterns of *BnaGRFs* under multiple hormone and abiotic stress treatments were also investigated in this study. Yang Lab developed the BnTIR database, presenting a highly comprehensive temporal-resolution analysis of the transcriptomes of nine different 'ZS11' tissues (cotyledon, root, stem peel, leaf, bud, flower, silique, silique wall, and seed) at three distinct developmental stages, and the transcriptomes of roots and leaves under multi-hormone and abiotic stress treatments (Liu et al., 2021). Spatial and temporal expression profiles showed that most of the *BnaGRFs* were expressed in the vast majority of tissues, except *BnaGRF15*, *BnaGRF23*, *BnaGRF28*, *BnaGRF36*, *BnaGRF42*, *BnaGRF45*, and *BnaGRF46*, which showed no expression in almost all tissues or organs. These results suggest that *BnaGRFs* play important roles in the regulation of plant growth and development in *B. napus*. Interestingly, the expression of *BnaGRF10*, *BnaGRF17*, *BnaGRF20*, *BnaGRF27*, and *BnaGRF38* was only detected in filament and silique sampled at 2 DAF; these genes were clustered into the ε group, which indicates that these genes function in floral organ development.

Phytohormones play a central role in the defense against environmental stress. Expression analysis showed most *BnaGRFs* responded to hormone and abiotic stress treatments, although the response was stronger to abiotic stresses than to hormones (**Figures 6B,C**). Compared with other hormones, ABA and JA treatment had a greater influence on the expression level of *BnaGRFs*. Because ABA and JA are closely related to abiotic and biotic stresses, other results hint at the involvement of *BnaGRFs* in the response to abiotic and biotic stresses. Almost all *BnaGRFs* responded to salt, drought, freezing, cold, heat, and osmotic stresses. In most cases, *BnaGRFs* were downregulated by these abiotic stresses. Expression levels of *BnaGRFs* differed significantly between the ε and non-ε groups; for instance, a higher percentage of *BnaGRFs* in the ε group was unexpressed or showed low-level expression in response to all abiotic stresses (5/17), whereas only two *BnaGRFs* in the non-ε group (*BnaGRF45* and *BnaGRF46*) showed this expression pattern. Compared with the non-ε group *BnaGRFs*, the ε group members showed a more dramatic increase or decrease in transcript levels. These results suggest that *BnaGRFs*, especially the ε group members, are extensively involved in the stress response in *B. napus*, and this involvement most likely occurs through various hormone signaling pathways.

Sclerotinia stem rot, caused by *S. sclerotiorum*, is the most serious disease affecting the yield of rapeseed, an agriculturally and economically important crop (Boland and Hall, 1994; Liu et al., 2018). JA, SA, and H_2O_2 signaling pathways are thought

to be central components of the mechanisms underlying the active defense response (Hu et al., 2021; Xu et al., 2021). OA is a toxic compound secreted by *S. sclerotiorum*, which plays an important role in the infection process (Magro et al., 1984; Liang et al., 2015). In the current study, we performed SA, H_2O_2, and OA treatments and *S. sclerotiorum* inoculation to evaluate changes in the expression levels of *BnaGRFs*. None of the *BnaGRFs* showed a response to H_2O_2 and OA treatments; however, 9 (19.57%) and 19 (41.30%) *BnaGRFs* showed differential expression upon the SA treatment and *S. sclerotiorum* inoculation, respectively (**Figure 7**). These results indicated that *BnaGRF* family may not participate in H_2O_2 and OA metabolic and accumulation processes in *B. napus*. In addition, changes in the expression levels of *BnaGRFs* were also detected upon the JA treatment (**Figure 6B**). The *cis*-element analysis of these gene promoters revealed that all of the 19 *BnaGRFs* promoters have MYB-binding sites. In addition, 18 of them show MYC and G-box element and 17 have ABRE and ARE elements. These elements may be involved in the response to *S. sclerotiorum*. Among the 19 *BnaGRFs* which response to *S. sclerotiorum* inoculation, 14 (73.69%) were clustered into the non-ε group, this is almost half of the non-ε group members. This data implied that the members of non-ε group paly more important roles in *S. sclerotiorum* resistance response. Together, these results suggest that *BnaGRFs* might participate in the response to *S. sclerotiorum via* the JA and SA signaling pathways. It has been reported that SA and JA signaling pathways are involved in the plant resistance to *S. sclerotiorum* in *B. napus*, whereas the specific regulatory process remains unknown (Wu et al., 2016). A comprehensive study on the function of GRFs and their interacting proteins will help to elucidate the response processes, and these GRFs may be further applied as genetic resources for breeding S. sclerotiorum-resistant plants in *B. napus*.

Conclusion

Overall, this study presents a comprehensive analysis of the *BnaGRF* gene family in rapeseed and provides evidence for their possible roles in the response to *S. sclerotiorum* infection. In total, 46 *BnaGRFs* were identified in the *B. napus* genome, and classified into the ε and non-ε groups. Analysis of *cis*-acting regulatory elements in *BnaGRF* promoters and evaluation of *BnaGRF* expression patterns in various tissues and under abiotic stresses revealed that these genes play important roles in plant development and stress responses. RNA-seq data showed that 41.30% of the *BnaGRFs* are involved in the response to *S. sclerotiorum* infection.

In summary, these findings provide a detailed characterization of *BnaGRFs* in *B. napus*, and could serve as a platform for the functional analysis and genetic improvement of agronomic traits in *B. napus*.

Data availability statement

The datasets presented in this study can be found in online repositories. The names of the repository/repositories and accession number(s) can be found in the article/**Supplementary material**.

Author contributions

QS and YPW designed the research. QS, YX, PL, YL, and YW performed the experiments. QS, YX, PL, and YL analyzed the data. QS, YX, and YPW wrote and revised the manuscript. All authors read and approved the current version of the manuscript.

Funding

This research was funded by the National Natural Science Foundation of China (U20A2028 and 31901504), the Natural Science Foundation of Jiangsu Province (BK20190894 and BE2022340), and the Priority Academic Program Development of Jiangsu Higher Education Institutions, Project of Special Funding for Crop Science Discipline Development (yzuxk202006).

Conflict of interest

The authors declare that the research was conducted in the absence of any commercial or financial relationships that could be construed as a potential conflict of interest.

Publisher's note

Supplementary material

The Supplementary Material for this article can be found online at: https://www.frontiersin.org/articles/10.3389/fpls.2022.986635/full#supplementary-material

References

Bailey, T. L., Johnson, J., Grant, C. E., and Noble, W. S. (2015). The MEME Suite. *Nucleic Acids Res.* 43, W39–W49. doi: 10.1093/nar/gkv416

Boland, G. J., and Hall, R. (1994). Index of plant hosts of *Sclerotinia sclerotiorum*. *Can. J. Plant Pathol.* 16, 93–108. doi: 10.1080/07060669409500766

Camoni, L., Visconti, S., Aducci, P., and Marra, M. (2018). 14-3-3 proteins in plant hormone signaling: doing several things at once. *Front. Plant Sci.* 9:297. doi: 10.3389/fpls.2018.00297

Catala, R., Lopez-Cobollo, R., Mar Castellano, M., Angosto, T., Alonso, J. M., Ecker, J. R., et al. (2014). The Arabidopsis 14-3-3 protein RARE COLD INDUCIBLE 1A links low-temperature response and ethylene biosynthesis to regulate freezing tolerance and cold acclimation. *Plant Cell* 26, 3326–3342. doi: 10.1105/tpc.114.127605

Chalhoub, B., Denoeud, F., Liu, S., Parkin, I. A. P., Tang, H., Wang, X., et al. (2014). Plant genetics. Early allopolyploid evolution in the post-Neolithic *Brassica napus* oilseed genome. *Science* 345, 950–953. doi: 10.1126/science.1253435

Chandna, R., Augustine, R., Kanchupati, P., Kumar, R., Kumar, P., Arya, G. C., et al. (2016). Class-specific evolution and transcriptional differentiation of 14-3-3 family members in mesohexaploid *Brassica rapa*. *Front. Plant. Sci.* 7:12. doi: 10.3389/fpls.2016.00012

Chang, I. F., Curran, A., Woolsey, R., Quilici, D., Cushman, J. C., Mittler, R., et al. (2009). Proteomic profiling of tandem affinity purified 14-3-3 protein complexes in *Arabidopsis thaliana*. *Proteomics* 9, 2967–2985. doi: 10.1002/pmic.200800445

Chang, L., Tong, Z., Peng, C., Wang, D., Kong, H., Yang, Q., et al. (2020). Genome-wide analysis and phosphorylation sites identification of the 14-3-3 gene family and functional characterization of MeGRF3 in cassava. *Physiol. Plant* 169, 244–257. doi: 10.1111/ppl.13070

Chen, C., Chen, H., Zhang, Y., Thomas, H. R., Frank, M. H., He, Y., et al. (2020). TBtools: An integrative toolkit developed for interactive analyses of big biological data. *Mol. Plant* 13, 1194–1202. doi: 10.1016/j.molp.2020.06.009

Chen, F., Li, Q., Sun, L., and He, Z. (2006). The rice 14-3-3 gene family and its involvement in responses to biotic and abiotic stress. *DNA Res.* 13, 53–63. doi: 10.1093/dnares/dsl001

Cheng, C., Wang, Y., Chai, F., Li, S., Xin, H., and Liang, Z. (2018). Genome-wide identification and characterization of the 14-3-3 family in Vitis vinifera L. during berry development and cold- and heat-stress response. *BMC Genomics* 19:579. doi: 10.1186/s12864-018-4955-8

DeLille, J. M., Sehnke, P. C., and Ferl, R. J. (2001). The Arabidopsis 14-3-3 family of signaling regulators. *Plant Physiol.* 126, 35–38. doi: 10.1104/pp.126.1.35

Ferl, R. J., Manak, M. S., and Reyes, M. F. (2002). The 14-3-3s. *Genome Biol.* 3:3010. doi: 10.1186/gb-2002-3-7-reviews3010

Finn, R. D., Clements, J., and Eddy, S. R. (2011). HMMER web server: interactive sequence similarity searching. *Nucleic Acids Res.* 39, W29–W37. doi: 10.1093/nar/gkr367

Holtman, W. L., Roberts, M. R., Oppedijk, B. J., Testerink, C., Van Zeijl, M. J., and Wang, M. (2000). 14-3-3 proteins interact with a 13-lipoxygenase, but not with a 9-lipoxygenase. *FEBS Lett.* 474, 48–52. doi: 10.1016/s0014-5793(00)01575-1

Hu, H., Tang, Y., Wu, J., Chen, F., Yang, Y., Pan, X., et al. (2021). *Brassica napus* mediator subunit16 induces BnMED25- and BnWRKY33-activated defense signaling to confer *Sclerotinia sclerotiorum* resistance. *Front. Plant Sci.* 12:663536. doi: 10.3389/fpls.2021.663536

Ito, T., Nakata, M., Fukazawa, J., Ishida, S., and Takahashi, Y. (2014). Scaffold function of Ca2+-dependent protein kinase: tobacco Ca2+-DEPENDENT PROTEIN KINASE1 transfers 14-3-3 to the substrate REPRESSION OF SHOOT GROWTH after phosphorylation. *Plant Physiol.* 165, 1737–1750. doi: 10.1104/pp.114.236448

Jaspert, N., Throm, C., and Oecking, C. (2011). Arabidopsis 14-3-3 proteins: Fascinating and less fascinating aspects. *Front. Plant Sci.* 2:96. doi: 10.3389/fpls.2011.00096

Jones, D. H., Ley, S., and Aitken, A. (1995). Isoforms of 14-3-3 protein can form homo- and heterodimers in vivo and in vitro: Implications for function as adapter proteins. *FEBS Lett.* 368, 55–58. doi: 10.1016/0014-5793(95)00598-4

Kaneko-Suzuki, M., Kurihara-Ishikawa, R., Okushita-Terakawa, C., Kojima, C., Nagano-Fujiwara, M., Ohki, I., et al. (2018). TFL1-Like proteins in rice antagonize rice FT-Like protein in inflorescence development by competition for complex formation with 14-3-3 and FD. *Plant Cell Physiol.* 59, 458–468. doi: 10.1093/pcp/pcy021

Konagaya, K.-I., Matsushita, Y., Kasahara, M., and Nyunoya, H. (2004). Members of 14-3-3 protein isoforms interacting with the resistance gene product N and the elicitor of Tobacco mosaic virus. *J. Gen. Plant Pathol.* 70, 221–231. doi: 10.1007/s10327-003-0113-4

Li, M., Ren, L., Xu, B., Yang, X., Xia, Q., He, P., et al. (2016). Genome-wide identification, phylogeny, and expression analyses of the 14-3-3 family reveal their involvement in the development, ripening, and abiotic stress response in banana. *Front. Plant Sci.* 7:1442. doi: 10.3389/fpls.2016.01442

Liang, X., Liberti, D., Li, M., Kim, Y. T., Hutchens, A., Wilson, R., et al. (2015). Oxaloacetate acetylhydrolase gene mutants of *Sclerotinia sclerotiorum* do not accumulate oxalic acid, but do produce limited lesions on host plants. *Mol. Plant Pathol.* 16, 559–571. doi: 10.1111/mpp.12211

Liu, D., Yu, L., Wei, L., Yu, P., Wang, J., Zhao, H., et al. (2021). BnTIR: An online transcriptome platform for exploring RNA-seq libraries for oil crop *Brassica napus*. *Plant Biotechnol. J.* 19, 1895–1897. doi: 10.1111/pbi.13665

Liu, F., Li, X. X., Wang, M. R., Wen, J., Yi, B., Shen, J. X., et al. (2018). Interactions of WRKY15 and WRKY33 transcription factors and their roles in the resistance of oilseed rape to *Sclerotinia infection*. *Plant Biotechnol. J.* 16, 911–925. doi: 10.1111/pbi.12838

Lyu, S., Chen, G., Pan, D., Chen, J., and She, W. (2021). Molecular analysis of 14-3-3 genes in *Citrus sinensis* and their responses to different stresses. *Int. J. Mol. Sci.* 22:568. doi: 10.3390/ijms22020568

Magro, P., Marciano, P., and Di Lenna, P. (1984). Oxalic acid production and its role in pathogenesis of *Sclerotinia sclerotiorum*. *FEMS Microbiol. Lett.* 24, 9–12.

Mayfield, J. D., Folta, K. M., Paul, A. L., and Ferl, R. J. (2007). The 14-3-3 Proteins mu and upsilon influence transition to flowering and early phytochrome response. *Plant Physiol.* 145, 1692–1702. doi: 10.1104/pp.107.108654

Mayfield, J. D., Paul, A. L., and Ferl, R. J. (2012). The 14-3-3 proteins of Arabidopsis regulate root growth and chloroplast development as components of the photosensory system. *J. Exp. Bot.* 63, 3061–3070. doi: 10.1093/jxb/ers022

Nakamura, T., Yamada, K. D., Tomii, K., and Katoh, K. (2018). Parallelization of MAFFT for large-scale multiple sequence alignments. *Bioinformatics* 34, 2490–2492. doi: 10.1093/bioinformatics/bty121

Pi, B., Pan, J., Xiao, M., Hu, X., Zhang, L., Chen, M., et al. (2021). Systematic analysis of CCCH zinc finger family in Brassica napus showed that BnRR-TZFs are involved in stress resistance. *BMC Plant Biol.* 21:555. doi: 10.1186/s12870-021-03340-8

Qin, C., Cheng, L., Shen, J., Zhang, Y., Cao, H., Lu, D., et al. (2016). Genome-wide identification and expression analysis of the 14-3-3 family genes in Medicago truncatula. *Front. Plant Sci.* 7:320. doi: 10.3389/fpls.2016.00320

Rahman, H., Xu, Y. P., Zhang, X. R., and Cai, X. Z. (2016). Brassica napus genome possesses extraordinary iigh number of CAMTA genes and CAMTA3 contributes to PAMP triggered immunity and resistance to *Sclerotinia sclerotiorum*. *Front. Plant Sci.* 7:581. doi: 10.3389/fpls.2016.00581

Robinson, M. D., Mccarthy, D. J., and Smyth, G. K. (2010). edgeR: A Bioconductor package for differential expression analysis of digital gene expression data. *Bioinformatics* 26, 139–140. doi: 10.1093/bioinformatics/btp616

Rosenquist, M., Alsterfjord, M., Larsson, C., and Sommarin, M. (2001). Data mining the Arabidopsis genome reveals fifteen 14-3-3 genes. expression is demonstrated for two out of five novel genes. *Plant Physiol.* 127, 142–149. doi: 10.1104/pp.127.1.142

Ryu, H., Cho, H., Kim, K., and Hwang, I. (2010). Phosphorylation dependent nucleocytoplasmic shuttling of BES1 is a key regulatory event in brassinosteroid signaling. *Mol. Cells* 29, 283–290. doi: 10.1007/s10059-010-0035-x

Schoonheim, P. J., Costa Pereira, D. D., and De Boer, A. H. (2009). Dual role for 14-3-3 proteins and ABF transcription factors in gibberellic acid and abscisic acid signalling in barley *(Hordeum vulgare)* aleurone cells. *Plant Cell Environ.* 32, 439–447. doi: 10.1111/j.1365-3040.2009.01932.x

Schoonheim, P. J., Sinnige, M. P., Casaretto, J. A., Veiga, H., Bunney, T. D., Quatrano, R. S., et al. (2007). 14-3-3 adaptor proteins are intermediates in ABA signal transduction during barley seed germination. *Plant J.* 49, 289–301. doi: 10.1111/j.1365-313X.2006.02955.x

Shao, W., Chen, W., Zhu, X., Zhou, X., Jin, Y., Zhan, C., et al. (2021). Genome-wide identification and characterization of wheat 14-3-3 genes unravels the role of TaGRF6-A in salt stress tolerance by binding MYB transcription factor. *Int. J. Mol. Sci.* 22, 1904. doi: 10.3390/ijms22041904

Song, J. M., Guan, Z., Hu, J., Guo, C., Yang, Z., Wang, S., et al. (2020). Eight high-quality genomes reveal pan-genome architecture and ecotype differentiation of Brassica napus. *Nat. Plants* 6, 34–45. doi: 10.1038/s41477-019-0577-7

Sun, G., Xie, F., and Zhang, B. (2011). Transcriptome-wide identification and stress properties of the 14-3-3 gene family in cotton (*Gossypium hirsutum* L.). *Funct. Integr. Genomics* 11, 627–636. doi: 10.1007/s10142-011-0242-3

Sun, X., Luo, X., Sun, M., Chen, C., Ding, X., Wang, X., et al. (2014). A Glycine soja 14-3-3 protein GsGF14o participates in stomatal and root hair development and drought tolerance in *Arabidopsis thaliana*. *Plant Cell Physiol.* 55, 99–118. doi: 10.1093/pcp/pct161

Takahashi, K., Hayashi, K., and Kinoshita, T. (2012). Auxin activates the plasma membrane H+-ATPase by phosphorylation during hypocotyl elongation in Arabidopsis. *Plant Physiol.* 159, 632–641. doi: 10.1104/pp.112.196428

Taoka, K., Ohki, I., Tsuji, H., Furuita, K., Hayashi, K., Yanase, T., et al. (2011). 14-3-3 proteins act as intracellular receptors for rice Hd3a florigen. *Nature* 476, 332–335. doi: 10.1038/nature10272

Tian, F., Wang, T., Xie, Y., Zhang, J., and Hu, J. (2015). Genome-wide identification, classification, and expression analysis of 14-3-3 gene family in Populus. *PLoS One* 10:e0123225. doi: 10.1371/journal.pone.0123225

Wang, D., Zhang, Y., Zhang, Z., Zhu, J., and Yu, J. (2010). KaKs_Calculator 2.0: A toolkit incorporating Gamma-Series methods and sliding window strategies. *Genom Proteom. Bioinform.* 8, 77–80. doi: 10.1016/s1672-0229(10)60008-3

Wang, H., Yang, C., Zhang, C., Wang, N., Lu, D., Wang, J., et al. (2011). Dual role of BKI1 and 14-3-3 s in brassinosteroid signaling to link receptor with transcription factors. *Dev. Cell* 21, 825–834. doi: 10.1016/j.devcel.2011.08.018

Wang, Y., Ling, L., Jiang, Z., Tan, W., Liu, Z., Wu, L., et al. (2019). Genome-wide identification and expression analysis of the 14-3-3 gene family in soybean (*Glycine max*). *PeerJ* 7:e7950. doi: 10.7717/peerj.7950

Wu, J., Cai, G. Q., Tu, J. Y., Li, L. X., Liu, S., Luo, X. P., et al. (2013). Identification of QTLs for resistance to sclerotinia stem rot and BnaC.IGMT5.a as a candidate gene of the major resistant QTL SRC6 in Brassica napus. *PLoS One* 8:e67740. doi: 10.1371/journal.pone.0067740

Wu, J., Zhao, Q., Yang, Q., Liu, H., Li, Q., Yi, X., et al. (2016). Comparative transcriptomic analysis uncovers the complex genetic network for resistance to *Sclerotinia sclerotiorum* in *Brassica napus*. *Sci. Rep.* 6:19007. doi: 10.1038/srep19007

Xia, L., He, X., Huang, X., Yu, H., Lu, T., Xie, X., et al. (2022). Genome-wide identification and expression analysis of the 14-3-3 gene family in mango (*Mangifera indica* L.). *Int. J. Mol. Sci.* 23, 1593. doi: 10.3390/ijms23031593

Xie, M., Zuo, R., Bai, Z., Yang, L., Zhao, C., Gao, F., et al. (2022). Genome-wide characterization of Serine/Arginine-rich gene family and its genetic effects on agronomic traits of *Brassica napus*. *Front. Plant. Sci.* 13:829668. doi: 10.3389/fpls.2022.829668

Xu, B., Gong, X., Chen, S., Hu, M., Zhang, J., and Peng, Q. (2021). Transcriptome analysis reveals the complex molecular mechanisms of *Brassica napus-Sclerotinia sclerotiorum* interactions. *Front. Plant. Sci.* 12:716935. doi: 10.3389/fpls.2021.716935

Yan, J., He, C., Wang, J., Mao, Z., Holaday, S. A., Allen, R. D., et al. (2004). Overexpression of the Arabidopsis 14-3-3 protein GF14 lambda in cotton leads to a "stay-green" phenotype and improves stress tolerance under moderate drought conditions. *Plant Cell Physiol.* 45, 1007–1014. doi: 10.1093/pcp/pch115

Yang, X., Wang, W., Coleman, M., Orgil, U., Feng, J., Ma, X., et al. (2009). Arabidopsis 14-3-3 lambda is a positive regulator of RPW8-mediated disease resistance. *Plant J.* 60, 539–550. doi: 10.1111/j.1365-313X.2009.03978.x

Yoon, G. M., and Kieber, J. J. (2013). 14-3-3 regulates 1-aminocyclopropane-1-carboxylate synthase protein turnover in Arabidopsis. *Plant Cell* 25, 1016–1028. doi: 10.1105/tpc.113.110106

Zhan, G.-M., Tong, J., Wang, H.-Z., and Hua, W. (2010). Molecular analysis and expression patterns of four 14-3-3 genes from Brassica napus L. *Agric. Sci. China* 9, 942–950. doi: 10.1016/S1671-2927(09)60175-9

Zuo, X., Wang, S., Xiang, W., Yang, H., Tahir, M. M., Zheng, S., et al. (2021). Genome-wide identification of the 14-3-3 gene family and its participation in floral transition by interacting with TFL1/FT in apple. *BMC Genomics* 22:41. doi: 10.1186/s12864-020-07330-2

frontiers | Frontiers in Plant Science

TYPE Original Research
PUBLISHED 06 September 2022
DOI 10.3389/fpls.2022.998698

OPEN ACCESS

EDITED BY
Cunmin Qu,
Southwest University, China

REVIEWED BY
Yongdong Sun,
Henan Institute of Science and Technology, China
Chunyu Zhang,
Huazhong Agricultural University, China
Weihua Long,
Jiangsu Academy of Agricultural Sciences (JAAS), China

*CORRESPONDENCE
Benbo Xu
benboxu@yangtzeu.edu.cn
Jing Dong
Dongjingsir061@163.com
XueKun Zhang
zhangxuekun@yangtzeu.edu.cn

SPECIALTY SECTION
This article was submitted to Plant Pathogen Interactions, a section of the journal Frontiers in Plant Science

RECEIVED 20 July 2022
ACCEPTED 16 August 2022
PUBLISHED 06 September 2022

CITATION
Zhai L, Xie L, Xu J, Xu B, Dong J and Zhang X (2022) Study on exogenous application of thidiazuron on seed size of *Brassica napus* L.Study on exogenous application of thidiazuron on seed size of *Brassica napus* L. *Front. Plant Sci.* 13:998698. doi: 10.3389/fpls.2022.998698

Study on exogenous application of thidiazuron on seed size of *Brassica napus* L.

Lu Zhai[1,2], Lingli Xie[1,2], JinSong Xu[1,3], Benbo Xu [1,2]*, Jing Dong[4]* and XueKun Zhang[1,3]*

[1]Engineering Research Center of Ecology and Agricultural Use of Wetland, Ministry of Education, Hubei Key Laboratory of Waterlogging Disaster and Agricultural Use of Wetland, Yangtze University, Hubei, China, [2]College of Life Science, Yangtze University, Hubei, China, [3]College of Agriculture, Yangtze University, Hubei, China, [4]Hubei Key Laboratory of Food Crop Germplasm and Genetic Improvement, Hubei, China

Thidiazuron (TDZ) is a novel and efficient cytokinin commonly used in tissue culture, and numerous studies have demonstrated that TDZ can increase berry size. However, no study to date has explored the effect of TDZ on seed size of *Brassica napus* and the mechanism. To shed light on the effect of TDZ on the seed size of *B. napus*, four different concentrations of TDZ were applied to *B. napus*. Results indicated that TDZ treatment could increase the seed diameter and silique length of *B. napus* to varying degrees and 100 and 200 μmol/L TDZ treatments were the most effective with a 3.6 and 4.6% increase in seed diameter, respectively. In addition, the yield of *B. napus* was also substantially increased under TDZ treatment. On the other hand, confocal micrographs of embryos and cotyledon cells suggested that embryos and their cotyledon epidermal cells treated with 200 μmol/L TDZ were obviously larger in size than the control. Furthermore, TDZ promoted the upregulation of some key maternal tissue growth-related genes, including two G-protein signaling genes (*AGG3* and *RGA1*) and two transcriptional regulators (*ANT* and *GS2*). The expression analysis of genes related to the auxin metabolic pathways, G-protein signaling, endosperm growth and transcriptional regulators confirmed that treatment with TDZ negatively regulated the key genes *ABI5*, *AGB1*, *AP2*, *ARF2,* and *ARF18* during bud development stage and florescence. The results strongly suggested that TDZ might regulate the transcriptional levels of key genes involved in auxin metabolic pathways, G-protein signaling, endosperm growth and transcriptional regulators, which resulted in bigger cotyledon epidermal cells and seed size in *B. napus*. This study explored the mechanism of TDZ treatment on the seed size of *B. napus* and provided an important reference for improving rapeseed yield.

KEYWORDS

***Brassica napus* L., thidiazuron, seed size, yield, gene expression**

Abbreviations: *B. napus*, *Brassica napus L.*; TDZ, thidiazuron; GA_3, gibberellic acid 3; DIC, differential inference lens; EDTA, ethylene diamine tetraacetic acid; DMSO, dimethyl sulfoxide; RT-qPCR, real time quantitative PCR; SS, seed number per silique; SL, silique length; SW, seed weight; BnPIR, *Brassica napus* Pan-genome Information Resource; BLAST, Basic Local Alignment Search Tool.

Introduction

Brassica napus (AACC, 2*n* = 38) is not only an important oilseed but also a valuable biofuel. It is one of the main sources of natural edible vegetable oils in people's daily life and has gradually become the green energy that people urgently need now. Nevertheless, owning to the dramatically increase of world population and sharply decrease in arable land area, although rapeseed has been widely cultivated all over the world, the supply of oilseed crop still can't adequate to the production demand.

Three direct determinants of oilseed rape yield include seed number per silique, silique number per plant and seed weight. Whether rapeseed productivity can be improved or not is greatly influenced by these components (Chen et al., 2007). In addition, both seed size and seed weight were positively correlated with oilseed rape yield and the former determined the latter (Orsi and Tanksley, 2009). Furthermore, seed size and seed number are also key factors closely related to crop domestication and evolutionary fitness in a variety of plants (Butruille et al., 1999; Shi et al., 2009). When analyzing the effect of seed size on the growth and development of cotton seedlings, it was found that the growth indexes of plants cultivated with large and full seeds were better than those of small and shriveled seeds (Huang et al., 2022). Although various traits in regard to seed size are essential for yield improvement in *B. napus*, there are still few commercially available chemical reagents that can promote seed size, and the underlying mechanisms by which it regulates seed size remain unclear.

Thidiazuron (TDZ) is a highly effective synthetic phenyl urea plant growth regulator, which not only has auxin-like activity, but also a cytokinin analogue (Chang et al., 2018). Nowadays, many scholars are devoted to the application of TDZ in cotton, and its main function in cotton is to promote the shedding of cotton leaves. Recent studies found that TDZ could induce cotton leaf abscission by increasing ethylene content and the activity of cell wall degrading enzymes (Du et al., 2014). Moreover, treatments with TDZ are capable of stimulating fruit growth, accelerating fruit ripening and promoting fruit enlargement, which will greatly improve fruit quality (Famiani et al., 1999). In addition to stimulating the enlargement of grape barriers and preventing fruit drop, TDZ also had an influence on the production of aroma volatiles in viticulture (Wang et al., 2020). Treatment with 20 to 60 mg/L TDZ revealed a significant reduction in fruit drop and an increase in fruitlet retention in "Hosui" and "Packham's Triumph" pears, especially at 60 mg/L TDZ, which resulted in the highest fruit number per tree and yields compared to other treatments (Carra et al., 2017). The same author also showed that fruit diameter and fruit weight was markedly increase in response to TDZ (Carra et al., 2021). Both of these increases should be attributed to the increasing TDZ rate, while the crop load and yield decreased linearly. Similarly, it was observed that both GA_3 and TDZ treatments promoted fruit maturity and significantly increased berry cracking rate compared to the control treatment (Lee et al., 2013). TDZ has been widely used in agricultural production and there have been tremendous physiological and biochemical researches on it, but few studies have been conducted on the role of exogenous TDZ reatments on seed size and related pathways and mechanisms in rapeseed.

Seed size is a major trait affecting crop yield and evolutionary fitness, and it is regulated by multiple genes in different metabolic pathways and signal transduction pathways. Several recent studies have testified that seed size is regulated by the relevant signaling pathways that control maternal tissue size (Li et al., 2019). Through delving deeply into the molecular mechanisms underlying these metabolic and signaling pathways revealed that the signaling pathways controlling seed size mainly include G-protein signaling, the ubiquitin-proteasome pathway, mitogen-activated protein kinase (MAPK) signaling, HAIKU (IKU) pathway, phytohormone and some transcriptional regulators (Li and Li, 2016; Li et al., 2019). Heterotrimeric GTP-binding proteins are conserved key regulators of signaling during eukaryotes growth and development. The structural G protein is a core protein complex composed of one Gα, one Gβ and the Gγ subunits (Johnston et al., 2007; Urano and Jones, 2014; Stateczny et al., 2016). The AGG3-like-γ-subunits has a function in regulating the size of seeds and organs. AGG3-deficient mutant in *Arabidopsis* was discovered to produce smaller seeds and organs. In contrast, *AGG3* overexpression resulted in increased seed size, seed weight and seed number per plant (Li et al., 2012; Roy Choudhury et al., 2014). The typical α subunit (*RGA1*) in the heterotrimeric G protein complex has been found to be involved in the regulation of grain weight and cell function during plant development by coupling extracellular signals sensed by receptors (Biswal et al., 2022).

Plant hormones have recently been shown to play an important role in seed size regulation. In particular, the biosynthesis and signal transduction of auxin in plants controlled the seed size to a great extent (Ishimaru et al., 2013; Liu L. C. et al., 2015). The *Auxin/INDOLE-3-ACETIC ACID* (*Aux/IAA*) transcriptional repressors and the *AUXIN RESPONSE FACTOR* (*ARF*) are jointly involved in the auxin signaling process (Weijers and Friml, 2009). The seeds produced after complete loss of *ARF2* gene function were up to 46% heavier than wild-type seed parents and affected seed size through maternal tissues due to enlarged integuments (Schruff et al., 2006). *AINTEGUMENTA* (*ANT*) is a transcription factor of the AP2-domain family members that mediates cell proliferation and growth control (Klucher et al., 1996; Krizek, 2003). Studies manifested that overexpression of *ANT* gene generated larger seeds (Mizukami and Fischer, 2000). Scholars also found that the *ANT* promoter combined with *ARF2* could directly regulate the expression of *COLD-REGULATED15A* (*COR15a*), and the mutants after knocking out cor15a displayed a smaller seed size phenotype, indicating that *COR15A* positively regulated seed size (Meng et al., 2015). Evidence from polyploid

B. napus revealed that *ARF18* determined the seed weight and silique length through an auxin-response pathway and maternal regulation. Meanwhile, the homodimers formed by *ARF18* regulated seed size by repressing auxin-responsive genes and restraining cell expansion in the silique wall (Liu J. et al., 2015). Furthermore, *BRASSINAZOLE-RESISTANT1* (*BZR1*) is considered to be an important seed growth regulator through maternal tissues (Kim et al., 2021). Some findings indicated that specific seed developmental pathways regulated by *BR* transcription resulted in altered seed size and seed shape (Jiang et al., 2013).

Transcription factors repress or enhance the expression of various genes in the process of plant growth and developmental. In particular, it plays significant role in regulating genes related to seed size, for instance, *GRAIN SIZE ON CHROMOSOME* (*GS2*), *APETALA2* (*AP2*) and *TRANSPARENT TESTA GLABRA2* (*TTG2*) (Western et al., 2001; Johnson et al., 2002; Hu et al., 2015). There are six *AP2* members in the *APETALA2*/ethylene response element binding protein (*AP2/EREBP*) transcription factor superfamily, which are mainly expressed in floral organs, ovules and seed coat development (Jofuku et al., 1994; Jofuku et al., 2005; Ohto et al., 2005, 2009). Among them, *AfAP2-2* is an *AP2* homologous gene with two conserved *AP2* structural domains. Compared with the vegetative period, its expression level is significantly higher in vegetative organs during the reproductive period. Since AfAP2-2-over-expressing *Arabidopsis* produced smaller seeds than the wild type (WT), and seed weight was also predominantly reduced relative to the WT, the above results demonstrated that *AfAP2-2* might be negatively correlated with seed size and weight (Lei et al., 2019). In summary, *AP2* is one of the major transcription factors affecting seed size and seed weight. *GS2* is a member of the *GRF* transcription factor family, which is a transcriptional activator encoding *OsGRF4* (van der Knaap et al., 2000). MicroRNA miR396c regulated *OsGRF4* in a targeted manner *in vivo*. The *GS2* mutation disrupted the interaction between *OsmiR396* and *OsGRF4*, leading to advanced expression level of *OsGRF4*, and bringing about larger grains and higher grain yield (Duan et al., 2016; Li et al., 2016).

To study the effect of TDZ on seeds, *B. napus* was treated with different concentration TDZ in this research, and the morphology and physiology of treated plants were determined. Laser confocal microscopy was used to observe embryos and cotyledon cells. Quantitative Real-time PCR (qRT-PCR) was used to measure the transcriptional levels of genes associated with maternal tissue growth (*AGG3*, *RGA1*, *ANT,* and *GS2*) and seed size (*ABI5*, *AGB1*, *AP2*, *ARF2,* and *ARF18*). The results provided the evidence that a molecular mechanism by which TDZ regulated seed size in *Brassica napus*, which greatly benefitted to the improvement of rapeseed yield.

Materials and methods

Plant materials and growth conditions

The field trials were conducted during growing season of 2020–2021 in Agricultural Science and Technology Industrial Park of Yangtze University, Hubei province, China (30°36′N 112°08′E). The area belongs to the subtropical monsoon humid climate zone, with an average annual temperature of 15.9–16.6℃, annual rainfall of 2600–3100 mm, and annual sunshine hours of 1800–2000 h. Changyou No. 1 cultivar of *B. napus* was used material in this study, which was a hybrid between zhongshuang 11 and a material from Czechia. It is a winter-hardy variety with high yield which is extremely sensitive to light and temperature. Completely randomized block method was used with 3 replicates and the area of each block was 18 m^2, with a planting density of 18 cm between the plant individuals and 25 cm between rows. Field management and pest and disease prevention were conducted based on local standard practices.

The plant growth regulator TDZ were sprayed at concentrations of 10, 100, 200, and 400 μmol/L on the leaves at the early development stage in March, 3–5 days before flowering. Plants treated with distilled water were used as control. All applications of TDZ were sprayed with hand sprayer. The buds and flowers selected for sampling at the flowering stage in April 9 were picked and stored at −80℃ for RT-qPCR. Siliques and seeds were harvested in May 28, 2021. At least 30 siliques and seeds from each concentration of the treatment were selected for growth and yield measurements. The harvested seeds were analyzed immediately.

Morphological and physiological measurements of seeds

Plants were monitored from April through May 2021. It started growing siliques on April 18. Seeds ripe completely after 40 days. In May 28, 2021, final seed diameters (cm), silique length (cm) and seed number per silique were recorded. Thirty uniformly growing plants from rape treated with different concentrations of TDZ were selected for the determination of growth and yield indicators. Meanwhile all siliques of the selected plants were measured. In order to analyze the effect of TDZ on seed size, the main stem of plants was divided into three parts: top, middle and bottom, according to the branching characteristics of rape. Total number of seeds per plant was added up by using a knife to open all siliques from each plant and counting the number of seeds in it. Additionally, the number of existing seeds and empty shells number were counted. Seed setting ratio was determined as the number of existing seeds divided by the sum of the number of existing seeds and the empty shells number. Seed diameter was measured with vernier calipers. Twenty siliques were selected at the optimal

concentration after TDZ treatment, and their silique lengths were measured with a ruler and photographed for comparison with the control. The seeds collected from each part of the plant were evenly mixed together and randomly selected 30 seeds from them to measure their seed diameter, then divided by the number of seeds to get the average seed diameter per plant. To calculate thousand-seed weight (g), 1,000 seeds per plant were randomly selected and weighed. Poured the seeds into the test tube to its 5 ml mark and weighed the seeds at this moment. Seed volume weight (g/ml) was determined as the seed weight divided by the volume of tick mark. The all seeds of each block was harvested separately and its yield was measured.

Confocal laser scanning microscope observation

A dissecting needle was used to dissect CK and seeds treated with 200 μmol/L TDZ under a microscope to isolate the embryos. Seeds of 10 days after flowering and mature seeds are treated in this way. Then, the embryos placed in DIC buffer (50 mM sodium phosphate, pH 7.0/10 mM EDTA/1% Triton X-100/1% DMSO) were incubated in 37°C constant temperature incubator overnight (at least 12 h), fixed with FAA fixative (10% formalin/5% acetic acid/45% ethanol/0.01% Triton X-100). The fixed embryos were dehydrated with 30, 50, 70, 80, 90, 95, and 100% ethanol (1 h for each stage) and then treated in Hoyer's solution (chloral hydrate: water: glycerol = 3:0.8:0.4) for 1 h (Ohto et al., 2005, 2009). The cellular morphology of the embryos was observed and photographed using a confocal laser scanning microscope observation (Leica TCS-SP8 SR, Germany) fitted with a differential interference lens (DIC). The cell number and cell size per unit area were counted by using ImageJ software (National Institute of Health, United States).

RNA extraction and quantitative real-time PCR

RNA prep Pure Plant Plus Kit (Tiangen, Beijing, China) was used to extract the total RNA from flowers and buds under different concentrations of TDZ treatment according to the manual. In short, samples were ground with a grinder (MB-24) after freezing about 100 mg of flowers and buds in liquid nitrogen. The concentration and purity of RNA was evaluated using Ultramicro ultraviolet spectrophotometer (QuaWell Q5000, United States) by determining absorption at 260 and 280 nm. Subsequently, 1 μg RNA was reverse transcribed into cDNA using HiScript® II Q RT SuperMix for qPCR Kit (Vazyme, Nanjing, China) according to the manufacturer's protocol.

To gain insights into the response of seed size-related genes to TDZ, transcription level of nine genes involved in seed growth was detected, including an endosperm growth-related gene (*ABI5*), three transcriptional regulatory factors (*ANT*, *AP2,* and *GS2*), three G-protein signaling genes (*AGB1*, *AGG3,* and *RGA1*) and two auxin metabolic relative genes (*BnARF18* and *ARF2*). The nine genes were searched directly or BLAST in the BnPIR genome browser by using the protein sequences of *Arabidopsis* as a query. Then, Vector NTI software was used to design the specific primers for qRT-PCR accord to the genes sequences related seed development (**Supplementary Table 2**). Relative transcriptional level of genes associated with seed size was analyzed by qRT-PCR. The experimental protocol was carried on CFX96TM Real-Time System (Bio-Rad, United States). The total reaction solution was 10 μL, containing 5 μL 2 ×ChamQ Universal SYBR qPCR Master Mix (Vazyme, Nanjing, China), 0.4 μL forward and reverse primer, 2.6 μL autoclaved sterile water and 2 μL of 10-fold diluted template. The qRT-PCR program was conducted using three-step cycling conditions of 95℃ predenaturation for 30 s, 40 cycles of 95℃ for 10 s, cooling down to 60℃ for 30 s and at 72℃ extending for 30 s. *Actin-2* was the selection of internal control genes in rape. The relative expression levels of genes related to seed size were calculated based on the method of $2^{-\Delta\Delta CT}$ (Livak and Schmittgen, 2001). Each sample corresponded to three technical replicates.

Statistical analysis

The experiment was carried out following a completely randomized devise with four replications at different concentrations of TDZ treatment. The phenotypic data of seed diameters, silique number per plant, seed number per silique, thousand-seed weight and seed volume weight were subjected to the mean ± standard error. The statistical analysis of total data was determined by applying Duncan's Test in DPS 8.50 (Data processing software, China). A significant difference was indicated when the p-value < 0.05. GraphPad Prism 9.0 (GraphPad Software, Inc., United States) was used to draw figures.

Results

Effect of thidiazuron treatments on seed morphology of *Brassica napus*

In length measurements of siliques, 200 μmol/L TDZ treatment increased the silique length located in the middle (**Figure 1A**). The application of 200 μmol/L TDZ achieved the greatest length (10.44 ± 0.19 cm), and control almost had a shorter siliques length, ranging from 7.70 to 10.40 cm

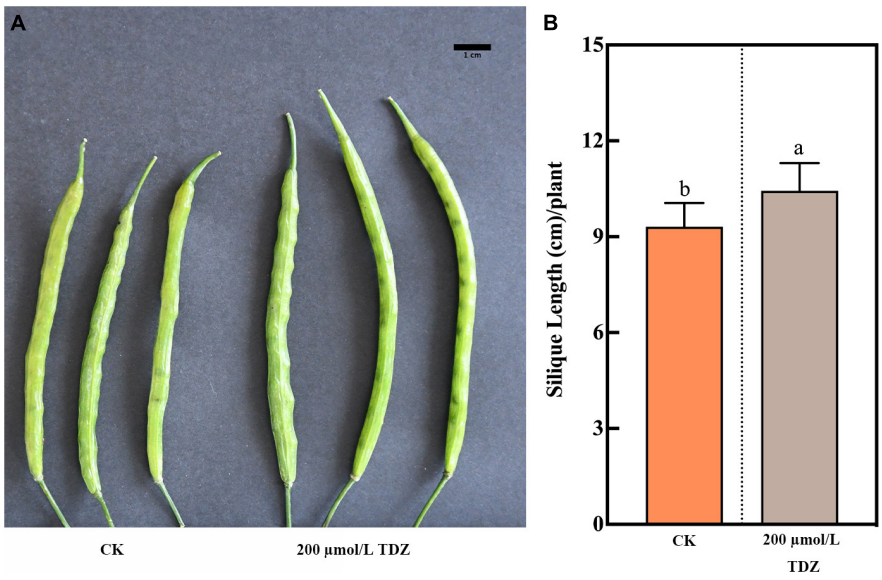

FIGURE 1
Effect of 200 μmol/L TDZ treatment on silique phenotype and silique length. **(A)** Comparisons of silique phenotype. **(B)** Comparison of silique length. Scale bar: 1 cm. Mean ± Standard error (n = 20). Different letters denote a significant difference (Student's t-test, $p \leq 0.05$).

(Figure 1B). The effect of different concentrations of TDZ on the seed size of *B. napus* at 40th day after full maturity is shown in Figure 2. It was observed that TDZ had a significant effect on seed size, as the seeds located in different parts under each concentration of TDZ treatment were obviously larger than the control. In the seeds growing in the top siliques, the seeds treated with TDZ at concentrations of 100, 200, and 400 μmol/L were greater than those of 10 μmol/L and the control (Figure 2A). The seed diameter (2.05–1.93 cm) under the all TDZ treatment was also simultaneously notably increased when compared to the control ($p \leq 0.05$) (Supplementary Table 1). Regarding the seeds in the middle silique, all TDZ-treated seeds became larger relative to the control (Figure 2B). Meanwhile, 200 μmol/L TDZ treatment had the longest seed diameter among all TDZ-treated seeds (2.04–1.92 cm), followed by 100 and 400 μmol/L TDZ, which were different from 10 μmol/L TDZ and the control ($p \leq 0.05$) (Supplementary Table 1). For the seeds growing in the bottom silique of the plant, the seed diameter varied from 2.05 to 1.99 cm. It was noticed that the TDZ treatment at the medium concentration (100 μmol/L) significantly increased seed size, and the seed diameter was the longest, followed by the other TDZ-treated seeds. Similarly, the seed diameter of the control remained the shortest in all cases ($p \leq 0.05$) (Supplementary Table 1 and Figure 2C). Additionally, comprehensive analysis for seed diameter within the silique of each part of the plant showed that application of medium TDZ concentration (100 and 200 μmol/L) promoted the longer seed diameter with an increased increment of 3.6 and 4.6%, respectively relative to the control. Overall, the above-mentioned results indicated that TDZ treatment notably affected the seed size of *B. napus*.

Effect of thidiazuron on yield-related traits in *Brassica napus*

Plants treated with TDZ showed basically consistent changes in the seed yield-related traits, including increases in thousand-seed weight, seed volume weight, the silique number per plant, yield and the seed number per silique relative to control. Thousand-seed weight is one of the important components of yield. The thousand-seed weight after treatment with 200 μmol/L TDZ was remarkably higher than control and the other concentrations of TDZ treatments. Additionally, as compared to control, the thousand-seed weight also significantly increased in the other TDZ treatment. As for seed volume weight, like thousand-seed weight, it also reached a maximum under the treatment of 200 μmol/L TDZ, while the effect of TDZ (400 μmol/L) treatment was statistically comparable to TDZ (10 and 100 μmol/L), but all of the seed volume weight treated with them was greater than that of control (Table 1).

Among the variables related to yield, the silique number per plant was one of the main factors, 200 and 400 μmol/L TDZ treatment significant increased silique number per plant ($p \leq 0.05$). Moreover, the 400 μmol/L TDZ treatment outperformed the other TDZ treatments (except for the 200 μmol/L TDZ treatment) both in terms of silique number per plant and yield ($p \leq 0.05$) (Table 1). On the other hand, the highest yield was obtained under the treatment with TDZ

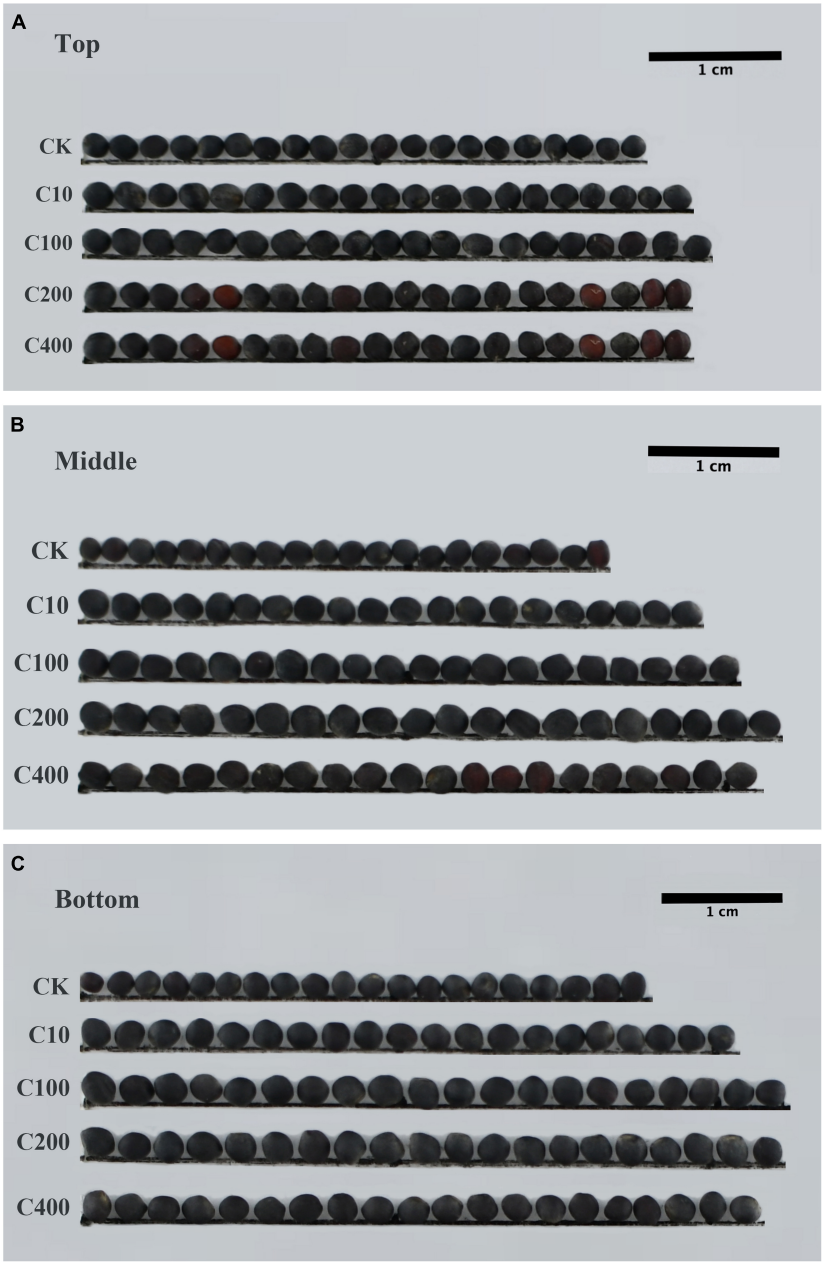

FIGURE 2
Effect of TDZ treatment on seed size of *B. napus*. **(A)** Siliques in the top; **(B)** siliques in the middle; **(C)** siliques in bottom; CK: control; C10: 10 μmol/L TDZ; C100: 100 μmol/L TDZ; C200: 200 μmol/L TDZ; C400: 400 μmol/L TDZ; Scale bars: 1 cm.

(200 μmol/L), followed by TDZ 100 and 400 μmol/L, TDZ 10 μmol/L also gave higher yield than the control (Table 1). The yield of the TDZ (200 μmol/L) treatment increased by 12.04% compared to the control plants. This might be attributed to the increase in seed size.

The empty shells number exhibited significance only in the siliques located in the middle, bottom and various portions of the plant. The average seed number per silique after 400 μmol/L TDZ treatment was significantly more than that in control and 100 μmol/L TDZ treatment, followed by 200 μmol/L TDZ treatment. Meanwhile, the control had the least seed number per silique in the top and middle siliques, followed by 100 μmol/L TDZ treatment. Among the siliques located in the middle, bottom and various portions of *B. napus*, the control had the most empty shells number and was significantly more than 10 μmol/L TDZ treatment. Additionally, in the siliques located in the bottom and various portion, the empty shells number in control was significantly higher than in 100

10.3389/fpls.2022.998698

TABLE 1 Effect of TDZ treatments on seed yield-related traits.

Treatment (μmol/L)	Thousand-seed weight (g)	Seed volume weight (g)	Silique number per plant	Seed number per silique	Yield (Kg/ha)
Control	2.91 ± 0.06c	0.6704 ± 0.0039b	263.25 ± 9.22b	19.01 ± 4.56c	2584.50 ± 6.56d
TDZ 10	3.27 ± 0.01bc	0.6732 ± 0.0047ab	267.25 ± 7.93b	19.77 ± 4.77bc	2666.75 ± 4.57c
TDZ 100	3.38 ± 0.04ab	0.6806 ± 0.0044ab	268.75 ± 6.24b	19.28 ± 4.70c	2763.75 ± 5.38b
TDZ 200	3.46 ± 0.04a	0.6846 ± 0.0019a	309.00 ± 6.06a	20.97 ± 4.93ab	2895.75 ± 4.57a
TDZ 400	3.16 ± 0.03d	0.6714 ± 0.0053ab	299.75 ± 4.27a	21.76 ± 3.79a	2767.00 ± 5.16b

Mean ± Standard error (SE), $n \geq 5$. For each group of comparisons, thousand-seed weight, seed volume weight, silique number per plant, seed number per silique and yield values followed by the same letter are not significantly different at the 0.05 significance level based on Duncan's multiple range test and ANOVA. The ANOVA was run for each seed yield-related traits.

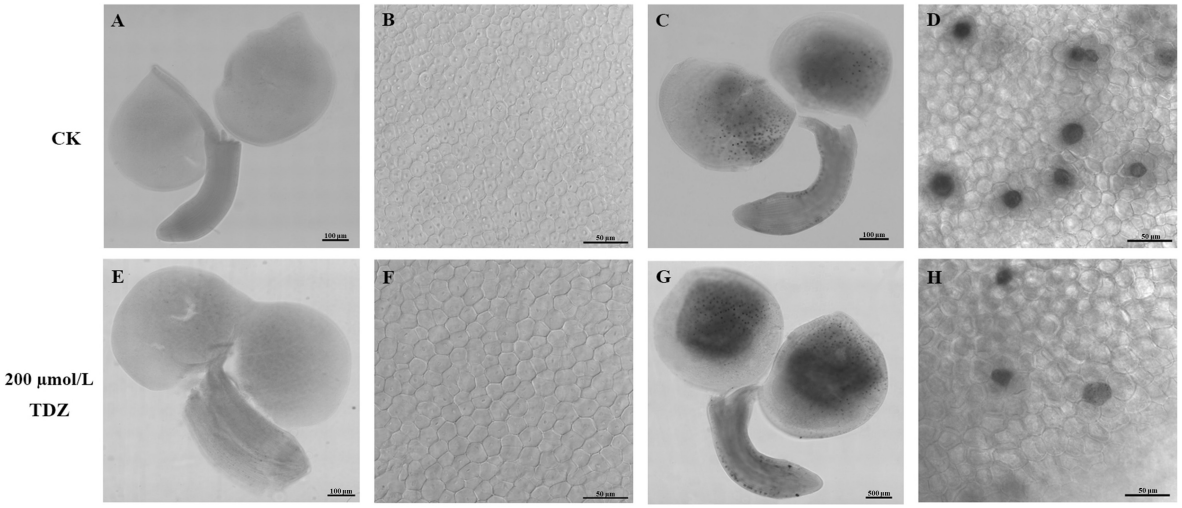

FIGURE 3
Effect of TDZ treatment on embryo cell size and number. **(A,E)** Immature embryos from seeds of 20 days after treatments; **(B,F)** epidermal cell layer from the central part of cotyledons from panels **(A,E)**; **(C,G)** mature embryos from mature dried seeds; **(D,H)** epidermal cell layer from the central region of cotyledons panels **(C,G)**. Scale bar: 100 μm in panels **(A,C,E)** and 500 μm in panel **(G)**, observation with 20× objective in DIC mode; 50 μm in panels **(B,D,F,H)**, 40× oil lens observation in DIC mode.

and 400 μmol/L TDZ treatments ($p \leq 0.05$) (Supplementary Table 1). Nevertheless, the effect of TDZ treatment on the seed number per silique and the empty shells number and the relationship between the two yield traits remain to be further investigated. The seed setting ratio with low and high concentrations (10 and 400 μmol/L) TDZ treatment was notably higher in the siliques in the bottom than in the untreated *B. napus* (Supplementary Table 1). For the siliques in the bottom, the seed setting ratio after two concentrations of TDZ treatment increased by 7.39 and 7.06% compared to the control, respectively.

Effect of thidiazuron treatments on embryo cell size and number

In order to explore the reasons for the larger seeds, a cytological analysis of the seeds was performed. The embryos were isolated and observed. The size of embryo and cotyledon cells in the siliques at 20th day after TDZ treatment is shown in Figure 3. Embryos treated with 200 μmol/L TDZ were significantly larger than that of control and the average cotyledon area in TDZ-treated embryos was 2.34 times larger than in the control (Figure 4A). Furthermore, it could be found from the laser confocal microscope image that the hypocotyl and radicle treated by TDZ was also appeared bigger than those of control (Figure 4A). Similarly, embryos in mature seeds treated with 200 μmol/L TDZ were also significantly larger than the control (Figures 3C,G), and the average area of cotyledons after TDZ treatment was 1.81 times larger than that of control (Figure 4A).

Epidermal cells in the middle of cotyledons treated with TDZ and control were selected respectively to measure the cell size. The results proved that TDZ treatments enlarged the epidermal cells of cotyledons. For the 20 days seeds after treatments, the average area of cotyledon epidermal cells was 1.24 times larger than the area of the corresponding control cells (Figures 3B,D,F,H). The cotyledon epidermal cell area in

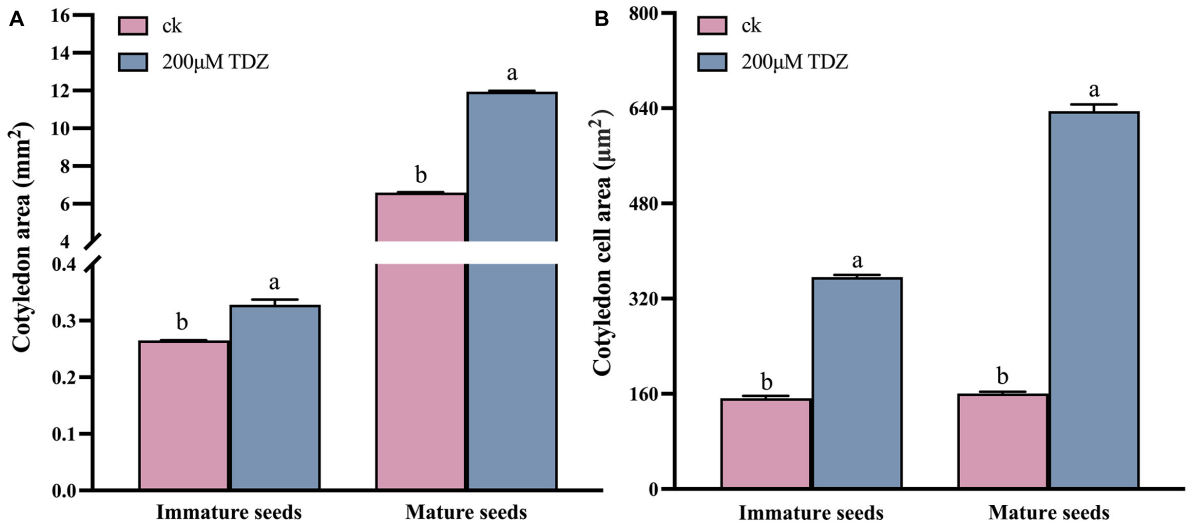

FIGURE 4
Cotyledon area **(A)** and cotyledon cell size **(B)** of immature seeds and mature seeds. Entire cotyledons from immature embryos and mature dried embryos or their central parts were cleared and photographed. Imaging analysis software was used to calculate areas. Mean ± Standard error (n = 3). Different values were marked with different letters at 0.05 significance level.

mature seeds treated with 200 μmol/L TDZ was 3.95 times larger than that of the control (Figure 4B). In immature seeds, the number of cotyledon cells treatmented with TDZ was approximately 1.89 times that of the control. Thus, TDZ treatment increased both cell size and number, which may lead to an increase in seed size as well.

Transcriptional levels of seed size-related genes of *Brassica napus* after thidiazuron treatment

As shown in Figures 5, 6, the transcriptional patterns of these genes were similar in the buds and flowers. Although the gene transcriptional levels differed slightly under different concentrations of TDZ treatment, the overall expression trends of individual genes located on different chromosomes were basically the same. The results showed that transcriptional levels of *ABI5* gene related to endosperm formation was significantly decreased in buds (Figure 5A). Compared with the control group, *AP2*, *ARF2*, *BnARF18* and *AGB1*, which played a negative regulatory role in seed size control, were also down-regulated in the same buds (Figures 5D–F,I). By contrast, compared with the control group, the transcriptional levels of the *AGG3*, *ANT*, *GS2,* and *RGA1* genes, which were positive regulators of seed size, were significantly increased after TDZ treatment in buds (Figures 5B,C,G,H). Simultaneously, the transcription of these genes showed the same trend in flowers (Figure 6). Overall, exogenous TDZ treatment induced the transcription of these genes to some extent. Interestingly, the transcriptional level of *AGG3*, *ANT*, *GS2,* and *RGA1* genes, which were all positive regulators of seed size, reached a maximum after TDZ treatment at relatively medium concentrations (100 or 200 μmol/L) in buds. In flowers, the transcriptional levels of *AGG3* and *ANT* also reached a maximum at moderate concentrations (100 or 200 μmol/L) of TDZ treatment. In contrast, compared to that of control, the transcriptional level of the genes *BnaA05.ABI5*, *AGB1* (except *BnaC01.AGB1*), *AP2* (except *BnaA03.AP2*) and *ARF18* reached a minimum when treated with TDZ at the same concentrations (100 or 200 μmol/L). Combined with the previous phenotypic and morphological results, it could be speculated that a medium concentration (100 or 200 μmol/L) of TDZ treatment may be the optimum concentration for increasing seed size. To summarize, TDZ might affect seed growth and regulate seed size by promoting or repressing the transcription of genes related to seed size.

Discussion

Thidiazuron can be used as a plant growth regulator to improve the yield of *Brassica napus*

Thidiazuron is considered as a substituted phenyl urea compound with strong auxin- and cytokinin-like activities. It has been proved to promote seed germination and stomatal formation on floral parts (Meng et al., 2004; Sharaf et al., 2011). What's more, TDZ has the effect of inducing and stimulating

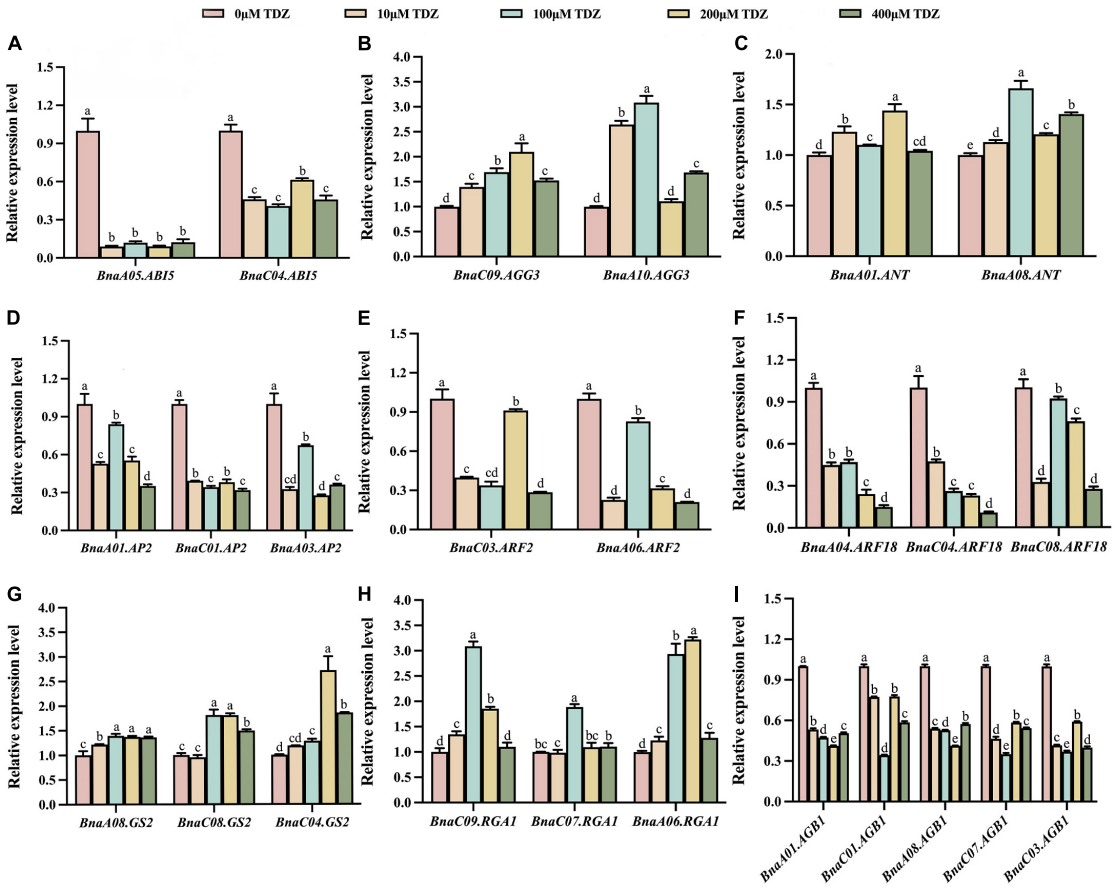

FIGURE 5
Relative transcriptional levels of seed size-related genes in buds of *B. napus*. **(A–I)** lists the relative transcriptional levels of nine genes associated with seed size located on different chromosomes in buds. Among them, the pink, orange, blue, yellow and green columns represent the relative transcriptional levels of genes in buds treated with 0 μmol/L, 10 μmol/L, 100 μmol/L, 200 μmol/L and 400 μmol/L TDZ, respectively. Three biological replicates and three technical replicates were carried out using buds from 3 to 5 days before flowering. Mean ± Standard error (n = 3). Different letters suggest significant differences (Duncan's multiple range test, $p \leq 0.05$).

cotyledon growth and development as well as increasing fruit weight, etc. (Guo et al., 2011). In fruit cultivation, studies have found that TDZ can effectively promote the fruit growth of various fruits such as apples (Greene, 1995), persimmons (Itai et al., 1995) and kiwis (Famiani et al., 1999; Famiani et al., 2002), increasing their size and seed setting ratio. Although many studies have demonstrated TDZ can promote fruit enlargement and increase fruit weight, there are few studies on its role in seed size.

Seed size is an important agronomic trait, which not only affects plant and environmental stress adaptation, but also crop quality and yield (Guo et al., 2020; Miao et al., 2020). Study has revealed that gibberellic acid in combination with 5 mg·L^{-1} TDZ increases berry width (Kimura et al., 1996). Based on previous study, TDZ treatments increased the fruit diameter led to a decrease in the fruit length/average diameter ratio, which caused a change in fruit shape, while an increase in fruit size and weight (Famiani et al., 1999). Additionally, spraying TDZ (20–30 mg·L^{-1}) on small-fruited "Spadona" and "Coscia" pears resulted in a significant increase in fruit size (Stern et al., 2003). The fact that fruit size was increased by exogenous application of TDZ was also reported in "Hosui" pears and "Gala" apples (Petri et al., 2001; Pasa et al., 2017). Altogether, above studies indicated that TDZ had an important regulatory role on seed size. *B. napus* is one of the most important oilseed crops widely grown worldwide. It has been reported that the determinants of seed yield in oilseed crops include effective silique number per plant and seed number per silique, and thousand-seed weight depending on the seed number and size (Ozer, 2003; Jiao et al., 2012). In this study, results indicated that TDZ treatment was effective in promoting seed size in *B. napus*. 100 and 200 μmol/L TDZ treatments significantly increased seed diameter of 40-day-old siliques of *B. napus*, and other concentrations of TDZ treatment also increased seed diameter compared with the control (**Supplementary Table 1**). Our study

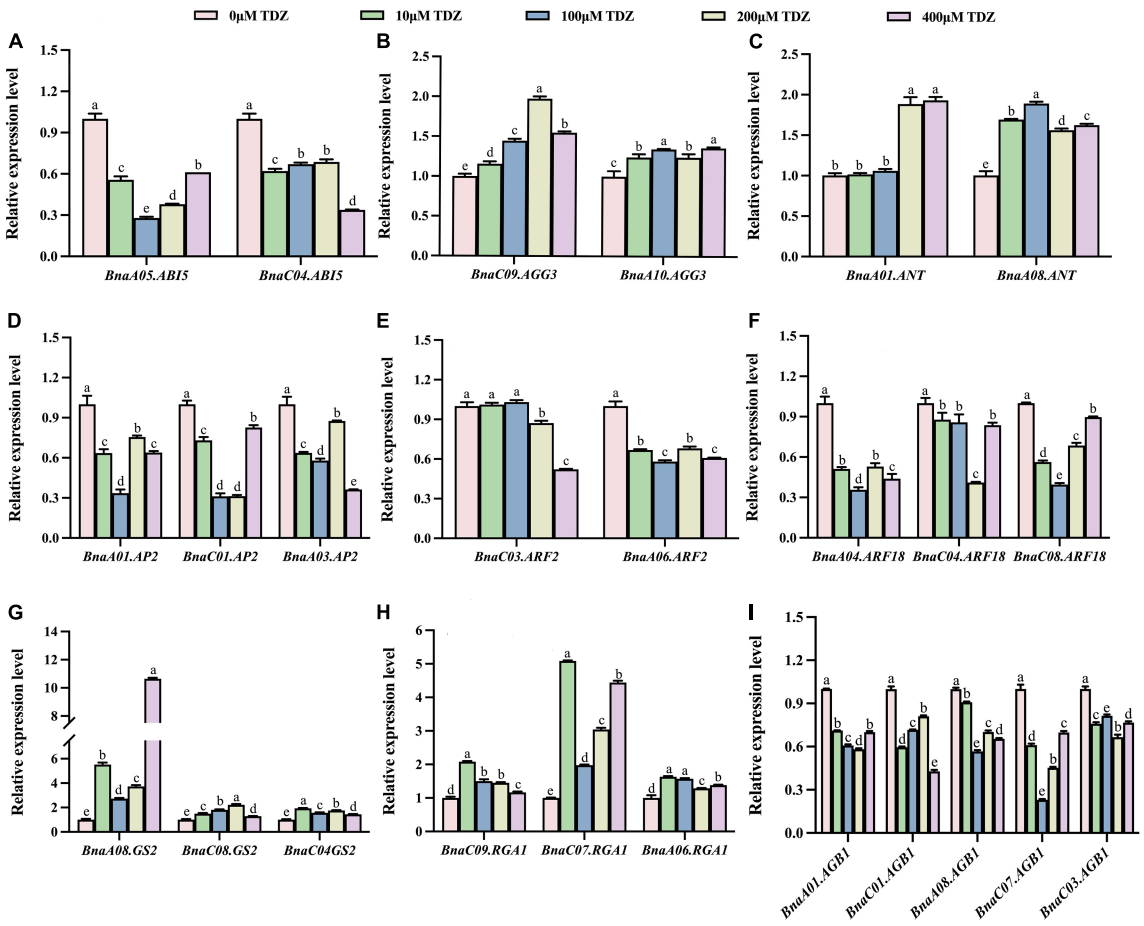

FIGURE 6
Relative transcriptional levels of seed size-related genes in flowers of *B. napus*. **(A–I)** lists the relative transcriptional levels of nine genes associated with seed size located on different chromosomes in flowers. Among them, the pink, green, blue, yellow and purple columns represent the relative transcriptional levels of genes in flowers treated with 0 μmol/L, 10 μmol/L, 100 μmol/L, 200 μmol/L and 400 μmol/L TDZ, respectively. Three biological replicates and three technical replicates were carried out using 10-day-old blooming flowers. Mean ± Standard error (n = 3). Different letters suggest significant differences (Duncan's multiple range test, $p \leq 0.05$).

proved that 200 μmol/L TDZ treatment had the most silique number per plant among all treatments (Table 1). Except for the siliques located in the bottom portion of the plant, the seed number per silique was significantly higher at a high concentration (400 μmol/L) than other concentrations of TDZ treatment, while the seed number per silique in all TDZ-treated plants was no less than in the control (Supplementary Table 1). In kiwifruit, TDZ greatly increased the fruit number with protruding distal ends at high concentrations. However, TDZ did not result in significant changes in seed number (Famiani et al., 1999). Similar results emerged from the study of small-fruited "Spadona" and "Coscia" pears by Stern et al. (2003) that TDZ treatment had no effect on fruit shape, seed number and yield in the following year. For the result that there was no difference in the seed number observed, the authors attributed this to low pollen utilization due to the lack of simultaneous flowering or the absence of pollinators. Nevertheless, our experiment does not have these problems and the research subjects are completely different, which may be the reason for the different results from the previous studies. Furthermore, both thousand-seed weight and seed volume weight reached their maximum values under the treatment with TDZ (200 μmol/L), and were higher than the control under other concentrations of TDZ treatment (Table 1). It was reported that TDZ treatment linearly increased the weight of bunches and berries, while reduced the total soluble solids content (Reynolds et al., 1992). Likewise, kiwifruit treated with different concentrations of TDZ were 50% or 60% heavier than untreated ones, the dry weight also increased substantially and to a similar increase extent at same treatment concentrations (Famiani et al., 1999). In our study, the yield of *B. napus* was higher than that of the control regardless of the application of any concentration of TDZ within the selected range of concentrations (Table 1). In terms of seed setting

ratio of the whole plant, compared to the control, the seed setting ratio per plant was increased by 5.3 and 6.04% under low and high concentrations (10 and 400 μmol/L) of TDZ treatment, respectively (**Supplementary Table 1**). Consistent with previous studies, Pasa et al. (2017) found that the application of TDZ to "Hosui" and "Packham's Triumph" pears significantly increased fruit setting, reduced fruit abscission and ultimately resulting in increased yield. Furthermore, in addition to "Hosui" and "Packham's Triumph" pears, foliar sprays of TDZ were also observed in "Shinseiki" pears to significantly increase fruit setting (Hawerroth et al., 2011). Application of TDZ during flowering significantly increased fruit setting and fruit weight in apple trees "Gala" and "Fuji" over seven growing seasons. The 7-year average fruit setting ratio for TDZ 10 mg L^{-1} was 112.7% compared to 51.3% for the control (Petri et al., 2001). These results indicated that TDZ treatment increased yield traits such as the silique number per plant, thousand-seed weight, seed volume weight, the yield and seed setting ratio, thereby greatly improving the yield of *B. napus*.

Thidiazuron treatments enlarger cell and increase the number of embryos of *Brassica napus*

Cell division and cell expansion control the size and shape of plant organs. In the present study, TDZ-treated rapeseed seeds were significantly larger than untreated seeds. The reason for this result could be that TDZ induced or prolonged the active phase of mitosis resulting in increased cell number, increased cell area or both (Celikel et al., 2021). The embryos of seeds in the siliques after 20 days of 200 μmol/L TDZ treatment were significantly larger than that of control (**Figures 3A,E**) and their average cotyledon area was 2.34 times larger than the control (**Figure 4A**). Similarly, embryos in mature seeds treated with 200 μmol/L TDZ were also significantly larger than the control (**Figures 3C,G**), and the average area of cotyledons after TDZ treatment was 1.81 times larger than that of control (**Figure 4A**). Both area and number of cotyledon epidermal cells increased after 200 μmol/L TDZ treatment (**Figure 4B**). Such a result demonstrated that exogenous application of TDZ induced an increase in cell size and number, which results in an increase in seed size of *B. napus*. Similar phenomena were observed in other plants. Shargal et al. (2006) suggested that the number of cells present at fruit setting, the number of subsequent cell divisions and cell expansion determined the fruit size of "Spadona" pears. The "Spadona" pear fruit treated with TDZ was significantly larger than the untreated fruit, and the cells between the parenchyma of the pulp were smaller but the number of parenchymal cells was significantly increased. On the other hand, according to the fluorescence-activated cell sorter (FACS) analysis, suggesting that TDZ affected pear fruit size by increasing cell number and prolonging the mitotically active period of pulp parenchyma cells (Shargal et al., 2006).

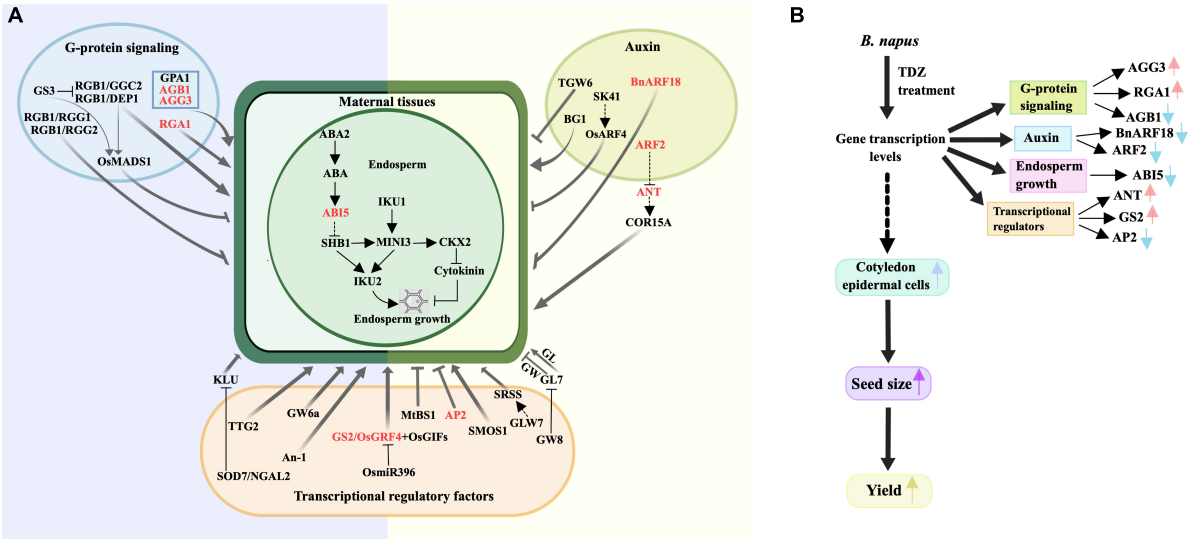

FIGURE 7
Diagram of signaling pathways associated with seed size **(A)** and a schematic diagram of a simulation mechanism explaining the regulation of seed size by TDZ **(B)**. **(A)** The image showed the genes related to the seed size in four different signaling pathways in *Arabidopsis*, rice and other species, where the red text represented the genes studied in this paper in *B. napus*, and the dashed lines indicated unclear genetic relationships (Li et al., 2019). ABA, abscisic acid; GL, grain length; GW, grain width. **(B)** TDZ treatment may initially affect changes in gene expression levels the yield of related to the seed size, resulting in larger cotyledon epidermal cells, increased seed size, and ultimately a substantial increase in *B. napus*.

10.3389/fpls.2022.998698

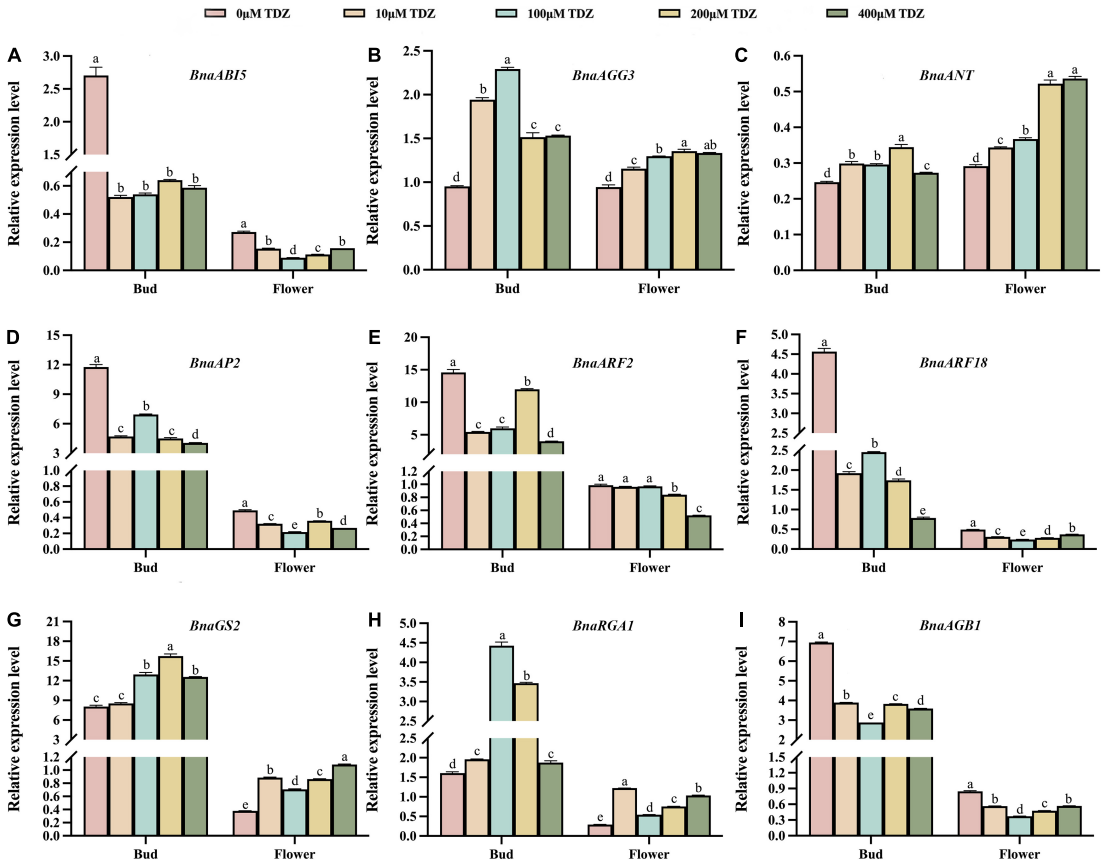

FIGURE 8
Comprehensive analysis of relative transcriptional levels of seed size-related genes in buds and flowers of *B. napus*. **(A–I)** lists the relative transcriptional levels of nine genes associated with seed size in buds and flowers. Among them, the pink, orange, blue, yellow and green columns represent the relative transcriptional levels of genes in buds and flowers treated with 0 μmol/L, 10 μmol/L, 100 μmol/L, 200 μmol/L and 400 μmol/L TDZ, respectively. Three biological replicates and three technical replicates were carried out using buds from 3 to 5 days before flowering and 10-day-old blooming flowers. Mean ± Standard error (n = 3). Different letters suggest significant differences (Duncan's multiple range test, $p \leq 0.05$).

Multiple seed development related pathways respond to thidiazuron treatments

A previous review showed that seed size is controlled by a combination of several different signaling pathways that regulate maternal tissues growth (Li et al., 2019). **Figure 7A** showed a partial signaling pathways diagram related to seed size involved in this study. The latest study found that KIX8/9 and PPD1/2 led to larger seeds by increasing cell proliferation and cell elongation, suggesting that the KIX-PPD-MYC-GIF1 pathway has a role in controlling seed size (Liu et al., 2020). Our real-time qPCR data revealed that these nine genes directly related to endosperm growth, G-protein signaling, auxin metabolic pathways and transcription factors controlling seed size were differentially regulated by TDZ in buds and flowers of *B. napus* at early developmental stages. **Figure 7B** is a schematic diagram of the simulation mechanism explaining how TDZ regulates the seed size of *B. napus*. Specifically, three genes (*AGB1*, *AGG3*, and *RGA1*) were identified in G-protein signaling, two genes (*BnARF18* and *ARF2*) in auxin metabolic pathway, three genes (*ANT*, *AP2*, and *GS2*) in transcriptional regulatory factors and an endosperm growth-related gene (*ABI5*). In order to more intuitively reflect the difference in the overall expression level of each gene between different tissues, we summed up the expression levels of genes located on different chromosomes. **Figure 8** showed the trend of the overall expression of each gene in buds and flowers after different concentrations of TDZ treatment. It can be seen from the figure that the change trend of the overall expression level of a single gene in different tissues is the same as the change trend of the expression level of the gene located on different chromosomes. Meanwhile, the expression patterns of these genes were similar in the buds and flowers. Exogenous application with TDZ in bud down-regulated the expression of auxin metabolic pathway genes, such as *ARF2* and *BnARF18*. Schruff et al. (2006) reported

that *ARF2* was a suppressor of cell division, tissue development and organ growth, and it determined seed size and weight by regulating integument growth and development. Subsequently, *ARF2* was shown to negatively regulate the expression of the homologous structural domain gene *HB33*, thereby controlling ABA-mediated primary root growth and seed germination (Wang et al., 2011). A recent study demonstrated that *ARF2* could negatively regulate the expression of *ANT* after binding to the *ANT* promoter region, which in turn regulated seed weight and drought resistance by promoting cell proliferation (Meng et al., 2015). In addition, *ARF18* was showed as a transcriptional repressor, which can activate downstream auxin genes to increase cell size, thereby regulating SL and SW (Liu J. et al., 2015). Our results also suggested that the expression levels of several genes involved in endosperm growth and G-protein signaling were down-regulated in response to TDZ treatment, such as *ABI5*, *AP2,* and *AGB1* (**Figure 7**). *ABI5* has the effect of attenuating or terminating ABA signaling during seed germination, hence *ABI5* can regulate seed dormancy, germination and seedling growth (Lopez-Molina et al., 2001). In *Arabidopsis*, ABA downstream signaling component *ABI5* have been proposed to decrease the expression of *SHB1* by combining with the *SHB1* promoter region during early seed development, which caused the seed size increased in abi5 (Cheng et al., 2014). The Gβ subunits in the heterotrimeric G protein complex play important roles in seed germination, seed size, stress adaptation, and stomatal opening and closing (Ullah et al., 2002; Xu et al., 2015). *AGB1* has been shown previously to function as a negative regulator in ABA responses (Pandey et al., 2006). The plasticity of fruit number, seed number per fruit and total seed yield were reduced in the agb1 mutant compared to Col (Nilson and Assmann, 2010). Interestingly, recent researches indicated that the transcription factor AP2/ERF-domain family gene *SlDREB3* also negatively regulated ABA responses in tomato and its over-expression reduced final fruit size (Gupta et al., 2022). In *Arabidopsis*, *AP2* was shown to be a negative regulator of seed size and weight. When *AP2* gene expression decreased, *ap2* mutants produced abnormally shaped large seeds in which not only the seed size and weight increased, but also the number and size of embryo cells increased simultaneously due to endosperm cellularization and outward growth of the central endosperm vacuole (Jofuku et al., 2005; Ohto et al., 2005, 2009). Thus, *AP2* has a negative regulatory effect on seed size and weight. Additionally, *AP2* genes have been found to have similar effects in other plant species, such as Larix Li et al. (2013) and *Aechmea fasciata* (Lei et al., 2019). Two G protein signaling-related genes and two transcriptional regulatory factors, such as *AGG3*, *RGA1*, *ANT*, *GS2* were up-regulated by TDZ treatment. Prior research in rice highlighted the importance of *RGA1* in dwarfism and set small seed, and this study identified *RGA1* as a positive regulator of cellular proliferation and dwarfism in d1 was caused by a decrease in the number of cells (Izawa et al., 2010). Consistent with previous studies, which demonstrated a positive regulatory role for *AGG3* in the control of seed and organ size in *Arabidopsis*, *AGG3* overexpression resulted in increased seed size, fruit length, and number of seeds per fruit. Instead, *AGG3* loss-of-function mutants had smaller seeds and reduced number of seeds per fruit (Chakravorty et al., 2011; Li et al., 2012; Roy Choudhury et al., 2014). The *ANT* gene is a key transcription factor for ovule development and organ growth in *Arabidopsis*. It has been proved that after overexpression of the *ANT* gene driven by the 35s promoter, ant mutants exhibit a larger seed phenotype due to cell expansion (Mizukami and Fischer, 2000). Recently, several researches have reported that when *GS2*/*OsGRF4* directly interacted with the transcriptional co-activator *OsGIF1*, the elevated expression levels of both resulted in increased cell size and number, which positively regulated grain size and grain weight, and significantly improved yield (Che et al., 2016; Duan et al., 2016; Li et al., 2016).

Conclusion

Thidiazuron treatment could increase the seed diameter and silique length of *B. napus* to varying degrees and greatly improve rapeseed yield. TDZ increased seed size by promoting cell elongation, cell division and regulating gene expression in several signaling pathways associated with maternal tissue growth. This study preliminarily explored the mechanism of TDZ treatment on the seed size of *B. napus* and provided an important reference for improving rapeseed yield.

Data availability statement

The original contributions presented in this study are included in the article/**Supplementary material**, further inquiries can be directed to the corresponding authors.

Author contributions

BX, JD, and XZ: designed the research. LZ: conducted the research and analyzed the data. JX: supplied the materials. LZ, LX, BX, JX, JD, and XZ: wrote and edited the manuscript. All authors scrutinized and corrected the manuscript.

Funding

This research was supported by the National Key R&D Program of China (2017YFD0101700), the Hubei Key Laboratory of Food Crop Germplasm and Genetic Improvement (2018lzjj11), and Open Project Fund of Henan

Key Laboratory of Water Pollution Control and Rehabilitation Technology (CJSP2021010).

Acknowledgments

Great appreciations are given to the editor and reviewers' critical comments on the improvement of the manuscript.

Conflict of interest

The authors declare that the research was conducted in the absence of any commercial or financial relationships that could be construed as a potential conflict of interest.

Publisher's note

Supplementary material

The Supplementary Material for this article can be found online at: https://www.frontiersin.org/articles/10.3389/fpls.2022.998698/full#supplementary-material

References

Biswal, A. K., Wu, T. Y., Urano, D., Pelissier, R., Morel, J. B., Jones, A. M., et al. (2022). Novel mutant alleles reveal a role of the extra-large G protein in rice grain filling, panicle architecture, plant growth, and disease resistance. *Front. Plant Sci.* 12:15. doi: 10.3389/fpls.2021.782960

Butruille, D. V., Guries, R. P., and Osborn, T. C. (1999). Linkage analysis of molecular markers and quantitative trait loci in populations of inbred backcross lines of *Brassica napus* L. *Genetics* 153, 949–964. doi: 10.1093/genetics/153.2.949

Carra, B., Fachinello, J. C., de Abreu, E. S., Pasa, M. D., Spagnol, D., Giovanaz, M. A., et al. (2017). Control of the vegetative growth of 'Shinseiki' pear trees by prohexadione calcium and root pruning. *Pesqui. Agropecu. Bras.* 52, 177–185. doi: 10.1590/s0100-204x2017000300005

Carra, B., Pasa, M. S., Abreu, E. S., Dini, M., Pasa, C. P., Ciotta, M. N., et al. (2021). Plant growth regulators to increase fruit set and yield of 'Rocha' pear trees in Southern Brazil. *An. Acad. Bras. Cienc.* 93:e20180680. doi: 10.1590/0001-3765202120180860

Celikel, F. G., Zhang, Q. C., Zhang, Y. L., Reid, M. S., and Jiang, C. Z. (2021). A Cytokinin Analog Thidiazuron Suppresses Shoot Growth in Potted Rose Plants via the Gibberellic Acid Pathway. *Front. Plant Sci.* 12:639717. doi: 10.3389/fpls.2021.639717

Chakravorty, D., Trusov, Y., Zhang, W., Acharya, B. R., Sheahan, M. B., McCurdy, D. W., et al. (2011). An atypical heterotrimeric G-protein γ-subunit is involved in guard cell K^+-channel regulation and morphological development in *Arabidopsis thaliana*. *Plant J.* 67, 840–851. doi: 10.1111/j.1365-313X.2011.04638.x

Chang, E. H., Jung, S. M., Hur, Y. Y., Nam, J. C., and Choi, I. M. (2018). Characteristics of the fruit quality and volatile compounds of 'Cheongsoo' grape by treatment with different plant growth regulators. *Hortic. Sci. Technol.* 36, 326–336. doi: 10.12972/kjhst.20180032

Che, R. H., Tong, H. N., Shi, B. H., Liu, Y. Q., Fang, S. R., Liu, D. P., et al. (2016). Control of grain size and rice yield by GL2-mediated brassinosteroid responses. *Nat. Plants* 2:15195. doi: 10.1038/nplants2016.2

Chen, W., Zhang, Y., Liu, X. P., Chen, B. Y., Tu, J. X., and Fu, T. D. (2007). Detection of QTL for six yield-related traits in oilseed rape (*Brassica napus*) using DH and immortalized F-2 populations. *Theor. Appl. Genet.* 115, 849–858. doi: 10.1007/s00122-007-0613-2

Cheng, Z. J., Zhao, X. Y., Shao, X. X., Wang, F., Zhou, C., Liu, Y. G., et al. (2014). Abscisic acid regulates early seed development in *Arabidopsis* by ABI5-mediated transcription of short hypocotyl under blue1. *Plant Cell* 26, 1053–1068. doi: 10.1105/tpc.113.121566

Du, M. W., Li, Y., Tian, X. L., Duan, L. S., Zhang, M. C., Tan, W. M., et al. (2014). The phytotoxin coronatine induces abscission-related gene expression and boll ripening during defoliation of cotton. *PLoS One* 9:e97652. doi: 10.1371/journal.pone.0097652

Duan, P. G., Ni, S., Wang, J. M., Zhang, B. L., Xu, R., Wang, Y. X., et al. (2016). Regulation of OsGRF4 by OsmiR396 controls grain size and yield in rice. *Nat. Plants* 2:15203. doi: 10.1038/nplants.2015.203

Famiani, F., Battistelli, A., Moscatello, S., Boco, M., and Antognozzi, E. (1999). Thidiazuron affects fruit growth, ripening and quality of *Actinidia deliciosa*. *J. Hortic. Sci. Biotechnol.* 74, 375–380. doi: 10.1080/14620316.1999.11511124

Famiani, F., Battistelli, A., Moscatello, S., Boco, M., Gardi, T., Proietti, S., et al. (2002). Thidiazuron increases current-year fruit size and production in *Actinidia deliciosa* without decreasing return bloom. *J. Hortic. Sci. Biotechnol.* 77, 116–119. doi: 10.1080/14620316.2002.11511466

Greene, D. W. (1995). Thidiazuron effects on fruit-set, fruit-quality, and return bloom of apples. *Hortscience* 30, 1238–1240. doi: 10.21273/hortsci.30.6.1238

Guo, B., Abbasi, B. H., Zeb, A., Xu, L. L., and Wei, Y. H. (2011). Thidiazuron: A multi-dimensional plant growth regulator. *Afr. J. Biotechnol.* 10, 8984–9000. doi: 10.5897/AJB11.636

Guo, Y., Gao, M. L., Liang, X. X., Xu, M., Liu, X. S., Zhang, Y. L., et al. (2020). Quantitative trait loci for seed size variation in cucurbits-a review. *Front. Plant Sci.* 11:304. doi: 10.3389/fpls.2020.00304

Gupta, A., Upadhyay, R. K., Prabhakar, R., Tiwari, N., Garg, R., Sane, V. A., et al. (2022). SlDREB3, a negative regulator of ABA responses, controls seed germination, fruit size and the onset of ripening in tomato. *Plant Sci.* 319:111249. doi: 10.1016/j.plantsci.2022.111249

Hawerroth, F. J., Herter, F. G., Fachinello, J. C., Petri, J. L., Prezotto, M. E., Haas, L. B., et al. (2011). Fruit production increase in Asian pear trees by use of plant growth regulators. *Cienc. Rural* 41, 1750–1754. doi: 10.1590/s0103-84782011001000012

Hu, J., Wang, Y. X., Fang, Y. X., Zeng, L. J., Xu, J., Yu, H. P., et al. (2015). A rare allele of GS2 enhances grain size and grain yield in Rice. *Mol. Plant* 8, 1455–1465. doi: 10.1016/j.molp.2015.07.002

Huang, L., Yang, S. X., Wu, L. Y., Xin, Y., Song, J. K., Wang, L., et al. (2022). Genome-wide analysis of the GW2-like genes in gossypium and functional characterization of the seed size effect of GhGW2-2D. *Front. Plant Sci.* 13:860922. doi: 10.3389/fpls.2022.860922

Ishimaru, K., Hirotsu, N., Madoka, Y., Murakami, N., Hara, N., Onodera, H., et al. (2013). Loss of function of the IAA-glucose hydrolase gene TGW6 enhances rice grain weight and increases yield. *Nat. Genet.* 45, 707–711. doi: 10.1038/ng.2612

Itai, A., Tanabe, K., Tamura, F., Susaki, S., Yonemori, K., and Sugiura, A. (1995). Synthetic cytokinins control persimmon fruit shape, size and quality. *J. Hortic. Sci.* 70, 867–873. doi: 10.1080/14620316.1995.11515362

Izawa, Y., Takayanagi, Y., Inaba, N., Abe, Y., Minami, M., Fujisawa, Y., et al. (2010). Function and expression pattern of the alpha subunit of the heterotrimeric G protein in rice. *Plant Cell Physiol.* 51, 271–281. doi: 10.1093/pcp/pcp186

Jiang, W. B., Huang, H. Y., Hu, Y. W., Zhu, S. W., Wang, Z. Y., and Lin, W. H. (2013). Brassinosteroid regulates seed size and shape in *Arabidopsis*. *Plant Physiol.* 162, 1965–1977. doi: 10.1104/pp.113.217703

Jiao, D. Y., Xiang, M. H., Li, W. G., and Cai, Z. Q. (2012). Dry-season irrigation and fertilisation affect the growth, reproduction, and seed traits of *Plukenetia*

volubilis L. plants in a tropical region. *J. Hortic. Sci. Biotechnol.* 87, 311–316. doi: 10.1080/14620316.2012.11512870

Jofuku, K. D., Den Boer, B., Van Montagu, M., and Okamuro, J. K. (1994). Control of *Arabidopsis* flower and seed development by the homeotic gene APETALA2. *Plant Cell* 6, 1211–1225. doi: 10.1105/tpc.6.9.1211

Jofuku, K. D., Omidyar, P. K., Gee, Z., and Okamuro, J. K. (2005). Control of seed mass and seed yield by the floral homeotic gene APETALA2. *Proc. Natl. Acad. Sci. U.S.A.* 102, 3117–3122. doi: 10.1073/pnas.0409893102

Johnson, C. S., Kolevski, B., and Smyth, D. R. (2002). Transparent testa glabra2, a trichome and seed coat development gene of *Arabidopsis*, encodes a WRKY transcription factor. *Plant Cell* 14, 1359–1375. doi: 10.1105/tpc.001404

Johnston, C. A., Taylor, J. P., Gao, Y., Kimple, A. J., Grigston, J. C., Chen, J. G., et al. (2007). GTPase acceleration as the rate-limiting step in *Arabidopsis* G protein-coupled sugar signaling. *Proc. Natl. Acad. Sci. U.S.A.* 104, 17317–17322. doi: 10.1073/pnas.0704751104

Kimura, P. H., Okamoto, G., and Hirano, K. (1996). Effects of gibberellic acid and streptomycin on pollen germination and ovule and seed development in Muscat Bailey A. *Am. J. Enol. Vitic.* 47, 152–156. doi: 10.1007/BF00223387

Kim, Y., Kim, S. H., Shin, D. M., and Kim, S. H. (2021). Atbs1-interacting factor 2 negatively modulates pollen production and seed formation in *Arabidopsis*. *Front. Plant Sci.* 12:704958. doi: 10.3389/fpls.2021.704958

Klucher, K. M., Chow, H., Reiser, L., and Fischer, R. L. (1996). The AINTEGUMENTA gene of *Arabidopsis* required for ovule and female gametophyte development is related to the floral homeotic gene APETALA2. *Plant Cell* 8, 137–153. doi: 10.1105/tpc.8.2.137

Krizek, B. A. (2003). AINTEGUMENTA utilizes a mode of DNA recognition distinct from that used by proteins containing a single AP2 domain. *Nucleic Acids Res.* 31, 1859–1868. doi: 10.1093/nar/gkg292

Lee, B., Kwon, Y., Park, Y., and Park, H. S. (2013). Effect of GA_3 and thidiazuron on seedlessness and fruit quality of 'Kyoho' grapes. *Korean J. Hortic. Sci. Technol.* 31, 135–140. doi: 10.7235/hort.2013.12065

Lei, M., Li, Z. Y., Wang, J. B., Fu, Y. L., and Xu, L. (2019). Ectopic expression of the *Aechmea fasciata* APETALA2 gene AfAP2-2 reduces seed size and delays flowering in *Arabidopsis*. *Plant Physiol. Biochem.* 139, 642–650. doi: 10.1016/j.plaphy.2019.03.034

Li, A., Zhou, Y. A., Jin, C., Song, W. Q., Chen, C. B., and Wang, C. G. (2013). LaAP2L1, a heterosis-associated AP2/EREBP transcription factor of Larix, increases organ size and final biomass by affecting cell proliferation in *Arabidopsis*. *Plant Cell Physiol.* 54, 1822–1836. doi: 10.1093/pcp/pct124

Li, N., and Li, Y. (2016). Signaling pathways of seed size control in plants. *Curr. Opin. Plant Biol.* 33, 23–32. doi: 10.1016/j.pbi.2016.05.008

Li, N., Xu, R., and Li, Y. H. (2019). "Molecular Networks of Seed Size Control in Plants," in *Annual Review of Plant Biology*, ed. S. S. Merchant (Palo Alto: Annual Reviews), 435–463. 095851 doi: 10.1146/annurev-arplant-050718-

Li, S., Liu, Y., Zheng, L., Chen, L., Li, N., Corke, F., et al. (2012). The plant-specific G protein γ subunit AGG3 influences organ size and shape in *Arabidopsis thaliana*. *New Phytol.* 194, 690–703. doi: 10.1111/j.1469-8137.2012.04083.x

Li, S. C., Gao, F. Y., Xie, K. L., Zeng, X. H., Cao, Y., Zeng, J., et al. (2016). The OsmiR396c-OsGRF4-OsGIF1 regulatory module determines grain size and yield in rice. *Plant Biotechnol. J.* 14, 2134–2146. doi: 10.1111/pbi.12569

Liu, J., Hua, W., Hu, Z. Y., Yang, H. L., Zhang, L., Li, R. J., et al. (2015). Natural variation in ARF18 gene simultaneously affects seed weight and silique length in polyploid rapeseed. *Proc. Natl. Acad. Sci. U.S.A.* 112:E5123–E5132. doi: 10.1073/pnas.1502160112

Liu, L. C., Tong, H. N., Xiao, Y. H., Che, R. H., Xu, F., Hu, B., et al. (2015). Activation of Big Grain1 significantly improves grain size by regulating auxin transport in rice (vol 112, pg 11102, 2015). *Proc. Natl. Acad. Sci. U.S.A.* 112:E5446–E5446. doi: 10.1073/pnas.1517098112

Liu, Z., Li, N., Zhang, Y., and Li, Y. (2020). Transcriptional repression of GIF1 by the KIX-PPD-MYC repressor complex controls seed size in *Arabidopsis*. *Nat. Commun.* 11:1846. doi: 10.1038/s41467-020-15603-3

Livak, K. J., and Schmittgen, T. D. (2001). Analysis of relative gene expression data using real-time quantitative PCR and the $2^{-\Delta\Delta CT}$ method. *Methods* 25, 402–408. doi: 10.1006/meth.2001.1262

Lopez-Molina, L., Mongrand, S., and Chua, N. H. (2001). A postgermination developmental arrest checkpoint is mediated by abscisic acid and requires the AB15 transcription factor in *Arabidopsis*. *Proc. Natl. Acad. Sci. U.S.A.* 98, 4782–4787. doi: 10.1073/pnas.081594298

Meng, L. S., Wang, Z. B., Yao, S. Q., and Liu, A. Z. (2015). The ARF2-ANT-COR15A gene cascade regulates ABA-signaling-mediated resistance of large seeds to drought in *Arabidopsis*. *J. Cell Sci.* 128, 3922–3932. doi: 10.1242/jcs.171207

Meng, R., Chen, T. H. H., Finn, C. E., and Li, Y. (2004). Improving In Vitro Plant Regeneration from Leaf and Petiole Explants of 'Marion' Blackberry. *HortScience* 39, 316–320. doi: 10.21273/hortsci.39.2.316

Miao, C. B., Wang, D., He, R. Q., Liu, S. K., and Zhu, J. K. (2020). Mutations in MIR396e and MIR396f increase grain size and modulate shoot architecture in rice. *Plant Biotechnol. J.* 18, 491–501. doi: 10.1111/pbi.13214

Mizukami, Y., and Fischer, R. L. (2000). Plant organ size control: AINTEGUMENTA regulates growth and cell numbers during organogenesis. *Proc. Natl. Acad. Sci. U.S.A.* 97, 942–947. doi: 10.1073/pnas.97.2.942

Nilson, S. E., and Assmann, S. M. (2010). Heterotrimeric G proteins regulate reproductive trait plasticity in response to water availability. *New Phytol.* 185, 734–746. doi: 10.1111/j.1469-8137.2009.03120.x

Ohto, M., Fischer, R. L., Goldberg, R. B., Nakamura, K., and Harada, J. J. (2005). Control of seed mass by APETALA2. *Proc. Natl. Acad. Sci. U.S.A.* 102, 3123–3128. doi: 10.1073/pnas.0409858102

Ohto, M. A., Floyd, S. K., Fischer, R. L., Goldberg, R. B., and Harada, J. J. (2009). Effects of APETALA2 on embryo, endosperm, and seed coat development determine seed size in *Arabidopsis*. *Sex. Plant Reprod.* 22, 277–289. doi: 10.1007/s00497-009-0116-1

Orsi, C. H., and Tanksley, S. D. (2009). Natural variation in an ABC transporter gene associated with seed size evolution in tomato species. *PLoS Genet.* 5:e1000347. doi: 10.1371/journal.pgen.1000347

Ozer, H. (2003). Sowing date and nitrogen rate effects on growth, yield and yield components of two summer rapeseed cultivars. *Eur. J. Agron.* 19, 453–463. doi: 10.1016/s1161-0301(02)00136-3

Pandey, S., Chen, J.-G., Jones, A. M., and Assmann, S. M. (2006). G-protein complex mutants are hypersensitive to abscisic acid regulation of germination and postgermination development. *Plant Physiol.* 141, 243–256. doi: 10.1104/pp.106.079038

Pasa, M. S., Da Silva, C. P., Carra, B., Brighenti, A. F., De Souza, A. L. K., and Petri, J. L. (2017). Thidiazuron (TDZ) increases fruit set and yield of 'Hosui' and 'Packham's Triumph' pear trees. *An. Acad. Bras. Cienc.* 89, 3103–3110. doi: 10.1590/0001-3765201720170644

Petri, J. L., Schuck, E., and Leite, G. B. (2001). Effects of thidiazuron (TDZ) on fruiting of temperate tree fruits. *Rev. Bras. Frutic.* 23, 513–517. doi: 10.1590/S0100-29452001000300012

Reynolds, A. G., Wardle, D. A., Zurowski, C., and Looney, N. E. (1992). Phenylureas CPPU and thidiazuron affect yield components, fruit composition, and storage potential of four seedless grape selections. *J. Am. Soc. Hortic. Sci.* 117, 85–89. doi: 10.21273/jashs.117.1.85

Roy Choudhury, S., Riesselman, A. J., and Pandey, S. (2014). Constitutive or seed-specific overexpression of *Arabidopsis* G-protein γ subunit 3 (AGG3) results in increased seed and oil production and improved stress tolerance in *Camelina sativa*. *Plant Biotechnol. J.* 12, 49–59. doi: 10.1111/pbi.12115

Schruff, M. C., Spielman, M., Tiwari, S., Adams, S., Fenby, N., and Scott, R. J. (2006). The auxin response factor 2 gene of *Arabidopsis* links auxin signaling, cell division, and the size of seeds and other organs. *Development* 133, 251–261. doi: 10.1242/dev.02194

Sharaf, A. R. N., Hamidoghli, Y., and Zakizadeh, H. (2011). In vitro seed germination and micropropagation of primrose (*Primula heterochroma* Stapf.) an endemic endangered Iranian species via shoot tip explants. *Hortic. Environ. Biotechnol.* 52, 298–302. doi: 10.1007/s13580-011-0129-1

Shargal, A., Golobovich, S., Yablovich, Z., Shlizerman, L. A., Stern, R. A., Grafi, G., et al. (2006). Synthetic cytokinins extend the phase of division of parenchyma cells in developing pear (*Pyrus communis* L.) fruits. *J. Hortic. Sci. Biotechnol.* 81, 915–920. doi: 10.1080/14620316.2006.11512159

Shi, J. Q., Li, R. Y., Qiu, D., Jiang, C. C., Long, Y., Morgan, C., et al. (2009). Unraveling the complex trait of crop yield with quantitative trait loci mapping in *Brassica napus*. *Genetics* 182, 851–861. doi: 10.1534/genetics.109.101642

Stateczny, D., Oppenheimer, J., and Bommert, P. (2016). G protein signaling in plants: Minus times minus equals plus. *Curr. Opin. Plant Biol.* 34, 127–135. doi: 10.1016/j.pbi.2016.11.001

Stern, R. A., Shargal, A., and Flaishman, M. A. (2003). Thidiazuron increases fruit size of 'Spadona' and 'Coscia' pear (*Pyrus communis* L.). *J. Hortic. Sci. Biotechnol.* 78, 51–55. doi: 10.1080/14620316.2003.11511586

Ullah, H., Chen, J. G., Wang, S. C., and Jones, A. M. (2002). Role of a heterotrimeric G protein in regulation of *Arabidopsis* seed germination. *Plant Physiol.* 129, 897–907. doi: 10.1104/pp.005017

Urano, D., and Jones, A. M. (2014). Heterotrimeric G protein–coupled signaling in plants. *Annu. Rev. Plant Biol.* 65, 365–384. doi: 10.1146/annurev-arplant-050213-040133

van der Knaap, E., Kim, J. H., and Kende, H. (2000). A novel gibberellin-induced gene from rice and its potential regulatory role in stem growth. *Plant Physiol*122, 695–704. doi: 10.1104/pp.122.3.695

Wang, L., Hua, D. P., He, J. N., Duan, Y., Chen, Z. Z., Hong, X. H., et al. (2011). Auxin Response Factor2 (ARF2) and its regulated homeodomain gene HB33 mediate abscisic acid response in *Arabidopsis*. *PLoS Genet.* 7:e1002172. doi: 10.1371/journal.pgen.1002172

Wang, W., Khalil-Ur-Rehman, M., Wei, L. L., Nieuwenhuizen, N. J., Zheng, H., and Tao, J. M. (2020). Effect of thidiazuron on terpene volatile constituents and terpenoid biosynthesis pathway gene expression of Shine Muscat (*Vitis labrusca* x *V. vinifera*) grape berries. *Molecules* 25:14. doi: 10.3390/molecules25112578

Weijers, D., and Friml, J. (2009). SnapShot: Auxin signaling and transport. *Cell* 136, 1172–1172.e1. doi: 10.1016/j.cell.2009.03.009

Western, T. L., Burn, J., Tan, W. L., Skinner, D. J., Martin-McCaffrey, L., Moffatt, B. A., et al. (2001). Isolation and characterization of mutants defective in seed coat mucilage secretory cell development in *Arabidopsis*. *Plant Physiol.* 127, 998–1011. doi: 10.1104/pp.127.3.998

Xu, D.-B., Chen, M., Ma, Y.-N., Xu, Z.-S., Li, L.-C., Chen, Y.-F., et al. (2015). A G-protein β subunit, AGB1, negatively regulates the ABA response and drought tolerance by down-regulating AtMPK6-related pathway in *Arabidopsis*. *PLoS One* 10:e0116385. doi: 10.1371/journal.pone.0116385

frontiers | Frontiers in Plant Science

TYPE Original Research
PUBLISHED 15 September 2022
DOI 10.3389/fpls.2022.970716

OPEN ACCESS

EDITED BY
Cunmin Qu,
Southwest University, China

REVIEWED BY
Yujie Fang,
Yangzhou University, China
Zhang Zhen Qian,
Hunan Agricultural University, China
Jiaqin Shi,
Oil Crops Research Institute (CAAS), China

*CORRESPONDENCE
Yun Zhao
zhaoyun@scu.edu.cn
Yongjun Lin
yongjunlin@mail.hzau.edu.cn
Jun Jiang
jiangjun227@163.com

†These authors have contributed equally to this work

SPECIALTY SECTION
This article was submitted to Plant Pathogen Interactions, a section of the journal Frontiers in Plant Science

RECEIVED 16 June 2022
ACCEPTED 06 July 2022
PUBLISHED 15 September 2022

CITATION
Yin M, Wang R, Li S, Luo M, Wei W, Wang M, Jiang J, Lin Y and Zhao Y (2022) High *Sclerotinia sclerotiorum* resistance in rapeseed plant has been achieved by *OsPGIP6*. *Front. Plant Sci.* 13:970716. doi: 10.3389/fpls.2022.970716

High *Sclerotinia sclerotiorum* resistance in rapeseed plant has been achieved by *OsPGIP6*

Meng Yin[1†], Rui Wang[1†], Shi Li[1], Mei Luo[1], Wei Wei[1], Maolin Wang[1], Jun Jiang[2*], Yongjun Lin[3*] and Yun Zhao[1*]

[1]Key Laboratory of Bio-Resource and Eco-Environment of Ministry of Education, College of Life Sciences, Sichuan University, Chengdu, China, [2]Institute of Crop Research, Sichuan Academy of Agricultural Sciences, Chengdu, China, [3]National Key Laboratory of Crop Genetic Improvement and National Centre of Plant Gene Research, Huazhong Agricultural University, Wuhan, China

Sclerotinia sclerotiorum, a worldwide distributed fungal pathogen, causes serious adverse effects on the yield and seed quality of rapeseed. Polygalacturonase-inhibiting proteins (PGIPs) can protect the cell wall from degradation by pathogen-secreted polygalacturonases (PGs). The present study found several PGIPs from *Oryza sativa*, especially OsPGIP6 and 3 have much higher inhibitory activities to SsPGs than BnPGIP2 from *Brassica napus*. Among them, *OsPGIP1, 4, 6* can significantly elevate the resistance of transgenic Arabidopsis to *S. sclerotiorum*. Subsequently, *OsPGIP1, 3, 4, 6* were subjected to SSR resistance assay in transgenic rapeseed plants. Among which, *OsPGIP6* showed the highest resistance to *S. sclerotiorum*. At 48 h after detached leaves inoculation, the lesion area of OE-OsPGIP6 rapeseed plants is only 17.93% of the non-transgenic line, and 22.17, 21.32, 52.78, 56.47%, compared to OE-BnPGIP2, OE-OsPGIP1, OE-OsPGIP2, OE-OsPGIP4, respectively. Furthermore, the lesion area of OE-OsPGIP6 reached 10.11% compared to WT at 72 hpi. Also, the lesion length on the stem of OE-OsPGIP6 plants was reduced by 36.83% compared to WT. These results reveal that *OsPGIP* family, especially *OsPGIP6*, has a great potential in rapeseed *S. sclerotiorum*-resistance breeding.

KEYWORDS

Sclerotinia sclerotiorum*, *Brassica napus*, PGIP, PG inhibitory activity, *Arabidopsis thaliana

Introduction

Sclerotinia sclerotiorum (Lib.) de Bary, one of the worldwide distributed necrotrophic fungal pathogens, can infect more than 400 plant species, including some important economic crops, such as rapeseed, soybean, sunflower, and so on, among which rapeseed (*Brassica napus* L.), as one of the most important oil crops worldwide, deserves great attention (Bolton et al., 2006). Studies show that Sclerotinia stem rot (SSR) caused by *S. sclerotiorum* can lead to severe yield loss,10%−70% yield loss per year, and results in low oil quality due to a decrease in oil content, erucic acid content, glucosinolate, and protein content. The *S. sclerotiorum* attack host during all growth stages especially in the flowering period, causing white watery lesions at the stem, siliques, and leaf,

which consequently affect the host physiological activities. For a long time, the obtained breeding materials were still compromised in further agricultural applications (Zhao and Wang, 2004; Liu et al., 2005; Mei et al., 2015). In addition, the pathogenesis mechanisms of SSR still remain elusive. Current research on the pathogenesis of SSR and the crop genetic improvement for SSR resistance mainly focuses on mining major genes associated with innate defense signaling pathways. Rice, as a typical model plant, have gained great attention, since it lives in high temperature and humidity and is susceptible to fungal infection. Therefore, the rice-derived resistance genes may have an important potential in fighting against fungal disease for other plants.

Till now, some breakthroughs have been made in the study of the pathogenicity and effector of *S. sclerotiorum*. Researchers proposed that the acidic environment rather than oxalic acid is the key factor in determining the virulence of *S. sclerotiorum*, namely PH-dependent theory (Liang et al., 2015; Xu et al., 2015, 2018). *S. sclerotiorum* can detoxify reactive oxygen species (ROS) by regulating the "copper ion import/transport" pathway. And the hosts competitively absorb copper ions in the lesion to restrict *S. sclerotiorum* (Dingid et al., 2020). In the face of the Brassicaceae plant's glucosinolate-myrosinase system, *S. sclerotiorum* metabolize isothiocyanates effectively *via* hydrolysis to amines that are not toxic to the fungus (Chen et al., 2020). In addition to the above studies, many other effectors involved in the pathogenicity of *S. sclerotiorum* have also been reported. For example, the SsCP1, a cerato-platanin protein, targeting host PR1 in apoplast facilitates the infection of *S. sclerotiorum* (Yang et al., 2018). The SsITL targets a chloroplast-localized calcium-sensing receptor (CAS) inhibiting SA accumulation during the early stage of infection and contributes to the virulence of *S. sclerotiorum* (Tang et al., 2020). The interaction between *S. sclerotiorum* and hosts remains to be further clarified.

It is well-known that during the early infection stage, *S. sclerotiorum* secretes a series of cell wall degrading enzymes (CWDEs) such as Polygalacturonases (PGs) to facilitate its colonization in the hosts. PGs can degrade the structural polysaccharides between the mesophytic layer and the primary cell wall of plants (Bolton et al., 2006). To fight against the PGs, hosts secrete polygalacturonase-inhibiting proteins (PGIPs) as the defender, which can specifically bind to the active site of PGs to inhibit their activities (Vorwerk et al., 2004; Shanmugam, 2005). Besides, PGIPs can attenuate the degradation of oligosaccharides which are able to elicit defense responses, and thus prolong the protection of the plant against pathogens (Mishra et al., 2012).

PGIPs have been widely studied with a transgenic approach in many species including Arabidopsis (Ferrari et al., 2012), rice (Lu et al., 2012; Wang et al., 2015; Feng et al., 2016), wheat (Janni et al., 2013), tobacco (Joubert et al., 2006), rapeseed (HuangFu et al., 2014; Wang et al., 2018), apple (Oelofse et al., 2006), cabbage (Hwang et al., 2010), tomato (Schacht et al., 2011), kiwi (Szankowski et al., 2003), grapevine (Szankowski et al., 2003; Richter et al., 2006; Nguema-Ona et al., 2013; Zhang et al., 2021), mulberry (Hu et al., 2012), and mungbean (Chotechung et al., 2016). The results suggest that *PGIPs* play crucial roles in plant fungi resistance. Therefore, *PGIPs* are considered effective candidate genes against *S. sclerotiorum*. Rice is an important crop as well as a model plant around the world. It is worth noting that rice is often cultivated in high-temperature and high-humidity environments, which makes it easier to confront with fungi. However, few studies have been carried out to discover and identify gene resources in rice that fight against fungal disease for other crops, such as oilseed rape. As for *OsPGIPs*, *OsPGIP1*, *OsPGIP2,* and *OsPGIP4* have been identified to be involved in the defense against sheath blight and bacterial leaf streak, respectively, in transgenic plants (Wang et al., 2015; Feng et al., 2016). And another research showed that *OsPGIP2* confers *S. sclerotiorum* resistance in *B. napus* through increased activation of defense mechanisms (Wang et al., 2018). Therefore, researchers have proposed that increasing the expression of *OsPGIPs* by transgenic technology might correspondingly increase the resistance to pathogens in transgenic lines.

In the present study, five *OsPGIPs* (*OsPGIP1*, *OsPGIP2*, *OsPGIP3*, *OsPGIP4, OsPGIP6*) and *BnPGIP2* were functionally identified for their resistance against *S. sclerotiorum* both *in vitro* and *in vivo*. OsPGIPs showed obvious inhibitory activities toward PGs from *S. sclerotiorum*, and remarkably OsPGIP6 and OsPGIP3 exhibited high-level inhibitory activities. The results of pathogenicity assays showed that overexpressing *OsPGIP2*, *OsPGIP3*, *OsPGIP4,* and *OsPGIP6* in rapeseed plants conferred significantly elevated resistance to *S. sclerotiorum*, and the *S. sclerotiorum* resistances were consistent with the SsPGs inhibitory activities. Among these genes, *OsPGIP6* showed the highest resistance to *S. sclerotiorum* in both pathogenicity assays and PGIP activity assays, suggesting their potential values in crop breeding for *S. sclerotiorum* resistance, and a batch of high-quality transgenic resistance materials represented by OE-OsPGIP6-3 have been screened in this study.

Materials and methods

Prokaryotic expression and western blot analysis

The total genomic DNA of Nipponbare and *B. napus* was used as a template to amplify *OsPGIP1*, *OsPGIP2*, *OsPGIP3*, *OsPGIP4*, *OsPGIP6,* and *BnPGIP2* (accession numbers: AM180652, AM180653, AM180654, AM180655, NM-001068720, and EU142024, respectively) with specific primers. The PCR-generated fragments were inserted into T-vector and confirmed by sequencing with primers SP6 and

T7. Sequence-confirmed clones containing the target genes were digested by corresponding restriction enzymes and, respectively, cloned into prokaryotic expression vector pMAL-c2X.

Positive recombinant plasmids were, respectively, transformed into *E. coli transetta (DE3)*, and then grown at 37°C. When the cultures reached an OD_{600} of 0.5, protein expression was induced by the addition of IPTG to 0.1 mM at 16°C for 20 h. Cells collected by centrifugation at 12,000 rpm for 1 min at 4°C were re-suspended in pre-cooled Hepes buffer (pH 7.0) and then broken by ultrasonication and centrifuged at 12,000 rpm for 10 min at 4°C. The supernatant and sediment were analyzed by SDS-PAGE.

For Western blot analysis, soluble proteins with different OsPGIP-MBP or MBP control were, respectively, transferred to PVDF membranes after SDS-PAGE. Western blot analysis was performed with Anti-MBP Monoclonal Antibody (New England Biolabs, E8032, 1:10,000 working dilution) as the primary antibody and HRP-conjugated murine antibody (1:10,000 working dilution) as the second antibody according to standard protocols.

SsPGs inhibitory activity *in vitro*

PGs from *S. sclerotiorum* were isolated according to a previous study. PGIP activities were determined by reducing end-group analysis with the 3, 5-Dinitrosalicylic Acid (DNS) method (HuangFu et al., 2014). Ten units of PG from *S. sclerotiorum* (strain Ep-1PNA367) were mixed with different prokaryotically expressed proteins and were then incubated for 30 min at 25°C. Then the mixtures were, respectively, added with polygalacturonic acid (2.5 mg/ml) and incubated for 1 h at 30°C. The experiment was performed in triplicate.

OsPGIPs overexpression vector construction and *Agrobacterium*-mediated transformation

Each PGIP was amplified with specific primers. Sequence-confirmed clones containing the target genes were digested by corresponding restriction enzymes and, respectively, cloned into pCHF3. The positive clones were transformed into the *Agrobacterium tumefaciens* strain *GV3101* by electroporation. Subsequently, all the constructs were introduced into Arabidopsis (ecotype Columbia-0) and rapeseed (Westar) by *Agrobacterium*-mediated transformation (Chotechung et al., 2016). The transformation procedures were carried out as previously described (Janni et al., 2013). Subsequently, PCR analysis was performed to determine the presence of the target genes in transgenic plants with the specific primers 35S-F and 35S-R.

Gene expression analysis

The total RNAs of the transgenic plants were extracted and reverse-transcribed as described previously (Lu et al., 2012). Reverse transcription PCR (RT-PCR), as well as quantitative real-time PCR (qRT-PCR), were performed according to the same reference. The relative expression levels were determined using $2_{\mathrm{T}}^{-\Delta\Delta C}$ method (Schmittgen and Livak, 2001).

Leaf inoculation and detached stem inoculation

The PCR-positive transformed plants and untransformed controls were grown in the field to the 9–10 leaf stage. And pathogenicity assay was performed with detached leaves as previously described (HuangFu et al., 2014). The sixth-eighth leaf of each transgenic plant was removed for detached leaf inoculation with *S. sclerotiorum* in a greenhouse. Maintaining a relatively high humidity is a key factor in this experiment. The leaf lesions were taken pictures and measured at 48 h and 72 h post-inoculation (hpi). Each treatment was performed with three independent biological replicates. And lesion sizes were measured using Image J. Normally growing rapeseed were screened for stem inoculation of *S. scleroterum*. Agar discs (8 mm in diameter) were excised from the edges of growing fungal colonies, which were then affixed onto rapeseed stems 50 cm from the ground. Disease severity was assessed by measuring lesion length per pathogen infection spot at 120 hpi. Inoculation, observation, and disease resistance were only determined for plants located in the center of blocks to avoid marginal effects.

Results

OsPGIP6 and OsPGIP3 showed high inhibitory activities against SsPGs

In order to characterize inhibitory activities of OsPGIPs including OsPGIP1, OsPGIP2, OsPGIP3, OsPGIP4, and OsPGIP6 to PGs from *S. sclerotiorum*, the OsPGIPs:MBP in-frame gene fusions were, respectively, expressed in *E.coli* Rosetta (DE3) cell (Figure 1). The SDS-PAGE results suggested that highly active fusion protein could be obtained in the supernatant (Figure 1A). Western blot assay further proved the target proteins were successfully obtained (Figure 1B).

The PGs isolated from *S. sclerotiorum* were used for OsPGIPs activity assay. *In vitro* activity assays showed that SsPGs inhibitory activities of different PGIPs are diverse (Figure 1C). PG inhibitory rate of OsPGIP6 is high up to 26.56%, followed by OsPGIP3, OsPGIP2, OsPGIP4, OsPGIP1, and BnPGIP2 in 100 ng purified protein treatment. The PGs inhibitory rate of each PGIP has increased as the amount of

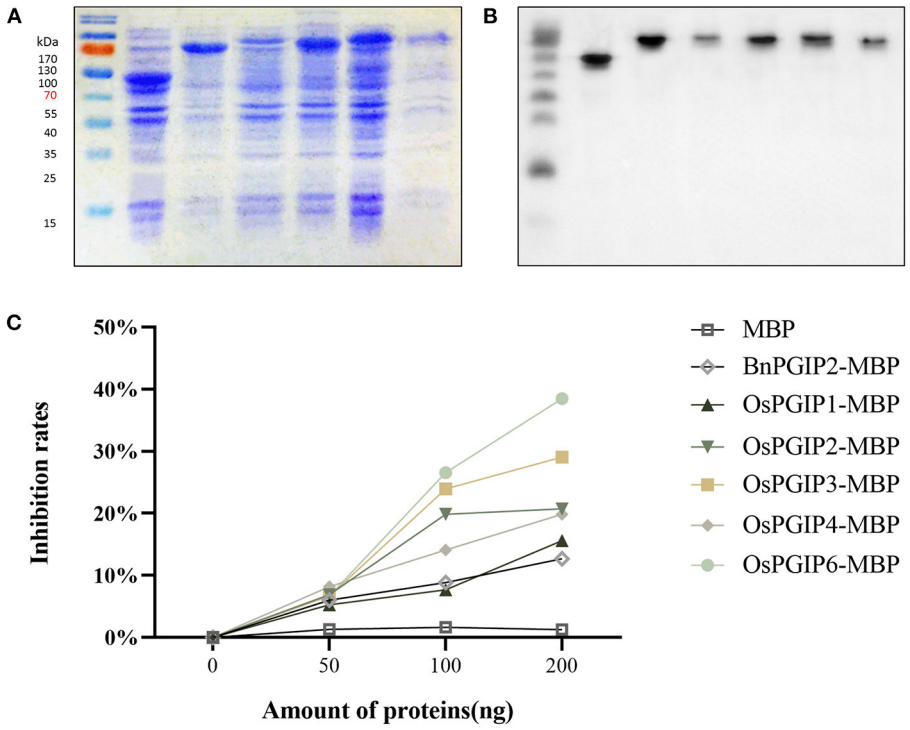

FIGURE 1
OsPGIPs show PG inhibitory activity of *S. sclerotiorum in vitro*. **(A)** Supernatant protein of prokaryotic expression. Expression of OsPGIPx in E. coli. M, marker; Lane 1, 20 h after IPTG inducement with MBP; Lane 2–6, 20 h after IPTG inducement with OsPGIP-MBP (Lane 2: OsPGIP1-MBP; Lane 3: OsPGIP2-MBP; Lane 4: OsPGIP3-MBP; Lane 5: OsPGIP4-MBP; Lane 6: OsPGIP6-MBP). **(B)** The corresponding immune signals of target proteins in **(A)** were generated by Western blot. Western blot was performed with Anti-MBP Monoclonal Antibody (1:10,000 working dilution) as primary antibody and HRP-conjugated murine antibody (1:10,000 working dilution) as second antibody. **(C)** OsPGIP activity assays. Variation of *S. sclerotiorum* PG activity with increasing amounts (0–200 ng) of different prokaryotically expressed proteins. Ten units of PG and 2.5 mg/ml polygalacturonic acid were used in the assays. *In vitro* inhibition of enzyme activity by purified PGIP protein equal the reduction percentage of D-GA in the reaction.

purified protein did. When elevated to 200 ng, the inhibition rates of different PGIPs were increased to 38.48, 29.06, 20.75, 19.86, 15.59, and 12.67%, respectively. The results indicate that the five OsPGIPs can significantly reduce the activity of PGs hydrolyzing polygalacturonic acid *in vitro*. Notably, OsPGIP6 performed outstandingly.

OEPGIP4, OEPGIP1, OEPGIP2, and OEPGIP6 exhibited significantly elevated resistance to *S. sclerotiorum* in Arabidopsis

Subsequently, the five OsPGIPs were subjected to in vivo resistance assay. Their expression levels in various tissues and organs throughout the entire life cycle of rice were shown in Figure 2A. The construct containing *OsPGIPs* under the control of *35S* promoter were, respectively, transformed into *Arabidopsis thaliana* (ecotype Columbia-0) (Figure 2B). Three overexpression transgenic lines of each OsPGIP were obtained after semi-quantitative PCR (Figure 2C) and quantitative real-time PCR (qRT-PCR) (Figure 2D) identification. The target gene was expressed at high levels in all transgenic lines, and we performed inoculation assay in these OE-*OsPGIPs* lines.

To determine the *in vivo* functions of the five *OsPGIPs* in *S. sclerotiorum*-plant interaction, the leaves detached from *OsPGIP* transgenic plants (OE-OsPGIPs) were, respectively, subjected to pathogenicity assay (Figure 3). 36 h after the inoculation of *S. sclerotiorum*, the infection phenotypes of the leaves were obviously diverse among different transgenic plants. The leaves of OE-OsPGIP1 and OE-OsPGIP4 showed the highest resistance to this pathogen; OE-OsPGIP2 and OE-OsPGIP6 also exhibited resistance, but it was lower than that of OE-OsPGIP1 and OE-OsPGIP4; while OE-OsPGIP3 showed no obviously elevated resistance. Furthermore, the sizes of the spreading lesions on the leaves from *OsPGIPx* transgenic plants (Figure 3B) indicated that their resistance to *S.*

10.3389/fpls.2022.970716

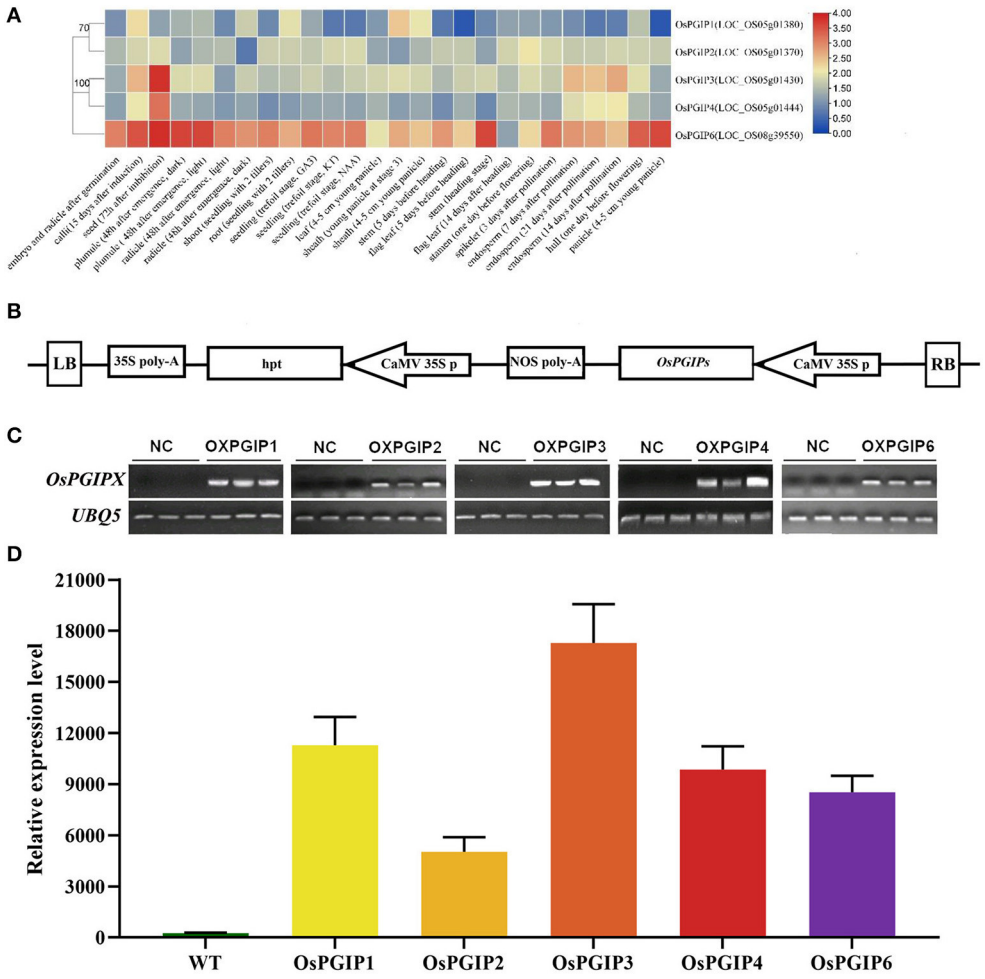

FIGURE 2
The expression analysis of OsPGIPs in rice and transgenic Arabidopsis plants. **(A)** The expression of OsPGIPs in various tissues and organs throughout the entire life cycle of rice. The color scale (representing |lg signal values|) is shown on the right. **(B)** Schemes of recombinant plasmids for overexpression. The expression level of each target gene was analyzed by RT-PCR **(C)** and qRT-PCR **(D)** with three independent transgenic lines. NC, negative control, Error bars indicate SE based on three independent biological replicates.

sclerotiorum followed the order of OE-OsPGIP4, OE-OsPGIP1, OE-OsPGIP2, OE-OsPGIP6, OE-OsPGIP3. Meanwhile, OE-OsPGIP4, OE-OsPGIP1, OE-OsPGIP2, and OE-OsPGIP6 showed significantly elevated resistance compared to the non-transgenic plants. These results also suggested that the *S. sclerotiorum* resistance of the transgenic plants overexpressing different *OsPGIPs* was in accordance with their inhibitory activities to PGs from this pathogen.

OsPGIPs overexpression conferred resistance to *S. sclerotiorum* in transgenic rapeseed plants

Quantitative real-time PCR (qRT-PCR) was used to detect the expression levels of target genes in transgenic rapeseed plants. Ten independent biological replicates in T_0 generation of each *PGIP* transgenic rapeseeds were subjected to expression analysis (Figure 4). Based on the results, five individual transgenic families of each *PGIP* with representative expression levels were selected for *S. sclerotiorum* resistance assay, their seed yields per plant were shown in Supplementary Figure 1.

The resistance of *S. sclerotiorum* was identified by leaf inoculation at the 9–10 leaf stage and detached stem inoculation at the flowering stage. The results told that 48 and 72 h after inoculation with *S. sclerotiorum*, the transgenic plant lesion areas were smaller than that of the wild-type material significantly. In the detached leaf inoculation, the transgenic lines, OE-OsPGIP6 and OE-OsPGIP3, showed a greatly improved resistance to SSR, especially OE-OsPGIP6. The lesion area of transgenic lines OE-OsPGIP6 and OE-OsPGIP3 are 43.63 and 57.64 mm^2, respectively, while the non-transgenic line

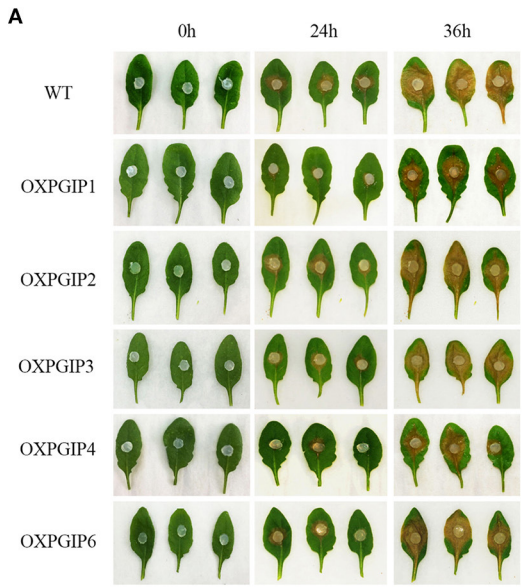

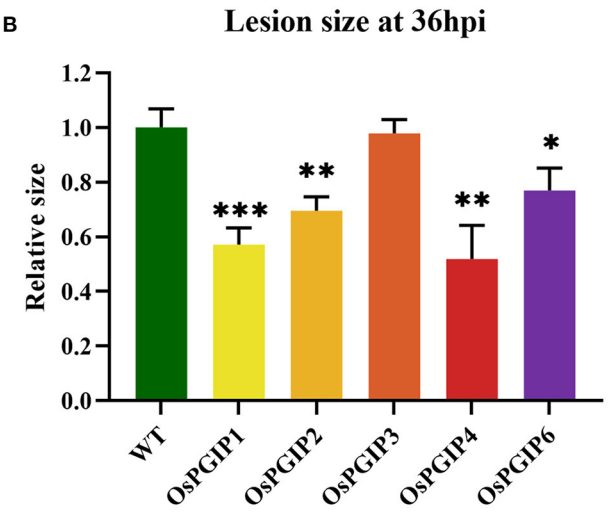

FIGURE 3
S. sclerotiorum resistance assay in *OsPGIPx* transgenic Arabidopsis. **(A)** Phenotypes of pathogenicity assays on detached leaves from different transgenic plants at 0 h, 24 h and 36 h after inoculation with *S. sclerotiorum*. **(B)** Statistical analysis of relative lesion sizes on the inoculated leaves at 36 hpi. Significant differences were showed by: ***$P < 0.001$, **$P < 0.01$, *$P < 0.05$. Error bars indicate SE based on three independent biological replicates.

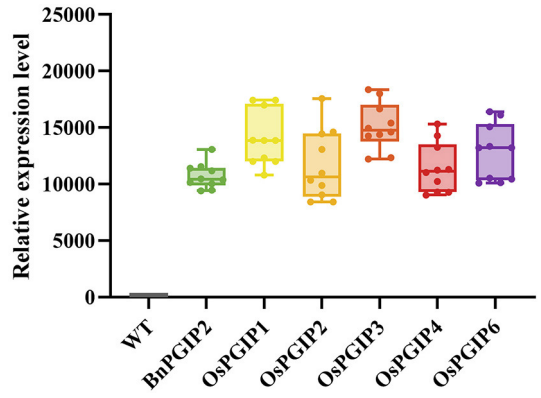

FIGURE 4
Relative expression of *OsPGIPx* in transgenic rapeseed plants. Ten individual plants in T_0 generation of each *PGIP* transgenic rapeseeds were subjected to expression analysis.

presented a lesion area of 243.36 mm^2 (Figure 5) at 48 hpi. At 72 hpi, the lesion area of OE-OsPGIP6 was even reduced to 10.11% compared to the non-transgenic lines. In addition, some other transgenic strains also showed enhanced *S. sclerotiorum* resistance by delaying pathogen infection. When living leaves were inoculated with *S. sclerotiorum*, the transgenic lines, OE-OsPGIP6 and OE-OsPGIP1, showed the best resistance to SSR, with a lesion area reduction of 88.52 and 84.38% at 72 hpi (Figure 6). In the green-pod stage, the resistance of *S. sclerotiorum* was further identified by detached stem inoculation. The experimental results showed that the resistances of the detached stems from OE-OsPGIP2, OE-OsPGIP3, OE-OsPGIP4, and OE-OsPGIP6 to *S. sclerotiorum* were significantly higher than that of the wild-type after 120 h inoculation with *S. sclerotiorum*, and the lesion length caused by *S. sclerotiorum* infection was significantly lower, with a reduction of 24.27, 25.33, 28.47, and 36.83%, respectively (Figure 7).

Discussion

In nature, rice live in high temperature and high humidity environments which are more susceptible to fungi. Considering that a dozen *PGIPs* have been found in *B. napus* while few have resistance to *S. sclerotiorum*, we speculated that the *PGIPs* family from rice may have more ideal resistance potential to fighting against SSR (Bashi et al., 2013; HuangFu et al., 2014). *BnPGIP2* was selected for its superior performance in *BnPGIPs* against *S. sclerotiorum* (Wang et al., 2021). Our study confirms this hypothesis, which shows that *OsPGIPs* have better *S. sclerotiorum* resistance than *BnPGIP2* when introduced in *B. napus*, providing a new implication for rapeseed *S. sclerotiorum*-resistance breeding.

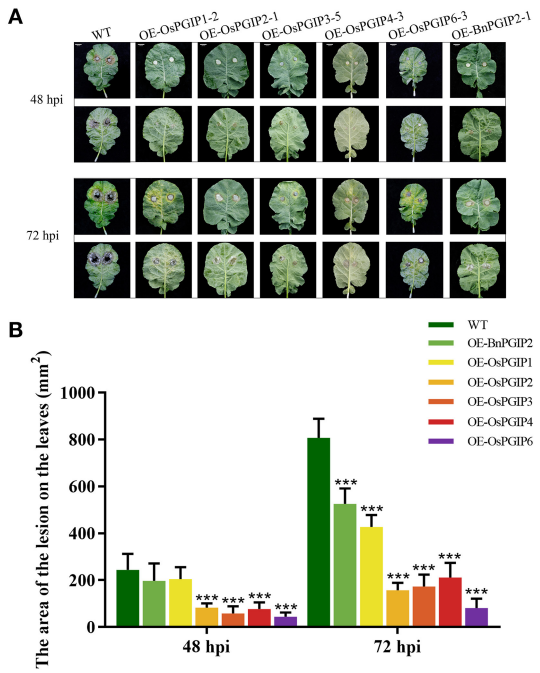

FIGURE 5
OsPGIPx overexpression conferred resistance to *S. sclerotiorum* in detached leaves inoculation. **(A)** Detached leaves of overexpression lines and non-transgenic line inoculated with 10-mm agar plugs of *S. sclerotiorum* hyphae at 22°C. Images were taken at 48 and 72 h post-inoculation (hpi). Scale bars are 20 mm. **(B)** Lesion on detached leaves at 48 and 72 hpi. Significant differences were showed by: ***$P < 0.001$. Error bars indicate SE based on five independent biological replicates.

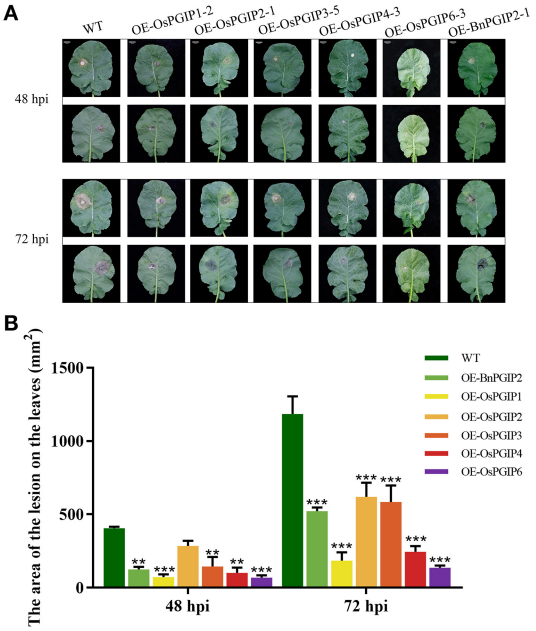

FIGURE 6
OsPGIPx overexpression conferred resistance to *S. sclerotiorum* in Living leaves inoculation. **(A)** Living leaves of overexpression lines and non-transgenic line inoculated with 10-mm agar plugs of *S. sclerotiorum* hyphae at 22°C. Lesion on living leaves at 48 and 72 hpi. Scale bars are 20 mm. **(B)** Lesion on living leaves at 48 and 72 hpi. Significant differences were showed by: ***$P < 0.001$, **$P < 0.01$. Error bars indicate SE based on five independent biological replicates.

Although *OsPGIP* has been reported for its resistance to *S. sclerotiorum*, the candidate gene was only confined to *OsPGIP2* (Wang et al., 2018). In this study, the performance of the living leaves of *OsPGIP2*-overexpressing rapeseed plants was not ideal compared to other *OsPGIPs*, which may be related to the functional specificity of different *PGIPs*. Therefore, the resistance gene screened by a detached test could not meet the needs of the application. Here, we found that rapeseeds overexpressing *OsPGIP6* performed much better than *OsPGIP2* in *S. sclerotiorum* invasion. Moreover, *OsPGIP6*-transgenic plants showed stable high resistances to *S. sclerotiorum* in different inoculation experiments. Hence, *OsPGIP6* is a valuable *S. sclerotiorum*-resistance gene both in theory and applications.

The present study demonstrates that the *PGIPs* family from rice can effectively elevate the resistance of transgenic plants to SSR. By *in vitro* assays, the PG inhibitory activities of OsPGIPs were all evaluated. Subsequently, these *OsPGIPs* were overexpressed in Arabidopsis for pathogenicity assays. Pathogenicity assays of transgenic plants showed that *OsPGIP1*, *OsPGIP2*, *OsPGIP4,* and *OsPGIP6* could significantly improve the resistance of Arabidopsis to *S. sclerotiorum*.

The PGIP activity assays showed that the inhibitory activities of different OsPGIPs to *S. sclerotiorum* PGs were widely divergent. OsPGIP6 and OsPGIP3 showed strong inhibitory activities, while OsPGIP1 showed relatively low inhibitory activity. The results are also consistent with the finding of previous reports, PGIPs are diverse in their inhibition specificities and potentials. Hence, it can be inferred that despite the conservation of *PGIPs* family across different species during evolution, each *PGIP* within the family is specific, especially in the domain involved in the interaction with PGs. In addition, five *OsPGIPs* in Arabidopsis and rapeseed showed inconsistent resistances to *S. sclerotiorum*, which may be caused by the complex polyploidy genome of *B. napus*. As an allotetraploid plant, a more complicated defense system could further improve or alter the effects of resistance genes.

The PGIP-PG interaction is a classic immune evolutionary system model for analyzing the resistant-protein and pathogenic factors. Pathogens produced varieties of PGs to enhance aggressivity, while the hosts have evolved corresponding resistant proteins to minimize harmlessness. Therefore, *PGIPs* are diverse in their inhibition specificities and potentials. Combined with the results, it can be inferred that *OsPGIP6* has a high potential in preventing *S. sclerotiorum* from degrading the

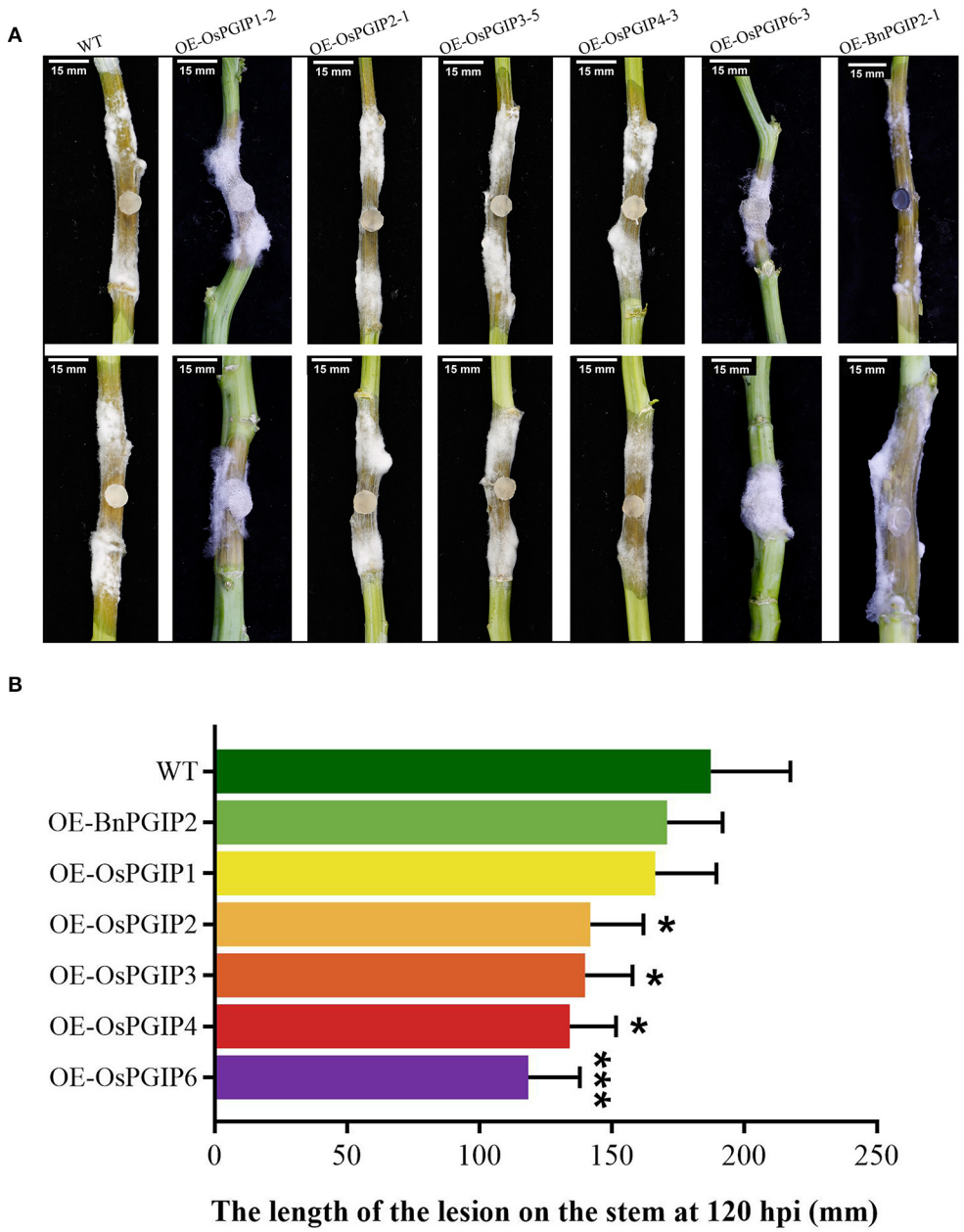

FIGURE 7
OsPGIPx overexpression conferred resistance to *S. sclerotiorum* in detached stem inoculation. **(A)** Stems of transgenic lines and non-transgenic line 120 h after inoculation with *S. sclerotiorum*. Scale bars are 15 mm. **(B)** Lesion on stem at 120 hpi. Significant differences were showed by: ***$P < 0.001$, *$P < 0.05$. Error bars indicate SE based on five independent biological replicates.

plant cell wall. The specific molecular mechanism needs to be elucidated in further study.

The results of living leaves pathogenicity assays showed that the *S. sclerotiorum* resistance of *OsPGIP2* transgenic plants was obviously lower than that of *OsPGIP4* transgenic plants, while the PG-inhibitory activity of OsPGIP2 was almost the same as that of OsPGIP4. This phenotype might arise from the less elevation of expression levels of the target gene in the *OsPGIP2*-overexpressing line compared with the *OsPGIP4*-overexpressing line. Our previous report also showed that the resistance of transgenic plants is related to the expression levels of *PGIP* (Wang et al., 2015). Since the potential PG-inhibitory ability of OsPGIP2 is like that of OsPGIP4, it can be inferred that if the expression level of *OsPGIP2* in transgenic plants is further elevated, the resistance of these plants will be further improved.

In this study, *S. sclerotiorum*-resistant rapeseed plants were obtained by introducing the rice-derived resistance genes, *OsPGIPs*, into *B. napus*, proved by *in vitro* and *in vivo* pathogenicity assays. Different *OsPGIPs* have diverse potential in *S. sclerotiorum* resistance. *OsPGIP6*-overexperssing lines showed vastly lesion reduction compared to the non-transgenic line, also other *OsPGIPs*- and *BnPGIP*- transgenic lines. Overall, our results show that *OsPGIPs* could provide substantial *S. sclerotiorum* resistance in rapeseeds and facilitate SSR-resistance crop breeding.

Data availability statement

The original contributions presented in the study are included in the article/Supplementary material, further inquiries can be directed to the corresponding author/s.

Author contributions

YZ, YL, RW, MY, SL, JJ, WW, and MW contributed to design of the study. MY and SL performed the data analysis and completed the original draft. JJ provided partial resources. All authors contributed to manuscript revision, read, and approved the submitted version.

Funding

This work was supported by the National Key Research and Development Program of China (2016YFD0100202), the National Key Research and Development Plan (2018YFD0100501), Sichuan Province (Grants 2021YJ0296, 2021YFYZ0018, and 2022ZDZX0015), and People's Republic of China. This research was also supported by the Fundamental Research Funds for the Central Universities (SCU2019D013).

Conflict of interest

The authors declare that the research was conducted in the absence of any commercial or financial relationships that could be construed as a potential conflict of interest.

Publisher's note

All claims expressed in this article are solely those of the authors and do not necessarily represent those of their affiliated organizations, or those of the publisher, the editors and the reviewers. Any product that may be evaluated in this article, or claim that may be made by its manufacturer, is not guaranteed or endorsed by the publisher.

Supplementary material

The Supplementary Material for this article can be found online at: https://www.frontiersin.org/articles/10.3389/fpls.2022.970716/full#supplementary-material

References

Bashi, Z. D., Rimmer, S. R., Khachatourians, G. G., and Hegedus, D. D. (2013). *Brassica napus* polygalacturonase inhibitor proteins inhibit *Sclerotinia sclerotiorum* polygalacturonase enzymatic and necrotizing activities and delay symptoms in transgenic plants. *Can. J. Microbiol.* 59,79–86. doi: 10.1139/cjm-2012-0352

Bolton, M. D., Thomma, B. P. H. J., and Nelson, B. D. (2006). *Sclerotinia sclerotiorum* (Lib.) de Bary: biology and molecular traits of a cosmopolitan pathogen. *Mol. Plant Pathol.* 7, 1–16. doi: 10.1111/j.1364-3703.2005.00316. x

Chen, J., Ullah, C., Reichelt, M., Beran, F., Yang, Z. L., Hammerbacher, A., et al. (2020). The phytopathogenic fungus *Sclerotinia sclerotiorum* detoxifies plant glucosinolate hydrolysis products via an isothiocyanate hydrolase. *Nat. Commun.* 11, 3090. doi: 10.1038/s41467-020-16921-2

Chotechung, S., Somta, P., Chen, J., Yimram, T., Chen, X., and Srinives, P. (2016). A gene encoding a polygalacturonase-inhibiting protein (PGIP) is a candidate gene for bruchid (Coleoptera: bruchidae) resistance in mungbean (*Vigna radiata*). *Theor. Appl. Genet.* 129, 1673–1683. doi: 10.1007/s00122-016-2731-1

Dingid, Y., Chai, Y., Mei, J., Yang, W., Mao, Y., Yan, B., et al. (2020). *Sclerotinia sclerotiorum* utilizes host-derived copper for ROS detoxification and infection. *PLoS Pathog.* 16, e1008919. doi: 10.1371/journal.ppat.1008919

Feng, C., Zhang, X., Wu, T., Yuan, B., Ding, X., Yao, F., et al. (2016). The polygalacturonase-inhibiting protein 4 (*OsPGIP4*), a potential component of the *qBlsr5a* locus, confers resistance to bacterial leaf streak in rice. *Planta* 243, 1297–1308. doi: 10.1007/s00425-016-2480-z

Ferrari, S., Sella, L., Janni, M., de Lorenzo, G., Favaron, F., and D'Ovidio, R. (2012). Transgenic expression of polygalacturonase-inhibiting proteins in Arabidopsis and wheat increases resistance to the flower pathogen *Fusarium graminearum*. *Plant Biol.* 14, 31–38. doi: 10.1111/j.1438-8677.2011. 00449.x

Hu, D., Dai, R., Wang, Y., Zhang, Y., Liu, Z., Fang, R., et al. (2012). Molecular cloning, sequence analysis, and expression of the polygalacturonase-inhibiting protein *(PGIP)* gene in mulberry. *Plant Mol. Biol. Rep.* 30, 176–186. doi: 10.1007/s11105-011-0324-3

HuangFu, H., Guan, C., Jin, F., and Yin, C. (2014). Prokaryotic expression and protein function of *Brassica napus PGIP2* and its genetic transformation. *Plant Biotechnol. Rep.* 8, 171–181. doi: 10.1007/s11816-013-0307-y

Hwang, B. H., Bae, H., Lim, H. S., Kim, K. B., Kim, S. J., Im, M. H., et al. (2010). Overexpression of polygalacturonase-inhibiting protein 2 (*PGIP2*) of Chinese cabbage (*Brassica rapa* ssp. *pekinensis*) increased resistance to the bacterial pathogen *Pectobacterium carotovorum* ssp. *carotovorum*. *Plant Cell Tissue Org.* 103, 293–305. doi: 10.1007/s11240-010-9779-4

Janni, M., Bozzini, T., Moscetti, I., Volpi, C., and D'Ovidio, R. (2013). Functional characterisation of wheat Pgip genes reveals their involvement in the local response to wounding. *Plant Biol.* 15, 1019–1024. doi: 10.1111/plb. 12002

Joubert, D. A., Slaughter, A. R., Kemp, G., Becker, J. V. W., Krooshof, G. H., Bergmann, C., et al. (2006). The grapevine polygalacturonase-inhibiting

protein (VvPGIP1) reduces *Botrytis cinerea* susceptibility in transgenic tobacco and differentially inhibits fungal polygalacturonases. *Transgenic Res.* 15, 687–702. doi: 10.1007/s11248-006-9019-1

Liang, X., Liberti, D., Li, M., Kim, Y., Hutchens, A., Wilson, R., et al. (2015). Oxaloacetate acetylhydrolase gene mutants of *Sclerotinia sclerotiorum* do not accumulate oxalic acid, but do produce limited lesions on host plants. *Mol. Plant Pathol.* 16, 559–571. doi: 10.1007/s41348-021-00509-z

Liu, S., Wang, H., Zhang, J., Fitt, B. D. L., Xu, Z., Evans, N., et al. (2005). *In vitro* mutation and selection of doubled-haploid *Brassica napus* lines with improved resistance to *Sclerotinia sclerotiorum*. *Plant Cell Rep.* 24, 133–144. doi: 10.1007/s00299-005-0925-0

Lu, L., Zhou, F., Zhou, Y., Fan, X., Ye, S., Wang, L., et al. (2012). Expression profile analysis of the polygalacturonase-inhibiting protein genes in rice and their responses to phytohormones and fungal infection. *Plant Cell Rep.* 31, 1173–1187. doi: 10.1007/s00299-012-1239-7

Mei, J., Liu, Y., Wei, D., Wittkop, B., Ding, Y., Li, Q., et al. (2015). Transfer of sclerotinia resistance from wild relative of *Brassica oleracea* into *Brassica napus* using a hexaploidy step. *Theor. Appl. Genet.* 128, 639–644. doi: 10.1007/s00122-015-2459-3

Mishra, A. K., Sharma, K., and Misra, R. S. (2012). Elicitor recognition, signal transduction and induced resistance in plants. *J. Plant Interact.* 7, 95–120. doi: 10.1080/17429145.2011.597517

Nguema-Ona, E., Moore, J. P., Fagerström, A. D., Fangel, J. U., Willats, W. G. T., Hugo, A., et al. (2013). Overexpression of the grapevine *PGIP1* in tobacco results in compositional changes in the leaf arabinoxyloglucan network in the absence of fungal infection. *BMC Plant Biol.* 13, 46. doi: 10.1186/1471-2229-13-46

Oelofse, D., Dubery, I. A., Meyer, R., Arendse, M. S., Gazendam, I., Berger, D. K., et al. (2006). Apple polygalacturonase inhibiting protein1 expressed in transgenic tobacco inhibits polygalacturonases from fungal pathogens of apple and the anthracnose pathogen of lupins. *Phytochemistry* 67, 255–263. doi: 10.1016/j.phytochem.2005.10.029

Richter, A., Jacobsen, H. J., de Kathen, A., de Lorenzo, G., Briviba, K., Hain, R., et al. (2006). Transgenic peas (*Pisum sativum*) expressing polygalacturonase inhibiting protein from raspberry (*Rubus idaeus*) and stilbene synthase from grape (*Vitis vinifera*). *Plant Cell Rep.* 25, 1166–1173. doi: 10.1007/s00299-006-0172-z

Schacht, T., Unger, C., Pich, A., and Wydra, K. (2011). Endo- and exopolygalacturonases of *Ralstonia solanacearum* are inhibited by polygalacturonase-inhibiting protein (PGIP) activity in tomato stem extracts. *Plant Physiol. Biochem.* 49, 377–387. doi: 10.1016/j.plaphy.2011.02.001

Schmittgen, T. D., and Livak, K. J. (2001). Analysis of relative gene expression data using real-time quantitative PCR and the 2(-Delta Delta C(T)) method. *Methods.* 25, 402–408. doi: 10.1006/meth.2001.1262

Shanmugam, V. (2005). Role of extracytoplasmic leucine rich repeat proteins in plant defence mechanisms. *Microbiol. Res.* 160, 83–94. doi: 10.1016/j.micres.2004.09.014

Szankowski, I., Briviba, K., Fleschhut, J., Schönherr, J., Jacobsen, H. J., and Kiesecker, H. (2003). Transformation of apple (*Malus domestica Borkh.*) with the stilbene synthase gene from grapevine (*Vitis vinifera* L.) and a PGIP gene from kiwi (*Actinidia deliciosa*). *Plant Cell Rep.* 22, 141–149. doi: 10.1007/s00299-003-0668-8

Tang, L. G., Yang, G. G., Ma, M., Liu, X. F., Li, B., Xie, J. T., et al. (2020). An effector of a necrotrophic fungal pathogen targets the calcium-sensing receptor in chloroplasts to inhibit host resistance. *Mol. Plant Pathol.* 21, 686–701. doi: 10.1111/mpp.12922

Vorwerk, S., Somerville, S., and Somerville, C. (2004). The role of plant cell wall polysaccharide composition in disease resistance. *Trends Plant Sci.* 9, 203–209. doi: 10.1016/j.tplants.2004.02.005

Wang, R., Lu, L., Pan, X., Hu, Z., Ling, F., Yan, Y., et al. (2015). Functional analysis of *OsPGIP1* in rice sheath blight resistance. *Plant Mol. Biol.* 87, 181–191. doi: 10.1007/s11103-014-0269-7

Wang, Z., Wan, L., Xin, Q., Chen, Y., Zhang, X., Dong, F., et al. (2018). Overexpression of *OsPGIP2* confers *Sclerotinia sclerotiorum* resistance in *Brassica napus* through increased activation of defense mechanisms. *J. Exp. Bot.* 69, 3141–3155. doi: 10.1093/jxb/ery138

Wang, Z. R., Wan, L., Zhang, X. H., Xin, Q., Song, Y. X., Hong, D. F., et al. (2021). Interaction between *Brassica napus* polygalacturonase inhibition proteins and *Sclerotinia sclerotiorum* polygalacturonase: implications for rapeseed resistance to fungal infection. *Planta* 253, 34. doi: 10.1007/s00425-020-03556-2

Xu, L., Li, G., Jiang, D., and Chen, W. (2018). *Sclerotinia sclerotiorum*: an evaluation of virulence theories. *Annu. Rev. of Phytopathol.* 56, 311–338. doi: 10.1146/annurev-phyto-080417-050052

Xu, L., Xiang, M., White, D., and Chen, W. (2015). pH dependency of sclerotial development and pathogenicity revealed by using genetically defined oxalate-minus mutants of *Sclerotinia sclerotiorum*. *Environ. Microbiol.* 17, 2896–2909. doi: 10.1111/1462-2920.12818

Yang, G., Tang, L., Gong, Y., Xie, J., Fu, Y., Jiang, D., et al. (2018). A cerato-platanin protein SsCP1 targets plant PR1 and contributes to virulence of *Sclerotinia sclerotiorum*. *N. Phytol.* 217, 739–755. doi: 10.1111/nph.14842

Zhang, Q., Yan, Q., Yuan, X., Lin, Y., Chen, J., Wu, R., et al. (2021). Two polygalacturonase-inhibiting proteins (VrPGIP) of *Vigna radiata* confer resistance to bruchids (*Callosobruchus* spp.). *J. Plant Physiol.* 153376, 258–259. doi: 10.1016/j.jplph.2021.153376

Zhao, Y., and Wang, M. L. (2004). Inheritance and agronomic performance of an apetalous flower mutant in *Brassica napus* L. *Euphytica.* 137, 381–386. doi: 10.1023/B:EUPH.0000040522.37048.7a

frontiers | Frontiers in Plant Science

TYPE Original Research
PUBLISHED 28 September 2022
DOI 10.3389/fpls.2022.1014376

OPEN ACCESS

EDITED BY
Cunmin Qu,
Southwest University, China

REVIEWED BY
Raj Kumar Joshi,
Rama Devi Women's University, India
Guizhen Gao,
Oil Crops Research Institute,
(CAAS), China
Zongyun Feng,
Sichuan Agricultural University, China

*CORRESPONDENCE
Maolin Wang
mlwang@scu.edu.cn

SPECIALTY SECTION
This article was submitted to Plant Pathogen Interactions, a section of the journal Frontiers in Plant Science

RECEIVED 08 August 2022
ACCEPTED 01 September 2022
PUBLISHED 28 September 2022

CITATION
Jiang X, Su Y and Wang M (2022) Mapping of a novel clubroot disease resistance locus in *Brassica napus* and related functional identification. *Front. Plant Sci.* 13:1014376. doi: 10.3389/fpls.2022.1014376

Mapping of a novel clubroot disease resistance locus in *Brassica napus* and related functional identification

Xuefei Jiang, Ying Su and Maolin Wang*

Key Laboratory of Bio-Resource and Eco-Environment of Ministry of Education, College of Life Sciences, Sichuan University, Chengdu, China

Clubroot disease, caused by *Plasmodiophora brassicae*, is a devastating disease that results in substantial yield loss in *Brassicaceae* crops worldwide. In this study, we identified a clubroot disease resistance (CR) *Brassica napus*, "Kc84R," which was obtained by mutation breeding. Genetic analysis revealed that the CR trait of "Kc84R" was controlled by a single dominant locus. We used the bulked segregant analysis sequencing (BSA-seq) approach, combined with genetic mapping based on single nucleotide polymorphism (SNP) markers to identify CR loci from the F_2 population derived from crossing CR "Kc84R" and clubroot susceptible "855S." The CR locus was mapped to a region between markers *Bn*SNP14198336 and *Bn*SNP14462201 on the A03 chromosome, and this fragment of 267 kb contained 68 annotated candidate genes. Furthermore, we performed the CR relation screening of candidate genes with the model species Arabidopsis. An ERF family transcriptional activator, *Bn*ERF034, was identified to be associated with the CR, and the corresponding Arabidopsis homozygous knockout mutants exhibited more pronounced resistance compared with the wild-type Col-0 and the transgenic lines of *BnERF034* in response to *P. brassicae* infection. Additionally, the expression analysis between resistant and susceptible materials indicated that *BnERF034* was identified to be the most likely CR candidate for the resistance in Kc84R. To conclude, this study reveals a novel gene responsible for CR. Further analysis of *BnERF034* may reveal the molecular mechanisms underlying the CR of plants and provide a theoretical basis for *Brassicaceae* resistance breeding.

KEYWORDS

clubroot disease, mapping, *Plasmodiophora brassicae*, *Brassica napus*, ERF transcription factor

1 Introduction

Clubroot disease caused by *Plasmodiophora brassicae* is one of the most devastating diseases affecting *Brassicaceae* crops, it is widespread throughout the world and causes significant economic losses every year (Dixon, 2009). *Brassica napus*, the largest planted oil crop in the *Brassicaceae* family, has been particularly badly affected (Hejna et al., 2019). *P. brassicae* is difficult to eradicate once the fields are contaminated because it can remain in the soil for years as resting spores. Furthermore, there are currently no good control measures for agricultural production (Webster and Dixon, 1991; Wallenhammar, 2010). On the whole, resistance breeding is one of the most effective and desirable approaches to deal with this disease (Piao et al., 2009).

Although there are many crops in the *Brassicaceae* family, limited resources are identified for clubroot disease resistance (CR) (Jiang et al., 2018). CR genes in *Brassica rapa* have been identified most frequently and studied most intensively (Sakamoto et al., 2008), among which two most well-studied CR genes, *CRa* (A03) (Matsumoto et al., 1998; Hayashida et al., 2008) and *Crr1a* (Hatakeyama et al., 2013) (A08), have been successfully isolated (Ueno et al., 2012). In addition, there are many CR loci for genes of undefined function, such as *Crr2* (Suwabe et al., 2003), *PbBa1.1* (Chen et al., 2013), *QS_B1.1* (Pang et al., 2014) (A01); *CRc* (Sakamoto et al., 2008), *Rcr8* (Yu et al., 2017) (A02); *PbBa3.1* (Chen et al., 2013), *PbBa3.3* (Chen et al., 2013), *Crr3* (Saito et al., 2006), *CRd* (Pang et al., 2018), *CRk* (Sakamoto et al., 2008), *CRb* (Kato et al., 2013), *QS_B3.1* (Pang et al., 2014), *Rcr1* (Yu et al., 2017), *Rcr4* (Yu et al., 2017), *Rpb1* (Chu et al., 2013) (A03); *Crr4* (Suwabe et al., 2006) (A06); *CRs* (Laila et al., 2019), *Crr1b, PbBa8.1* (Chen et al., 2013), *Rcr9* (Yu et al., 2017) (A08), and most of these loci contain typical disease resistance proteins. In *Brassica oleracea*, relatively few CR loci have been reported (Piao et al., 2009; Ce et al., 2021), such as *CR2a* (Grandclément and Thomas, 1996), *CR2b* (Grandclément and Thomas, 1996), *Pb3* (Voorrips et al., 1997), *Pb4* (Voorrips et al., 1997) and *PbBo1* (Rocherieux et al., 2004), and most of them exhibit quantitative traits controlled by polygenic. In *B. napus*, it appears to have many disease resistance loci (more than 30 CR loci) reported (Hejna et al., 2019), but these are either less (only two) dominant loci or from a single source (most of CR loci have been mapped by Werner et al.) (Werner et al., 2008). Notably that all these CR loci are still poorly studied in terms of disease resistance function and resistance mechanisms.

At present, the utilization of CR loci primarily uses intraspecific or interspecific mating to generate new CR materials. For instance, Sakamoto and Suwabe et al. have developed numerous CR cabbages using European fodder turnips as a source of resistance (Suwabe et al., 2003; Sakamoto et al., 2008). Because *B. napus* is a natural amphidiploid between *B. oleracea* and *B. rapa* (Piao et al., 2009), Diederichsen et al. used the interspecific cross of CR turnip and CR kale material to produce two novel CR *B. napus*, "Mendel" and "Tosca" (Diederichsen and Sacristan, 1996; Diederichsen et al., 2006), which were found to be resistant to the clubroot disease both in the laboratory and field identification. Furthermore, Zhan et al. developed a new conventional variety, Huashuang 5R, and a new hybrid variety, Huayouza 62R, with excellent CR by interspecific crosses of *B. napus* material containing the resistance locus *PbBa8.1* with CR turnips ECD04 and CR Chinese cabbage, respectively (Zhan et al., 2020, Li et al., 2021b). Shah et al. combined two CR genes, *CRb* and *PbBa8.1*, which originated from two homozygous *B. napus* CR varieties 305R and 409R, respectively, and developed CR homozygous lines through marker-assisted selection (MAS) (Shah et al., 2019). However, in general, CR resources, especially in *B. napus*, are still scarce and the use of resistance loci is mostly limited by the source of resistance. And the interspecific crosses require a long breeding cycle, so it is still important to identify CR resources from *B. napus* for the creating of varieties of *B. napus* resistant to clubroot disease.

In our study, a novel CR material, "Kc84R," and a susceptible material, "855S," of *B. napus* were used to develop a new segregation population. We performed the inheritance analysis to determine that the CR trait of Kc84R is a qualitative trait controlled by a dominant locus. The CR loci were identified by bulk segregation analysis sequencing (BSA-Seq) strategy, which is based on genome resequencing in two sets of extreme pools. The target region was then gradually narrowed and located on a 267 kb fragment of the A03 chromosome. Furthermore, we performed the CR relation screening of candidate genes with the model species Arabidopsis. A candidate gene, *BnERF034*, encoding a transcriptional activator, was shown to be strongly associated with disease resistance. Our study identifies a new type of CR gene, and provides important information for future resistance breeding in *Brassicaceae* species.

2 Materials and methods

2.1 Plant materials and pathogen isolates

Two *B. napus* materials: CR material (previously, a *B. napus* material was screened out with excellent resistance to a *P. brassicae* isolate of Sichuan Guanghan during years of field cultivation) "Kc84R," a selected line of Kc84-1, which comes from the "2013-84" mutagenized by Atmospheric and Room Temperature Plasma (ARTP), followed by more than six generations of successive self-pollinated and selection pressure of clubroot disease in field cultivation; susceptible material "855S," which verified by field cultivation, were selected as parents to produce F_1 progenies, and F_1 plants were self-pollinated to develop F_2 segregating population.

Arabidopsis thaliana: Wild-type Columbia-0 (Col-0), the mutant T-DNA single insertion lines *wrky12* (salk_204550c),

erf034 (salk_087049c), *atg8e* (salk_126394c), *tcp9* (salk_201398c), *urm1* (cs812600), *pub15* (salk_120989c), *skp1* (salk_042202) in Col-0 background were obtained from Arabidopsis Biological Resource Center (http://www.arabidopsis.org/abrc/), *pme17* (salk_059908c) was obtained from Arashare (https://www.arashare.cn/index/). Homozygous mutant plants were selected and tested for T-DNA insertion and homozygosity by PCR using primers obtained by T-DNA Primer Design Tool (http://signal.salk.edu/tdnaprimers.2.html) (Supplementary Table 1).

The *P. brassicae* pathotypes: *P. brassicae* infection tests were comprised of pathotypes 2, 4, 7, and 11 in Williams system supplied by Piao, in addition, the local *P. brassicae* isolate collected from Guanghan, Sichuan Province, China (E104.1797, N31.0382), named it *Pb*Gh, which has been identified as Pb3, according to the sinitic clubroot differential set (SCD) system (Pang et al., 2020).

2.2 Pathogen preparation and inoculation

All pathogen isolates were propagated with kinds of *B. napus* materials, and fresh galls were stored at −20°C for resting spore extraction. Preparation of *P. brassicae* resting spores was taken with sucrose gradient centrifugation. In brief, the infected plant galls were homogenized with sterile water using a grinder after surface cleaning and sterilization. The homogenate was filtered through 8 layers of cheesecloth, then the filtrate was collected and centrifuged at 3 100 rpm, the sediment was washed several times with sterile water and suspended in 50% sucrose solution. The supernatant was retained after centrifugation, and then centrifuged with additional sterile water. The sediment was collected, and washed several times again, the resting spores were obtained.

In soil culture infection, the inoculation of resting spores was taken with the injection. Firstly, holes were dug in the substrate to be transplanted, and 2 g sterilized vermiculite was added. Then, 1 mL of adjusted concentrations of *P. brassicae* resting spores were carefully injected into the vermiculite, and the roots of plants to be transplanted were then wrapped in the infiltrated vermiculite. The inoculation concentration depended on different experiments.

In hydroponic culture infection, ½ Hogland nutrient solution was used as the medium with the same temperature and light conditions. The resting spores of *P. brassicae* were diluted into 1×10^7 mL^{-1}. *A. thaliana* was treated in 6 well cell culture plates, and *B. napus* was placed in 50 mL conical flasks.

2.3 Disease index evaluation and phenotypic investigation

Disease symptoms of *B. napus* were evaluated at 28 days post inoculation (dpi) with *P. brassicae*. After thorough cleaning of the roots, disease symptoms were scored as follows: 0, no obvious galls; 1, a few small galls mainly on lateral roots; 3, larger galls on the lateral roots or small galls on the main roots; and 5, large galls both on the lateral and main roots (Huang et al., 2017) (Supplementary Figure 1).

Symptoms of *A. thaliana* were assessed on a 0–5 scale at 21 and 28 dpi, respectively, where 0, no obvious galls; 1, small galls mainly on lateral roots; 3, obvious galls on the main roots and plant growth were inhibited; 5, severe galls on the whole roots and extending to the hypocotyl, plant growth was severely affected (Supplementary Figure 2).

The disease index (DI) was calculated as following:

$$\mathrm{DI}\ (\%) = \frac{\sum\ (\text{rating class}) \times\ (\#\ \text{plants in rating class})}{(\text{total}\ \#\ \text{plants in treatment}) \times\ 5} \times\ 100$$

Hypocotyl width: the plants used to calculate hypocotyl width were selected randomly from trays, with 4 plants per tray for each material.

Hydroponic culture infection observation: the infection phenotype of the root hairs and main roots of *A. thaliana* that need to be observed were obtained from corresponding sampling points. The phenotypes were photographed with microscope (Nikon DS-Ri2, Tokyo, Japan).

2.4 Selection of pathogen pathotypes for mapping

"Kc84R" was inoculated with *P. brassicae* pathotypes 2, 4, 7, 11 and the local *P. brassicae* isolate, respectively. "855S" was inoculated with the *P. brassicae* pathotypes that "Kc84R" showed disease resistance in previous tests. The concentration of resting spores was 1×10^7/mL.

2.5 Population genetic analysis

"Kc84R," "855S," the F_1 population from 855S (female) × "Kc84R" (male) (more than 60 plants), and the segregating population obtained from F_1 self-fertilization (F_2 lines) (560 plants), were inoculated with *P. brassicae* pathotypes for mapping. The concentration of resting spores was 1×10^7/mL.

2.6 BSA-seq analysis

To construct reliable extreme separation pools, the F_2 segregating populations were randomly divided into 5 groups, in which each group contained about 200 F_2 lines. Total 20/20 extreme R/S plants were selected from the 5 groups. Individual plants genomic DNA was extracted from young leaves of two parents (10 plants per material) and the extreme lines following

the manufacturer's instructions of Plant Genomic DNA Kit (TIANGEN, Beijing, China). R and S pools were constructed by mixing an equal volume of DNA from the extreme R and S lines within each group, the parental pools were constructed in the same way. The two separation pools and two parental pools were subjected to perform whole-genome sequencing on the illumina HiSeqTM PE150 platform by Novogene (Beijing, China). Read pairs with adapters were removed; the paired reads with N ratio over 10% were removed; the paired reads that low quality ($Q \leq 5$) bases exceeds 50% of the length, need to be removed. Then, the clean reads were mapped to the reference genome of *B. napus* (https://ftp.ncbi.nlm.nih.gov/genomes/genbank/plant/Brassica_napus/latest_assembly_versions/GCA_000686985.2_Bra_napus_v2.0/) with BWA (mem -t 4 -k 32 -M), followed by de-duplication with SAMTOOLS (rmdup).

2.7 SNP discovery and mapping

Clean reads were used for the detection of SNPs and InDels. The detection of multiple sample SNPs with the Unified Genotyper module of GATK3.8 software, Variant Filtration for filtering with the parameters –cluster Window Size 4, –filter Expression "QD< 4.0 || FS > 60.0 || MQ< 40.0," -G_filter "GQ<20." The InDels detection also used Unified Genotyper module of GATK3.8 software, Variant Filtration for filtering with the filter parameter –filter Expression "QD< 4.0 || FS > 200.0." SNP and InDel annotation using ANNOVAR. The parents were selected as a reference, and SNP/InDel-index (frequency of SNPs/InDels) was calculated for each SNP/InDel loci between the parents and R/S pools. SNP loci with SNP-index less than 0.3 and SNP depth less than 7 in both R and S were filtered out; SNP loci with a missing SNP-index in one offspring pool were filtered out; InDels loci that were missing in the offspring pools were filtered out.

Δ(SNP/InDel-index) curve: 1 Mb was chosen as the window, 1 kb was chosen as the step size, and the mean of SNP/InDel-index was calculated to reflect the SNP/InDel-index distribution of the two offspring pools in each window. Δ(SNP/InDel-index) = SNP/InDel index (extreme trait B) - SNP/InDel index (extreme trait A), 1,000 permutation tests were performed and the 95% confidence level was selected as the threshold for screening. The preliminary candidate interval was confirmed by the Δ(SNP/InDel-index) curve.

2.8 SNP genotyping and identification of target region

Appropriate SNP/InDel loci (17 SNPs and 3 InDels) were selected as markers on target chromosomes (Supplementary Table 2), especially candidate intervals, based on SNP/InDel_index in BSA-seq. SNP genotyping of the 810 F_2 lines was performed by SNaPshot and genetic distances were calculated using QTL IciMapping (Version 4.2.53) with the F_2 population approach for genetic distance calculation, with parameters set to default. The primers used are listed in Supplementary Table 3.

2.9 Gene synteny analysis of the target region

B. napus ZS11 genome (Bra_napus_v2.0) and *A. thaliana* genome (Arabidopsis_thaliana. TAIR 10) were downloaded from the NCBI and ENA (European Nucleotide Archive) respectively. Then, the sequences and GFFs of each genome were extracted by One-Step MCScanX module of TBtools (Version 1.09876) with parameter set as default. Finally, the gene synteny analysis was performed with the CDS of the candidate chromosome as queries and CDS of the *A. thaliana* genome as subject with Dual Systeny Plot for MCscan X (Chen et al., 2020).

2.10 Quantitative RT-PCR

The whole roots were collected from "Kc84R" and "855S" at 14 and 28 dpi with *P. brassicae* in soil, and with three biological replications for RNA extraction, each repeat contains 3-6 roots. The whole roots were collected from "Kc84R" and "855S" at 12 and 24 hours, 3-, 5-, and 7-days post inoculation with *P. brassicae* in hydroponic culture, and with three biological replications for RNA extraction, each repeat contains 6-9 roots. RNAprep Pure Kit TSP411 (TSINGKE; Beijing, China) with on-column deoxyribonuclease (DNase) digestion was used for RNA extraction from each sample following the manufacturer's instructions. The RNA concentration and quality were checked using a Nano-400A Micro-Spectrophotometer (ALLSHENG, Hangzhou, China). The preparation of cDNA libraries performed by *TransScript*® Uni All-in-One First-Strand cDNA Synthesis SuperMix for qPCR (One-Step gDNA Removal) (Transgene; Beijing, China). PCR was conducted using the Taq Pro Universal SYBR qPCR Master Mix (Vazyme; Nanjing, China) following manufacturer's instruction. Cycling conditions were 95°C for initial 30 s followed by 42 cycles of 10 s at 95°C, 30 s at 60°C. Melt-curve profiling and agarose gel electrophoresis was conducted to evaluate the specificity of the reaction and the absence of primer dimers. *BnACTIN* was used as an endogenous control to normalize the expression levels of target genes. The primers used in this part are listed in Supplementary Table 4.

2.11 Bioinformatic analysis of candidate genes

The expression data of *A. thaliana* in response to *P. brassicae* infection was downloaded from the ENA (https://www.ebi.ac.

uk/ena/) under the identifier PRJEB12261 (Malinowski et al., 2016; Olszak et al., 2019).

The visual expression data of the target genes in *A. thaliana* and *B. napus* were downloaded from eFP Browser (http://bar.utoronto.ca/eplant/) and *Bn*TAIR (*Brassica napus* transcriptome information resource) (http://yanglab.hzau.edu.cn/BnTIR/eFP).

The protein spatial structure of the target gene is downloaded from Swiss-model (https://swissmodel.expasy.org/), and made by PyMol (https://pymol.org/2/).

2.12 Subcellular localization

The full-length coding sequences of *Bn*ERF034-855S and *Bn*ERF034-Kc84R were fused with eGFP at C-terminus and inserted into the pBI121 vector, respectively. The primers used are included in Supplementary Table 4. Then, the recombinant vectors and pBI121 were transformed into *A. tumefaciens* strain GV3101, with infiltration into 4- to 6-week-old *Nicotiana benthamiana* leaves. *N. benthamiana* leaves were harvested at 2 days post infiltration (dpi) and imaged using a fluorescence microscope (Leica DM4 B, Weztlar, Germany).

2.13 Transactivation assay in yeast cells

The yeast strain AH109, containing the *lacZ* and *HIS3* reporter genes, was used as an assay system. The yeast vector pGBKT7-BD with DNA binding domain (DNA-BD) but lacking an activation domain was used to verify the transcriptional activation effect of the transcription factor. The coding sequences of *Bn*ERF034-855S and *Bn*ERF034-Kc84R proteins were obtained by PCR. The primers used are included in the Supplementary Table 4. Then, the PCR products were cloned into pGBKT7-BD vector containing the GAL4 DNA-binding domain to obtain plasmids for testing of transcriptional activation. The recombinant vectors named "*Bn*ERF034-855S" and "*Bn*ERF034-Kc84R," the positive control pGAL4 named "GAL4," the negative control named "PUB15" and the blank group pBD vector, were all transformed into the yeast host strain AH109. All transformants were successively dropped onto YPAD, SD/-Trp and SD/-Trp/-His plates. Transcriptional activation activities were evaluated according to their growth status. Transfected yeast cells were also transferred onto SD/-Trp/-His and incubated in the presence of X-α-gal to check the β-galactosidase activity by monitoring the generation of blue.

2.14 Generation of transgenic Arabidopsis plants

The *BnERF034* full-length CDS was amplified from Kc84R and 855S cDNA libraries. PCR products with the restriction sites at both ends were cloned into the binary vector pFGC5941 to produce the constructs *35S::BnERF034* using the methods of enzyme digestion and enzyme ligation. The primers used are listed in the Supplementary Table 4. The recombinant vectors were transformed into *A. tumefaciens* GV3101 by the heat shock method. Wild-type Col-0 was transformed using the Agrobacterium- mediated floral dip method (Clough and Bent, 1998). Transgenic T_1 was selected by spraying 1/1500 Basta solution onto the leaves. PCR and qPCR identification of the surviving positive lines were performed using specific primers of recombinant vectors, the *AtACTIN2* was used as an internal reference control (Supplementary Table 4). Ten positive lines were selected from the T_2 generation with a basta resistance separation ratio of 3:1 to generate homozygous transgenic plants (T_3) for further analysis.

3 Results

3.1 Mapping of resistance loci

To verify the *P. brassicae* pathotype resistance profile of Kc84R and characterize the identity of CR genes, Kc84R was inoculated respectively by five different *P. brassicae* isolates, which are pathotypes 2, 4, 7, 11 that classified based on the differential system of Williams and *P. brassicae* isolate collected from Guanghan, namely, *Pb*Gh. The disease index was investigated at 28 days post inoculated (dpi). As shown in Figure 1, Kc84R showed significant resistance to pathotype 7 (DI 2.83) and *Pb*Gh (DI 1.24), typical susceptibility characteristics to pathotypes 2 (DI 82.31) and 11 (DI 95.76), and lower susceptibility to pathotype 4 (DI 76.33) than pathotypes 2 and 11 (Table 1). The susceptible parent material, 855S, used for population construction, was also tested for resistance to several *P. brassicae* isolates (pathotype 7 and *Pb*Gh). The results showed that 855S was significantly susceptible to *Pb*Gh (DI 92), and low susceptibility to the pathotype 7 (DI 18.06) (Table 1). Therefore, we selected the *P. brassicae* isolate *Pb*Gh for phenotypic identification of the resistant gene mapping population.

To confirm the genetic characteristics of the CR loci on Kc84R, we crossed the resistant material Kc84R with the susceptible material 855S and established a segregating population for genetic mapping. And phenotypic identification was performed on the relevant material in the disease-resistant localization population. The results showed that the tested F_1 generation materials were basically free of disease (Figure 2A), while the separation ratio of the F_2 population roughly conformed to 3:1 ($\chi^2 = 3.125$, $P > 0.05$) (Table 2). In summary, we inferred that the CR phenotype of Kc84R is a qualitative trait controlled by a dominant locus.

To identify the locus that controls the CR trait, BSA-seq based on the second-generation sequencing was carried out.

10.3389/fpls.2022.1014376

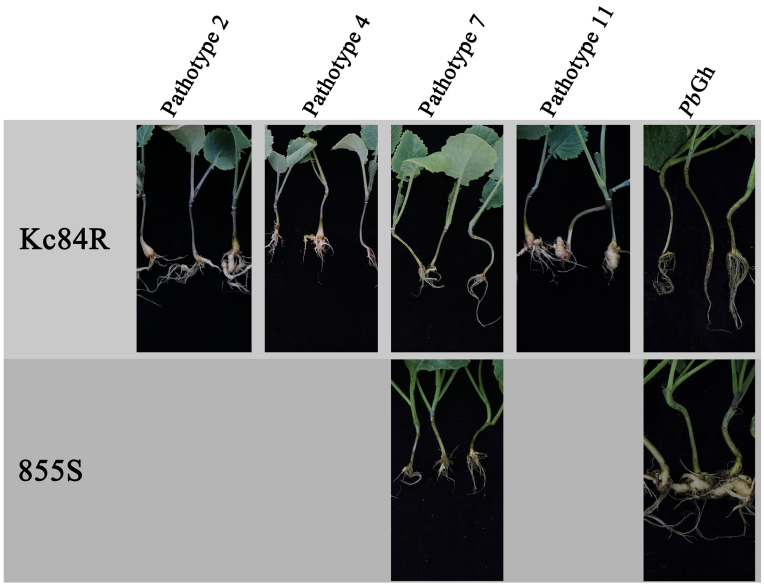

FIGURE 1
Phenotypes of parent materials to *P. brassicae* pathotypes.

TABLE 1 Disease investigation for susceptibility of parent materials to *P. brassicae* pathotypes.

Materials	Pathotype	DI (Disease Index)
Kc84R	2	82.31 ± 1.74^{b}
	4	76.33 ± 4.30^{b}
	7	2.83 ± 0.12^{d}
	11	95.76 ± 3.26^{a}
	*Pb*Gh	1.24 ± 0.81^{d}
855S	7	18.06 ± 4.73^{c}
	*Pb*Gh	92.00 ± 1.32^{a}

Significance analysis of disease index was performed using the one-way ANOVA method, Tukey's test, and different letters indicate a significant difference ($p < 0.05$).

Genomic DNA of two extreme F_2 pools (R-pool and S-Pool) and two parent pools (Kc84R, 855S) was sequenced. A total of 25,521,831,000 bp and 24,151,904,400 bp raw reads were generated from the R- and S-pools, respectively. The raw reads of 13,317,282,600 bp and 13,233,702,000 bp were obtained from the resistant and susceptible parent pools, respectively. The Q30 are all over 91% (Supplementary Table 5). After filtering, more than 98% of the reads passed the quality control standard and remained. The genome of *B. napus* (Bra_napus_v2.0) was mapped, and the overall mapping rates exceeded 97% (Supplementary Table 6). SNP/InDel was used to calculate the SNP/InDel frequency distribution (Supplementary Table 7), ΔSNPS/InDel was plotted against the genomic positions. According to the ΔSNPS/InDel peak value, an interval of about 2.6 Mb from 11.9 Mb to 14.5 Mb on A03 chromosome was determined, which may be related to the CR gene on Kc84R (Figure 2B). To further narrow down the candidate interval, we screened 20 SNP/InDel markers (Supplementary Table 2) to genotype 810 F_2 individual plants. The analysis results showed that the CR locus was located between *Bn*SNP14462201 and *Bn*SNP14198336, in an interval of 1.06 cM (Figure 2C).

3.2 Identification and expression analysis of candidate genes

*Bn*SNP14198336 was located in the gene LOC106438228, and *Bn*SNP14462201 was located in the gene LOC106438265. The physical distance between these two markers (including these two genes) was 267,362 bases. There were 68 genes annotated in this target region according to reference genome (Bra_napus_v2.0). And in the disease resistant material Kc84R, numerous SNP/InDel events (Supplementary Table 8) were included in these candidate genes compared to the reference genome and the susceptible material 855S.

To confirm the sequence characteristics of the candidate genes and perform functional analysis of these candidate genes using *A. thaliana*, we performed covariance analysis of the *B. napus* A03 chromosome with the *A. thaliana* chromosomes. As shown in Figure 3, this candidate interval was highly homologous to the interval from AT2G44730 to AT2G45750

10.3389/fpls.2022.1014376

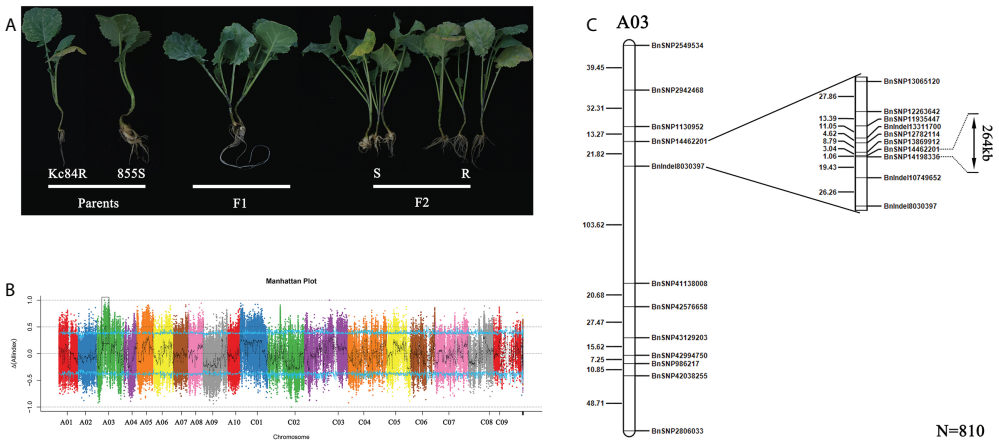

FIGURE 2
Mapping of candidate CR locus. **(A)** Phenotype identification of two parent lines and their crossed offspring after inoculation with *Pb*Gh. **(B)** The CR loci identified by BSA-sequencing (BSA-seq). **(C)** Fine mapping of the CR locus based on SNP markers using 810 F_2 individuals. The genetic distance is shown on the left, the physical locations of SNP markers are included in the names.

TABLE 2 Disease phenotype statistics in F_1 population from cross of Kc84R and 855S.

Population	Disease rating				Total	Incidence Rate	χ^2	$\chi^2_{0.05}$
	0	1	3	5				
Kc84R (R parent)	60	1	0	0	61	1.64		
855S (S parent)	0	0	3	61	64	100		
F_1	64	2	0	0	66	3.03		
F_2	430	2	12	116	560	23.21	0.0029	3.841

R, resistant; S, susceptible. A rating of "0" was defined as R, "1," "3," "5" as S.

on Arabidopsis chromosome 2. The functional annotations of all candidate genes are shown in Table 3. Based on the expression data of Arabidopsis in response to *P. brassicae* infection, most genes within the candidate interval exhibited differential expression, some showed high expression and some showed reduced expression levels (Figure 4A). Part of differentially expressed genes (LOC106443642, WRKY12-like; LOC106438231, *ERF034*; LOC106438243, *ATG8E*; LOC106438246, *PME17*; LOC106438256, *TCP9*; LOC106443648, *URM1*; LOC106438258, *PUB15*; and LOC106438265, *SKP1*) were selected for further analyses for their expression patterns in response to *P. brassicae* infection in *B. napus* (Kc84R and 855S) (Figure 4B). The results showed that the expression level of *WRKY12-like* was low in both Kc84R and 855S. The expression level of *ERF034* in Kc84R was significantly lower than that in 855S, especially in the early stage of infection (14 dpi). The expression level of *ATG8E* in Kc84R was significantly higher than that in 855S in the blank group (Mock), and the down-regulated expression in response to *P. brassicae* infection was also significant. *PME17* is also a gene down-regulated by *P. brassicae* infection, but the overall expression level in Kc84R is significantly higher than that in 855S. At 14 dpi, the expression levels of *TCP9* in Kc84R were much higher than that in 855S. *URM1* is a gene up-regulated at 14 dpi, and the expression level of the two materials was not significantly different. *PUB15* is also a gene down-regulated by *P. brassicae* infection, and the expression level in Kc84R is higher than that in 855S. The differential expression of *SKP1* infected by *P. brassicae* at 14 dpi was not significant, and there was no significant difference between the two materials. These differentially expressed genes, especially those differentially expressed in different materials, may have important relationships with clubroot disease resistance.

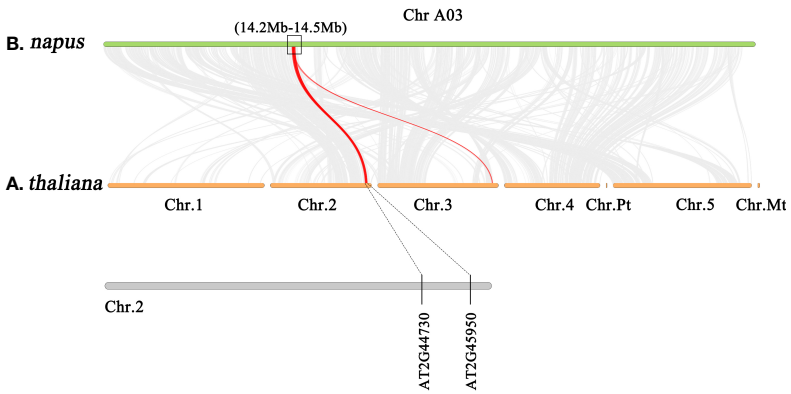

FIGURE 3
Gene synteny analysis between A03 chromosome of *B. napus* and all chromosomes of *A. thaliana*.

3.3 Resistance function screening of candidate genes

3.3.1 The clubroot disease is significantly reduced in *erf034* mutant during soil culture

Clubroot disease affects most members of the *Brassicaceae* plants, including the model species Arabidopsis, which can conveniently be used to study the biological basis of *P. brassicae*-plant interactions (Walerowski et al., 2018). To further explore the role of these candidate genes in the CR locus, Arabidopsis was taken as the test material. The wild-type *A. thaliana* (Col-0), knockout lines of each candidate gene were obtained and infected by *P. brassicae*. These phenotypes were then recorded and screened. To correctly evaluate the clubroot disease state of *A. thaliana*, we used the Col-0 to establish a rating system for *P. brassicae* infection adapting to our laboratory culture conditions (Supplementary Figure 2). According to the phenotypes, two time points, the 21 and 28 dpi were taken as the key disease investigation nodes. The DI, shoot and root phenotype, hypocotyl width and hydroponic infection phenotype were recorded, respectively.

The results of disease investigation showed that the *erf034* mutant (DI 27.5 and 46.25, respectively), corresponding to *ERF034*, had the lowest DI at both 21 and 28 dpi, and was significantly lower than Col-0 plants (DI 49.8 and 76.8, respectively). Other mutants, like *pme17*, *pub15*, and *skp1* also had significantly lower DI than Col-0 plants at 21 dpi. However, the difference between *pme17* and Col-0 was not significant at 28 dpi. While *skp1* and *pub15* had significant differences compared with Col-0, they were still reflected in relatively severe DI. Alternatively, the three mutants *atg8e*, *urm1*, and *tcp9* showed a more severe susceptibility phenotype than Col-0 plants at 21 dpi, but were not significantly different from Col-0 plants at 28 dpi (Table 4).

To visualize the phenotypic response of each mutant to *P. brassicae* infection, the roots and above-ground phenotypes of infected plants were photographed at 21 and 28 dpi, respectively (Figure 5A). The roots of wild-type Col-0 were significantly expansive growth at 21 dpi, and the ends of some severely infected main roots had started to rot, but most of the relatively healthy lateral roots were still preserved. While the roots of the more severely susceptible *atg8e*, *urm1*, and *tcp9* mutants showed obvious symptoms, such as rot of main roots and disappearance of lateral roots. The roots of *erf034*, *pme17*, *pub15*, and *skp1* mutants were less susceptible, especially the *erf034* mutant, which had robust lateral roots and many roots without obvious infection. The phenotype of the infected plants was more visually reflected in the above-ground parts by 28 dpi. The severely affected plants showed symptoms of wilting and dryness, whereas the less affected plants showed a clear purple coloration and senescence.

At the later stage of *P. brassicae* infection, the root expansion would gradually extend to the hypocotyl, so the thickness of the hypocotyl can also reflect the infection level of host plants. We counted the hypocotyl diameter of each Arabidopsis material at 21 dpi. As shown in Figure 5B, the width of *erf034* hypocotyls, expanded by an average 1.08 mm, was the smallest and significantly lower than that of the wild-type Col-0 and other mutants, showing the lowest degree of susceptibility. While the width of the primary roots of some mutants differed did not show significance, which was related to the characteristics of different materials in response to *P. brassicae* infection. Some of the mutants had earlier decay of the primary roots after the onset of infection and could not develop to a later stage, such as *atg8e*, *urm1*.

3.3.2 The development of *P. brassicae* is inhibited in *erf034* mutant during hydroponic culture

To further determine the differential response of each material in response to *P. brassicae* infection, we conducted hydroponic culture infection experiments on each material. In early infection of *P. brassicae*, root hair infection was the first to occur, but previous

TABLE 3 Homologs of candidate genes in *A. thaliana* and functional annotation.

Gene ID	ID in *A. thaliana*	Sort by percent identity (%)	Description of gene functions in *A. thaliana*
LOC106438228	AT2G44730	81.48	Alcohol dehydrogenase transcription factor Myb/SANT-like family protein
LOC106443641	AT2G44740	89.68	cyclin p4;1
LOC106443642	AT2G44745	85.57	WRKY family transcription factor
LOC106441903	AT2G44770	91.61	ELMO/CED-12 family
LOC106438229	AT2G44790	77.99	uclacyanin 2
LOC106438230	AT3G60320	80.50	bZIP domain class transcription factor (DUF630 and DUF632)
LOC106438231	AT2G44940	78.01	Ethylene-responsive transcription factor 34
LOC106441904	AT2G45060	88.52	alanine-tRNA ligase
LOC106438232	AT2G45060	85.02	alanine-tRNA ligase
LOC106438234	AT2G45070	85.88	Preprotein translocase Sec, Sec61-beta subunit protein
LOC106443643	AT2G45080	89.35	cyclin p3;1
LOC106443644	AT2G45110	80.77	expansin B4
LOC106438235	/AT2G40360	85.71	Transducin/WD40 repeat-like superfamily protein
LOC106438238	AT2G45120	79.69	C2H2-like zinc finger protein
LOC106438239	AT2G45130	84.71	SPX domain protein 3
LOC106438240	AT2G45140	87.93	plant VAP homolog 12
LOC106438237	AT2G45150	88.97	cytidinediphosphate diacylglycerol synthase 4
LOC106438236	AT2G45160	79.06	GRAS family transcription factor
LOC106438243	AT2G45170	89.60	AUTOPHAGY 8E
LOC106438242	AT2G45180	86.01	Bifunctional inhibitor/lipid-transfer protein/seed storage 2S albumin superfamily protein
LOC106438241	AT2G45190	88.71	Plant-specific transcription factor YABBY family protein
LOC106438245	AT2G45200	89.00	golgi snare 12
LOC106443645	AT2G45210	77.87	SAUR-like auxin-responsive protein family
LOC106438246	AT2G45220	88.27	Plant invertase/pectin methylesterase inhibitor superfamily
LOC106438247	AT2G45260	85.80	myosin-4 protein (DUF641)
LOC106438248	AT2G45300	89.35	RNA 3'-terminal phosphate cyclase/enolpyruvate transferase, alpha/beta
LOC106438249	AT2G45310	85.23	UDP-D-glucuronate 4-epimerase 4
BNAA03G56780D	AT2G45320	87.82	polyphosphatidylinositol phosphatase
LOC106438251	/AT4G17910	87.25	transferases, transferring acyl groups
LOC106441905	/AT1G10720	24.49	BSD domain-containing protein
LOC106443646	AT2G45510	82.69	cytochrome P450, family 704, subfamily A, polypeptide 2
LOC106438252	AT2G45510	87.38	cytochrome P450, family 704, subfamily A, polypeptide 2
LOC106441906	AT2G45640	85.15	SIN3 associated polypeptide P18
LOC106443647	AT2G45650	86.71	AGAMOUS-like 6
LOC106438253	AT2G45660	93.49	AGAMOUS-like 20
LOC106441907	/		/
LOC106441908	/AT5G04590	86.82	sulfite reductase
LOC111214396	AT2G45670	85.00	lysophosphatidylethanolamine acyltransferase 2
LOC106438255	AT2G45670	87.11	lysophosphatidylethanolamine acyltransferase 2
LOC106438256	AT2G45680	85.80	TCP family transcription factor
LOC106438257	AT2G45690	86.65	shrunken seed protein (SSE1)
LOC106443648	AT2G45695	87.19	Ubiquitin related modifier 1
LOC106443650	AT3G61110	86.92	ribosomal protein S27
LOC106438258	AT2G45720	87.07	ARM repeat superfamily protein
LOC106438259	AT2G45730	88.86	eukaryotic initiation factor 3 gamma subunit family protein
LOC106443651	AT2G45760	77.81	BON association protein 2
LOC106438263	AT2G45790	89.09	Phosphomannomutase (PPM)
LOC106438262	AT2G45800	87.11	GATA type zinc finger transcription factor family protein (PLIM2a)

(Continued)

TABLE 3 Continued

Gene ID	ID in *A. thaliana*	Sort by percent identity (%)	Description of gene functions in *A. thaliana*
LOC106438264	AT2G45940	81.40	hypothetical protein (DUF295)
LOC106443652	AT2G45930	75.98	hypothetical protein
LOC106438265	AT2G45950	52.07	SKP1-like 20

"/" represents that the candidate genes in *B. napus* have no homologous sequences in *A. thaliana*.

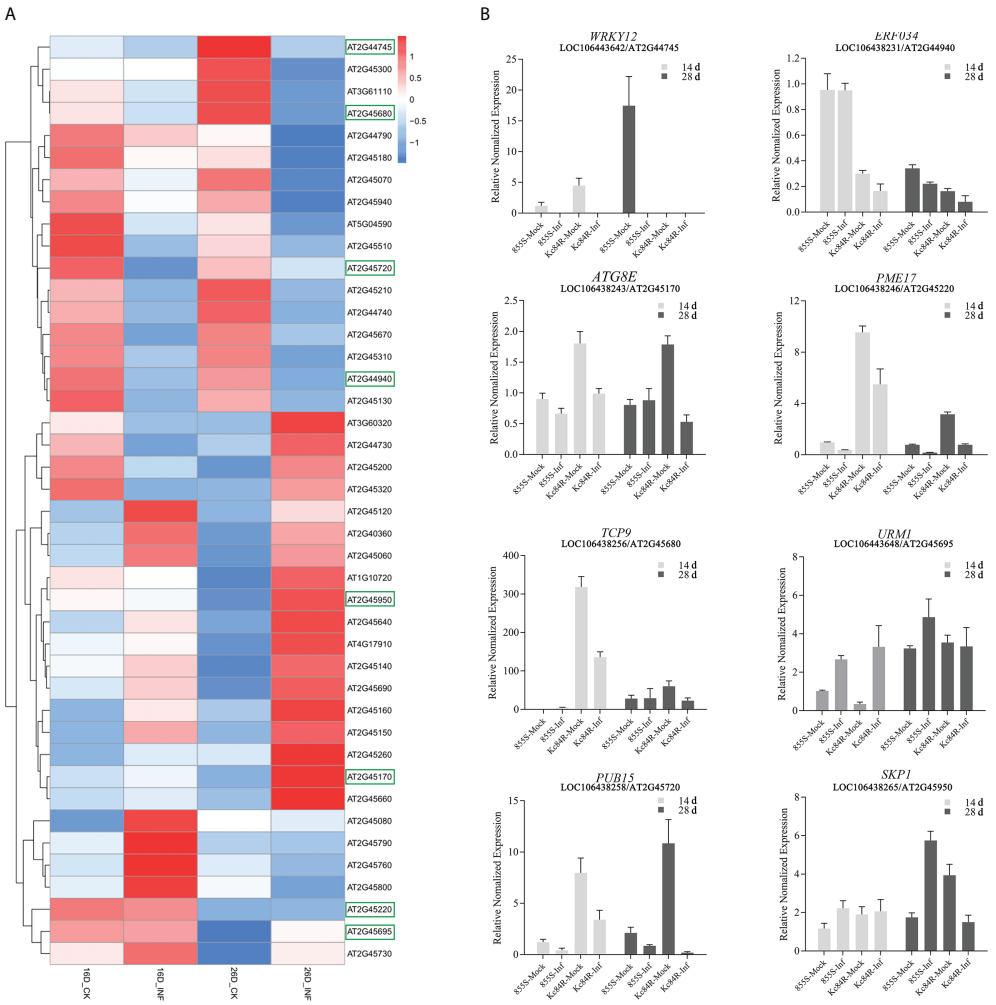

FIGURE 4
Expression patterns of candidate genes. **(A)** Expression patterns of candidate genes of homologous in *A. thaliana* roots in response to *P. brassicae*, INF indicates the treatment with *P. brassicae*, CK indicates the treatment with sterile water, the boxes indicate genes selected for quantification in *B. napus*; **(B)** transcript levels of selected candidate genes at 14- and 28-days post inoculation (dpi) in *B. napus* Kc84R and 855S. The inoculation with *P. brassicae* was taken as treatment group (Inf) and sterile water as blank control (Mock).

studies have shown that root hair infection lacks specificity, and many non-host plants of *P. brassicae* also underwent this link (Ren et al., 2016). For the host plants, successful cortical infection is the key to *P. brassicae* colonization, continuous observation of cortical infection under hydroponic culture can help us determine the differences in resistance levels of different materials to *P. brassicae* infection. As shown in Figure 6, wild-type Col-0 was taken as a reference, the occurrence mainly was adsorption of *P. brassicae* resting spores or primary zoospores during the first 12 h of infection. By the 24th hour, root hair infection could already be

TABLE 4 Results of disease investigation of *A. thaliana* inoculated with *P. brassicae*.

Materials	DI (Disease Index)	
	21 dpi	28 dpi
Col-0	49.8 ± 1.35^{b}	76.80 ± 2.41^{ab}
atg8e	60 ± 0.72^{a}	79.58 ± 1.05^{a}
erf034	27.5 ± 0.72^{e}	46.25 ± 1.10^{d}
pme17	43.9 ± 0.74^{c}	71.72 ± 1.01^{bc}
pub15	35.51 ± 1.74^{d}	65.97 ± 1.73^{c}
skp1	37.5 ± 0.36^{d}	69.72 ± 0.503^{c}
urm1	59.22 ± 1.58^{a}	80.83 ± 1.27^{a}
tcp9	63.31 ± 1.17^{a}	80.83 ± 0.96^{a}

Significance analysis of the disease index in the table was performed using the one-way ANOVA method, and different letters indicate a significant difference ($p < 0.05$).

observed, and some small primary plasmodia began to appear. By the 48th hour, the invasion of *P. brassicae* began to be detected in the cortex cells of Arabidopsis main root. Secondary plasmodium could be observed, and from then on to the period of 3 and 5 dpi, cortical infection gradually increased, and various developmental secondary plasmodia could be observed in cortex cells. Compared with wild-type Col-0, the cortical infection of *atg8e* and *urm1*, which showed more susceptible in soil culture infection, were not observed earlier than that of Col-0, but numerous secondary plasmodia could be observed at 3 dpi. While the cortical infection of the *tcp9* mutant was significantly earlier, few secondary plasmodia could be observed at 12 h post inoculation. On the other hand, the materials that showed less susceptibility in soil culture infection, such as *pme17* and *skp1*, which were not significantly different from Col-0. The observed infection time points of *pub15* were not significantly different, but the number of infected cortex cells was significantly less than that of Col-0 at the same points. In the case of *erf034*, the performance of hydroponic culture infection was also significantly different from that of Col-0. Not only was the time of cortical infection delayed, but also the state of secondary plasmodia in the cortical infection could be observed. In Col-0 and other susceptible materials, the secondary plasmodia of *P. brassicae* developed so fast that they took up most of the infected cells, or even filled a whole cortical cell, while in *erf034*, the secondary plasmodia were mostly in an undeveloped or early developing state just entering the root cortex cells, which was consistent with the results observed at 3 and 5 dpi.

3.3.3 The *erf034* mutant has significant disease tolerance under high concentrations *P. brassicae* inoculation

Combining the results of soil culture and hydroponic culture infection, it can be tentatively concluded that *erf034* was an Arabidopsis mutant with the most prominent CR characteristic relative to wild-type Col-0 and other mutants, *pub15* was able to show some level of resistance, while *tcp9*, *urm1*, and *atg8e* may be more susceptible. To confirm this phenotype, we performed the resistance retesting with higher concentrations of resting spores and continuously recorded the phenotypes of each growth period. As shown in Figure 7, there were no significant phenotypic differences between the treatment (Inf) and control groups (Mock) for all materials at 10 dpi, while at 14 dpi, differences in plant size began to appear in two treatments of each material. The growth of infected plants was inhibited and their size was significantly smaller than that of control plants. This difference was further amplified by 21 dpi. Among the different materials, *tcp9* and *atg8e* showed stronger growth inhibition than *pub15* and Col-0, and this difference was more pronounced relative to *erf034*. These intergroup differences were also more pronounced at 28 dpi. For the sake of observation, the phenotypes at 28 dpi we listed were the photographic records of the treatment and control groups after stem cutting, while the uncut treatment groups showed that there were extremely obvious phenotypic differences in the two groups of different materials. On the one hand, *erf034* can shoot and flower normally and produce silique despite the stress of infection. On the other hand, the differentiation of flower buds was inhibited, and the number of shoots was less than that of the control group, especially the wild-type Col-0 was almost unable to shoot normally at 28 dpi. The infected plants were dwarf, the leaves started to wilt, and turned purple or yellow. The *pub15* varied considerably among individuals, with plants capable of normally flowering or dwarf and purple, which were similar to the phenotype of the more susceptible *tcp9*, but the overall growth and development were significantly inhibited. The susceptible plants *atg8e* were more extreme, showing purple leaves and even withering of the whole plants. In summary, the mutant *erf034* had the best CR phenotype in response to *P. brassicae* infection.

3.4 ERF034 is a transcriptional activator in response to biotic stresses

To further clarify the role of *ERF034* in the process of clubroot disease, relevant bioinformatics analysis and functional exploration of *ERF034* was performed. *ERF034* was abundantly expressed in the roots of *B. napus* and *A. thaliana* during the seedling stage (Supplementary Figure 3), and *AtERF034* showed down-regulated expression in various biotic stress states (Supplementary Figure 4). Transcription factors of the ERF family generally contain a highly conserved ERF domain, which is composed of 4 α-helices and 3 β-sheets, of which 1 α-helix and 3 β-sheets at the N-terminal are the key to the interaction of proteins with cis-elements (Figure 8A). The Valine 14 and Glutamicacid 19 on β-sheet are required for binding to cis-elements, and the flanking sequences affect the efficiency of ERF protein binding to cis-acting elements (Tournier et al., 2003; Canella et al., 2010). According to the structural prediction, *At*ERF034 had this typical ERF domain (Figure 8B). Furthermore, the protein sequences encoded by *BnERF034* did not differ much in the two materials, especially the β-fold sequence, encoded the ability to bind specific motifs

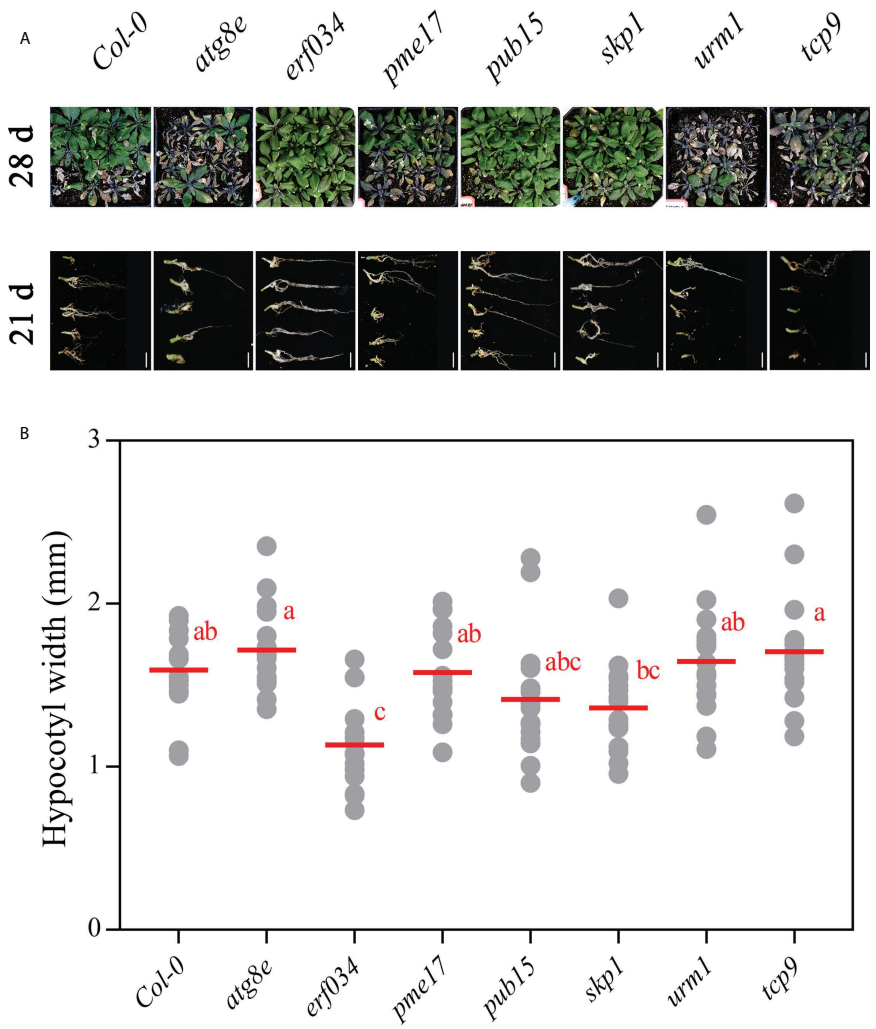

FIGURE 5
Phenotypes of *A. thaliana* inoculated with *P. brassicae* in soil culture. **(A)** Above-ground parts of Col-0 and each mutant material at 28 dpi, roots at 21 dpi; scale bars represent 2 cm. **(B)** Hypocotyl width of *A. thaliana* inoculated with *P. brassicae* at 21 dpi. Scatter plots present individual hypocotyl width measurements (12 replicates for each treatment), calculated means and SEs. Different letters indicate significant differences between means (Tamhane's test, $p < 0.05$).

was highly consistent (Figure 8C). This implies that the differences of resistance levels in different materials were not caused by functional differences of ERF034. To further clarify the location of *Bn*ERF034, *Bn*ERF034-855S-eGFP, and *Bn*ERF034-Kc84R-eGFP were expressed in *N. benthamiana* leaves, and fluorescent signals were detected by fluorescence microscope. The results showed that enhanced green fluorescent protein (eGFP) fluorescent signals were localized in the cell nucleus (Figure 8D). The transactivation abilities of *Bn*ERF034-855S and *Bn*ERF034-Kc84R were analyzed using a yeast assay system. As shown in Figure 8E, the transformants harboring GAL4, *Bn*ERF034-855S, and *Bn*ERF034-Kc84R grew well, while the cells containing pBD and PUB15 could not grow on the same medium. The X-α-gal staining for β-galactosidase activity showed blue in cells having GAL4, *Bn*ERF034-855S and *Bn*ERF034-Kc84R. These results indicate that the *Bn*ERF034-855S and *Bn*ERF034-Kc84R have transactivation capacity.

3.5 Heterogeneous expression of *BnERF034* enhanced the virulence of *P. brassicae*

Additionally, we generated transgenic *A. thaliana* lines expressing *BnERF034* (from 855S and Kc84R, respectively) to further investigate the effect of *BnERF034* in clubroot disease. The positive plants and expression of *BnERF034* were confirmed by Basta solution, PCR and RT-qPCR, respectively

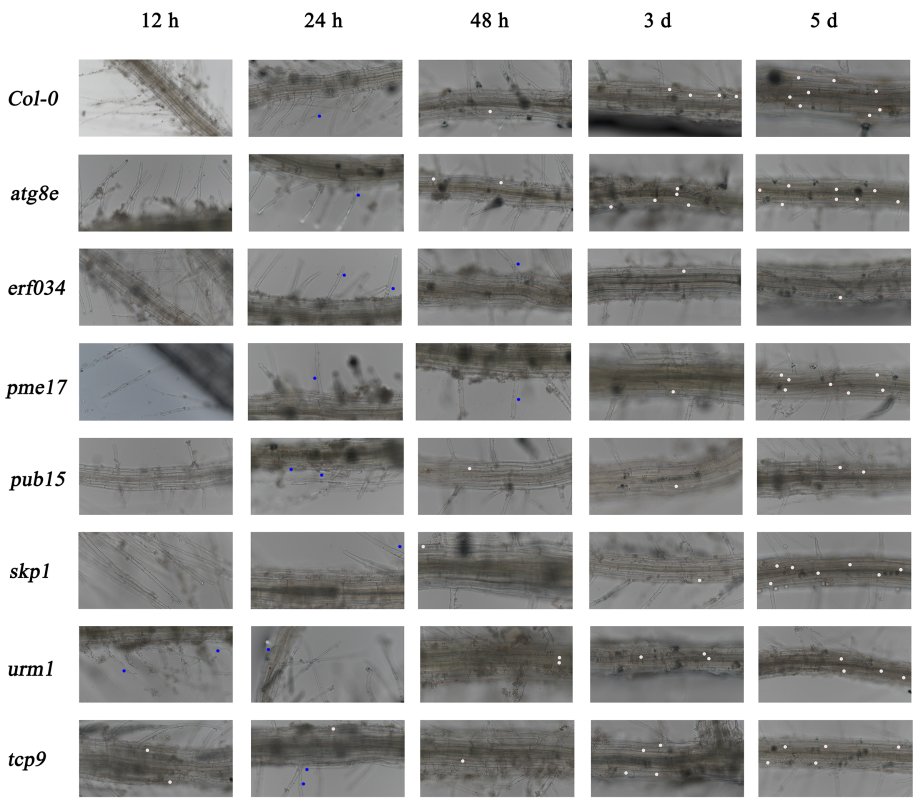

FIGURE 6
Roots observation of *A. thaliana* inoculated with *P. brassicae* in hydroponic culture. Blue dots indicate the *P. brassicae* of root hair-infected stage, white dots indicate the *P. brassicae* of cortex-infected.

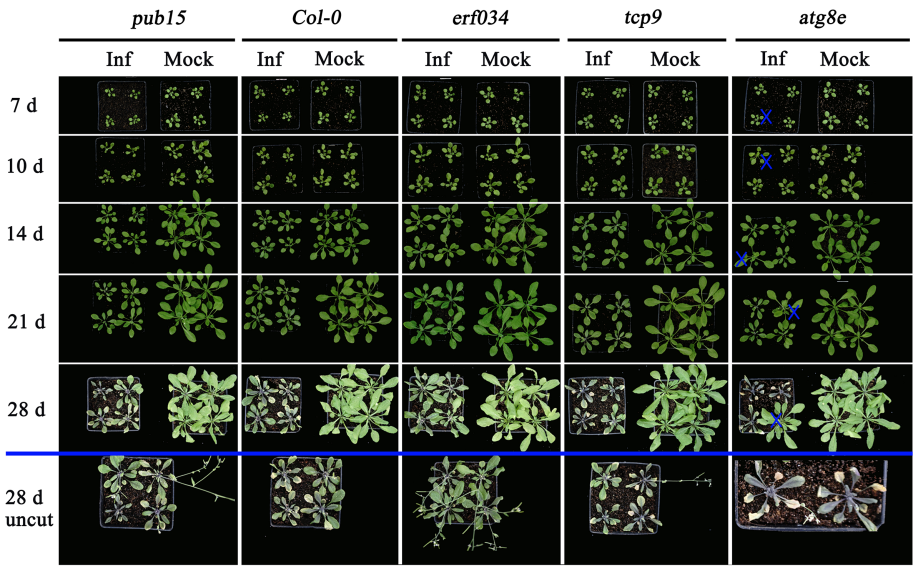

FIGURE 7
Clubroot disease development in *A. thaliana* for retesting. The plants below the blue line indicates the uncut above-ground portion, "×" indicates the single plants inoculated with sterile water in the *atg8e* treatment group.

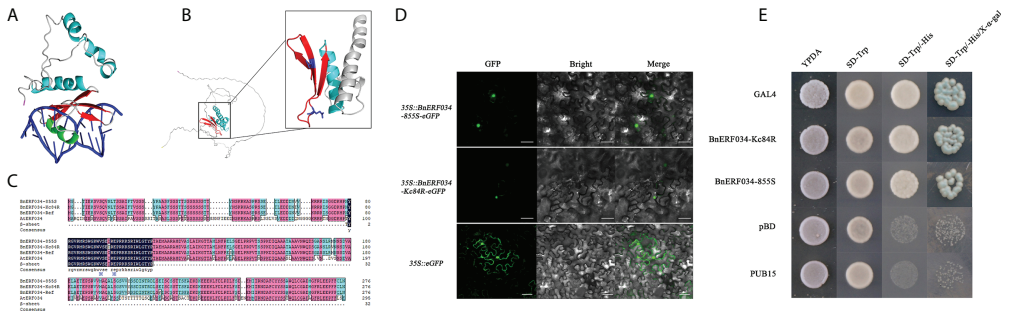

FIGURE 8
Bioinformatics analysis and related functional analysis of ERF034. **(A)** Conserved structural domain elements of ERF transcription factors. **(B)** Structure prediction of *At*ERF034 and characterization of its ERF structural domain. **(C)** Comparison of the ERF034 and β-sheet sequences from 855S, Kc84R and *A. thaliana*. **(D)** Subcellular localization of *Bn*ERF034-eGFP, scale bars represent 50 μm. **(E)** Transcriptional activation activity verification of *Bn*ERF034.

(Supplementary Figure 5). All transgenic lines, mutants and wild type Col-0 were inoculated with *P. brassicae*. Above-ground partial phenotype photography and the occurrence of clubroot disease were investigated at 21 dpi. Root phenotypes were photographed and collected at 28 dpi. The results showed that the *BnERF034* transgenic plants were more severely susceptible to the clubroot disease under the same infection conditions (Figure 9A). In the wild type Col-0, the percentage of medium to severe galls (disease classes 3 and 5) was 63.3%, and the percentage of small galls (disease classes 0 and 1) was 36.7%. In the *BnERF034* heterogeneous expression lines, the percentage of medium to severe galls was higher, with a value of 98.4% in *35S::BnERF034-Kc84R*#1, 88.89% in *35S::BnERF034-Kc84R*#2, 93.33% in *35S::BnERF034-Kc84R*#3, 87.09% in *35S::BnERF034-855S*#1 and 91.66% in *35S::BnERF034-855S*#2. The percentage of medium to severe galls with a value of 16.13% in *erf034* mutants (Figure 9B). On the other hand, the hypocotyl width of infected plants was significantly decreased in the *erf034* mutant (on average by 62.25 at 28 dpi; Figures 9C, D), and significantly increased in the *BnERF034* transgenic lines (on average by 262.07% at 28 dpi; Figures 9C, D), in relation to Col-0 controls. These results illustrate that *BnERF034* enhanced the virulence of *P. brassicae* and promoted plant susceptibility to clubroot disease in *A. thaliana*, and further suggested that ERF034 was an important factor controlling CR trait and exhibited the characteristics of negative regulation.

To explore the relationship between the CR trait and *ERF034*, we further compared the transcript level of *ERF034* in response to the *P. brassicae* infection between Kc84R and 855S in hydroponic culture. The results showed that the transcript level of *BnERF034* in 855S gradually increased over time, but it did not strictly increase with the infection stage. There was no significant change in all stages in Kc84R, and compared with 855S, the transcript level of *BnERF034* was significantly lower (Figure 10A). Combined with the data from soil culture (Figure 4B), the transcript levels of *BnERF034* in Kc84R at each time point we tested were the same significantly lower than 855S. We further analyzed the segments containing the promoter sequence in Kc84R and 855S according to the BSA-Seq files and found that Kc84R had many deletions and mutations in the segment predicted to be *BnERF034* promoter element, relative to 855S (Figure 10B). In particular, in the predicted promoter region from 1,779 bp to 1,729 bp upstream of the 5'-UTR, there was an AT deletion and a G→A base substitution, and there was also a 16 bp fragment deletion downstream adjacent to this region, which may directly affect the transcript level of *BnERF034*.

4 Discussion

With the development of modern agriculture, *P. brassicae* has rapidly spread among major oilseed producing areas in China. Clubroot disease has become one of the most serious diseases affecting *Brassicaceae* crop production (Dixon, 2009; Chai et al., 2014). Therefore, it is urgent to choose more economical and effectively management measures to control clubroot disease. Clubroot disease resistance breeding has proven to be a powerful approach, however, there are still two important problems for the resistance breeding: one is the lack of CR resources, especially in *B. napus* (Werner et al., 2008); Another is the complex genetic basis and relatively genetic variation of *P. brassicae*. These make it necessary to screen and breed corresponding CR materials for different *P. brassicae* isolates (Strelkov et al., 2016). The pathotype in Guanghan, Sichuan province (*Pb*Gh) used in this study has been identified as Pb3, according to the sinitic clubroot differential set (SCD) system (Pang et al., 2020). In our study, Kc84R is a selected line of *B. napus* "Kc84-1," which is obtained from ARTP mutagenesis and has stable *Pb*Gh CR trait. In view of the current status of CR genes in *B. napus*, the CR locus in Kc84R has great potential to

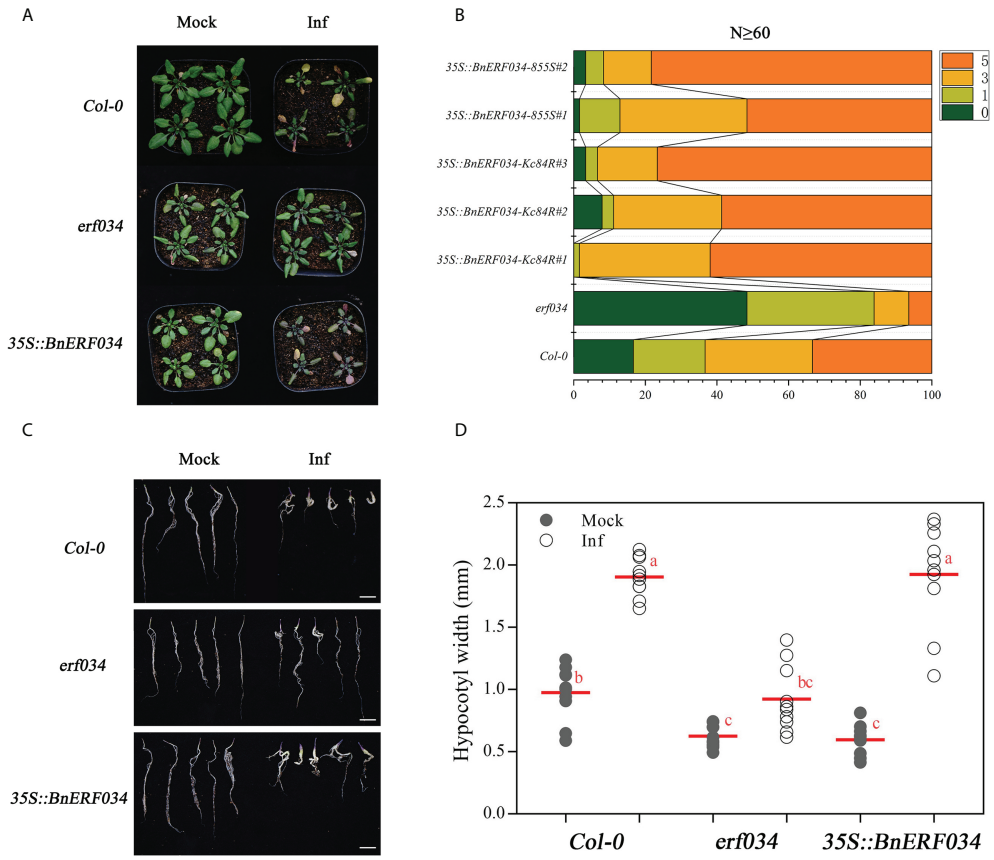

FIGURE 9
BnERF034 enhanced the severity of clubroot disease in *A. thaliana*. **(A)** Above-ground phenotype of *A. thaliana* Col-0, *erf034*, and transgenic lines of *BnERF034* at 21 dpi. **(B)** Results of disease survey, 0-5 indicates disease grade. **(C)** Root phenotypes of *A. thaliana* materials at 28 dpi, scale bars represent 2 cm. **(D)** Hypocotyl width of different *A. thaliana* materials at 28 dpi in sterile water-inoculated (Mock) and *P. brassicae*-inoculated (Inf). Scatter plots present individual hypocotyl width measurements (10 replicates for each treatment), calculated means and SEs. Different letters indicate significant differences between means (Tamhane's test, $p < 0.05$).

be studied. In this study, the CR locus mapping population was performed with BSA-seq approach and SNP genotyping. Before that, the parents ("Kc84R" and "855S" respectively), the F_1 and F_2 populations were inoculated with the *Pb*Gh isolate, respectively. The phenotype of F_1 and F_2 populations infected showed that the CR trait was controlled by a dominant locus (Table 2, Figure 2A). A single peak was identified on the A03 chromosome, and the CR locus was further narrowed down to an interval of 267 kb. This result differed from previous reports of resistance to clubroot disease in *B. napus*.

Generally, plant disease resistance refers to the interaction between plant innate immune system and pathogens, that is, the interaction of pathogen-associated molecular patterns (PAMPs) and effector proteins with PTI (PAMP-triggered immunity) or ETI (effector-triggered immunity) (Deng et al., 2020). Therefore, the current mapping of disease resistance genes generally refers to identifying genes that can participate in the plant immune system, and then exploring their role in the disease resistance process. Firstly, there are numerous immune receptors consisting of receptor-like proteins (RLPs) and receptor kinases (RKs) on the cell surface of host plants, which can recognize the PAMPs of invading pathogens (Tang et al., 2017; Zhou and Zhang, 2020). A series of immune responses are subsequently activated, such as calcium influx, reactive oxygen species (ROS) burst, production of defense hormones and activation of mitogen-activated protein kinase (MAPK) cascades, etc. (Tang et al., 2017). In addition, plant intracellular immune receptors can be classified into three major subgroups according to their N-terminal domains: TIR-NBS-LRR (TNL) proteins carrying a Toll Interleukin-1 Receptor (TIR) domain, CC-NBS-LRR (CNL) proteins carrying a coiled coil (CC) domain, and RPW8-NB-ARC-LRR (RNL) proteins carrying a RPW8-like (CC R) domain (Wang and Chai, 2020), all of which can specifically sense various pathogen effector proteins that are delivered into the plant cell (Zhou and Zhang, 2020). Subsequently, the corresponding downstream defense responses are also activated, such as programmed cell death or

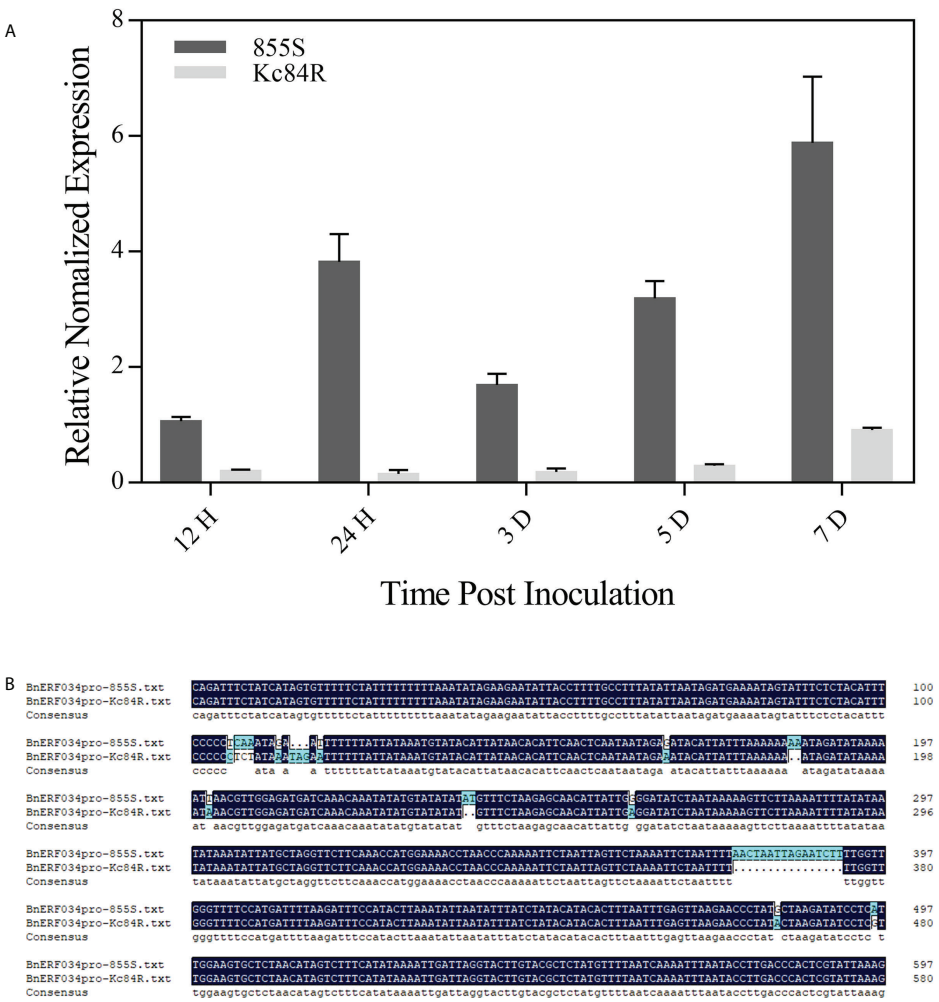

FIGURE 10
Expression patterns and predicted promoter regions of *BnERF034* in Kc84R and 855S. **(A)** Expression patterns of *BnERF034* in Kc84R and 855S in hydroponic culture infection with *P. brassicae*. **(B)** Sequence alignment of predicted promoter regions of *BnERF034* in Kc84R and 855S.

called hypersensitive response (HR), SA biosynthesis, ROS burst, MAPK cascades and other immune responses (Zhang et al., 2017; Yuan et al., 2021). It turns out that in both immune pathways, plants ultimately rely on various immune responses to resist the infection by pathogens. The mapping of disease resistance genes is the search for genes involved in plant immune responses. Although the reported CR loci either directly encode (only two CR genes, namely, *CRa* and *Crr1a*) or contain TIR-NB-LRR proteins, the mechanisms of resistance involved in these disease resistance proteins have rarely been studied.

As there are no common CR genes belonging to TNL gene families in the target region, we need to perform functional annotation and screening of all candidate genes. It is well known that the interaction between host plants and pathogens is a complex process. In face of pathogens invasion, host plants have evolved various ways to resist the attack, including but not limited to autophagy (blocking further colonization by discarding the infected part) (Zhang et al., 2021), ubiquitin pathway (targeting certain proteins are involved in disease resistance response, enhancing the system's disease resistance response) (Christians et al., 2009; Li et al., 2012), and some broad-spectrum resistance, such as systemic acquired resistance (SAR), in which an important defense hormone, salicylic acid (SA), plays a major role (Century et al., 1997; Zheng et al., 2015). By analyzing the candidate genes, we found that *ATG8E* annotated to participate in autophagy, *PUB15*, *URM1* and *SKP1* involved in ubiquitination, and the transcription factor *TCP9* is related to salicylic acid synthesis (Wang et al., 2015). However, these *A. thaliana* lines corresponding to the candidate genes showed relatively less effect on CR. For example, the 742nd position of

the *PUB15* encoding sequence in Kc84R, mutated from C to T, has been early terminated (Supplementary Figures 6A, B). The functional domain of *BnPUB15* is mainly composed of 3 ARM domains, which contains many polypeptides binding sites (Supplementary Figure 6C). This implies that *BnPUB15* may regulate the clubroot disease by targeting a certain protein. We carried out the infection tests with the relevant lines of *BnPUB15*, and the results showed that the transgenic lines were not more obvious than the wild-type Col-0, some of them showed even more susceptible (Supplementary Figure 6D). *BnTCP9* was the largest difference in transcript level between Kc84R and 855S (Figure 4B). In the previous infection experiments, we also found that *tcp9* mutants showed earlier infected symptoms (Figures 5A, 6). Correlation analysis and functional verification experiments showed that *BnTCP9* was a nuclear localized protein, its homologous sequence in *A. thaliana* had a typical transcription factor domain (Supplementary Figures 7A, B). Additionally, TCP9 can bind to the promoter region of *ICS1* and positively regulate the expression of *ICS1* (Wang et al., 2015) (Supplementary Figure 7E). But similar to the results of other studies, the SA pathway cannot resist the infection of *P. brassicae* alone, and a relatively high content of SA can only relatively alleviate the disease symptoms (Lovelock et al., 2016). Therefore, even though the infected *BnTCP9* transgenic lines had delayed leaf senescence compared with Col-0 and *tcp9*, the galls were not significantly reduced compared to Col-0 (Supplementary Figures 7C, D). Furthermore, we also constructed transgenic lines for several other genes, but some were unsuccessfully transformed in the construction of transgenic lines and others were missing during the passaging process due to various problems. The mining of CR-related genes in target region still needs to be further developed.

In our study, ERF034 is a negative regulator participating in clubroot disease, but the corresponding regulation pathway is still unclear. ERF is a major sub-family of AP2/ERF transcription factor, and generally contains only an AP2/EREBP domain. The cis-acting elements that can be combined mainly include two categories: GCC boxes and DRE/CRT (DRE: Dehydration-Responsive Element, CRT: C Repeat); (Qin et al., 2004). GCC box (conservative sequence is GCCGCC) exists in a large number of *PR* gene promoters (Büttner and Singh, 1997). DRE/CRT components (conservative sequences are CCGAC) mostly exist in the genes involved in low temperature response or are drought induced (Liu et al., 1998). ERF transcription factors can regulate the expression of most target genes through these two types of cis-acting elements with occasional exceptions (Chakravarthy et al., 2003). Additionally, ERF transcription factors play an important role in both abiotic stress responses and biotic stress responses in plants. Previous studies have used knockout mutants and overexpression materials of the ERF family genes to verify their function in the disease resistance response of *A. thaliana*. For example, the resistance of plants overexpressing *AtERF4* to *Fusarium oxysporum* was significantly reduced, while the resistance of loss-of-function mutant *erf4* was enhanced, indicating that *AtERF4* can negatively regulate Fusarium wilt resistance, and overexpression of *AtERF2* can improve *A. thaliana* resistance to Fusarium Wilt (McGrath et al., 2005). Onate-Sanchez et al. tested *erf14* mutants and *AtERF14* overexpressing lines and found that loss of *ERF14* function resulted in reduced resistance to Fusarium wilt in *A. thaliana*, whereas overexpression enhanced this resistance (Oñate-Sánchez et al., 2007). In addition, the overexpression of *AtERF14* can suppress JA-ethylene responsive *AtPDF1.2* while activate SA-responsive *AtPR1/5* genes (Zhang et al., 2016). *AtERF019* can interact with the transcriptional co-repressor NINJA, and transgenic Arabidopsis overexpressing *ERF019* is more susceptible to *Botrytis cinerea* (Huang et al., 2019). All these studies have shown that ERF family transcription factor is highly related to biotic stress. As for ERF034, *At*ERF034 is a nuclear-localized transcription factor, which can bind the core cis-acting element DRECRTCOREAT, and upregulate the promoter activity of *CESA1* (cellulose synthase catalytic subunit 1) (Schwacke et al., 2007; Saelim et al., 2019). *At*ERF034 can also interact with *TMO6* (AT5G60200) and participate in the regulatory network of Arabidopsis root development (Brady et al., 2011). Furthermore, the regulatory network analysis of *BnERF034* homologous participating in *A. thaliana* and *B. rapa* showed that the genes annotated as *RAP2.7* (*TOE1*) and *TOE2* were present in both materials (Supplementary Figure 8, Supplementary Tables 9, 10). The miR172/TOE1-TOE2 is an important regulatory module in plants, involved in plant development regulation, morphogenesis and innate immunity (Zou et al., 2018; Werner et al., 2021). There has been reported that this module in response to *P. brassicae* infection in *B. napus* (Li et al., 2021a). In summary, the exploration of the CR mechanism involving *ERF034* can be carried out from these three aspects: (i) hormone regulation associated with *ERF034*, including ethylene, SA, jasmonic acid (JA), etc.; (ii) target genes that *ERF034* can regulate through cis-acting elements; (iii) modules related to plant immunity involving *ERF034*, such as miRNAs, etc. Therefore, in-depth exploration of *ERF034* is helpful to explain its involvement in the CR.

Data availability statement

The data presented in the study are deposited in the Genome Sequence Archive in National Genomics Data Center repository, accession number CRA008099.

Author contributions

MW and XJ designed and directed the experiments. XJ and YS performed most of the experiments and analysed the data. XJ

wrote the manuscript. All authors contributed to the article and approved the submitted version.

Funding

This research was funded by The National Key Research and Development Plan, grant numbers 2016YFD0100202 and 2018YFD0100501, and Sichuan Province Breeding Project, grant number 2016NYZ0031.

Conflict of interest

The authors declare that the research was conducted in the absence of any commercial or financial relationships that could be construed as a potential conflict of interest.

Publisher's note

Supplementary material

The Supplementary Material for this article can be found online at: https://www.frontiersin.org/articles/10.3389/fpls.2022.1014376/full#supplementary-material

References

Brady, S. M., Zhang, L., Megraw, M., Martinez, N. J., Jiang, E., Yi, C. S., et al. (2011). A stele-enriched gene regulatory network in the arabidopsis root. *Mol. Syst. Biol.* 7, 459. doi: 10.1038/msb.2010.114

Büttner, M., and Singh, K. B. (1997). *Arabidopsis thaliana* ethylene-responsive element binding protein (*At*EBP), an ethylene-inducible, GCC box DNA-binding protein interacts with an ocs element binding protein. *Proc. Natl. Acad. Sci. U.S.A.* 94, 5961–5966. doi: 10.1073/pnas.94.11.5961

Canella, D., Gilmour, S. J., Kuhn, L. A., and Thomashow, M. F. (2010). DNA Binding by the *Arabidopsis* CBF1 transcription factor requires the PKKP/RAGRxKFxETRHP signature sequence. *Biochim. Biophys. Acta* 1799, 454–462. doi: 10.1016/j.bbagrm.2009.11.017

Ce, F., Mei, J., He, H., Zhao, Y., Hu, W., Yu, F., et al. (2021). Identification of candidate genes for clubroot-resistance in *Brassica oleracea* using quantitative trait loci-sequencing. *Front. Plant Sci.* 12. doi: 10.3389/fpls.2021.703520

Century, K. S., Shapiro, A. D., Repetti, P. P., Dahlbeck, D., Holub, E., and Staskawicz, B. J. (1997). NDR1, a pathogen-induced component required for arabidopsis disease resistance. *Science* 278, 1963–1965. doi: 10.1126/science.278.5345.1963

Chai, A. L., Xie, X. W., Shi, Y. X., and Li, B. J. (2014). Research status of clubroot (*Plasmodiophora brassicae*) on cruciferous crops in China. *Can. J. Plant Pathol.* 36, 142–153. doi: 10.1080/07060661.2013.868829

Chakravarthy, S., Tuori, R. P., D'Ascenzo, M. D., Fobert, P. R., Despres, C., and Martin, G. B. (2003). The tomato transcription factor Pti4 regulates defense-related gene expression *via* GCC box and non-GCC box cis elements. *Plant Cell* 15, 3033–3050. doi: 10.1105/tpc.017574

Chen, C., Chen, H., Zhang, Y., Thomas, H. R., Frank, M. H., He, Y., et al. (2020). TBtools: An integrative toolkit developed for interactive analyses of big biological data. *Mol. Plant* 13, 1194–1202. doi: 10.1016/j.molp.2020.06.009

Chen, J., Jing, J., Zhan, Z., Zhang, T., Zhang, C., and Piao, Z. (2013). Identification of novel QTLs for isolate-specific partial resistance to *Plasmodiophora brassicae* in *Brassica rapa*. *PloS One* 8, e85307. doi: 10.1371/journal.pone.0085307

Christians, M. J., Gingerich, D. J., Hansen, M., Binder, B. M., Kieber, J. J., and Vierstra, R. D. (2009). The BTB ubiquitin ligases ETO1, EOL1 and EOL2 act collectively to regulate ethylene biosynthesis in arabidopsis by controlling type-2 ACC synthase levels. *Plant J.* 57, 332–345. doi: 10.1111/j.1365-313X.2008.03693.x

Chu, M., Yu, F., Falk, K. C., Liu, X., Zhang, X., Chang, A., et al. (2013). Identification of the clubroot resistance gene *Rpb1* and introgression of the resistance into canola breeding lines using a marker-assisted approach. *Acta Hortic.* 1005, 599–605. doi: 10.17660/ActaHortic.2013.1005.74

Clough, S. J., and Bent, A. F. (1998). Floral dip: a simplified method for agrobacterium-mediated transformation of *Arabidopsis thaliana*. *Plant J.* 16, 735–743. doi: 10.1046/j.1365-313x.1998.00343.x

Deng, Y., Ning, Y., Yang, D. L., Zhai, K., Wang, G. L., and He, Z. (2020). Molecular basis of disease resistance and perspectives on breeding strategies for resistance improvement in crops. *Mol. Plant* 13, 1402–1419. doi: 10.1016/j.molp.2020.09.018

Diederichsen, E., Beckmann, J., Schondelmeier, J., and Dreyer, F. (2006). *Genetics of clubroot resistance in brassica napus ´Mendel´* (Leuven, Belgium: International Society for Horticultural Science (ISHS), 307–312.

Diederichsen, E., and Sacristan, M. D. (1996). Disease response of resynthesized *Brassica napus* l. lines carrying different combinations of resistance to *Plasmodiophora brassicae* wor. *Plant Breed.* 115, 5–10. doi: 10.1111/j.1439-0523.1996.tb00862.x

Dixon, G. R. (2009). The occurrence and economic impact of *Plasmodiophora brassicae* and clubroot disease. *J. Plant Growth Regul.* 28, 194–202. doi: 10.1007/s00344-009-9090-y

Grandclément, C., and Thomas, G. (1996). Detection and analysis of QTLs based on RAPD markers for polygenic resistance to *Plasmodiophora brassicae* woron in *Brassica oleracea* l. *Theor. Appl. Genet.* 93, 86–90. doi: 10.1007/BF00225731

Hatakeyama, K., Suwabe, K., Tomita, R. N., Kato, T., Nunome, T., Fukuoka, H., et al. (2013). Identification and characterization of *Crr1a*, a gene for resistance to clubroot disease (*Plasmodiophora brassicae* woronin) in *Brassica rapa* l. *PloS One* 8, e54745. doi: 10.1371/journal.pone.0054745

Hayashida, N., Takabatake, Y., Nakazawa, N., Aruga, D., Nakanishi, H., Taguchi, G., et al. (2008). Construction of a practical SCAR marker linked to clubroot resistance in Chinese cabbage, with intensive analysis of HC352b genes. *J. Japan Soc Hortic. Sci.* 77, 150–154. doi: 10.2503/jjshs1.77.150

Hejna, O., Havlickova, L., He, Z., Bancroft, I., and Curn, V. (2019). Analysing the genetic architecture of clubroot resistance variation in *Brassica napus* by associative transcriptomics. *Mol. Breed.* 39, 112. doi: 10.1007/s11032-019-1021-4

Huang, Z., Peng, G., Liu, X., Deora, A., Falk, K. C., Gossen, B. D., et al. (2017). Fine mapping of a clubroot resistance gene in Chinese cabbage using SNP markers identified from bulked segregant RNA sequencing. *Front. Plant Sci.* 8. doi: 10.3389/fpls.2017.01448

Huang, P. Y., Zhang, J., Jiang, B., Chan, C., Yu, J. H., Lu, Y. P., et al. (2019). NINJA-associated ERF19 negatively regulates *Arabidopsis* pattern-triggered immunity. *J. Exp. Bot.* 70, 1033–1047. doi: 10.1093/jxb/ery414

Jiang, Y., Zhan, Z., Piao, Z., and Zhang, C. (2018). Progresses and prospects of germplasms innovation for clubroot resistance and genetic improvement in *Brassica napus*. *Acta Agron. Sin.* 44, 1592–1599. doi: 10.3724/sp.J.1006.2018.01592

Kato, T., Hatakeyama, K., Fukino, N., and Matsumoto, S. (2013). Fine mapping of the clubroot resistance gene *CRb* and development of a useful selectable marker in *Brassica rapa*. *Breed. Sci.* 63, 116–124. doi: 10.1270/jsbbs.63.116

Laila, R., Park, J. I., Robin, A. H. K., Natarajan, S., Vijayakumar, H., Shirasawa, K., et al. (2019). Mapping of a novel clubroot resistance QTL using ddRAD-seq in Chinese cabbage (*Brassica rapa* l.). *BMC Plant Biol.* 19, 13. doi: 10.1186/s12870-018-1615-8

Li, W., Ahn, I. P., Ning, Y., Park, C. H., Zeng, L., Whitehill, J. G., et al. (2012). The U-Box/ARM E3 ligase PUB13 regulates cell death, defense, and flowering time in arabidopsis. *Plant Physiol.* 159, 239–250. doi: 10.1104/pp.111.192617

Li, Q., Shah, N., Zhou, Y., Hou, Z., Gong, J., Liu, J., et al. (2021b). Breeding of a novel clubroot disease-resistant *Brassica napus* variety huayouza 62R. *Acta Agron. Sin.* 47, 210–223. doi: 10.3724/SP.J.1006.2021.04086

Li, Q., Shah, N., Zhou, X., Wang, H., Yu, W., Luo, J., et al. (2021a). Identification of micro ribonucleic acids and their targets in response to *Plasmodiophora brassicae* infection in *Brassica napus*. *Front. Plant Sci.* 12. doi: 10.3389/fpls.2021.734419

Liu, Q., Kasuga, M., Sakuma, Y., Abe, H., Miura, S., Yamaguchi-Shinozaki, K., et al. (1998). Two transcription factors, DREB1 and DREB2, with an EREBP/AP2 DNA binding domain separate two cellular signal transduction pathways in drought- and low-temperature-responsive gene expression, respectively, in arabidopsis. *Plant Cell* 10, 1391–1406. doi: 10.1105/tpc.10.8.1391

Lovelock, D. A., Šola, I., Marschollek, S., Donald, C. E., Rusak, G., van Pée, K. H., et al. (2016). Analysis of salicylic acid-dependent pathways in *Arabidopsis thaliana* following infection with *Plasmodiophora brassicae* and the influence of salicylic acid on disease. *Mol. Plant Pathol.* 17, 1237–1251. doi: 10.1111/mpp.12361

Malinowski, R., Novák, O., Borhan, M. H., Spíchal, L., Strnad, M., and Rolfe, S. A. (2016). The role of cytokinins in clubroot disease. *Eur. J. Plant Pathol.* 145, 543–557. doi: 10.1007/s10658-015-0845-y

Matsumoto, E., Yasui, C., Ohi, M., and Tsukada, M. (1998). Linkage analysis of RFLP markers for clubroot resistance and pigmentation in Chinese cabbage (*Brassica rapa* ssp. *pekinensis*). *Euphytica* 104, 79. doi: 10.1023/A:1018370418201

McGrath, K. C., Dombrecht, B., Manners, J. M., Schenk, P. M., Edgar, C. I., Maclean, D. J., et al. (2005). Repressor- and activator-type ethylene response factors functioning in jasmonate signaling and disease resistance identified *via* a genome-wide screen of arabidopsis transcription factor gene expression. *Plant Physiol.* 139, 949–959. doi: 10.1104/pp.105.068544

Olszak, M., Truman, W., Stefanowicz, K., Sliwinska, E., Ito, M., Walerowski, P., et al. (2019). Transcriptional profiling identifies critical steps of cell cycle reprogramming necessary for *Plasmodiophora brassicae*-driven gall formation in arabidopsis. *Plant J.* 97, 715–729. doi: 10.1111/tpj.14156

Oñate-Sánchez, L., Anderson, J. P., Young, J., and Singh, K. B. (2007). *At*ERF14, a member of the ERF family of transcription factors, plays a nonredundant role in plant defense. *Plant Physiol.* 143, 400–409. doi: 10.1104/pp.106.086637

Pang, W., Fu, P., Li, X., Zhan, Z., Yu, S., and Piao, Z. (2018). Identification and mapping of the clubroot resistance gene *CRd* in Chinese cabbage (*Brassica rapa* ssp. *pekinensis*). *Front. Plant Sci.* 9. doi: 10.3389/fpls.2018.00653

Pang, W., Liang, S., Li, X., Li, P., Yu, S., Lim, Y. P., et al. (2014). Genetic detection of clubroot resistance loci in a new population of *Brassica rapa*. *Hortic. Environ. Biotechnol.* 55, 540–547. doi: 10.1007/s13580-014-0079-5

Pang, W., Liang, Y., Zhan, Z., Li, X., and Piao, Z. (2020). Development of a sinitic clubroot differential set for the pathotype classification of *Plasmodiophora brassicae*. *Front. Plant Sci.* 11. doi: 10.3389/fpls.2020.568771

Piao, Z., Ramchiary, N., and Lim, Y. P. (2009). Genetics of clubroot resistance in *Brassica* species. *J. Plant Growth Regul.* 28, 252–264. doi: 10.1007/s00344-009-9093-8

Qin, F., Sakuma, Y., Li, J., Liu, Q., Li, Y. Q., Shinozaki, K., et al. (2004). Cloning and functional analysis of a novel DREB1/CBF transcription factor involved in cold-responsive gene expression in *Zea mays* l. *Plant Cell Physiol.* 45, 1042–1052. doi: 10.1093/pcp/pch118

Ren, L., Xu, L., Liu, F., Chen, K., Sun, C., Li, J., et al. (2016). Host range of *Plasmodiophora brassicae* on cruciferous crops and weeds in China. *Plant Dis.* 100, 933–939. doi: 10.1094/pdis-09-15-1082-re

Rocherieux, J., Glory, P., Giboulot, A., Boury, S., Barbeyron, G., Thomas, G., et al. (2004). Isolate-specific and broad-spectrum QTLs are involved in the control of clubroot in *Brassica oleracea*. *Theor. Appl. Genet.* 108, 1555–1563. doi: 10.1007/s00122-003-1580-x

Saelim, L., Akiyoshi, N., Tan, T. T., Ihara, A., Yamaguchi, M., Hirano, K., et al. (2019). Arabidopsis group IIId ERF proteins positively regulate primary cell wall-type *CESA* genes. *J. Plant Res.* 132, 117–129. doi: 10.1007/s10265-018-1074-1

Saito, M., Kubo, N., Matsumoto, S., Suwabe, K., Tsukada, M., and Hirai, M. (2006). Fine mapping of the clubroot resistance gene, *Crr3*, in *Brassica rapa*. *Theor. Appl. Genet.* 114, 81–91. doi: 10.1007/s00122-006-0412-1

Sakamoto, K., Saito, A., Hayashida, N., Taguchi, G., and Matsumoto, E. (2008). Mapping of isolate-specific QTLs for clubroot resistance in Chinese cabbage (*Brassica rapa* l. ssp. *pekinensis*). *Theor. Appl. Genet.* 117, 759–767. doi: 10.1007/s00122-008-0817-0

Schwacke, R., Fischer, K., Ketelsen, B., Krupinska, K., and Krause, K. (2007). Comparative survey of plastid and mitochondrial targeting properties of transcription factors in arabidopsis and rice. *Mol. Genet. Genomics* 277, 631–646. doi: 10.1007/s00438-007-0214-4

Shah, N., Sun, J., Yu, S., Yang, Z., Wang, Z., Huang, F., et al. (2019). Genetic variation analysis of field isolates of clubroot and their responses to *Brassica napus* lines containing resistant genes *CRb* and *PbBa8.1* and their combination in homozygous and heterozygous state. *Mol. Breed.* 39, 153. doi: 10.1007/s11032-019-1075-3

Strelkov, S. E., Hwang, S.-F., Manolii, V. P., Cao, T., and Feindel, D. (2016). Emergence of new virulence phenotypes of *Plasmodiophora brassicae* on canola (*Brassica napus*) in Alberta, Canada. *Eur. J. Plant Pathol.* 145, 517–529. doi: 10.1007/s10658-016-0888-8

Suwabe, K., Tsukazaki, H., Iketani, H., Hatakeyama, K., Fujimura, M., Nunome, T., et al. (2003). Identification of two loci for resistance to clubroot (*Plasmodiophora brassicae* woronin) in *Brassica rapa* l. *Theor. Appl. Genet.* 107, 997–1002. doi: 10.1007/s00122-003-1309-x

Suwabe, K., Tsukazaki, H., Iketani, H., Hatakeyama, K., Kondo, M., Fujimura, M., et al. (2006). Simple sequence repeat-based comparative genomics between *Brassica rapa* and *Arabidopsis thaliana*: the genetic origin of clubroot resistance. *Genetics* 173, 309–319. doi: 10.1534/genetics.104.038968

Tang, D., Wang, G., and Zhou, J. M. (2017). Receptor kinases in plant-pathogen interactions: More than pattern recognition. *Plant Cell* 29, 618–637. doi: 10.1105/tpc.16.00891

Tournier, B., Sanchez-Ballesta, M. T., Jones, B., Pesquet, E., Regad, F., Latché, A., et al. (2003). New members of the tomato ERF family show specific expression pattern and diverse DNA-binding capacity to the GCC box element. *FEBS Lett.* 550, 149–154. doi: 10.1016/s0014-5793(03)00757-9

Ueno, H., Matsumoto, E., Aruga, D., Kitagawa, S., Matsumura, H., and Hayashida, N. (2012). Molecular characterization of the *CRa* gene conferring clubroot resistance in *Brassica rapa*. *Plant Mol. Biol.* 80, 621–629. doi: 10.1007/s11103-012-9971-5

Voorrips, R. E., Jongerius, M. C., and Kanne, H. J. (1997). Mapping of two genes for resistance to clubroot (*Plasmodiophora brassicae*) in a population of doubled haploid lines of *Brassica oleracea* by means of RFLP and AFLP markers. *Theor. Appl. Genet.* 94, 75–82. doi: 10.1007/s001220050384

Walerowski, P., Gündel, A., Yahaya, N., Truman, W., Sobczak, M., Olszak, M., et al. (2018). Clubroot disease stimulates early steps of phloem differentiation and recruits SWEET sucrose transporters within developing galls. *Plant Cell* 30, 3058–3073. doi: 10.1105/tpc.18.00283

Wallenhammar, A. C. (2010). Monitoring and control of *Plasmodiophora brassicae* in spring oilseed *brassica* crops. *Acta Hortic.* 867, 181–190. doi: 10.17660/ActaHortic.2010.867.23

Wang, J., and Chai, J. (2020). Molecular actions of NLR immune receptors in plants and animals. *Sci. China Life Sci.* 63, 1303–1316. doi: 10.1007/s11427-019-1687-6

Wang, X., Gao, J., Zhu, Z., Dong, X., Wang, X., Ren, G., et al. (2015). TCP Transcription factors are critical for the coordinated regulation of isochorismate synthase 1 expression in *Arabidopsis thaliana*. *Plant J.* 82, 151–162. doi: 10.1111/tpj.12803

Webster, M. A., and Dixon, G. (1991). Boron, pH and inoculum concentration influencing colonization by *Plasmodiophora brassicae*. *Mycol. Res.* 95, 64–73. doi: 10.1016/S0953-7562(09)81363-4

Werner, S., Bartrina, I., and Schmülling, T. (2021). Cytokinin regulates vegetative phase change in *Arabidopsis thaliana* through the miR172/TOE1-TOE2 module. *Nat. Commun.* 12, 5816. doi: 10.1038/s41467-021-26088-z

Werner, S., Diederichsen, E., Frauen, M., Schondelmaier, J., and Jung, C. (2008). Genetic mapping of clubroot resistance genes in oilseed rape. *Theor. Appl. Genet.* 116, 363–372. doi: 10.1007/s00122-007-0674-2

Yuan, M., Jiang, Z., Bi, G., Nomura, K., Liu, M., Wang, Y., et al. (2021). Pattern-recognition receptors are required for NLR-mediated plant immunity. *Nature* 592, 105–109. doi: 10.1038/s41586-021-03316-6

Yu, F., Zhang, X., Peng, G., Falk, K. C., Strelkov, S. E., and Gossen, B. D. (2017). Genotyping-by-sequencing reveals three QTL for clubroot resistance to six pathotypes of *Plasmodiophora brassicae* in *Brassica rapa*. *Sci. Rep.* 7, 4516. doi: 10.1038/s41598-017-04903-2

Zhang, H., Hong, Y., Huang, L., Li, D., and Song, F. (2016). Arabidopsis *At*ERF014 acts as a dual regulator that differentially modulates immunity against *Pseudomonas syringae* pv. *tomato* and *Botrytis cinerea*. *Sci. Rep.* 6, 30251. doi: 10.1038/srep30251

Zhang, Z., Liu, Y., Huang, H., Gao, M., Wu, D., Kong, Q., et al. (2017). The NLR protein SUMM2 senses the disruption of an immune signaling MAP kinase cascade *via* CRCK3. *EMBO Rep.* 18, 292–302. doi: 10.15252/embr.201642704

Zhang, B., Shao, L., Wang, J., Zhang, Y., Guo, X., Peng, Y., et al. (2021). Phosphorylation of ATG18a by BAK1 suppresses autophagy and attenuates plant resistance against necrotrophic pathogens. *Autophagy* 17, 2093–2110. doi: 10.1080/15548627.2020.1810426

Zhan, Z., Jiang, Y., Shah, N., Hou, Z., Zhou, Y., Dun, B., et al. (2020). Association of clubroot resistance locus *PbBa8.1* with a linkage drag of high erucic acid content in the seed of the European turnip. *Front. Plant Sci.* 11. doi: 10.3389/fpls.2020.00810

Zheng, X. Y., Zhou, M., Yoo, H., Pruneda-Paz, J. L., Spivey, N. W., Kay, S. A., et al. (2015). Spatial and temporal regulation of biosynthesis of the plant immune signal salicylic acid. *Proc. Natl. Acad. Sci. U.S.A.* 112, 9166–9173. doi: 10.1073/pnas.1511182112

Zhou, J. M., and Zhang, Y. (2020). Plant immunity: Danger perception and signaling. *Cell* 181, 978–989. doi: 10.1016/j.cell.2020.04.028

Zou, Y., Wang, S., Zhou, Y., Bai, J., Huang, G., Liu, X., et al. (2018). Transcriptional regulation of the immune receptor FLS2 controls the ontogeny of plant innate immunity. *Plant Cell* 30, 2779–2794. doi: 10.1105/tpc.18.00297

frontiers | Frontiers in Plant Science

TYPE Original Research
PUBLISHED 12 October 2022
DOI 10.3389/fpls.2022.1008665

OPEN ACCESS

EDITED BY
Qi Peng,
Jiangsu Academy of Agricultural Sciences (JAAS), China

REVIEWED BY
Shuijin Hua,
Zhejiang Academy of Agricultural Sciences, China
Zheng Wang,
Jiangsu University, China
Yong Liu,
Sichuan Academy of Agricultural Sciences, China

*CORRESPONDENCE
Xiong Zhang
hbzhangxiong@126.com

†These authors have contributed equally to this work

SPECIALTY SECTION
This article was submitted to Plant Pathogen Interactions, a section of the journal Frontiers in Plant Science

RECEIVED 01 August 2022
ACCEPTED 20 September 2022
PUBLISHED 12 October 2022

CITATION
Cheng X, Zhao C, Gao L, Zeng L, Xu Y, Liu F, Huang J, Liu L, Liu S and Zhang X (2022) Alternative splicing reprogramming in fungal pathogen *Sclerotinia sclerotiorum* at different infection stages on *Brassica napus*. *Front. Plant Sci.* 13:1008665. doi: 10.3389/fpls.2022.1008665

Alternative splicing reprogramming in fungal pathogen *Sclerotinia sclerotiorum* at different infection stages on *Brassica napus*

Xiaohui Cheng[1†], Chuanji Zhao[1†], Lixia Gao[2], Lingyi Zeng[1], Yu Xu[3], Fan Liu[1], Junyan Huang[1], Lijiang Liu[1], Shengyi Liu[1] and Xiong Zhang[1*]

[1]Key Laboratory of Biology and Genetic Improvement of Oil Crops, Ministry of Agriculture of the People's Republic of China (PRC), Oil Crops Research Institute, Chinese Academy of Agricultural Sciences, Wuhan, China, [2]State Key Laboratory of Agricultural Microbiology, Huazhong Agricultural University, Wuhan, China, [3]Hebei Provincial Academy of Ecological and Environmental Sciences, Shijiazhuang, China

Alternative splicing (AS) is an important post-transcriptional mechanism promoting the diversity of transcripts and proteins to regulate various life processes in eukaryotes. Sclerotinia stem rot is a major disease of *Brassica napus* caused by Sclerotinia sclerotiorum, which causes severe yield loss in *B. napus* production worldwide. Although many transcriptome studies have been carried out on the growth, development, and infection of S. sclerotiorum, the genome-wide AS events of S. sclerotiorum remain poorly understood, particularly at the infection stage. In this study, transcriptome sequencing was performed to systematically explore the genome-scale AS events of *S. sclerotiorum* at five important infection stages on a susceptible oilseed rape cultivar. A total of 130 genes were predicted to be involved in AS from the *S. sclerotiorum* genome, among which 98 genes were differentially expressed and may be responsible for AS reprogramming for its successful infection. In addition, 641 differential alternative splicing genes (DASGs) were identified during *S. sclerotiorum* infection, accounting for 5.76% of all annotated *S. sclerotiorum* genes, and 71 DASGs were commonly found at all the five infection stages. The most dominant AS type of *S. sclerotiorum* was found to be retained introns or alternative 3′ splice sites. Furthermore, the resultant AS isoforms of 21 DASGs became pseudogenes, and 60 DASGs encoded different putative proteins with different domains. More importantly, 16 DASGs of *S. sclerotiorum* were found to have signal peptides and possibly encode putative effectors to facilitate the infection of *S. sclerotiorum*. Finally, about 69.27% of DASGs were found to be non-differentially expressed genes, indicating that AS serves as another important way to regulate the infection of *S. sclerotiorum* on

plants besides the gene expression level. Taken together, this study provides a genome-wide landscape for the AS of *S. sclerotiorum* during infection as well as an important resource for further elucidating the pathogenic mechanisms of *S. sclerotiorum*.

KEYWORDS

***Sclerotinia sclerotiorum*, transcriptome sequencing, alternative splicing, reprogramming, secreted proteins**

Introduction

Alternative splicing (AS) of precursor mRNAs is an important mechanism to increase transcriptome and proteome diversity through the production of multiple mRNA isoforms from a single coding gene (Chaudhary et al., 2019). The splicing is catalyzed by two unique spliceosomes designated as major U2-dependent spliceosome and minor U12-dependent spliceosome. Notably, the U2-dependent spliceosome mainly processes GT-AG introns, while the U12-dependent spliceosome processes AT-AC introns (Turunen et al., 2013). AS events can be classified into five major types: alternative 3′ splice site (A3SS), alternative 5′ splice site (A5SS), exon skipping (ES), retained intron (RI), and mutually exclusive exon (MXE). Specifically, RI is the most frequent type of AS in plants (Reddy et al., 2013), whereas ES is the most frequent type in animals (Pan et al., 2009). About 95% of human and 60% of *Arabidopsis* genes undergo AS events during expression, and many of these genes can generate multiple splicing isoforms (Pan et al., 2009; Zhang et al., 2017a)—for example, the small-sized *Arabidopsis* genome encodes 82,190 nonredundant isoforms from 34,212 genes (Zhang et al., 2017a). The most extreme example of AS is the *Drosophila melanogaster* gene *DSCAM*, which potentially encodes 38,016 distinct isoforms through AS (Graveley, 2005). AS has likewise been reported in microbial eukaryotes, and the ratio ranges from 0.2% in the non-pathogenic yeast *Saccharomyces cerevisiae* (Grutzmann et al., 2014) to 24% in the plant-pathogenic oomycete *Pseudoperonospora cubensis* (Burkhardt et al., 2015), which is much lower than that in plants and animals.

As a major posttranscriptional regulatory event of eukaryotes, AS plays essential roles in various cellular functions and adaptation to environmental changes. In humans, aberrant AS is associated with several diseases, such as cancer (Bonnal et al., 2020), muscular dystrophies (Pistoni et al., 2010), and neurodegenerative diseases (Tollervey et al., 2011). In plants, AS is important for growth and development (Wang et al., 2020), circadian clock (James et al., 2012), stress response (Palusa and Reddy, 2015), and immune response (Huang et al., 2020). Despite the great progress in related research, AS events and regulation in microbial eukaryotes remain largely elusive, especially in plant pathogens. A genome-wide study of 23 fungal genomes has revealed that pathogenic species have much higher AS rates than non-pathogenic species (Grutzmann et al., 2014). Host-specific and infection-specific AS were observed in *S. sclerotiorum* and *Magnaporthe oryzae* (Ibrahim et al., 2021; Jeon et al., 2022), respectively. In *Ustilago maydis*, the two core glycolysis enzymes, GAPDH and PGK, can generate two isoforms through AS, one of which is located on the peroxisome, and the deletion of the peroxisome-located isoform would reduce its virulence to maize (Freitag et al., 2012). Intriguingly, signal peptide-containing proteins and putative effectors were observed to undergo AS in *P. cubensis* (Burkhardt et al., 2015). Based on these findings, it can be speculated that AS is functionally regulated during the host colonization of plant pathogens.

S. sclerotiorum is a notorious pathogen infecting more than 400 host plants all over the world, including some economically important crops, such as tomato (*Solanum lycopersicum*), common bean (*Phaseolus vulgaris*), sunflower (*Helianthus annuus*), and oilseed rape (*Brassica napus* L.) (Bolton et al., 2006). Sclerotinia stem rot caused by *S. sclerotiorum* is a major yield-limiting factor, causing about $200 million of annual economic loss in the United States alone (Bolton et al., 2006). For successful infection, *S. sclerotiorum* has evolved intricate strategies to disrupt host recognition (Kabbage et al., 2015). Among these strategies, oxalic acid has attracted great research attention since it manipulates the host redox environment and pH signaling to promote pathogenicity during *S. sclerotiorum* disease development (Williams et al., 2011). In addition, some effectors, such as an integrin-like protein SsITL (Zhu et al., 2013), a putative Ca^{2+} binding protein Ss-caF1 (Xiao et al., 2014), an uncharacterized protein SsSSVP1 (Lyu et al., 2016), and a cerato-platanin protein SsCP1 (Yang et al., 2018), are commonly involved in the virulence of *S. sclerotiorum*. Overall, most studies of *S. sclerotiorum* pathogenicity have been mainly focused on oxalic acid, effectors, transcription factors, and cell-wall-degrading enzymes (Xu et al., 2018). Although there have been increasing transcriptomic data to determine the gene expression profiles of *S. sclerotiorum* (Peng et al., 2017; Westrick et al., 2019; Chittem et al., 2020; Xu et al., 2021), the

prevalence of genome-wide AS in *S. sclerotiorum* at different infection stages remains elusive.

Clarification of how this pathogen infects hosts will improve our understanding of *S. sclerotiorum* and facilitate the development of disease-resistant crops. High-throughput transcriptome profiling is a powerful approach for the quantitative profiling of AS (Wang et al., 2008; Wang et al., 2009). However, AS events across different infection stages are still largely unknown. Although host-specific AS has been characterized in *S. sclerotiorum*, the study was based on samples collected at only one infection stage. In the present study, we used RNA-seq technology to detect the genome-wide AS events of *S. sclerotiorum* across different stages of infection, including mycelia (MY) and at 2, 6, 12, 24, and 36 h post-inoculation (hpi) on susceptible oilseed rape. The AS characteristics in *S. sclerotiorum* were elucidated, and more importantly, the effects of AS on the function of proteins were comprehensively analyzed, particularly secreted proteins. The findings provide a comprehensive landscape of AS during *S. sclerotiorum* infection and important gene resources for future research on its pathogenic mechanisms.

Materials and methods

RNA-seq sample collection

The S. *sclerotiorum* strain 1980 was collected from oilseed rape stems in the field and grown on potato dextrose agar (PDA) to produce a hyphal inoculum. Susceptible oilseed rape (*Brassica napus* cv Westar) was used as the host in this study. The plants were grown in a growth chamber at 25°C, 80% humidity, and 14-h light/8-h dark cycle. Once germinated, the seedlings were watered when necessary and fertilized once a week with 20–20–20 fertilizer. At 4weeks after planting, the plants were infected with *S. sclerotiorum.*

Mycelia were collected from the cellophane placed on the PDA immediately prior to inoculation (time 0) and at 2, 6, 12, 24, and 36 h post-inoculation (hpi). The collected samples were immediately frozen in liquid nitrogen and stored at −80°C for RNA extraction.

RNA isolation, RNA-seq library preparation, and sequencing

Total RNA was extracted from the collected samples using the EZNA total RNA kit I (Omega BioTek, Norcross, GA, USA) following the manufacturer's instructions. RNA quality was checked using a Qubit fluorometer (Life Technologies, New York, NY, USA) and Bioanalyzer 2100 (Agilent Technologies, Santa Clara, CA, USA). The libraries were then constructed and sequenced on Illumina HiSeq X Ten using the paired-end mode (Novogene Co. Ltd., Beijing, China). Three biological replicates were used for each analysis. All raw sequence data generated in this study have been deposited in the NCBI Sequence Read Archive (available online) under Bioproject ID PRJNA777355.

Transcriptomic analysis

Adapter trimming and low-quality read filtering were carried out by fastp (Chen et al., 2018) with default settings. The *S. sclerotiorum* near complete reference genome sequence (Derbyshire et al., 2017) and gene model annotation files were retrieved from the FTP site provided by NCBI. The paired-end clean reads were mapped to the reference genome by the software TopHat v2.0.12 (Trapnell et al., 2009) using the following option: -an 8 -m 0 with an anchor length of more than 8 nt for the spliced alignments. The gene expression levels were quantified by fragments per kilobase of transcript sequence per million base pairs mapped reads (FPKM) (Trapnell et al., 2010). The similarity between samples at the expression level was estimated by calculating the Pearson correlation coefficient and then visualized using R package pheatmap. Differentially expressed genes (DEGs) were determined by the R package DESeq (Anders and Huber, 2010) with an adjusted *P*-value <0.05 (false discovery rate = 0.05), and the absolute value of the $\log_2$ fold change ratio was >2. Fold change values were the ratio of FPKM of the different samples to that of the control.

Identification of differential alternative splicing

All putative AS events were extracted from the abovementioned high-quality transcript GTF file using rMATS (Shen et al., 2014). Five major types of AS were detected, including A5SS, A3SS, ES, IR, and MXE. The events with a *P*-value <0.05 calculated by rMATS were identified as significantly differential events. The Sashimi plot was constructed using rmats2sashimiplot (https://github.com/Xinglab/rmats2sashimiplot).

Gene function analysis

For secretome annotation, SignalP 3.0 (Bendtsen et al., 2004) and TMHMM v. 2.0 (Krogh et al., 2001) software were used to predict the presence of signal peptides and transmembrane (TM) domains, respectively. Proteins with signal peptides but no TM domains were considered as candidate secreted proteins. *S. sclerotiorum* gene ontology (GO) terms were obtained from a previous study (Derbyshire et al., 2017). GO enrichment analysis was performed using the OmicShare tools, a free online platform for data analysis (www.omicshare.com/tools). A protein–protein interaction network was constructed using the STRING database (http://string-db.org) with a combined score of >0.4. Sources in

STRING include experimentally determined interactions, curated databases, and information of neighborhood, co-occurrence, text mining, co-expression, and homology (Szklarczyk et al., 2021).

qRT-PCR validation of candidate genes

Total RNA samples were isolated at different infection stages. First-strand cDNA was obtained with the Prime Script RT reagent kit (Takara Bio, Beijing, China), and then real-time PCR was run on the CFX Connect Real-time PCR system (Bio-Rad, Hercules, CA, USA). The *S. sclerotiorum* actin gene (*Sscle_14g099090*) was used to normalize the gene expression. Three biological replicates were performed per sample, and the relative gene expression levels were calculated using the $2^{-\Delta\Delta Ct}$ method (Livak and Schmittgen, 2001). The primers are listed in Supplementary Table S1.

Results

Time-course transcriptome of *S. sclerotiorum* infection on *B. napus*

To characterize the transcriptome and AS patterns of *S. sclerotiorum* at different infection stages on *B. napus*, RNA-seq of *S. sclerotiorum* was performed at 0 (mycelia), 2, 6, 12, 24, and 36 hpi with three biological replicates. After data trimming and quality filtering, a total of 354.78 million clean paired-end reads were obtained for 18 samples, with the reads for each sample ranging from 16.14 to 28.57 million (Supplementary Table S2). Approximately 83.56% of the clean reads were mapped to the *S. sclerotiorum* 1980 UF-70 reference genome (Derbyshire et al., 2017). As a result, among the 11,130 protein-coding genes (Derbyshire et al., 2017), 9,512 genes were defined as expressed genes (FPKM ≥1.0) in at least one sample, indicating that the RNA-seq analysis had sufficient coverage.

To confirm the quality of the transcriptome generated in this study, Pearson correlation coefficient (r^2) was calculated between biological replicates based on the FPKM values of all the detected genes. Hierarchical clustering analysis showed that the data of three replicates were tightly clustered together, and independent treatments were clearly separated from each other (Supplementary Figure S1A), indicating the reliability of the experiments. The separation was even more evident in the principal component analysis (Supplementary Figure S1B). To further test the reliability of the RNA-seq results from Illumina sequencing data, 12 genes were randomly selected to carry out quantitative real-time PCR (qRT-PCR) validation, and the yielded results were consistent with our RNA-seq data (Figure 1). These results further confirmed that our RNA-seq data are accurate and reliable.

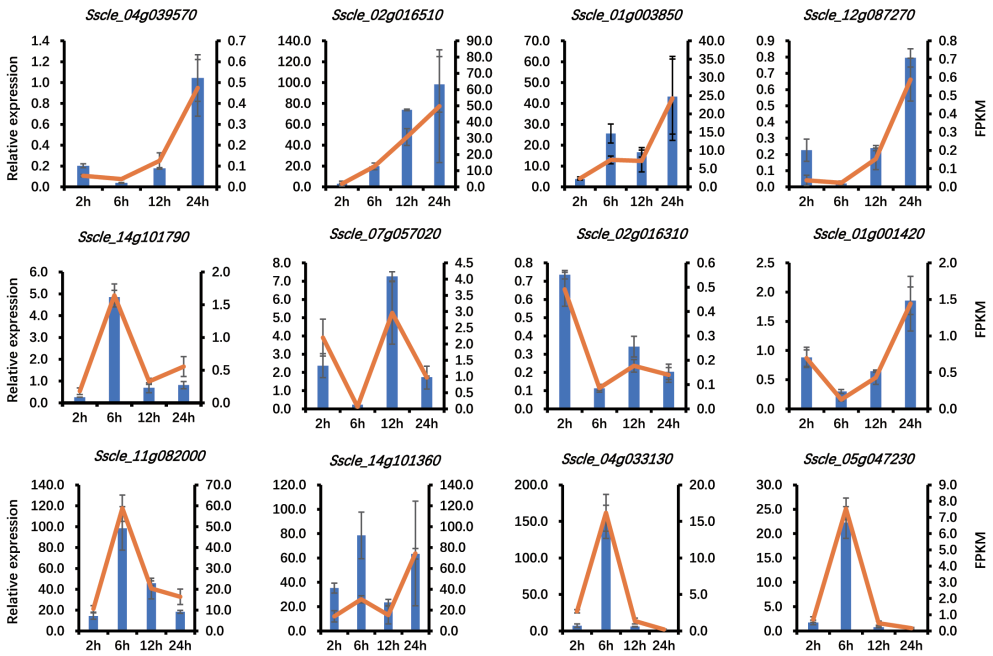

FIGURE 1
RNA-seq data validation by quantitative real-time PCR (qRT-PCR). The qRT-PCR results are presented as relative expression using actin as a reference gene. The expression levels are presented as the mean of three biological replicates, and the error bars show the standard deviation.

Splicing-related genes are active at different infection stages

Pre-mRNA splicing is catalyzed by a higher-order protein complex termed as the spliceosome, which comprises a range of proteins called splicing-related proteins (Will and Luhrmann, 2011; Matera and Wang, 2014). The abundance and the activity of splicing-related genes govern the AS patterns of target genes and their expression patterns under different environmental conditions (Syed et al., 2012; Papasaikas et al., 2015). To gain more insights into the genome-wide AS of *S. sclerotiorum* at different infection stages, 116 potential splicing-related genes previously identified in *S. sclerotiorum* genome (Ibrahim et al., 2021) were subjected to expression analysis (Figure 2 and Supplementary Table S3). As a result, all genes were expressed at detectable levels (FPKM ≥1.0) except for *Sscle02g018420*, which encodes a U2AF, and 105 genes showed high expression (FPKM ≥20.0) in at least one infection stage (Figure 2). Importantly, among the 116 splicing-related genes, 93 genes were differentially expressed at the five infection stages compared with the mycelium stage, including 31 upregulated genes and 65 downregulated genes—for example, *Sscle_01g006670*, which encodes an LSM2 homolog, was upregulated by 8.3 folds at 36 hpi, while the RNA helicase p68-coding gene *Sscle_03g029880* displayed 53.6-fold downregulation at 6 hpi. Interestingly, *Sscle_16g108670*, which encodes a Snu13 homolog, was dramatically downregulated at 2 hpi but upregulated at 36 hpi. Moreover, the SMG1-coding gene *Sscle_05g041300* and the SmD1-coding gene *Sscle_04g039900* were both downregulated at 2 hpi but upregulated at 6 hpi.

Additionally, we identified 14 other splicing-related genes based on the GO terms. Similarly, these genes also exhibited high expression levels at all infection stages, and there were five DEGs (one upregulated and four downregulated) relative to the mycelium stage (Figure 2 and Supplementary Table S3)—for example, *Sscle_01g008200* was dramatically downregulated at 2, 6, 12, and 24 hpi, while *Sscle_05g041930* showed an increase in expression at 6 hpi. Overall, these results demonstrated that *S. sclerotiorum* infection has significant effects on spliceosome components.

Prevalent changes in mRNA alternative splicing are observed in *S. sclerotiorum* during infection

To determine the dynamic changes of AS in *S. sclerotiorum* pre-mRNA during infection on *B. napus*, we detected the host-induced differential alternative splicing (DAS) events in *S. sclerotiorum* by comparing the infection samples with the mycelium sample from the RNA-seq data. The number of DAS events ranged from 371 at 36 hpi to 480 at 6 hpi, and there was a total of 2,149 DAS events covering 641 gene loci (Figure 3A). Among these genes, 71 genes were found in all infection stages (Supplementary Figure S2A), and each DAS gene corresponded to an average of 3.35 DAS events. These DAS genes (DASGs) accounted for 6.74% of the 9,512 genes expressed in *S. sclerotiorum* genome. In terms of the distribution of different types of AS, retained intron (RI; 30.47 ± 1.32%) was the most detected, followed by alternative 3′ splice site (A3SS; 27.49 ± 2.26%), alternative 5′ splice site (A5SS; 22.95 ± 0.49%), exon skipping (ES; 16.06 ± 1.43%), and mutually exclusive exon (MXE; 3.02 ± 1.51%). Most genes had a single type of DAS, and there were 117 genes exhibiting multiple types of DAS (Supplementary Figure S2B).

To investigate the regulatory mechanism of AS during infection, a pairwise comparison of DEGs and DASGs was further performed. A total of 2,941 DEGs were detected, including 1,022, 2,270, 1,206, 908, and 1,058 DEGs at 2, 6, 12, 24, and 36 hpi, respectively (Figure 3B). The results showed that the gene overlapping rate between all DEGs and DASGs was as low as 5.82%. Specifically, the number of overlapping genes was 25 for 2 hpi, 100 for 6 hpi, 44 for 12 hpi, 44 for 24 hpi, and 31 for 36 hpi, whereas 263, 233, 293, 263, and 242 DASGs were not differentially expressed at 2, 6, 12, 24, and 36 hpi, respectively (Figure 3B). The fact that most DASGs were not differentially expressed at different infection stages indicated that AS is independent of gene expression regulation during the infection process of *S. sclerotiorum*. Indeed the GO enrichment analysis revealed that there were significant differences in the biological process between DASGs and DEGs. As shown in Table 1 and Supplementary Figure S3, DASGs were enriched in processes such as the cellular modified amino acid metabolic process (GO:0006575), organonitrogen compound catabolic process (GO:1901565), and heterocycle biosynthetic process (GO:0018130), while DEGs were enriched in ribosome biogenesis (GO:0042254), ribonucleoprotein complex biogenesis (GO:0022613), and rRNA processing (GO:0006364).

Alternative splicing variants with modified functions

To evaluate the potential impacts of AS on protein function, we examined the transcript isoforms of genes resulting from AS events and the resultant protein sequences. As a result, the AS isoforms of 21 genes were found to be truncated in the open reading frames to less than 30 amino acids, and therefore these alternative isoforms should be pseudogenized (Table 2). Among these 21 genes, a *Fusarium graminearum* pre-mRNA-splicing factor srp1 (Zhang et al., 2017b) homolog-coding gene *Sscle_09g071470*, a myb-like domain-containing protein-coding gene *Sscle_05g047440*, and an enolase-phosphatase E1-coding gene *Sscle_03g030320* were found at all infection stages, while 11 genes were detected at only one infection stage, and eight genes were found in two to four infection stages. We then found that

10.3389/fpls.2022.1008665

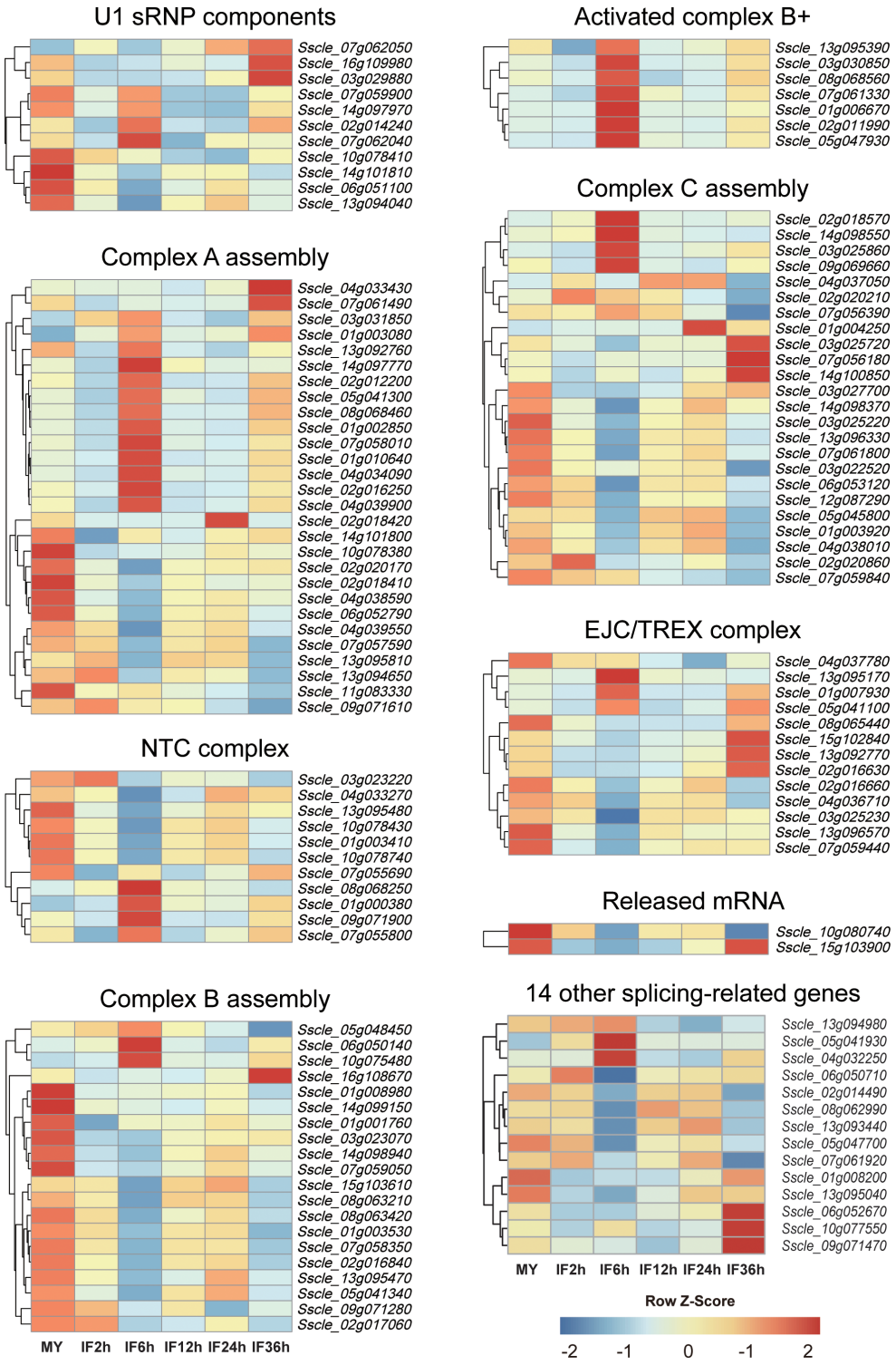

FIGURE 2
Expression patterns of splicing-related genes during *S. sclerotiorum* infection on *Brassica napus*. The gene ID of splicing factors is listed in the heat map. Blue to red indicate gene expression values from low to high. *Z* score normalization was applied for the transcription levels of genes at all stages. Cluster analysis was performed using the R package pheatmap.

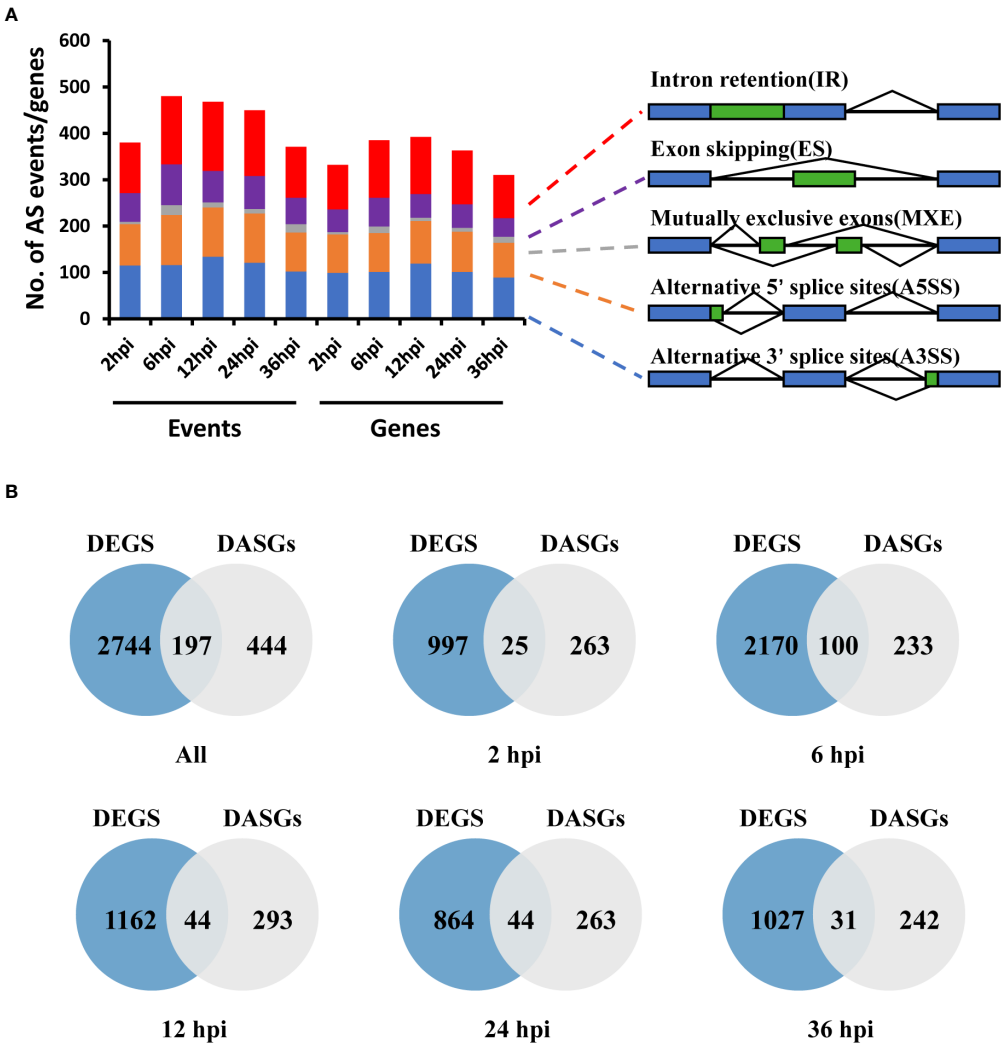

FIGURE 3
Differential alternative splicing genes (DASGs) and differentially expressed genes (DEGs) in *S. sclerotiorum* at different infection stages. **(A)** Number of different types of differentially expressing events and corresponding genes identified in different infected samples. A3SS, alternative 3′ splice site; A5SS, alternative 5′ splice site; ES, exon skipping; RI, retained intron; MXE, mutually exclusive exon. **(B)** Venn diagram of the overlap of DEGs and DASGs.

all AS types led to pseudogenization except for MXE—for example, the A3SS, A5SS, SE, and RI types of AS led to the pseudogenization of a dynactin subunit-coding gene *Sscle_03g022490*, a thiamine thiazole synthase-coding gene *Sscle_01g000960*, a calmodulin-1-coding gene Sscle_01g010310, and an ACT_7 domain-containing protein coding gene *Sscle_01g007440*, respectively (Supplementary Figure S4).

To determine whether there are changes in the domain structures of protein isoforms resulting from AS, we predicted the domain structures of all AS isoforms. In total, 60 DASGs were found to have variations in protein domain structure. Among the proteins encoded by these DASGs, 48 protein isoforms exhibited a loss of domains, seven showed a gain of domains, and six displayed more complex changes in domains. RRM_1, LRR_8, and Fungal_trans were the three most frequently modified domains (Figure 4A). Only three of the 60 DASGs underwent changes in domain at all five infection stages, *i.e.*, a probable prefoldin subunit-coding gene *Sscle_13g096300*, a *F. graminearum* pre-mRNA-factor srp2 (Zhang et al., 2020b) homologous-coding gene *Sscle_13g096570*, and a D-arabinitol dehydrogenase-coding gene *Sscle_16g110540*. Sscle_13g096300, Sscle_13g096570, and Sscle_16g110540 isoforms lost the prefoldin domain, RRM_1 domain, and ADH_zinc_N domain, respectively. Both RI and SE types were found to contribute to the loss of ADH_zinc_N domain in the Sscle_16g110540 isoforms.

Furthermore, the interaction network of all 81 DASGs with pseudogenization and/or domain changes was constructed. As shown in Figure 4B, 31 DASGs and 10 other genes interact with

TABLE 1 Top 10 biological processes from the Gene Ontology (GO) enrichment analysis of differentially expressed genes (DEGs) and differential alternative splicing genes (DASGs).

GO description (DEGs)	*P*-value	GO description (DASGs)	*P*-value
Ribosome biogenesis	7.57E-25	Cellular modified amino acid metabolic process	7.71E-05
Ribonucleoprotein complex biogenesis	1.32E-21	Organonitrogen compound catabolic process	1.01E-04
rRNA processing	1.08E-17	Heterocycle biosynthetic process	2.42E-04
rRNA metabolic process	1.08E-17	Nucleobase-containing compound biosynthetic	3.50E-04
ncRNA processing	1.62E-11	Kynurenine metabolic process	4.02E-04
Carbohydrate metabolic process	4.68E-09	Aromatic compound biosynthetic process	5.36E-04
ncRNA metabolic process	1.38E-08	Tryptophan catabolic process	1.12E-03
Cellular component biogenesis	1.28E-06	Amine catabolic process	1.12E-03
Polysaccharide catabolic process	3.64E-06	Cellular biogenic amine catabolic process	1.12E-03
Polysaccharide metabolic process	7.84E-06	Indole-containing compound catabolic process	1.12E-03

each other, resulting in 73 protein–protein associations. Two proteins, Sscle_03g023610 and A7EAG4 (Sscle_04g033520), had more than 10 connections with other proteins, suggesting that they are hub genes in the network. *Sscle_03g023610* encodes a tubulin gamma chain, while *A7EAG4* encodes cell division control protein 2, which belongs to the protein kinase superfamily. In addition, we found that these two hub genes were highly expressed during infection (Supplementary Figure S5). Overall, the interaction network showed that part of the DASGs were biologically connected and two hub genes might play crucial roles in the infection process.

S. sclerotiorum infection activates the AS of secreted proteins

During infection and colonization, various plant pathogens target the intracellular processes of plant cells *via* deploying secreted proteins (Arroyo-Velez et al., 2020). To determine whether secreted proteins undergo AS during infection, we predicted the signal peptide and transmembrane domain of all AS isoforms. In total, 16 predicted secreted protein-coding genes were found to be alternatively spliced during infection (Figure 5A). The expression analysis revealed that 75.0% of

TABLE 2 Differential alternative splicing genes with pseudogenization.

Gene ID	AS type	Infection stage	Description
Sscle_07g059110	RI	2 hpi	IMP-specific 5′-nucleotidase
Sscle_12g091700	A5SS	2 hpi	Alkaline ceramidase
Sscle_01g010310	SE	2 hpi	Calmodulin-1
Sscle_08g065510	A5SS	6 hpi	GH16 domain-containing protein
Sscle_03g022490	A3SS	6 hpi	Dynactin subunit
Sscle_04g033380	RI	6 hpi	Ubiquitin-conjugating enzyme E2
Sscle_04g037580	SE	6 hpi	Uncharacterized protein
Sscle_05g045150	A3SS	6 hpi	Tyrosine-protein phosphatase
Sscle_08g066420	SE	12 hpi	C2H2-type domain-containing protein
Sscle_04g032930	SE	12 hpi	Ubiquitin fusion degradation protein
Sscle_01g000960	A5SS	36 hpi	Thiamine thiazole synthase
Sscle_01g003590	SE	6/36 hpi	Ras-related protein
Sscle_01g006710	SE	2/6/24 hpi	RNA polymerase III subunit
Sscle_07g055740	RI	6/12/24 hpi	Defective in cullin neddylation protein
Sscle_06g048720	A3SS	2/12/24 hpi	D-/L-hydantoinase subunit
Sscle_01g007440	RI	2/6/12/24 hpi	ACT_7 domain-containing protein
Sscle_02g021320	RI	6/12/24/36 hpi	Transcription factor kapC
Sscle_09g071090	A5SS	2/6/12/24 hpi	Uncharacterized protein
Sscle_09g071470	RI	All stages	Pre-mRNA-splicing factor srp1
Sscle_05g047440	SE	All stages	Myb-like domain-containing protein
Sscle_03g030320	SE	All stages	Enolase-phosphatase E1

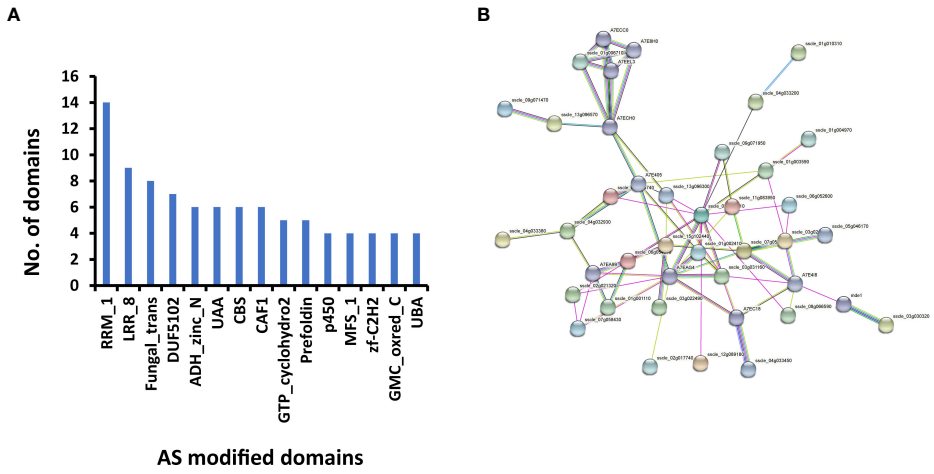

FIGURE 4
Differential alternative splicing genes (DASGs) with modified functions in *S. sclerotiorum*. **(A)** Fifteen most frequently modified domains in DASGs. **(B)** The network was constructed using STRING (https://string-db.org/). There are 41 protein nodes and 73 protein–protein association edges in the network. Seven differently colored lines represent the types of evidence used in predicting associations. Light blue line, database evidence; purple line, experimental evidence; green line, neighborhood evidence; blue line, co-occurrence evidence; yellow line, text mining evidence; black line, co-expression evidence; and dark blue lines, protein homology evidence.

secreted DASGs (12 out of 16) were significantly upregulated in at least one infection stage (Figure 5A), and the ratio was much higher than that of the total DASGs and secreted proteins.

Among the 16 spliced secreted proteins, two isoforms were predicted to lose the secretion function because no signal peptide (a cellulase coding gene *Sscle_01g005720* and a putative gas1-like protein coding gene *Sscle_03g029210*) was detected. One isoform was found to gain a transmembrane domain (a WSC domain-containing protein-coding gene *Sscle_04g035680*, Figure 5B), and two isoforms (a GH16 domain-containing protein-coding gene *Sscle_08g065510* and an RRM domain-containing protein-coding gene *Sscle_09g071470*) underwent pseudogenization. Intriguingly, there were three secreted proteins with altered domains in alternative isoforms, namely, a glutaminase-coding gene *Sscle_14g100290*, a NAD-dependent protein deacetylase-coding gene *Sscle_04g033450*, and a cytochrome p450 protein-coding gene *Sscle_03g025570*—for example, *Sscle_14g100290* encodes two secreted protein isoforms, namely, a reference protein Sscle_14g100290.1 and an alternative protein Sscle_14g100290.2: the former contained a signal peptide and three domains of unknown function (DUF4965, DUF5127, and DUF1793), while the latter contained a signal peptide and a domain of unknown function (DUF5127). In addition, loss of signal peptides and changes in domains were not observed in the alternative isoforms of the other nine secreted proteins.

Discussion

Plant diseases pose serious impacts on global agriculture, causing significant losses in crop productivity and great threats to global food security. As a filamentous ascomycete fungus, *S. sclerotiorum* causes a devastating disease for many important crops worldwide, particularly *B. napus* (Bolton et al., 2006). Therefore, a better understanding of the pathogenic mechanisms during *S. sclerotiorum* infection is of great importance to both basic and applied research on the development of effective strategies for disease resistance in breeding. Although the gene profiles in *S. sclerotiorum* have been extensively reported and well characterized (Peng et al., 2017; Westrick et al., 2019; Chittem et al., 2020; Xu et al., 2021), gene regulation at the post-transcriptional level, such as alternative splicing across all stages of infection, remains poorly understood. In the present study, we systematically characterized the genome-wide AS in *S. sclerotiorum* at five infection stages on *B. napus*.

Genome-wide AS events have been extensively investigated for plants and animals in their response to various biotic and abiotic stresses (Reddy et al., 2013). Only a few genome-wide AS events have been identified in fungi. It has been reported that the ratio of AS events ranges from 0.2% in the non-pathogenic *Saccharomyces cerevisiae* to 9.5% in the filamentous fungus *Aspergillus niger* (Grutzmann et al., 2014) and from 2.3 to 18.2% in human pathogenic fungi (Stepankiw et al., 2015). A recent study showed that 1,487 *S. sclerotiorum* genes exhibited alternative isoforms on diverse host plants, which may contribute to expanding the host spectrum of *S. sclerotiorum* (Ibrahim et al., 2021). However, genome-wide AS across all stages of fungi infection is largely unknown, which can reflect how AS is regulated during pathogenesis. In this study, we found 2,149 AS events among 641 genes in *S. sclerotiorum*, accounting for 5.8% of all the annotated genes and suggesting a genome-

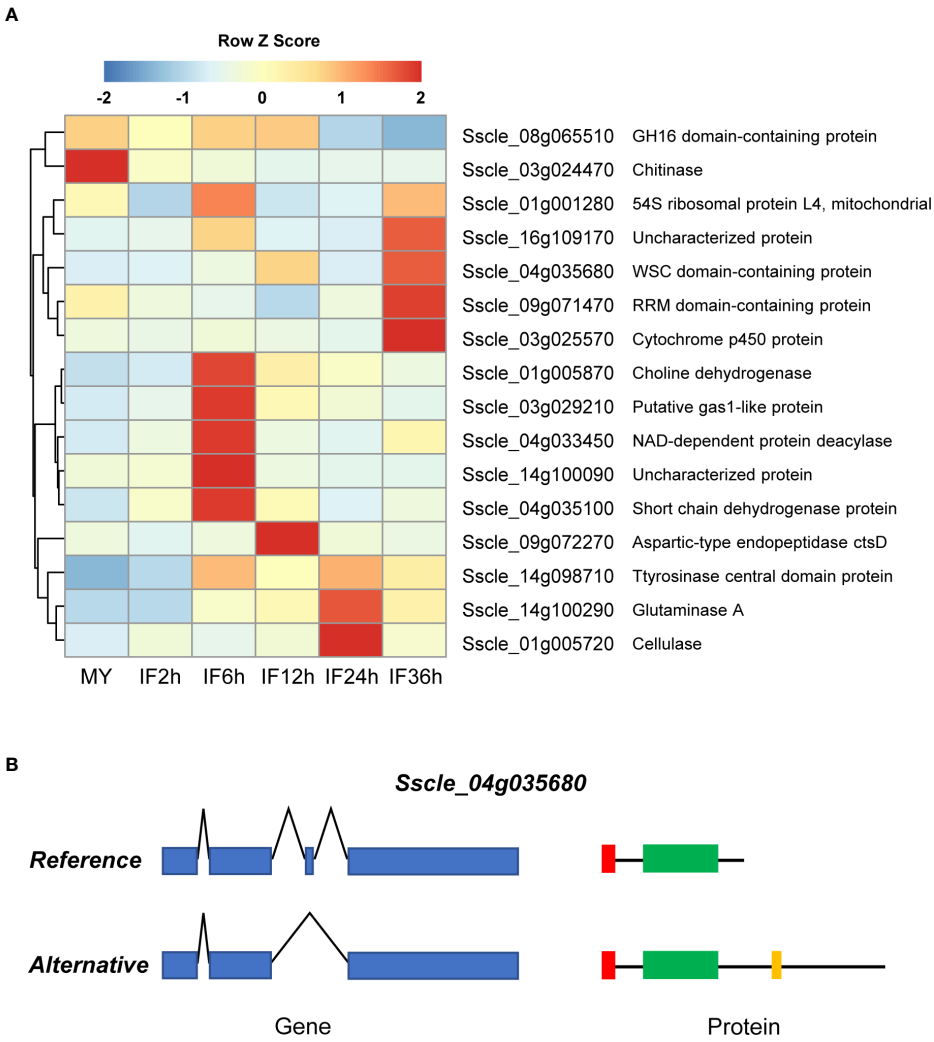

FIGURE 5
Modified functions of secreted protein-coding genes by alternative splicing (AS) in *S. sclerotiorum*. **(A)** The expression patterns of the secreted protein-coding genes undergo AS. **(B)** Schematic representation of *Sscle_04g035680* produced by AS. The blue boxes and polylines indicate the exons and introns, respectively. The red boxes, green boxes, and yellow box indicates the signal peptides, WSC domains, and transmembrane domain, respectively.

wide regulation of AS process during the colonization of *S. sclerotiorum* in the host plant. Among the 641 differential alternative splicing genes identified at five post-infection time points, only 71 DASGs were shared by all five time points, indicating dramatic changes in AS during *S. sclerotiorum* infection. In terms of the different types of AS events in *S. sclerotiorum*, the most common AS type was retained intron (30.47 ± 1.32%), which is consistent with the findings in a previous study (Ibrahim et al., 2021) and in plants (Reddy et al., 2013). However, in mammals, exon skipping is the dominant AS event (Pan et al., 2009). Thus, further research should be conducted on the post-transcriptional regulation of host-induced DASGs in a plant–pathogen interaction.

Previous studies have demonstrated that gene expression comprises both the gene expression level and AS, which are independent layers in some species (Huang et al., 2019; Huang et al., 2020). To better understand the transcriptomic dynamics of AS at different infection stages, we also investigated the DEGs in *S. sclerotiorum*. A comparison between DASGs and DEGs revealed that there were only 197 common genes in these two gene sets. A further GO enrichment analysis revealed that DASGs are mainly involved in the cellular modified amino acid metabolic process, organonitrogen compound catabolic process, and heterocycle biosynthetic process. By contrast, DEGs are associated with ribosome biogenesis, ribonucleoprotein complex biogenesis, and rRNA processing.

These results strongly suggest that AS can serve as an independent mechanism for gene regulation in *S. sclerotiorum* infection on *B. napus*.

A crucial issue to be addressed in this study is how S. *sclerotiorum* infection shapes AS. Numerous studies have demonstrated that AS events are directed by splicing factors and regulators in plants and animals—for example, the SR proteins in *Arabidopsis* have been shown to significantly influence the AS efficiency of their own pre-mRNAs and several other genes (Yan et al., 2017). Notably, some splicing factors have been described to be involved in the pathogenicity of fungi. In *F. graminearum*, the splicing factors FgSRP1 (Zhang et al., 2017b), FgSRP2 (Zhang et al., 2020b), and FgSRK1 (Wang et al., 2018) are essential for the infection process and AS process. In this study, we examined the changes in the transcript levels and alternatively spliced variants of S. *sclerotiorum* splicing-related genes. A total of 130 genes annotated as splicing-related factors or regulators were obtained. Most of these genes are highly expressed during infection, among which 98 are differentially expressed. Moreover, these spliceosome components showed a dynamic expression during infection, particularly at the early stage of infection, possibly to evade plant defense and establish infection. This regulation indicates a potentially strong defense pressure on *S. sclerotiorum* during early infection on *B. napus*. In addition, two predicted splicing factors Sscle_09g071470 and Sscle_13g096570, which are homologs of *F. graminearum* FgSRP1 and FgSRP2, respectively, undergo AS at all infection stages, indicating that they are promising targets for future research.

AS can expand proteome diversity and plays a crucial role in the evolution of species (Blencowe, 2006). This study is focused on the analysis of DASGs with pseudogenization, domain changes, and secretion. The results demonstrate that 21 genes are pseudogenized in alternative isoforms, which might be degraded through the nonsense-mediated decay pathway (Nickless et al., 2017). In terms of DASGs with changes in domains, RRM_1 and LRR_8 were the two most frequently modified domains. RRM_1 domain is known to bind with single-stranded RNAs, and proteins containing this domain have critical functions in regulating gene expression in eukaryotic cells, such as AS, mRNA transport, RNA editing, and modulation of mRNA translation (Zhang et al., 2016). VdNop12, a protein containing the RRM_1 domain, is a crucial factor of pathogenicity and cold adaption in *Verticillium dahliae* (Zhang et al., 2020a). LRR-containing proteins have been reported to be essential in the development and pathogenicity of *Phytophthora sojae* (Si et al., 2021). Two hub genes were identified in the protein–protein interaction network, which may be involved in regulating the pathogenicity of *S. sclerotiorum*. More importantly, 16 spliced secreted proteins were identified in this study. Secreted effectors are key virulence determinants in plant pathogens (Arroyo-Velez et al., 2020). Thus, we believe that AS reprogramming confers fitness benefits to *S. sclerotiorum* at different infection stages, and these secreted proteins undergoing AS are of great significance for the infection of *S. sclerotiorum*.

In this study, we performed the genome-wide AS analysis of *S. sclerotiorum* across all stages of infection. Our results demonstrate that AS is prevalent in *S. sclerotiorum*. In addition, we found that AS can give rise to functionally divergent proteins, and *S. sclerotiorum* infection activates the AS of secreted proteins. Taken together, our findings shed a new light on the landscape of AS and its potential contribution to *S. sclerotiorum* infection.

Data availability statement

The datasets presented in this study can be found in online repositories. The names of the repository/repositories and accession number(s) can be found in the article/Supplementary Material.

Author contributions

XZ and SL directed the project. XC, CZ, LG, YX, and LL analyzed the data. LZ, LF, JH, and XZ performed the experiments. XC and XZ wrote the manuscript. All authors contributed to the article and approved the submitted version.

Funding

The project was supported by the Central Public-Interest Scientific Institution Basal Research Fund (Y2020YJ03 and 1610172021001), the China Agriculture Research System of MOF and MARA (CAAS-12), and the Agricultural Science and Technology Innovation Program of the Chinese Academy of Agricultural Sciences (CAAS-ASTIP-2013-OCRI and CAAS-OCRI-XKPY-202104).

Conflict of interest

The authors declare that the research was conducted in the absence of any commercial or financial relationships that could be construed as a potential conflict of interest.

Publisher's note

All claims expressed in this article are solely those of the authors and do not necessarily represent those of their affiliated organizations, or those of the publisher, the editors and the reviewers. Any product that may be evaluated in this article, or

claim that may be made by its manufacturer, is not guaranteed or endorsed by the publisher.

Supplementary material

The Supplementary Material for this article can be found online at: https://www.frontiersin.org/articles/10.3389/fpls.2022.1008665/full#supplementary-material

SUPPLEMENTARY FIGURE 1
Correlation between the RNA-seq data. **(A)** Hierarchical clustering analysis of the gene expression levels in *S. sclerotiorum* at 0, 2, 6, 12, 24, and 36 hpi. The color bar represents the distance between samples, with red signifying a short distance and blue signifying a long distance between samples. The color bar (from blue to red) refers to the distance metric used for clustering, with red indicating the maximum correlation value and blue representing the minimum correlation value. **(B)** Principal component analysis of the gene expression levels in *S. sclerotiorum* at different infection stages. Each treatment has three independent biological replicates.

SUPPLEMENTARY FIGURE 2
Venn diagram of differential alternative splicing genes (DASGs). **(A)** Venn diagram of DASGs at different infection stages. **(B)** Venn diagram of DASGs under five alternative splicing types. A3SS, alternative 3′ splice site; A5SS, alternative 5′ splice site; ES, exon skipping; RI, retained intron; MXE, mutually exclusive exon.

SUPPLEMENTARY FIGURE 3
Top 20 Gene Ontology (GO) enrichment biological processes of differentially expressed genes and differential alternative splicing genes. The *x*-axis represents the negative $\log_{10}$ of the *P*-values for each GO term, and the *y*-axis indicates the GO terms.

SUPPLEMENTARY FIGURE 4
Sashimi plots for differential alternative splicing genes (DASGs) in each alternative splicing type. The plots indicate the average RNA-seq read density and splice junction counts for each DASG. The *x*-axis indicates genomic coordinates, and the *y*-axis indicates per-base expression. The numbers in the figure show the count of reads across this junction or in this area. The bottom track represents the exon–intron structure (exons in black and introns as lines) of alternative isoforms. **(A)** Sashimi plot of gene *Sscle_03g022490* with A3SS event. **(B)** Sashimi plot of gene *Sscle_01g000960* with A5SS event. **(C)** Sashimi plot of gene *Sscle_01g010310* with SE event. **(D)** Sashimi plot of gene *Sscle_01g007440* with RI event.

SUPPLEMENTARY FIGURE 5
Expression patterns of two hub genes in the STRING network. The *x*-axis represents the infection stages. The *y*-axis represents the fragments per kilobase of transcript sequence per million base pairs mapped reads value of the transcriptome.

References

Anders, S., and Huber, W. (2010). Differential expression analysis for sequence count data. *Genome Biol.* 11, R106. doi: 10.1186/gb-2010-11-10-r106

Arroyo-Velez, N., Gonzalez-Fuente, M., Peeters, N., Lauber, E., and Noel, L. D. (2020). From effectors to effectomes: Are functional studies of individual effectors enough to decipher plant pathogen infectious strategies? *PloS Pathog.* 16, e1009059. doi: 10.1371/journal.ppat.1009059

Bendtsen, J. D., Nielsen, H., Von Heijne, G., and Brunak, S. (2004). Improved prediction of signal peptides: SignalP 3.0. *J. Mol. Biol.* 340, 783–795. doi: 10.1016/j.jmb.2004.05.028

Blencowe, B. J. (2006). Alternative splicing: New insights from global analyses. *Cell* 126, 37–47. doi: 10.1016/j.cell.2006.06.023

Bolton, M. D., Thomma, B. P. H. J., and Nelson, B. D. (2006). Sclerotinia sclerotiorum (Lib.) de bary: biology and molecular traits of a cosmopolitan pathogen. *Mol. Plant Pathol.* 7, 1–16. doi: 10.1111/j.1364-3703.2005.00316.x

Bonnal, S. C., Lopez-Oreja, I., and Valcarcel, J. (2020). Roles and mechanisms of alternative splicing in cancer - implications for care. *Nat. Rev. Clin. Oncol.* 17, 457–474. doi: 10.1038/s41571-020-0350-x

Burkhardt, A., Buchanan, A., Cumbie, J. S., Savory, E. A., Chang, J. H., and Day, B. (2015). Alternative splicing in the obligate biotrophic oomycete pathogen pseudoperonospora cubensis. *Mol. Plant-Microbe Interact.* 28, 298–309. doi: 10.1094/MPMI-09-14-0300-FI

Chaudhary, S., Jabre, I., Reddy, A. S. N., Staiger, D., and Syed, N. H. (2019). Perspective on alternative splicing and proteome complexity in plants. *Trends Plant Sci.* 24, 496–506. doi: 10.1016/j.tplants.2019.02.006

Chen, S. F., Zhou, Y. Q., Chen, Y. R., and Gu, J. (2018). Fastp: an ultra-fast all-in-one FASTQ preprocessor. *Bioinformatics* 34, 884–890. doi: 10.1093/bioinformatics/bty560

Chittem, K., Yajima, W. R., Goswami, R. S., and Mendoza, L. E. D. (2020). Transcriptome analysis of the plant pathogen sclerotinia sclerotiorum interaction with resistant and susceptible canola (Brassica napus) lines. *PloS One* 15, e0229844. doi: 10.1371/journal.pone.0229844

Derbyshire, M., Denton-Giles, M., Hegedus, D., Seifbarghi, S., Rollins, J., Van Kan, J., et al. (2017). The complete genome sequence of the phytopathogenic fungus sclerotinia sclerotiorum reveals insights into the genome architecture of broad host range pathogens. *Genome Biol. Evol.* 9, 593–618. doi: 10.1093/gbe/evx030

Freitag, J., Ast, J., and Bolker, M. (2012). Cryptic peroxisomal targeting *via* alternative splicing and stop codon read-through in fungi. *Nature* 485, 522–U135. doi: 10.1038/nature11051

Graveley, B. R. (2005). Mutually exclusive splicing of the insect dscam pre-mRNA directed by competing intronic RNA secondary structures. *Cell* 123, 65–73. doi: 10.1016/j.cell.2005.07.028

Grutzmann, K., Szafranski, K., Pohl, M., Voigt, K., Petzold, A., and Schuster, S. (2014). Fungal alternative splicing is associated with multicellular complexity and virulence: A genome-wide multi-species study. *DNA Res.* 21, 27–39. doi: 10.1093/dnares/dst038

Huang, W., Chen, X., Guan, Q. J., Zhong, Z. H., Ma, J., Yang, B. X., et al. (2019). Changes of alternative splicing in arabidopsis thaliana grown under different CO2 concentrations. *Gene* 689, 43–50. doi: 10.1016/j.gene.2018.11.083

Huang, J., Lu, X. Y., Wu, H. W., Xie, Y. C., Peng, Q., Gu, L. F., et al. (2020). Phytophthora effectors modulate genome-wide alternative splicing of host mRNAs to reprogram plant immunity. *Mol. Plant* 13, 1470–1484. doi: 10.1016/j.molp.2020.07.007

Ibrahim, H. M. M., Kusch, S., Didelon, M., and Raffaele, S. (2021). Genome-wide alternative splicing profiling in the fungal plant pathogen sclerotinia sclerotiorum during the colonization of diverse host families. *Mol. Plant Pathol.* 22, 31–47. doi: 10.1111/mpp.13006

James, A. B., Syed, N. H., Bordage, S., Marshall, J., Nimmo, G. A., Jenkins, G. I., et al. (2012). Alternative splicing mediates responses of the arabidopsis circadian clock to temperature changes. *Plant Cell* 24, 961–981. doi: 10.1105/tpc.111.093948

Jeon, J., Kim, K. T., Choi, J., Cheong, K., Ko, J., Choi, G., et al. (2022). Alternative splicing diversifies the transcriptome and proteome of the rice blast fungus during host infection. *RNA Biol.* 19, 373–385. doi: 10.1080/15476286.2022.2043040

Kabbage, M., Yarden, O., and Dickman, M. B. (2015). Pathogenic attributes of sclerotinia sclerotiorum: Switching from a biotrophic to necrotrophic lifestyle. *Plant Sci.* 233, 53–60. doi: 10.1016/j.plantsci.2014.12.018

Krogh, A., Larsson, B., Von Heijne, G., and Sonnhammer, E. L. L. (2001). Predicting transmembrane protein topology with a hidden Markov model: Application to complete genomes. *J. Mol. Biol.* 305, 567–580. doi: 10.1006/jmbi.2000.4315

Livak, K. J., and Schmittgen, T. D. (2001). Analysis of relative gene expression data using real-time quantitative PCR and the 2(T)(-delta delta c) method. *Methods* 25, 402–408. doi: 10.1006/meth.2001.1262

Lyu, X. L., Shen, C. C., Fu, Y. P., Xie, J. T., Jiang, D. H., Li, G. Q., et al. (2016). A small secreted virulence-related protein is essential for the necrotrophic interactions of sclerotinia sclerotiorum with its host plants. *PloS Pathog.* 12, e1005435. doi: 10.1371/journal.ppat.1005435

Matera, A. G., and Wang, Z. F. (2014). A day in the life of the spliceosome. *Nat Rev Mol Cell Biol* 15, 108–121. doi: 10.1186/s13578-017-0153-7

Nickless, A., Bailis, J. M., and You, Z. S. (2017). Control of gene expression through the nonsense-mediated RNA decay pathway. *Cell Bioscience* 7, 26. doi: 10.1186/s13578-017-0153-7

Palusa, S. G., and Reddy, A. S. N. (2015). Differential recruitment of splice variants from SR pre-mRNAs to polysomes during development and in response to stresses. *Plant Cell Physiol.* 56, 421–427. doi: 10.1093/pcp/pcv010

Pan, Q., Shai, O., Lee, L. J., Frey, B. J., and Blencowe, B. J. (2009). Deep surveying of alternative splicing complexity in the human transcriptome by high-throughput sequencing (vol 40, pg 1413, 2008). *Nat. Genet.* 41, 762–762. doi: 10.1038/ng0609-762d

Papasaikas, P., Tejedor, J. R., Vigevani, L., and Valcarcel, J. (2015). Functional splicing network reveals extensive regulatory potential of the core spliceosomal machinery. *Mol. Cell* 57, 7–22. doi: 10.1016/j.molcel.2014.10.030

Peng, Q., Xie, Q. X., Chen, F., Zhou, X. Y., Zhang, W., Zhang, J. F., et al. (2017). Transcriptome analysis of sclerotinia sclerotiorum at different infection stages on brassica napus. *Curr. Microbiol.* 74, 1237–1245. doi: 10.1007/s00284-017-1309-8

Pistoni, M., Ghigna, C., and Gabellini, D. (2010). Alternative splicing and muscular dystrophy. *RNA Biol.* 7, 441–452. doi: 10.4161/rna.7.4.12258

Reddy, A. S. N., Marquez, Y., Kalyna, M., and Barta, A. (2013). Complexity of the alternative splicing landscape in plants. *Plant Cell* 25, 3657–3683. doi: 10.1105/tpc.113.117523

Shen, S. H., Park, J. W., Lu, Z. X., Lin, L., Henry, M. D., Wu, Y. N., et al. (2014). rMATS: Robust and flexible detection of differential alternative splicing from replicate RNA-seq data. *Proc. Natl. Acad. Sci. United States America* 111, E5593–E5601. doi: 10.1073/pnas.1419161111

Si, J. R., Pei, Y., Shen, D. Y., Ji, P. Y., Xu, R. F., Xue, X., et al. (2021). Phytophthora sojae leucine-rich repeat receptor-like kinases: diverse and essential roles in development and pathogenicity. *Iscience* 24, 102725. doi: 10.1016/j.isci.2021.102725

Stepankiw, N., Raghavan, M., Fogarty, E. A., Grimson, A., and Pleiss, J. A. (2015). Widespread alternative and aberrant splicing revealed by lariat sequencing. *Nucleic Acids Res.* 43, 8488–8501. doi: 10.1093/nar/gkv763

Syed, N. H., Kalyna, M., Marquez, Y., Barta, A., and Brown, J. W. (2012). Alternative splicing in plants–coming of age. *Trends Plant Sci.* 17, 616–623. doi: 10.1016/j.tplants.2012.06.001

Szklarczyk, D., Gable, A. L., Nastou, K. C., Lyon, D., Kirsch, R., Pyysalo, S., et al. (2021). The STRING database in 2021: customizable protein-protein networks, and functional characterization of user-uploaded gene/measurement sets. *Nucleic Acids Res.* 49, D605–D612. doi: 10.1093/nar/gkab835

Tollervey, J. R., Wang, Z., Hortobagyi, T., Witten, J. T., Zarnack, K., Kayikci, M., et al. (2011). Analysis of alternative splicing associated with aging and neurodegeneration in the human brain. *Genome Res.* 21, 1572–1582. doi: 10.1101/gr.122226.111

Trapnell, C., Pachter, L., and Salzberg, S. L. (2009). TopHat: discovering splice junctions with RNA-seq. *Bioinformatics* 25, 1105–1111. doi: 10.1093/bioinformatics/btp120

Trapnell, C., Williams, B. A., Pertea, G., Mortazavi, A., Kwan, G., Van Baren, M. J., et al. (2010). Transcript assembly and quantification by RNA-seq reveals unannotated transcripts and isoform switching during cell differentiation. *Nat. Biotechnol.* 28, 511–515. doi: 10.1038/nbt.1621

Turunen, J. J., Niemela, E. H., Verma, B., and Frilander, M. J. (2013). The significant other: splicing by the minor spliceosome. *Wiley Interdiscip Rev. RNA* 4, 61–76. doi: 10.1002/wrna.1141

Wang, Z., Gerstein, M., and Snyder, M. (2009). RNA-Seq: a revolutionary tool for transcriptomics. *Nat. Rev. Genet.* 10, 57–63. doi: 10.1038/nrg2484

Wang, E. T., Sandberg, R., Luo, S. J., Khrebtukova, I., Zhang, L., Mayr, C., et al. (2008). Alternative isoform regulation in human tissue transcriptomes. *Nature* 456, 470–476. doi: 10.1038/nature07509

Wang, G. H., Sun, P., Gong, Z. W., Gu, L. F., Lou, Y., Fang, W. Q., et al. (2018). Srk1 kinase, a SR protein-specific kinase, is important for sexual reproduction, plant infection and pre-mRNA processing in fusarium graminearum. *Environ. Microbiol.* 20, 3261–3277. doi: 10.1111/1462-2920.14299

Wang, L., Yang, T., Wang, B., Lin, Q., Zhu, S., Li, C., et al. (2020). RALF1-FERONIA complex affects splicing dynamics to modulate stress responses and growth in plants. *Sci. Adv.* 6, eaaz1622. doi: 10.1126/sciadv.aaz1622

Westrick, N. M., Ranjan, A., Jain, S., Grau, C. R., Smith, D. L., and Kabbage, M. (2019). Gene regulation of sclerotinia sclerotiorum during infection of glycine max: on the road to pathogenesis. *BMC Genomics* 20, 157. doi: 10.1186/s12864-019-5517-4

Williams, B., Kabbage, M., Kim, H. J., Britt, R., and Dickman, M. B. (2011). Tipping the balance: Sclerotinia sclerotiorum secreted oxalic acid suppresses host defenses by manipulating the host redox environment. *PloS Pathog.* 7, e1002107. doi: 10.1371/journal.ppat.1002107

Will, C. L., and Luhrmann, R. (2011). Spliceosome structure and function. *Cold Spring Harb. Perspect. Biol.* 3. doi: 10.1101/cshperspect.a003707

Xiao, X. Q., Xie, J. T., Cheng, J. S., Li, G. Q., Yi, X. H., Jiang, D. H., et al. (2014). Novel secretory protein ss-Caf1 of the plant-pathogenic fungus sclerotinia sclerotiorum is required for host penetration and normal sclerotial development. *Mol. Plant-Microbe Interact.* 27, 40–55. doi: 10.1094/MPMI-05-13-0145-R

Xu, B. J., Gong, X., Chen, S., Hu, M. L., Zhang, J. F., and Peng, Q. (2021). Transcriptome analysis reveals the complex molecular mechanisms of brassica napus-sclerotinia sclerotiorum interactions. *Front. Plant Sci.* 12. doi: 10.3389/fpls.2021.716935

Xu, L. S., Li, G. Q., Jiang, D. H., and Chen, W. D. (2018). Sclerotinia sclerotiorum: An evaluation of virulence theories. *Annu. Rev. Phytopathol.* 56, 311–338. doi: 10.1146/annurev-phyto-080417-050052

Yang, G. G., Tang, L. G., Gong, Y. D., Xie, J. T., Fu, Y. P., Jiang, D. H., et al. (2018). A cerato-platanin protein SsCP1 targets plant PR1 and contributes to virulence of sclerotinia sclerotiorum. *New Phytol.* 217, 739–755. doi: 10.1111/nph.14842

Yan, Q. Q., Xia, X., Sun, Z. F., and Fang, Y. D. (2017). Depletion of arabidopsis SC35 and SC35-like serine/arginine-rich proteins affects the transcription and splicing of a subset of genes. *PloS Genet.* 13, e1006663. doi: 10.1371/journal.pgen.1006663

Zhang, R. X., Calixto, C. P. G., Marquez, Y., Venhuizen, P., Tzioutziou, N. A., Guo, W. B., et al. (2017a). A high quality arabidopsis transcriptome for accurate transcript-level analysis of alternative splicing. *Nucleic Acids Res.* 45, 5061–5073. doi: 10.1093/nar/gkx267

Zhang, J., Cui, W. Y., Haseeb, H., and Guo, W. (2020a). VdNop12, containing two tandem RNA recognition motif domains, is a crucial factor for pathogenicity and cold adaption inVerticillium dahliae. *Environ. Microbiol.* 22, 5387–5401. doi: 10.1111/1462-2920.15268

Zhang, Y. M., Dai, Y. F., Huang, Y., Wang, K., Lu, P., Xu, H. F., et al. (2020b). The SR-protein FgSrp2 regulates vegetative growth, sexual reproduction and pre-mRNA processing by interacting with FgSrp1 in fusarium graminearum. *Curr. Genet.* 66, 607–619. doi: 10.1007/s00294-020-01054-2

Zhang, Y. M., Gao, X. L., Sun, M. L., Liu, H. Q., and Xu, J. R. (2017b). The FgSRP1 SR-protein gene is important for plant infection and pre-mRNA processing in fusarium graminearum. *Environ. Microbiol.* 19, 4065–4079. doi: 10.1111/1462-2920.13844

Zhang, S., Zhou, J. T., Hu, H. L., Gong, H. P., Chen, L. G., Cheng, C., et al. (2016). A deep learning framework for modeling structural features of RNA-binding protein targets. *Nucleic Acids Res.* 44, e32. doi: 10.1093/nar/gkv1025

Zhu, W. J., Wei, W., Fu, Y. P., Cheng, J. S., Xie, J. T., Li, G. Q., et al. (2013). A secretory protein of necrotrophic fungus sclerotinia sclerotiorum that suppresses host resistance. *PloS One* 8, e53901. doi: 10.1371/journal.pone.0053901

frontiers | Frontiers in Plant Science

TYPE Original Research
PUBLISHED 03 November 2022
DOI 10.3389/fpls.2022.1040511

OPEN ACCESS

EDITED BY
Cunmin Qu,
Southwest University, China

REVIEWED BY
Mingli Yan,
Hunan Academy of Agricultural Sciences, China
Liezhao Liu,
Southwest University, China
Zhiyong Hu,
Oil Crops Research Institute, Chinese Academy of Agricultural Sciences, China

*CORRESPONDENCE
Zhongsong Liu
zsliu48@sohu.com
Zhenqian Zhang
zzq770204@163.com

†These authors have contributed equally to this work and share first authorship

SPECIALTY SECTION
This article was submitted to Plant Pathogen Interactions, a section of the journal Frontiers in Plant Science

RECEIVED 09 September 2022
ACCEPTED 05 October 2022
PUBLISHED 03 November 2022

CITATION
Gan Q, Luan M, Hu M, Liu Z and Zhang Z (2022) Functional study of *CYP90A1* and *ALDH3F1* gene obtained by transcriptome sequencing analysis of *Brassica napus* seedlings treated with brassinolide.
Front. Plant Sci. 13:1040511.
doi: 10.3389/fpls.2022.1040511

Functional study of *CYP90A1* and *ALDH3F1* gene obtained by transcriptome sequencing analysis of *Brassica napus* seedlings treated with brassinolide

Qingqin Gan[1†], Mingbao Luan[2†], Maolong Hu[3], Zhongsong Liu[1*] and Zhenqian Zhang[1*]

[1]College of Agriculture, Hunan Agricultural University, Changsha, China, [2]Institute of Bast Fiber Crops, Chinese Academy of Agricultural Sciences/Key Laboratory of Stem-Fiber Biomass and Engineering Microbiology, Ministry of Agriculture, Changsha, China, [3]Institute of Industrial Crops, Jiangsu Academy of Agricultural Science, Nanjing, China

Sclerotinia disease and weeds of *Brassica napus* greatly reduce crop yields. However, brassinolides can improve the resistance of plants to sclerotinia diseases and herbicides. In this study, we investigated the effects of brassinolide on the occurrence, physiological indices, yield, and gene expression of Fanming No. 1 seeds under sclerotinia and glufosinate stress. The results showed that soaking of the seeds in 0.015% brassinolide for 6 h reduced the incidence of sclerotinia by 10%. Additionally, in response to glufosinate stress at the seedling stage, the enzyme activities of catalase and superoxide dismutase increased by 9.6 and 19.0 U/gFW/min, respectively, and the soluble sugar content increased by 9.4 mg/g, increasing the stress resistance of plants and yield by 2.4%. *LHCB1*, *fabF*, *psbW*, *CYP90A1*, *ALDH3F1*, *ACOX1*, *petF*, and *ACSL* were screened by transcriptome analysis. *ALDH3F1* and *CYP90A1* were identified as key genes. Following glufosinate treatment, transgenic plants overexpressing ALDH3F1 and CYP90A1 were found to be resistant to glufosinate, and the expression levels of the *ALDH3F1* and *CYP90A1* were 1.03–2.37-fold as high as those in the control. The expression level of *ATG3*, which is an antibacterial gene related to sclerotinia disease, in transgenic plants was 2.40–2.37-fold as high as that in the control. Our results indicate that these two key genes promote plant resistance to sclerotinia and glufosinate. Our study provides a foundation for further studies on the molecular mechanisms of rapeseed resistance breeding and selection of new resistant varieties.

KEYWORDS

Sclerotinia, herbicide, *Brassica napus*, brassinolide, *ALDH3F1*, *CYP90A1*, overexpression

1 Introduction

Rapeseed is the second-largest oilseed crop (Asaduzzaman et al., 2014). As one of the fastest growing global sources of edible oilseeds, rapeseed is among the few species with the potential for meeting the growing edible oil requirements of many countries in Asia, Africa, and America (Sharma et al., 2012).

Weed infestation during the rapeseed seedling stage is a major factor reducing yield (Krato and Petersen, 2012). Although chemical herbicides can effectively and easily control weeds, pesticide residues are extremely harmful to the growth of crops, particularly rapeseed (Gondo et al., 2021). Sclerotiorum is one of the main pathogens that causes serious stem rot disease in *Brassica napus L.* (Bolton et al., 2006). The serious stem rot disease in Brassica napus L. that is caused by sclerotiorum results in a yield loss of 10-70% in rapeseed cultivation (Del Río et al., 2007; Derbyshire and Denton-Giles, 2016). Disease control in rapeseed relies mainly on partially resistant lines which is resist sclerotiorum (Wang et al., 2018). The molecular mechanisms underlying the response of the rapeseed plant to this pathogen are poorly understood (Zhang et al., 2022).

Brassinolides improve plant adaptation to biotic and abiotic stresses, such as those caused by heavy metals, pesticides, herbicides, and organic pollutants (Rajewska et al., 2016; Yuan et al., 2017; Xia et al., 2018). Cytochrome P450 participates in the biosynthesis of endogenous lipophilic compounds, such as fatty acids, brassinolides, and gibberellins, and it enables the oxidative detoxification of many herbicides (Mary, 2010). *CYP90A1* engages in the most important step in brassinolide biosynthesis (Szekeres et al., 1996). In wheat (*Triticum aestivum*), a series of P450s mediate the N-demethylation and cyclo-methylhydroxylation of phenylurea herbicides such as primosulfuron (Frear DS); in soybean, *CYP71A10* N-demethylates a range of phenylurea herbicides and ring-methyl hydroxylates chlortoluron (Siminszky et al., 1999).

ALDH belongs to a family of NAD(P)+-dependent enzymes with broad substrate specificity and catalyzes the oxidation of various toxic aldehydes to carboxylic acids. Transgenic *Arabidopsis* plants overexpressing *Ath-ALDH3* show improved tolerance to dehydration, NaCl, heavy metals, and methyl viologen (Sunkar et al., 2003). In contrast, deletion of *ALDH* affects photosynthesis in plants. The protective effects of *ALDH3F1* are required to maintain membrane fluidity and support leaf gas exchange and photosynthesis (Zhao, J. Y. et al., 2017).

We previously showed that ATG3 can improve rapeseed resistance to *Sclerotinia sclerotiorum* (Wang et al., 2019). Treatment of *Brassica napus* seeds with brassinolides can improve resistance to herbicides (glufosinate-ammonium) at the seedling stage. Transcriptome analysis revealed that *ALDH3F1* and *CYP90A1* were involved in these effects. Overexpression of *ALDH3F1* and *CYP90A1* improved the tolerance of rapeseed to glufosinate-ammonium and enhanced *ATG3* expression. In this study, we investigated the underlying mechanisms influencing stress resistance, which may help accelerate molecular breeding of herbicide-resistant rapeseed plants.

2 Materials and methods

2.1 Plant material

Fanming No. 1 was cultivated in an experimental field at the Yunyuan Experimental Base of Hunan Agricultural University (Changsha, Hunan Province) at a planting density of 30 × 30 cm. Experiments were performed in triplicate according to planned regular regional experiments for Fanming No. 1. The plot area was 10 m^2, and the plants were planted in rows.

At the seedling stage, the control was soaked in water and sprayed with 88.8% ammonium glyphosate (dilution ratio 400×) and 200 g/L glufosinate (dilution ratio 400×). Young leaf tissue samples were collected on days 7, 10, and 13 after treatment, with five samples collected per treatment. The samples were divided into two parts: one part was immediately frozen at −80°C and the other was used to extract RNA. We performed physicochemical analysis of the frozen samples. For the samples evaluating using quantitative reverse transcription polymerase chain reaction (qRT-PCR), the first sampling time was October 28, 2021 and the last sampling time was November 3, 2021. The first sampling time for samples used to analyze physicochemical traits was November 3, 2021 and the last sampling time was April 27, 2022. Mature *B. napus* plants were harvested on May 3, 2022, and agronomic traits were determined.

2.2 Measurement items and methods

2.2.1 Effect of brassinolide on Fanming No. 1

2.2.1.1 Treatment methods

Fanming No. 1 seeds (n = 100) were soaked in water or 0.15% and 0.015% brassinolide solutions for 0, 2, 4, 6, 8, and 10 h. The germination rate was measured to determine the optimum concentration and soaking time.

2.2.1.2 Effects of brassinolide on the physiology, biochemistry, yield, and quality of Fanming No. 1

Leaf samples were taken from the third-to-last leaf of the plant to measure superoxide dismutase (SOD) (Gao, 2006), peroxidase (Bestwick et al., 1998), and catalase activities (Hayat et al., 2016). The contents of malondialdehyde (Vos et al., 1991), protein (Bradford, 1976), total sugar (Dubois et al., 1951), and total chlorophyll (Anis et al., 2020) were determined

using a U 8000 spectrophotometer (METASH, Shanghai, China). All experiments included three biological replicates, each containing five plants.

To determine the agronomic traits, the field growth of Fanming No. 1 was investigated in January 2022. The agronomic traits, yield, and quality of rapeseed at maturity were investigated in May 2022. All experiments were performed in five biological replicates.

2.2.2 Field disease investigation

At 35 days after pollination of Fanming No. 1, the presence of disease (sclerotiorum) was evaluated on all plants of each line, as described by Wang et al. (2019).

2.2.3 Key differential gene screening

2.2.3.1 RNA extraction from plant samples

The third-to-last leaf at the 5–6 leaf stage of Fanming No. 1 was collected, and more than three leaves from the brassinolide soaking treatment and control groups were collected. One sample was frozen in liquid nitrogen (−80°C). The TransZol Up Plus RNA Kit reagent was used for RNA extraction (Beijing TransGen Biotech Co., Ltd., Beijing, China). RNA quality was evaluated using a Nanodrop2000 (Thermo Fisher Scientific, Waltham, MA, USA) and 2100 Bioanalyzer (Agilent Technologies, Santa Clara, CA, USA).

2.2.3.2 Transcriptome sequencing

Transcriptome sequencing analysis was performed by Nanjing Pesennuo Gene Technology Ltd. (Nanjing, China).

2.2.3.3 Sequencing result analysis

We focused on metabolic pathways related to herbicide resistance, such as photosynthesis (Song et al., 2020), pyruvate metabolism (Leslie and Baucom, 2014), aromatic amino acid synthesis (Zhao N. et al., 2017), and screened key differential genes combined with functional annotations provided by NCBI.

2.2.4 Functional gene screening

The third to last leaves of each treatment sample were collected at different stages from more than three plants. One sample was cryopreserved in liquid nitrogen at −80°C and RNA was extracted using a TransZol Up Plus RNA Kit (Beijing TransGen Biotech Co., Ltd., Beijing, China). RNA quality was detected using a Nanodrop 2000 (Thermo Fisher Scientific) and 2100 Bioanalyzer (Agilent Technologies). cDNA was synthesized using approximately 0.5 μg of RNA and PrimeScript RT Master Mix (Aidlab Biotechnologies Co., Ltd., Changsha, China). qRT-PCR was performed for each sample using a Bio-Rad CFX96 Touch Detection System (Hercules, CA, USA) and SYBR Green PCR Master Mix (Aidlab Biotechnologies Co., Ltd.). Primers for the qRT-PCR experiments (Table 1) were designed using NCBI, and eight glufosinate resistance-related genes were analyzed. We used a qRT-PCR system and procedure developed using the SYBR Green PCR Master Mix Kit (Aidlab Biotechnologies Co., Ltd.). After PCR amplification, quantitative changes in each gene were analyzed using the delta Ct method (Livak and Schmittgen, 2001).

2.2.5 Gene function verification

2.2.5.1 Gene cloning and construction of overexpression vector

RNA was extracted using the TransZol Up Plus RNA kit. First-strand cDNA was synthesized from 1 μg of RNA using a Maxima H Minus First-Strand cDNA Synthesis Mix Kit (Thermo Fisher Scientific) according to the manufacturer's instructions. Synthetic cDNA was used to amplify the coding sequences of *ALDH3F1* and *CYP90A1* with the primers listed in Table 1. The amplified product was detected using 1% agarose gel electrophoresis and 0.1% GelRed nucleic acid gel staining, inserted into the PEASY vector (TransGen Biotech), and verified by sequencing. The *ALDH3F1* and *CYP90A1* sequences were inserted into the XbaI and BamHI restriction sites of the vector PBI121 to construct recombinant plasmids. The *ALDH3F1*-PBI121 and *CYP90A1*-PBI121 recombinant plasmids were introduced into *Agrobacterium tumefaciens* strain LBA4404 to overexpress *Brassica napus* (Zhongshuang 11).

2.2.5.2 Agrobacterium-mediated transformation of Zhongshuang 11

Rape hypocotyls were obtained and transformed as described by Eva et al. (2011). The explants were subcultured in the medium every 15 days. Selected green calli were transferred to induction medium. After two months, the selected shoots were transferred to the rooting medium. The medium formulation was prepared as described by Baskar et al. (2016).

2.2.5.3 Gene function verification

To verify *ALDH3F1* and *CYP90A1* genes function, glufosinate (2000× solution) was applied to the unfolded leaves of each rape seedling as described by Cui et al. (2016) with some modifications. Leaf performance was observed on day 7, after which the leaves were collected for qRT-PCR analysis.

2.3 Statistical analysis

Microsoft Excel 2010 software (Redmond, WA, USA) was used to sort data. All experimental data are presented as the average of three independent biological replicates. Data were analyzed by one-way analysis of variance using SPSS software (version 22.0; SPSS, Inc., Chicago, IL, USA). Different letters indicate significantly different means within the same group ($p < 0.05$, Duncan's multiple range test).

10.3389/fpls.2022.1040511

TABLE 1 Primer sequences.

Gene name	Primer name	Sequence (5'-3')
BnActin	BnActin -F	CGTTGGTGGAGTTGCACTTG
	BnActin -R	AGCACGTTACGGGATTGGTT
psbW	psbW -F	CTGGTCTTTCTCTCTGAACAT
	psbW -R	AACAACAAGAAACCAGAAGATCA
petF	petF -F	CCTTCCAAAAGCCACTGCCC
	petF -R	AGAGACTCGCACTGTAGCCA
LHCB1	LHCB1 -F	CTCCATGTTTGGATTCTTTGTA
	LHCB1 -R	ACATCACATTCAAGATTTAACAA
fabF	fabF -F	ATCTCTACCGCTTGTGCTACTT
	fabF -R	TGTGACAATGCCCTACAAGC
ACSL	ACSL -F	AATGGATAGTTGCTGGGATG
	ACSL -R	GAGAGAGTTTCCCAGCTTTA
ALDH3F1	ALDH3F1 -F	TCTTGTCAGAAACATCGTCAG
	ALDH3F1 -R	GAGGGTATCGAGCTTCCAGAT
ACOX1	ACOX1 -F	CCTTTTATCTCGTCGTCTCC
	ACOX1 -R	CGATCTCTAGATGACAGCAC
CYP90A1	CYP90A1 -F	CTCATGCTTGATATTGACCG
	CYP90A1 -R	AGAAGAGAGGGAGAGGTATTG
ALDH3F1	K-ALDH3F1 -F	CTTCTGAACAGAGTCGAGGG
	K-ALDH3F1 -R	TGTGTGTGTTTCTCTTATCGCT
ALDH3F1	A-XbaI-F	gagaacacgggggactctagaATGGAAGCCATGAAGGAGACTG
	A-BamAI-R	gcccttgctcaccatggatccTCTTTTAAGACCGAGCATTAAGAGG
CYP90A1	K-CYP90A1 -F	CCACTCTCCCCCTCTCCATT
	K-CYP90A1 -R	CAAGTAGCGGATAAGCCACCA
CYP90A1	C-XbaI-F	gagaacacgggggactctagaATGGCTTTCTCCTTCTCCTCCA
	C-BamAI-R	gcccttgctcaccatggatccAGTAGCGGATAAGCCACCATCA
ATG 3	ATG 3-F	TCGGCGTTCAAGGAGAAG
	ATG 3-R	TGCCAGGGTCACCAGATT

3 Results

3.1 Optimum conditions for brassinolide processing

Seeds from *B. napus* (Fanming No. 1) were soaked in brassinolide solution or water indoors (approximately 25°C). The effect of the soaking time on the germination rate is shown in Table 2. Soaking in 0.015% brassinolide for 6 h showed the better than other treatments.

Herbicide spraying was performed at the 4–5 leaf stage (early November) of Fanming No. 1. The plants showed similar growth under different treatments, namely, A (blank control) and B (brassinolide treatment). The growth of rapeseed in group C (brassinolide treatment and herbicide glufosinate-ammonium treatment) was strongly affected, with the leaves turning yellow and continuing to grow after 13 days (Figure 1). Group D plants (brassinolide and herbicide glyphosate treatments) withered on day 13 and died on the day after glyphosate treatment. In group E (herbicide glufosinate-ammonium treatment), after glufosinate treatment, the whole plant turned yellow on day 7 and died on this day. These results demonstrate that soaking of Fanming No. 1 seeds in brassinolide improved the resistance of seedlings to glufosinate.

TABLE 2 The soaking time test of brassinolide.

Soaking time (h)		0	2	4	6	8	10
Germination rate (%) Germination percentage	Water	100	100	100	94	88	82
	0.15% Brassinolide	100	100	96	92	86	78
	0.015% Brassinolide	100	100	100	100	90	86

10.3389/fpls.2022.1040511

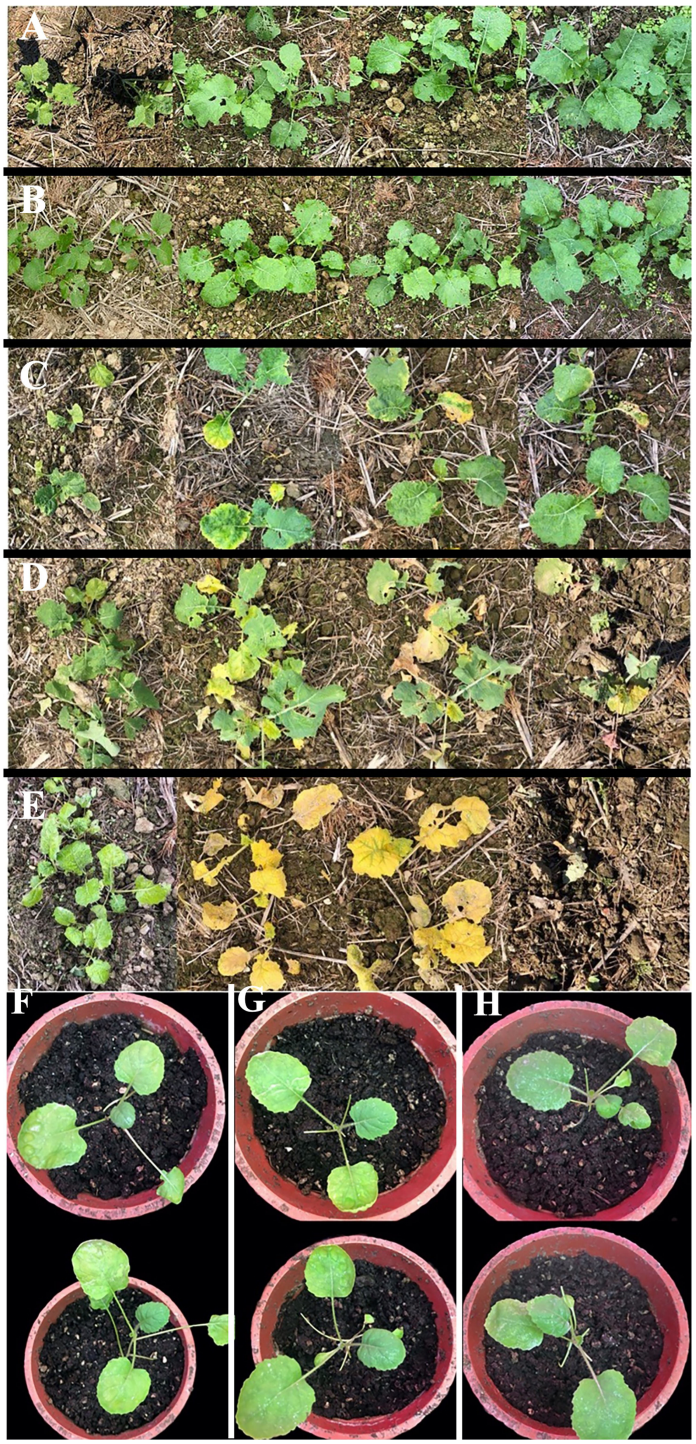

FIGURE 1
Brassica napus under different treatments. **(A)** water treatment, **(B)** 0.015% brassinolide treatment, **(C)** 0.015% brassinolide treatment and glufosinate-ammonium dilution ratio of 400× treatment, **(D)** 0.015% brassinolide treatment and glyphosate dilution ratio of 400× treatment, and **(E)** water treatment and dilution ratio of 400× glufosinate-ammonium treatment. **(A–E)** Performance of Fanming No. 1 under different treatments at 0, 7, 10, and 13 days after herbicide treatment. **(F–H)** *Brassica napus*, *ALDH3F1* transgenic *B napus*, and *CYP90A1* transgenic *B napus*, respectively; day 7 after smearing the leaves with 2000X glufosinate solution.

3.2 Effect of brassinolide treatment on Fanming No. 1

3.2.1 Analysis of physiological and biochemical indices of Fanming No. 1

The physiological and biochemical indicators of CK1 (blank control), CK2 (brassinolide treatment only), and A2 (brassinolide treatment followed by glufosinate treatment) leaves at different growth stages were measured. The results showed that the catalase activity (Figure 2G), SOD activity (Figure 2E), soluble sugar content (Figure 2C), and malondialdehyde content (Figure 2A) after A2 treatment were significantly higher than those of the control at the seedling stage. After entering the 5–6 leaf period, the content of soluble

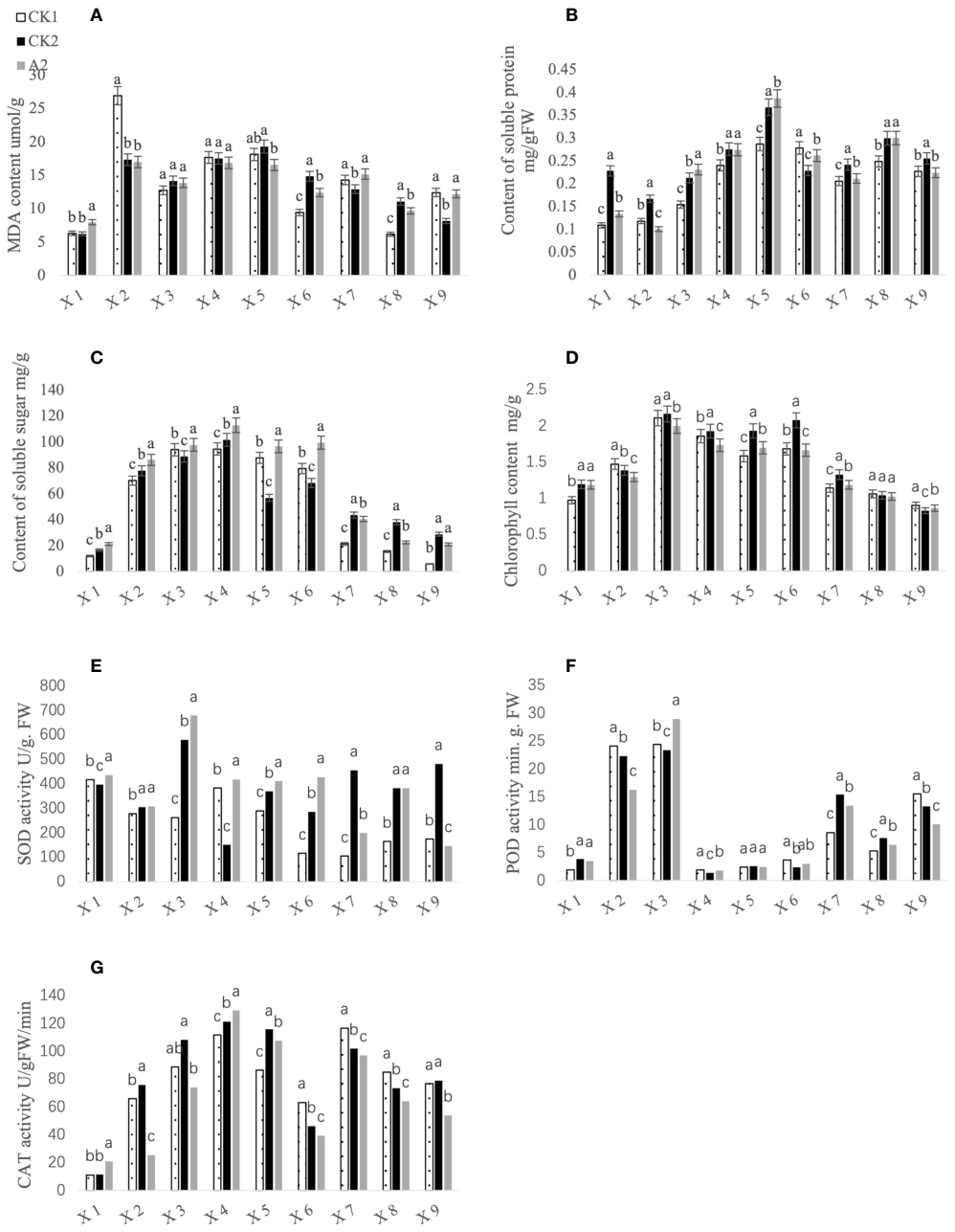

FIGURE 2
Effects of different treatments on physiological and biochemical indices of Fanming No. 1 leaves. X1–X9 represent the seedling period, 5–6-leaf period, bud stage, initial bloom stage, full bloom stage, final bloom stage, day 21 of pod growth, day 26 of pod growth, and day 31 of pod growth, respectively. **(A–G)** represents MDA content, Content of soluble protein, Content of soluble protein, Content of soluble sugar, Chlorophyll content, SOD activity, POD activity and CAT activity, respectively. Different letters indicate significant differences ($p < 0.05$).

substances in the A2 treatment group increased and was significantly higher than that in the control group. The contents of soluble sugar and soluble protein (Figure 2B) first increased and then decreased, and the content of soluble sugar in the A2 treatment group was highest in the initial bloom stage, whereas the highest soluble protein content was observed in the full bloom stage. Peroxidase activity (Figure 2F) and SOD activity in the A2 treatment group were highest at the bud stage and were significantly higher than those in the control group. The chlorophyll content (Figure 2D) was higher in the CK2 treatment group than in the other treatments, except for at the 5–6 leaf periods and at days 26 and 31 of pod growth.

3.2.2 Analysis of agronomic character index of Fanming No. 1

The results of the prewinter survey are shown in Table 3. Except for the largest leaf length, the growth of Fanming No. 1 under A2 treatment was poor, followed by CK2 and CK1 treatments. These results indicate that brassinolide treatment alleviated the effects of glufosinate. Table 4 shows the growth status of Fanming No. 1 at the maturity stage of different treatments, CK2 outperforms both CK1 and A2 treatments in terms of plant height (cm), primary effective branch site (cm), effective length of the main inflorescence (cm), number of effective branches at a time, number of effective pods on the main inflorescence, and grain weight per plant (g). The number of effective pods in the whole plant of the A2 treatment group was higher than that in the CK1 and CK2 groups, and the pod length and seed number per plant of the CK1 treatment pods were larger than those in the CK2 and A2 groups.

3.2.3 Analysis of disease resistance of Fanming No. 1

The disease survey results; disease index. As shown in Table 5, CK2 had the lowest disease index (<7.5) and incidence (<15%), followed by A2, whereas CK1 had the

TABLE 3 The growth status of rapeseed seedlings under different treatments before winter.

Materials	Green leaves of main stem	Total leaves of main stem	The largest leaf		Width of rootstock (cm)	Plant height (cm)
			Length (cm)	Width (cm)		
CK1	10.8 ± 1.92^{a}	12.8 ± 1.30^{a}	27.8 ± 2.51^{a}	19.5 ± 2.72^{a}	1.994 ± 0.40^{a}	22.2 ± 2.17^{a}
CK2	9.6 ± 1.52^{a}	11.4 ± 1.52^{ab}	26.5 ± 3.34^{a}	19.1 ± 2.58^{a}	1.74 ± 0.39^{ab}	19.6 ± 3.13^{b}
A2	9.4 ± 1.14^{a}	10.8 ± 1.10^{b}	28.62 ± 1.08^{a}	19.06 ± 0.86^{a}	1.38 ± 0.08^{b}	17.72 ± 3.20^{b}

CK1, blank control, CK2 brassinolide treatment only; A2, brassinolide treatment followed by glufosinate treatment. Different letters indicate significant differences ($p < 0.05$).

TABLE 4 Analysis of agronomic characters of Fanming No. 1 under different treatments.

Materials	Plant height (cm)	Primary effective branch site (cm)	Effective length of main inflorescence (cm)	Number of effective branches at a time	Number of effective pods on main inflorescence	Effective pods number of whole plant	Pod length (cm)	Seeds number of per pod	Grain weight of per plant (g)
CK1	177.4 ± 6.80^{b}	86.4 ± 2.07^{c}	36.0 ± 2.54^{c}	9.8 ± 1.79^{c}	48.0 ± 6.04^{b}	328.4 ± 8.53^{c}	6.22 ± 0.36^{a}	23.88 ± 1.53^{a}	29.3 ± 0.66^{c}
CK2	184.0 ± 3.32^{a}	122.2 ± 5.50^{a}	60.0 ± 2.83^{a}	12.4 ± 1.52^{a}	71.6 ± 8.44^{a}	434 ± 29.89^{a}	5.88 ± 0.44^{a}	21.6 ± 4.93^{a}	31.3 ± 1.09^{a}
A2	172.0 ± 3.08^{b}	105.4 ± 2.41^{b}	46.8 ± 2.17^{b}	11.8 ± 0.84^{b}	48.0 ± 2.55^{b}	500 ± 17.14^{b}	5.89 ± 0.36^{a}	22.8 ± 3.15^{a}	31.0 ± 1.54^{b}

CK1, blank control, CK2 brassinolide treatment only; A2, brassinolide treatment followed by glufosinate treatment. Different letters indicate significant differences ($p < 0.05$).

TABLE 5 Disease survey results.

Sample	Grading of disease/plant					Total/plant	Disease index	Morbidity/%
	Lever 0	Lever 1	Lever 2	Lever 3	Lever 4			
CK 1	15	2	1	1	1	20	13.75	25%
CK 2	17	1	1	1	0	20	7.5	15%
A 2	16	2	0	1	1	20	11.25	20%

CK1, blank control, CK2 brassinolide treatment only; A2, brassinolide treatment followed by glufosinate treatment.

highest. These results indicate that CK2 had stronger resistance to sclerotinia and that brassinolide improves the disease resistance of Fanming No. 1.

3.2.4 *ATG3* expression analysis

The expression level of *ATG3* in Fanming No. 1 different treatment groups and at different periods was measured. As shown in Figure 3A, both CK2 and A2 treatments showed upregulated ATG3 expression 7, 10, and 13 days after herbicide treatment, with the highest *ATG3* expression observed after CK 2 and A2 treatment in the first period. These results indicate that brassinolide treatment improved the resistance of Fanming No. 1 to sclerotinia disease. Furthermore, in transgenic seedlings overexpressing *ALDH3F1* and *CYP90A1*, the expression of *ATG3* was 3.39–6.11- and 2.29–3.13-fold higher than that in the control (Figure 3B), respectively.

3.3 Differential gene screening

3.3.1 Transcriptome analysis of seedlings

3.3.1.1 Sequencing quality statistics

The leaves of glufosinate-treated Fanming No. 1 plants on day 7 after treatment and leaves of control plants were collected to extract RNA and evaluate RNA quality. The RNA integrity number values of extracted RNA after each treatment were higher, with an OD260/280 and OD260/230 >2. The samples were sequenced and the sequencing data were further filtered. The contents of Q20, Q30, clean reads, and clean data were >90% (Table 6), indicating that the sequencing results were reliable. The upgraded version of HISAT2 (http://ccb.jhu.edu/software/hisat2/index.shtml) software of TopHat2 was used to align the filtered reads to the reference genome; >90% of the total reads were mapped (Table 6), indicating that the reference genome was selected appropriately and was free of contamination.

3.3.1.2 Analysis of expression differences

The R language Pheatmap software package was used to perform bidirectional clustering analysis on the union for cluster and samples with differentially expressed genes (DEGs) in each group. The expression of the evaluated genes differed, as shown in Figure 4.

3.3.2 Analysis of functional enrichment of DEGs

3.3.2.1 Gene Ontology enrichment analysis

Gene Ontology (GO) enrichment analysis showed that the DEGs were mainly enriched in metabolic pathways, such as the photosynthetic membrane (135 DEGs), photosystem (122 DEGs), thylakoid (137 DEGs), thylakoid part (137 DEGs), photosynthesis (146 DEGs), and cellular biosynthetic processe (1692 DEGs) (Figure 5). Glufosinate mainly affected the photosynthesis and cell growth of *B. napus*.

3.3.2.2 Kyoto Encyclopedia of Genes and Genomes enrichment analysis

According to Kyoto Encyclopedia of Genes and Genomes enrichment analysis of the DEGs, 121 metabolic pathways showed differences, among which 40 showed the *p*-value below a specific threshold and false discovery rate <0.3. These pathways were mainly divided into lipid metabolism (9), amino acid metabolism (8), carbohydrate metabolism (5), cofactor and vitamin metabolism (4), other secondary metabolite synthesis (2), signaling (2), nucleotide metabolism

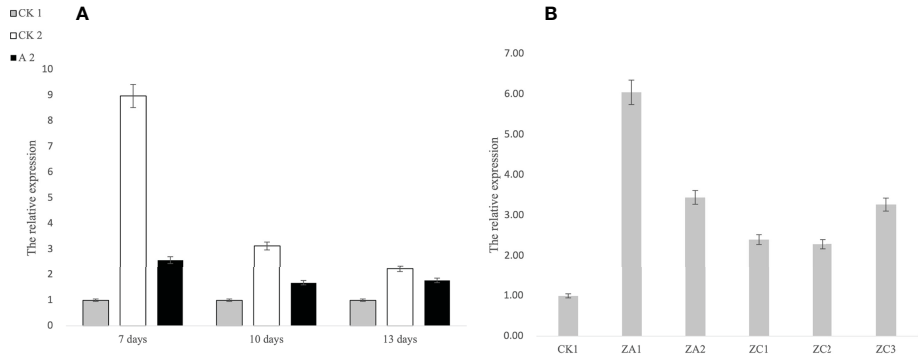

FIGURE 3
Expression levels of *ATG3* at different stages under different treatments in *Brassica napus*. **(A)** 1–3 correspond to 7, 10, and 13 days after herbicide treatment, respectively; **(B)** CK1 is the control, ZA1 and ZA2 are the *ALDH3F1* transgenic rape specimens, and ZC1–ZC3 are the *CYP90A1* transgenic rape specimens.

10.3389/fpls.2022.1040511

TABLE 6 Assessment of library quality and analysis of comparison results.

Sample	Reads no.	Q20 (%)	Q30 (%)	Clean reads no.	Clean data (%)	Total mapped (%)	Uniquely mapped (%)	Mapped to gene (%)	Mapped to exon (%)
C1	49408952	97.46	92.72	45079408	91.23	41583542 (92.25%)	39534424 (95.07%)	36651293 (92.71%)	36135281 (98.59%)
C2	46986734	97.96	94.23	43036380	91.59	39781094 (92.44%)	37880284 (95.22%)	35044120 (92.51%)	34513797 (98.49%)
C3	47377334	98	94.25	43534556	91.88	40298130 (92.57%)	38594626 (95.77%)	35802265 (92.76%)	35272204 (98.52%)
CK1	45548330	97.46	93.14	41737090	91.63	38667067 (92.64%)	36646044 (94.77%)	34708273 (94.71%)	34316012 (98.87%)
CK2	48413974	97.49	93.18	44289076	91.47	41008648 (92.59%)	38809486 (94.64%)	36749688 (94.69%)	36342188 (98.89%)
CK3	46391096	97.5	93.25	42261758	91.09	39125218 (92.58%)	37065052 (94.73%)	35109083 (94.72%)	34722181 (98.90%)

CK1-CK3, blank control, C1-C3 is brassinolide treatment followed by glufosinate treatment.

(2), folding (2), transport and catabolism (2), energy metabolism (1), other amino acid metabolism (1), terpenoid and polyketide metabolism (1), and glycan biosynthesis and metabolism (1) (Table 7). Amino acid metabolism, secondary metabolite synthesis, energy metabolism, carbohydrate metabolism, lipid metabolism, other amino acid metabolism, and metabolism of terpenoids and polyketides are closely related to growth and development, indicating that soaking

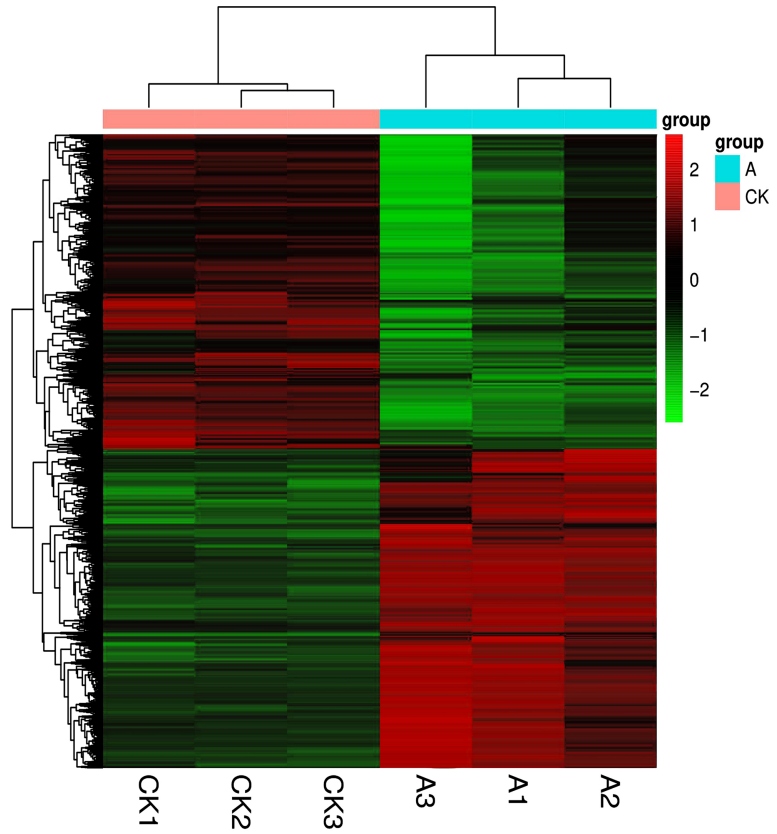

FIGURE 4
Clustering of differentially expressed genes. The horizontal direction represents genes; each column is a sample; red indicates highly expressed genes, and green indicates low gene expression.

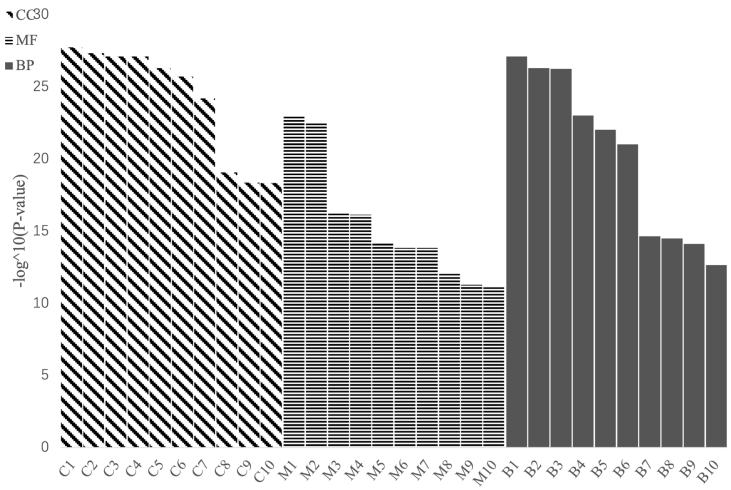

FIGURE 5
Histogram of Gene Ontology (GO) enrichment analysis (CC, cell components; MF, molecular functions; BP, biological processes). C1–C10 represent GO:0034357 photosynthetic membrane, GO:0009521 photosystem, GO:0009579 thylakoid, GO:0044436 thylakoid part, GO:0009523 photosystem II, GO:0042651 thylakoid membrane, GO:0009654 photosystem II evolving oxygen complex, GO:0005840 ribosome, GO:1990204 oxidoreductase complex and GO:0030529 intracellular ribonucleoprotein complex; M1–M10 respectively GO:0005198 structural molecule activity, GO:0003735 structural constituent of ribosome, GO:0003824 catalytic activity, GO:0036094 small molecule binding, GO:0004713 protein tyrosine kinase activity, GO:0000166 nucleotide binding, GO:1901265 nucleoside phosphate binding, GO:0043168 anion binding, GO:0004674 protein serine/threonine kinase activity and GO:0016740 transferase activity; B1–B10 represent GO:0015979 photosynthesis, GO:0044249 cellular biosynthetic process, GO:1901576 organic substance biosynthetic process, GO:0009058 biosynthetic process, GO:0044237 cellular metabolic process, GO:1901566 organonitrogen compound biosynthetic process, GO:0009987 cellular process, GO:0044271 cellular nitrogen compound biosynthetic process, GO:0008152 metabolic process, GO:0043043 peptide biosynthetic process.

of Fanming No. 1 seedlings in brassinolide mainly affected growth and development.

3.3.3 Glufosinate-related metabolic pathway analysis

We performed GO and Kyoto Encyclopedia of Genes and Genomes pathway enrichment analyses, focusing on DEGs in herbicide-related pathways, including photosynthesis (Song et al., 2020), pyruvate metabolism (Leslie and Baucom, 2014), and amino acid metabolism (Zhao, N. et al., 2017).

3.3.3.1 Photosynthesis

After spraying with glufosinate, nine DEGs were identified in photosystem I, all of which were downregulated. Nine DEGs were identified in photosystem II, of which two genes were upregulated. Seven genes were downregulated in photosystem II. One DEG in the cytochrome b6/f complex was downregulated. There were four DEGs involved in photosynthetic electron transport, with one node gene that was upregulated and three genes that were downregulated. Three F-type ATPases were downregulated (Figure 6).

3.3.3.2 Pyruvate metabolism

EPSP synthase is an enzyme involved in synthesizing aromatic amino acids by catalyzing the reaction of shikimate-3-phosphate and phosphoenolpyruvate to synthesize 5-enolpyruvylshikimate-3-phosphate. After spraying with pesticides, 114 genes in the pyruvate metabolic pathway showed differences in expression levels. Among them, three gene nodes were upregulated, five gene nodes were downregulated, and ten gene nodes were both upregulated and downregulated. Most of these genes are related to EPSP synthase, indicating that glufosinate affects the biosynthesis of pyruvate and leads to changes in EPSP synthase.

3.3.3.3 Amino acid metabolism

After spraying with glufosinate, 669 genes were differentially expressed in amino acid metabolism pathways, including in arginine biosynthesis; tyrosine metabolism; and glycine, serine, and threonine metabolism, of which 269 genes were downregulated and 400 genes were upregulated.

10.3389/fpls.2022.1040511

TABLE 7 Kyoto Encyclopedia of Genes and Genomes enrichment pathway analysis of DEGs.

Pathway ID	Pathway	Up number	Down number	Level
bna00500	Starch and sucrose metabolism	59	111	Carbohydrate metabolism
bna00010	Glycolysis/gluconeogenesis	45	113	
bna00053	Ascorbate and aldarate metabolism	15	46	
bna00620	Pyruvate metabolism	32	85	
bna00520	Amino sugar and nucleotide sugar metabolism	58	109	
bna00910	Nitrogen metabolism	24	36	Energy metabolism
bna00260	Glycine, serine and threonine metabolism	36	87	Amino acid metabolism
bna00350	Tyrosine metabolism	28	29	
bna00220	Arginine biosynthesis	19	40	
bna00360	Phenylalanine metabolism	42	26	
bna00250	Alanine, aspartate and glutamate metabolism	25	57	
bna00270	Cysteine and methionine metabolism	62	98	
bna00340	Histidine metabolism	8	30	
bna00330	Arginine and proline metabolism	49	33	
bna00073	Cutin, suberine and wax biosynthesis	4	46	Lipid metabolism
bna00591	Linoleic acid metabolism	9	9	
bna00564	Glycerophospholipid metabolism	61	60	
bna00062	Fatty acid elongation	9	39	
bna00592	alpha-Linolenic acid metabolism	41	18	
bna00561	Glycerolipid metabolism	44	59	
bna00565	Ether lipid metabolism	21	16	
bna00071	Fatty acid degradation	36	28	
bna00600	Sphingolipid metabolism	24	12	
bna00960	Tropane, piperidine and pyridine alkaloid biosynthesis	23	32	Biosynthesis of other secondary metabolites
bna00945	Stilbenoid, diarylheptanoid and gingerol biosynthesis	18	2	
bna00906	Carotenoid biosynthesis	22	34	Metabolism of terpenoids and polyketides
bna00670	One carbon pool by folate	3	32	Metabolism of cofactors and vitamins
bna00785	Lipoic acid metabolism	0	11	
bna00780	Biotin metabolism	7	24	
bna00740	Riboflavin metabolism	3	18	
bna00450	Selenocompound metabolism	11	18	Metabolism of other amino acids
bna04146	Peroxisome	49	78	Transport and catabolism
bna04136	Autophagy – other	54	4	
bna04016	MAPK signaling pathway-plant	124	55	Signal transduction
bna04075	Plant hormone signal transduction	256	131	
bna00240	Pyrimidine metabolism	29	60	Nucleotide metabolism
bna00230	Purine metabolism	45	90	
bna04141	Protein processing in endoplasmic reticulum	124	152	Folding, sorting and degradation
bna03060	Protein export	16	62	
bna00514	Other types of O-glycan biosynthesis	2	3	Glycan biosynthesis and metabolism

3.4 qRT-PCR analysis of glufosinate resistance-related genes

According to the sequencing results, numerous genes affected glufosinate resistance in Fanming No. 1, including *LHCB1* (*BnaA05g09410D*, Figure 7A), *fabF* (*BnaA06g36060D*, Figure 7B), *psbW* (*BnaA04g17660D*, Figure 7C), *CYP90A1* (*BnaA10g24860D*, Figure 7D), *ALDH3F1* (*BnaA03g59170D*, Figure 7E), *ACOX1* (*BnaC08g23150D*, Figure 7F), *petF* (*BnaA03g22350D*, Figure 7G), and *ACSL* (*BnaC01g15670D*, Figure 7H). We collected samples from the CK1 (Figure 1A) and CK2 (Figure 1B), glufosinate-only treatment (death on day 7; Figure 1E), A1 (glyphosate-only treatment, death on day 15, Figure 1D), A2 (survival, Figure 1C), 7 and 10 days after glufosinate treatment, and 13-day groups to determine the expression levels of each gene at different stages.

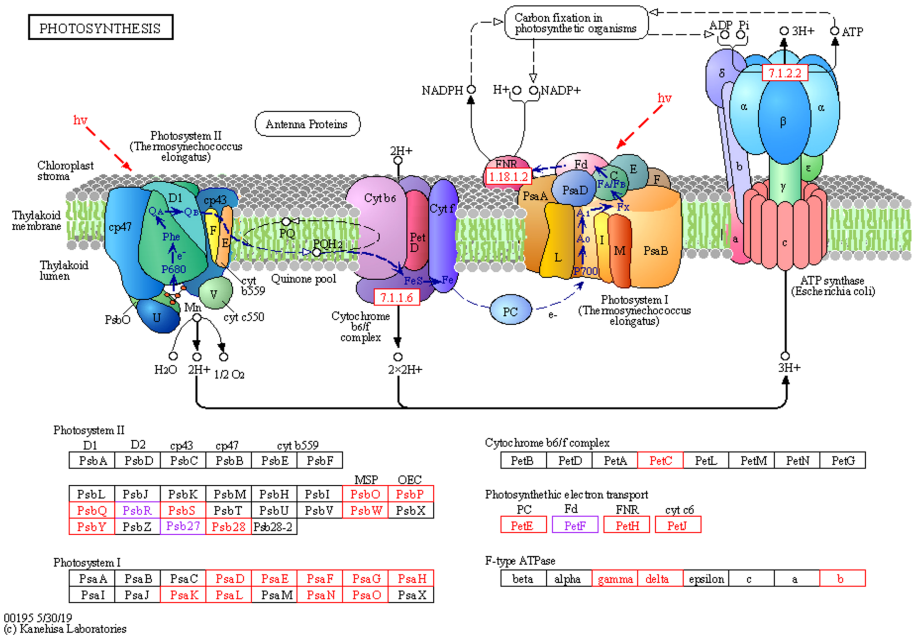

FIGURE 6
Photosynthesis metabolic pathways involving differentially expressed genes. Photosystem II, photosystem I, cytochrome b6/f complex, photosynthetic electron transport, F-type ATPase, carbon fixation in photosynthetic organisms, chloroplast stroma, thylakoid membrane, and thylakoid lumen.

This eight key glufosinate resistance genes were evaluated using qRT-PCR. Figure 7 shows the expression levels of these genes at 7 days after glufosinate treatment. The first period of each graph revealed changes in the expression level of each gene according to qRT-PCR (A2) and RNA-Seq. Figure 6 shows that the trends in the expression levels determined in qRT-PCR and RNA-Seq were highly similar, indicating that the expression data obtained using RNA-Seq are reliable.

3.5 Functional validation of two key differential genes

3.5.1 Agrobacterium-mediated transformation of the hypocotyl of *B. napus*

Because *B. napus* died 13 days after treatment following A1 treatment and the specimen in the A2 group turned green 13 days after treatment, gene expression was compared in the two (herbicide) treatment groups. In gene-corresponding protein function analysis, two key genes were identified, *CYP90A1* and *ALDH3F1*. *Agrobacterium*-mediated hypocotyl transformation was performed to transform the recombinant expression vectors pBI121-CYP90A1 and pBI121-ALDH3F1 into *B. napus* Zhongshuang 11 to obtain transgenic *B. napus* plants. DNA was extracted from the transgenic plants for PCR verification and pBI121 was obtained: pBI121-ALDH3F1 (Figure 8A) and pBI121-CYP90A1 (Figure 8B). Next, the expression levels of *CYP90A1* and *ALDH3F1* in the PCR positive plants were evaluated using qRT-PCR. Under the action of strong promoters, the *CYP90A1* expression levels of positive plant ZC1, ZC2 and ZC3 increased by 1.43, 1.27- and 1.19-fold, respectively (Figure 7J). In the control, the *ALDH3F1* expression levels of positive plant ZA1 and ZA2 were 1.40- and 2.06-fold as high as those in the control, respectively (Figure 7I).

3.5.2 Resistance identification of transgenic plants

After treatment of control and transgenic rape seedlings with glufosinate for 7 days, the leaves of plants in the blank control group showed yellowing and shrinkage. The leaves of *ALDH3F1* transgenic rape seedlings shrank significantly, although no yellowing was observed (Figure 1G). *CYP90A1* transgenic rape seedlings showed slight shrinkage without yellowing (Figure 1H). After 7 days of glufosinate treatment, samples were collected for qRT-PCR. In the overexpression lines ZA1-1 and ZA2-1, the relative expression levels of *ALDH3F1* were 1.04- and 1.63-fold as high as that in the control, respectively (Figure 7I). In the overexpression lines ZC1-1,ZC2-1 and ZC3-1, the *CYP90A1* expression was 2.37-, 2.09-, and 1.03-fold as high as that in the control (Figure 7J). The expression levels of

10.3389/fpls.2022.1040511

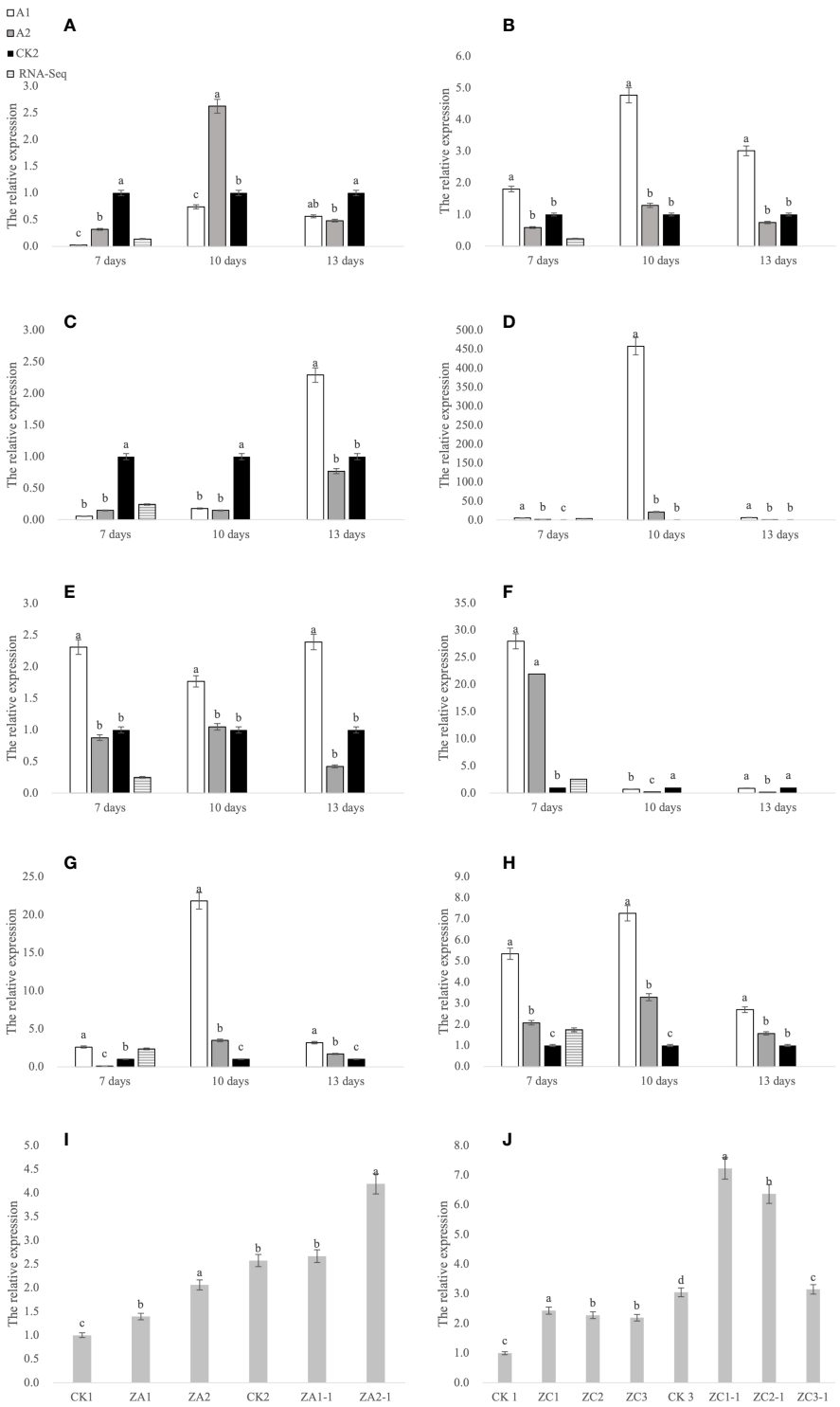

FIGURE 7
qRT-PCR analysis of genes. **(A–H)** Gene expression at 7, 10, and 13 days after glufosinate treatment. The relative expression levels of A1 and A2 in the same period were divided by the relative expression levels of CK2, and CK2 was set to 1. **(I, J)** CK1 is the blank control; CK2 and CK3 are the expression levels of *ALDH3F1* and *CYP90A1* at 7 days after non-transgenic *Brassica napus* seedlings were treated with glufosinate-ammonium, respectively; ZA1 and ZA2 are the expression levels of *ALDH3F1* in the transgenic *ALDH3F1* seedlings; ZC1–ZC3 denote the expression level of *CYP90A1* in *CYP90A1* transgenic seedlings; and ZA1-1, ZA2-1, and ZC1-1–ZC3-1 denote the expression levels of corresponding genes in transgenic seedlings treated with glufosinate. Different letters indicate significant differences ($p < 0.05$).

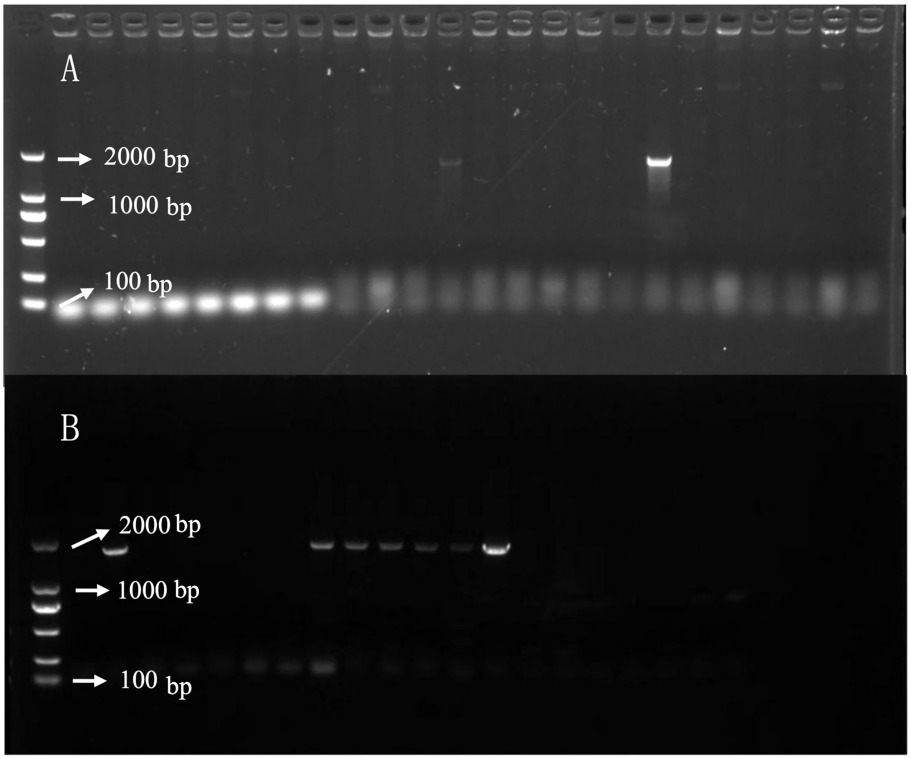

FIGURE 8
DNA detection of *ALDH3F1* and *CYP90A1* in transgenic plants. **(A, B)** are PCR detection of transgenic plants overexpression ALDH3F1 and CYP90A1 respectively.

ALDH3F1 and *CYP90A1* were higher in the overexpression lines than in control plants.

4 Discussion

4.1 Key genes in response to glufosinate stress under brassinolide treatment

When plants are externally stimulated, their gene expression is altered to mitigate changes in the environment. We found that *B. napus* pre-treated with brassinolide developed resistance to sclerotinia and glufosinate. Following transcriptome analysis, the GO enrichment results were mainly concentrated in the photosynthetic membrane, photosystem, and photosynthesis. The Kyoto Encyclopedia of Genes and Genomes enrichment results were also concentrated in carbohydrate metabolism, energy metabolism, and amino acid metabolism, indicating that pre-treatment with brassinolide affected plant growth and development and alleviated glufosinate stress in Fanming No. 1.

During the plant stress response, we evaluated the expression of eight key glufosinate resistance genes. The expression levels of *CYP90A1* and *ALDH3F1* were significantly different compared to in the control, with the expression levels gradually decreasing as the plants recovered. These two genes were further analyzed.

4.2 Overexpression of *CYP90A1* and *ALDH3F1* contributes to resistance of *B. napus* to glufosinate

Aldehydes are intermediates in several fundamental metabolic pathways. Aldehyde dehydrogenase (ALDH) enzymes belong to a family of $NAD(P)^+$-dependent enzymes, which exhibit substrate specificity and catalyze the oxidation of various aldehydes to the corresponding carboxylic acids, thereby reducing lipid peroxidation (Kirch et al., 2004). Plant family 2 ALDHs have been suggested to oxidize acetaldehyde generated *via* ethanolic fermentation, producing acetate for acetyl-CoA biosynthesis *via* acetyl-CoA synthetase, similar to the yeast pathway named as “pyruvate dehydrogenase bypass” (Wei et al., 2009). Transgenic *Arabidopsis* plants overexpressing *ALDH3F1* are more tolerant to salt (NaCl and/or KCl), dehydration, and oxidative stress (Stiti et al., 2011). Activation of NADPH oxidase results in higher levels of H_2O_2, which

triggers the relevant sensor to stimulate the mitogen-activated protein kinase cascade in plants under Cd stress. Mitogen-activated protein kinase activates the function of *trans*-regulatory elements in the nucleus to bind *cis*-regulatory elements and subsequently enhance the transcriptional levels of SOD and catalase to alleviate plant stress (Planas-Riverola et al., 2019), which is consistent with our results. We found that *ALDH3F1* was highly expressed under the influence of glufosinate-ammonium stress; over time, the plants gradually recovered and *ALDH3F1* expression decreased. These results suggest that high *ALDH3F1* expression enhances the tolerance of Zhongshuang 11 plants to glufosinate.

The functions of cytochrome P450 monooxygenase *CYP90A1/CPD* (mutants identified in *Arabidopsis*) include constitutive photomorphogenesis and dwarfism (cpd; *CYP90A1* deficiency). The expression levels of *CYP90A1/CPD* are correlated with the spatial allocation of the *CYP90A1* substrate 6-deoxocatha-sterone, suggesting that *CYP90* genes contribute to the regulation of brassinolide biosynthesis (Bancoş et al., 2002). Most herbicides such as prosulfuron, diclofop and chlortoluron can be converted into several metabolites by P450 (Danièle et al., 2000). P450 primarily catalyzes the monooxygenation of lipophilic xenobiotics, including herbicides, and plays a major role in the oxidation of most classes of herbicides (Frear, 1995). We found that *CYP90A1* was highly expressed during glufosinate stress. Over time, the plants gradually recovered, and *CYP90A1* expression decreased. These results suggest that high *CYP90A1* expression enhances the tolerance of Zhongshuang 11 tolerance to glufosinate.

4.3 Overexpression of *CYP90A1* and *ALDH3F1* leads to upregulated *ATG3* expression

ATG3 is crucial for responses to various biotic and abiotic stressors in animals and plants. A study of autophagy regulation in tomato showed that the heat shock transcription factor HsfA1a confers drought tolerance and induces autophagy by activating ATG (Wang et al., 2015). In this study, we found that the incidence of sclerotinia in samples treated with brassinolide and herbicides after brassinolide treatment was lower than that in the control, and the expression of *ATG3* was upregulated at all three time points evaluated. These results indicate that upregulation of *ATG3* expression can enhance the resistance of rape to sclerotiorum, which is consistent with the results of Wang et al. (2019).

ATG3 was highly expressed in plants overexpressing *ALDH3F1* and *CYP90A1*. These results indicate that upregulated expression of *ALDH3F1* and *CYP90A1* leads to upregulated expression of *ATG3*, which may cause Zhongshuang 11 to be resistant to sclerotiorum. The incidence of sclerotinia in later stages will be verified in follow-up experiments.

5 Conclusion

Soaking of *B. napus* seeds in 0.015% brassinolide for 6 h resulted in the germination rate. Brassinolide treated plants started to turn green and continued to grow on day 7 of glufosinate application, indicating that the treatment conferred some resistance to glufosinate. The incidence of sclerotinia disease was reduced by 10% and the disease index was reduced by 6 points in the brassinolide-pre-treated group compared to in the control. Additionally, the activities of catalase and SOD increased under brassinolide pre-treatment, increasing the content of soluble substances. Transgenic seedlings overexpressing *ALDH3F1* shrunk but did not show yellowing, whereas seedlings overexpressing *CYP90A1* showed only slight shrinkage, suggesting that transgenic Zhongshuang No. 11 was strongly resistant to glufosinate. Moreover, the expression level of related genes in transgenic plants and expression level of the antibacterial *S. sclerotiorum* gene *ATG3* in transgenic plants were higher than those in the control. These results indicate that *ALDH3F1* and *CYP90A1* are improve the resistance of *B. napus* to sclerotium disease. Our results provide a theoretical basis for the molecular breeding of *B. napus* to improve disease and glufosinate resistance, thereby promoting the development of the rapeseed industry.

Data availability statement

The datasets presented in this study can be found in online repositories. The names of the repository/repositories and accession number(s) can be found below: https://www.ncbi.nlm.nih.gov/, PRJNA877382.

Author contributions

ZZ developed the experimental plan. ZL designed the experiments. QG conducted the experiments. ML wrote the manuscript. MH analyzed the data. All authors have read and approved the manuscript.

Funding

This study was supported by the Natural Science Foundation of Changsha (kq2007015), National Transgenic Research Projects of China (2018ZX08020001), Agricultural Science, Technology Innovation Program (ASTIP) of CAAS (Grant

No.2021IBFC), and Natural Science Foundation of China (31201240).

Conflict of interest

The authors declare that this research was conducted in the absence of any commercial or financial relationships that could be construed as potential conflicts of interest.

Publisher's note

All claims expressed in this article are solely those of the authors and do not necessarily represent those of their affiliated organizations, or those of the publisher, the editors and the reviewers. Any product that may be evaluated in this article, or claim that may be made by its manufacturer, is not guaranteed or endorsed by the publisher.

References

Anis, A. S., Shakil, A., Muhammad, A., and Nasim, A. Y. (2020). Seed priming with 3-epibrassinolide alleviates cadmium stress in cucumis sativus through modulation of antioxidative system and gene expression. *Sci. Hortic.* 265 (C), 109203. doi: 10.1016/j.scienta.2020.109203

Asaduzzaman, M., Pratley, J. E., An, M., Luckett, D. J., and Lemerle, D. (2014). Canola interference for weed control. *Springer Sci. Rev.* 2 (1-2), 63–74. doi: 10.1007/s40362-014-0022-2

Bancoş, S., Nomura, T., Sato, T., Molnár, G., Bishop, G. J., Koncz, C., et al. (2002). Regulation of transcript levels of the arabidopsis cytochrome p450 genes involved in brassinosteroid biosynthesis. *Plant Physiol.* 130 (1), 504–513. doi: 10.1104/pp.005439

Baskar, V., Gangadhar, B. H., Park, S. W., and Nile, S. H. (2016). A simple and efficient agrobacterium tumefaciens-mediated plant transformation of *Brassica rapa* ssp. pekinensis. *3 Biotech* 6 (1), 88. doi: 10.1007/s13205-016-0402-1

Bestwick, C. S., Brown, I. R., and Mansfield, J. W. (1998). Localized changes in peroxidase activity accompany hydrogen peroxide generation during the development of a nonhost hypersensitive reaction in lettuce. *Plant Physiol.* 118, 1067–1078. doi: 10.1104/pp.118.3.1067

Bolton, M. D., Thomma, B. P. H. J., and Nelson, B. D. (2006). *Sclerotinia sclerotiorum* (Lib.) de bary: Biology and molecular traits of a cosmopolitan pathogen. *Mol. Plant Pathol.* 7, 1–16. doi: 10.1111/j.1364-3703.2005.00316.x

Bradford, M. M. (1976). A rapid and sensitive method for the quantitation of microgram quantities of protein utilizing the principle of protein-dye binding anal. *Biochem* 72, 248–254. doi: 10.1016/0003-2697(76)90527-3

Cui, Y., Huang, S. Q., Liu, Z. D., Yi, S. Y., Zhou, F., Chen, H., et al. (2016). Development of novel glyphosate-tolerant japonica rice lines: A step toward commercial release. *Front. Plant Sci.* 7. doi: 10.3389/fpls.2016.01218

Danièle, W. R., Alain, H., and Luc, D. (2000). Cytochromes P450 for engineering herbicide tolerance. *Trends Plant Sci.* 5 (3), 116–123. doi: 10.1016/S1360-1385(00)01567-3

Del Río, L., Bradley, C., Henson, R., Endres, G., Hanson, B., Mckay, K., et al. (2007). Impact of sclerotinia stem rot on yield of canola. *Plant Dis.* 91, 191–194. doi: 10.1094/PDIS-91-2-0191

Derbyshire, M. C., and Denton-Giles, M. (2016). The control of sclerotinia stem rot on oilseed rape (*Brassica napus*): Current practices and future opportunities. *Plant Pathol.* 65, 859–877. doi: 10.1111/ppa.12517

Dubois, M., Gilles, K., Hamilton, J. K., Rebers, P. A., and Smith, F. (1951). A colorimetric method for the determination of sugars. *Nature* 168 (4265), 167. doi: 10.1038/168167a0

Eva, B., Jana, L., Ildiko, M., Zuzana, P., Martin, J., Maria, B., et al. (2011). Agrobacterium-mediated genetic transformation of economically important oilseed rape cultivars. *Plant Cell Tissue Organ Culture (PCTOC)* 107 (2), 317–323. doi: 10.1007/s11240-011-9982-y

Frear, D. S. (1995). Wheat microsomal cytochrome P450 monooxygenases: characterization and importance in the metabolic detoxification and selectivity of wheat herbicides. *Drug Metabol Drug Interact.* 12, (3–4). doi: 10.1515/dmdi.1995.12.3-4.329

Gao, J. (2006). "Photosynthesis: determination of chlorophyll content," in *Experimental guidance for plant physiology*. Ed. J. Gao (Beijing: Higher Education Press), 74–77.

Gondo, T. F., Kamakama, M., Oatametse, B., Samu, T., Bogopa, J., and Keikotlhaile, B. M. (2021). Pesticide residues in fruits and vegetables from the southern part of Botswana. *Food Addit. Contam. Part B Surveill.* 14 (4), 271–280. doi: 10.1080/19393210.2021.1950845

Hayat, S., Cheng, Z., Ahmad, H., Ali, M., Chen, X., and Wang, M. (2016). Garlic, from remedy to stimulant: evaluation of antifungal potential reveals diversity in phytoalexin allicin content among garlic cultivars; allicin containing aqueous garlic extracts trigger antioxidants in cucumber. *Front. Plant Sci.* 7. doi: 10.3389/fpls.2016.01235

Kirch, H., Bartels, D., Wei, Y. L., Schnable, S. P., and Wood, A. J. (2004). The *ALDH* gene superfamily of arabidopsis. *Trends Plant Sci.* 9, 371–377. doi: 10.1016/j.tplants.2004.06.004

Krato, C., and Petersen, J. (2012). Gene flow between imidazolinone-tolerant and – susceptible winter oilseed rape varieties. *Weed Res.* 52 (2), 187–196. doi: 10.1111/j.1365-3180.2012.00907.x

Leslie, T., and Baucom, R. S. (2014). *De novo* assembly and annotation of the transcriptome of the agricultural weed ipomoea purpurea uncovers gene expression changes associated with herbicide resistance. *G3 (Bethesda)* 4 (10), 2035–2047. doi: 10.1534/g3.114.013508

Livak, K. J., and Schmittgen, T. D. (2001). Analysis of relative gene expression data using real-time quantitative PCR and the 2(-delta delta C(T)) method. *Methods* 25 (4), 402–408. doi: 10.1006/meth.2001.1262

Mary, A. (2010). Plant cytochrome P450 monooxygenases. *Crit. Rev. Plant Sci.* 15 (3), 235–284. doi: 10.1080/07352689609701942

Planas-Riverola, A., Gupta, A., Betegón-Putze, I., Bosch, N., Ibañes, M., and and Caño-Delgado, A. T. (2019). Brassinosteroid signaling in plant development and adaptation to stress. *Development* 146 (5), dev151894. doi: 10.1242/dev.151894

Rajewska, I., Talarek, M., and Bajguz, A. (2016). Brassinosteroids and response of plants to heavy metals action. *Front. Plant Sci.* 7. doi: 10.3389/fpls.2016.00629

Sharma, M., Gupta, S. K., and Mondal, A. K. (2012). "Production and trade of major world oil crops," in *Technological innovations in major world oil crops*, vol. 1. Ed. S. Gupta (New York, NY: Springer). doi: 10.1007/978-1-4614-0356-2_1

Siminszky, B., Corbin, F. T., Ward, E. R., Fleischmann, T. J., and Dewey, R. E. (1999). Expression of a soybean cytochrome P450 monooxygenase cDNA in yeast and tobacco enhances the metabolism of phenylurea herbicides. *Proc. Natl. Acad. Sci. U. S. A.* 96 (4), 1750–1755. doi: 10.1073/pnas.96.4.1750

Song, T., Chu, M., Zhang, J., Wen, R., Lee, J., Gossen, B. D., et al. (2020). Transcriptome analysis identified the mechanism of synergy between sethoxydim herbicide and a mycoherbicide on green foxtail. *Sci. Rep.* 10 (1), 21690. doi: 10.1038/s41598-020-78290-6

Stiti, N., Missihoun, T. D., Kotchoni, S. O., and Kirch, H. (2011). Bartels dorothea. aldehyde dehydrogenases in arabidopsis thaliana: Biochemical requirements, metabolic pathways, and functional analysis. *Front. Plant Sci.* 2. doi: 10.3389/fpls.2011.00065

Sunkar, R., Bartels, D., and Kirch, H. H. (2003). Overexpression of a stress-inducible aldehyde dehydrogenase gene from arabidopsis thaliana in transgenic plants improves stress tolerance. *Plant J.* 35 (4), 452–464. doi: 10.1046/j.1365-313x.2003.01819.x

Szekeres, M., Nemeth, K., Koncz-Kalman, Z., Mathur, J., Kauschmann, A., Altmann, T., et al. (1996). Brassinosteroids rescue the deficiency of CYP90, a cytochrome P450, controlling cell elongation and de-etiolation in arabidopsis. *Cell* 85, 171–182. doi: 10.1016/S0092-8674(00)81094-6

Vos, C. H. R. D., Schat, H., Waal, M. A. M. D., Vooijs, R., and Ernst, W. H. O. (1991). Increased resistance to copper-induced damage of the root cell plasmalemma in copper tolerant silene cucubalus. *Physiol. Plant* 82, 523–528. doi: 10.1111/j.1399-3054.1991.tb02942.x

Wang, Y., Cai, S., Yin, L., Shi, K., Xia, X., Zhou, Y., et al. (2015). Tomato HsfA1a plays a critical role in plant drought tolerance by activating ATG genes and inducing autophagy. *Autophagy* 11, 2033–2047. doi: 10.1080/15548627.2015.1098798

Wang, X. D., Chen, H., Zhang, Z. Q., and Guan, C. Y. (2019). Relationship between two resistance gene and diseases in high oleic acid rapeseed. *J. Nucl. Agric. Sci.* 33 (05), 894–901. doi: 10.11869/j.issn.100-8551.2019.05.0894

Wang, Z., Wan, L., Xin, Q., Chen, Y., Zhang, X., Dong, F., et al. (2018). Overexpression of OsPGIP2 confers sclerotinia sclerotiorum resistance in brassica napus through increased activation of defense mechanisms. *J. Exp. Bot.* 69, 3141–3155. doi: 10.1093/jxb/ery138

Wei, Y., Lin, M., Oliver, D. J., and Schnable, P. S. (2009). The roles of aldehyde dehydrogenases (ALDHs) in the PDH bypass of arabidopsis. *BMC Biochem.* 25, 10:7. doi: 10.1186/1471-2091-10-7

Xia, X. J., Fang, P. P., Guo, X., Qian, X. J., Zhou, J., Shi, K., et al. (2018). Brassinosteroid-mediated apoplastic H_2O_2 -glutaredoxin 12/14 cascade regulates antioxidant capacity in response to chilling in tomato. *Plant Cell Environ.* 41 (5), 1052–1064. doi: 10.1111/pce.13052

Yuan, X. Y., Zhang, L. G., Huang, L., Yang, H. J., Zhong, Y. T., Ning, N, et al. (2017). Spraying Brassinolide improves Sigma Broad tolerance in foxtail millet (Setaria italica L.) through modulation of antioxidant activity and photosynthetic capacity. *Sci. Rep.* 7 (1), 11232. doi: 10.1038/s41598-017-11867-w

Zhang, K., Zhuo, C. J., Wang, Z. X., Liu, F., Wen, J., Yi, B., et al. (2022). BnaA03.MKK5-BnaA06.MPK3/BnaC03.MPK3 module positively contributes to sclerotinia sclerotiorum resistance in brassica napus. *Plants* 11 (5), 609–609. doi: 10.3390/plants11050609

Zhao, N., Li, W., Bai, S., Guo, W. L., Yuan, G. H., Wang, F., et al. (2017). Transcriptome profiling to identify genes involved in mesosulfuron-methyl resistance in alopecurus aequalis. *Front. Plant Sci.* 8, 1309. doi: 10.3389/fpls.2017.01391

Zhao, J. Y., Missihoun, D. T., and Bartels, D. (2017). The role of arabidopsis aldehyde dehydrogenase genes in response to high temperature and stress combinations. *J. Exp. Bot.* 68 (15), 4295–4308. doi: 10.1093/jxb/erx194

frontiers | Frontiers in Plant Science

TYPE Original Research
PUBLISHED 10 November 2022
DOI 10.3389/fpls.2022.996862

OPEN ACCESS

EDITED BY
Qi Peng,
Jiangsu Academy of Agricultural Sciences (JAAS), China

REVIEWED BY
Peiqing Liu,
Fujian Academy of Agricultural Sciences, China
Wenkun Huang,
Institute of Plant Protection (CAAS), China
Yi Cheng,
Chinese Academy of Agricultural Sciences (CAAS), China

*CORRESPONDENCE
Hong Jian Zhu
hongjian62@hunau.edu.cn
Feng Liu
liufengrich@126.com

SPECIALTY SECTION
This article was submitted to Plant Pathogen Interactions, a section of the journal Frontiers in Plant Science

RECEIVED 18 July 2022
ACCEPTED 11 October 2022
PUBLISHED 10 November 2022

CITATION
Xie FL, Zhou XY, Xiao R, Zhang CJ, Zhong J, Zhou Q, Liu F and Zhu HJ (2022) Discovery and exploration of widespread infection of mycoviruses in *Phomopsis vexans*, the causal agent of phomopsis blight of eggplant in China.
Front. Plant Sci. 13:996862.
doi: 10.3389/fpls.2022.996862

Discovery and exploration of widespread infection of mycoviruses in *Phomopsis vexans*, the causal agent of phomopsis blight of eggplant in China

Fang Ling Xie[1,2], Xin Yu Zhou[1], Rong Xiao[3], Chao Jun Zhang[1], Jie Zhong[1], Qian Zhou[1], Feng Liu[2*] and Hong Jian Zhu[1*]

[1]College of Plant Protection, Hunan Agricultural University, Changsha, China, [2]College of Horticulture, Hunan Agricultural University, Changsha, China, [3]Hunan Institute of Microbiology, Changsha, China

Phomopsis vexans, which causes Phomopsis blight of eggplant, has been reported worldwide. To study the biocontrol of this disease, 162 leaf and fruit samples of eggplant Phomopsis blight were collected from Hunan, Hubei, Jiangxi, Sichuan, Zhejiang, Fujian, Guangdong and Anhui Provinces from 2017 to 2019. Eighty-seven pathogenic fungus isolates were identified as *P. vexans*. The following studies were conducted: screening of sporulation medium, spore morphology analysis, mycovirus detection and identification of novel mycoviruses in these isolates. The results showed that eggplant tissue medium was the most suitable medium for rapid sporulation, and all isolates had mycoviruses consisting of mainly mixed infections. The genome of these mycoviruses varied from 1-15 kb. Five novel mycoviruses infecting *P. vexans* were obtained, including "*Phomopsis vexans* fusarivirus 1" (PvFV1), "*Phomopsis vexans* ourmia-like virus 1" (PvOLV1), "*Phomopsis vexans* endornavirus 2" (PvEV2), "*Phomopsis vexans* partitivirus 1" (PvPV1) and "*Phomopsis vexans* victorivirus L1" (PvVVL1). Thus, PvVVL1 displays a unique genome structure, and this is the first report of a victorivirus consisting of two segments and of a deltapartitivirus infecting the fungus host.

KEYWORDS

phomopsis blight of eggplant, *Phomopsis vexans*, mycoviruses, mixed infections, deep sequencing

1 Introduction

Mycoviruses are viruses that infect and replicate in fungal cells (Hollings, 1962; Son et al., 2015). Most mycoviruses infect their fungal hosts asymptomatically (cryptic infections). However, several mycoviruses clearly can result in phenotypic alterations in the host, such as hypovirulence and debilitation. Therefore, mycoviruses have great potential to be exploited as biological agents against fungal diseases (Nuss, 2005; Jiang et al., 2013; Ghabrial et al., 2015; Li et al., 2019). Since *Cryphonectria hypovirus* 1 (CHV1) was successfully used to control chest blight disease in Europe (Nuss, 1992; Xie and Jiang, 2014; Ghabrial et al., 2015), an increasing number of hypoviruses have been detected in fungi, such as *Sclerotinia sclerotiorum*, *Botrytis cinerea*, and *Botryosphaeria dothidea* (Xiao et al., 2014; Hao et al., 2018; Azhar et al., 2019; Zhai et al., 2019). The mycovirus SSHADV-1 was used to transform the pathogenic fungus *Sclerotinia sclerotiorum* into an endophytic fungus that could coexist with, promote the growth and enhance the disease resistance of rape. The novel concept of a "plant vaccine" for the control of fungal diseases has been proposed, and it has also been pointed out that mycoviruses might be an important factor in the formation of endophytic fungi. Mycoviruses plays a significant role in the interaction between plants and fungi (Zhang et al., 2020). The development and application of high-throughput next-generation sequencing (NGS) technologies and bioinformatics have greatly enhanced the discovery of new viruses in many organisms, including fungi (Marzano et al., 2016; Zhang et al., 2018).

Some mycoviruses with attenuated virulence may not affect the growth rate of the host after infection but show physiological phenotypic changes under abiotic stress. For example, *Penicillium digitatum* polymycovirus 1 (PdPmV1) and *Penicillium digitatum* Narna-like virus 1 (PdNLV1) have no significant effect on the growth morphology of the host when coinfected with *Penicillium digitatum*; however, they reduce the sensitivity of the host to fungicides (Niu et al., 2018). Torres-Trenas et al., using a GFP fluorescence labeling technique, demonstrated that mycoviruses in *Fusarium oxysporum* affect its fixed speed and spatial distribution in plant roots (Torres-Trenas et al., 2019).

Mycoviruses can also promote the virulence of their fungal hosts. Curvularia thermal tolerance virus (CThTV) in the endophytic fungus *Curvularia protuberate* can enhance the heat tolerance of its fungal host and the plants simultaneously (Marquez et al., 2007), which provides material for studying the tripartite interaction among viruses, fungi and plants. Kotta-Loizou and Coutts found that mycoviruses can improve the pathogenicity of *Beauveria bassiana* to *Galleria mellonella* (Kotta-Loizo and Coutts, 2017). *Talaromyces marneffe* partitivirus 1 (TmPV1) can enhance the pathogenicity and tolerance of host fungi and increase the lethality of the host to mice in *Talaromyces marneffe* (Lau et al., 2018).

Mycoviruses are divided into five categories according to the nucleic acid type: retroviruses, negative single-stranded RNA viruses, positive single-stranded RNA viruses, double-stranded RNA viruses and DNA viruses. Double-stranded RNA viruses are divided into 7 families: Totiviridae, Partitiviridae, Chysoviridae, Endornaviride, Reoviridae, Quadriviridae and Megabirnaviridae. Negative single-stranded RNA viruses include the single-stranded negative-stranded RNA virological family (Mymonaviridae); DNA viruses comprise the Geminivirus-like family (Genomoviridae); retroviruses include the transposable virofamily (Metaviridae) and pseudoviridae (Pseudoviridae); positive single-stranded RNA viruses approved by the International Commission for the Classification of Virology include eight families: Alphaflexiviridae, Gammaflexiviridae, Deltaflexiviridae, Barnaviridae, Botourmiaviridae, Narnaviridae, Hypoviridae and Endornaviridae (King et al., 2012). Fusariviridae is a recently proposed family of + ssRNA viroviridae. The genome size of Fusariviruses is 6-10 kbp, and the larger ORF encodes replicase-related proteins.

In recent decades, a number of phytopathogenic and plant-associated fungi have been screened for viruses from a few perspectives, such as virological control practices (biological use of viruses) and basic virus research. The tested fungi were shown to be infected by viruses at different incidence rates, ranging from a few to over 90% (Hillman et al., 2018). These studies have revealed the great diversity of fungal viruses and provided insights into their evolutionary histories (Xie and Jiang, 2014; Marzano and Domier, 2016; Marzano et al., 2016). For example, dsRNA analysis has revealed that of the 79 *R. necatrix* isolates tested (62 Spanish, 1 Italian and 16 Israeli), 11 tested positive for the presence of dsRNA (Arjona-López et al., 2018). Luo isolated 13 *B. dothidiea* strains in Wuhan city of Hubei Province. After dsRNA detection, 12 were found to carry mycoviruses, and the carrying rate was as high as 92.31% (Luo et al., 2019). All 31 *Entoleuca* sp. isolates showed mycovirus infection. New virus-carrying Entoleuca sp. isolates were obtained, which are capable of controlling avocado white root rot (Arjona-López and López-Herrera, 2021). All *P. vexans* isolated from eggplant in this study also carried mycoviruses.

Eggplant is an economically important crop with a long cultivation history. It is widely planted in China, India, Pakistan, Menggara, the Philippines and other countries (Kumar et al., 2011). Eggplant brown streak (Phomopsis blight of eggplant) caused by *P. vexans* is an important disease that limits eggplant production (Rangaswami and Madevan, 1998; Khan, 1999; Akhtar and Chaube, 2006; Jayaramaiah et al., 2013), causing leaf and stem death or fruit rot. The disease was shown to decrease the production of eggplant by 20-50% in one season (Akhtar and Chaube, 2006; Pandey, 2010). The pathogen of eggplant brown streak can pass through the infected seed coat, cotyledon and hypocotyl (Thippeswamy et al., 2012), resulting in a low seed

germination rate and poor seed vigor. The seed yield is often reduced or even lost in breeding fields due to the spread of the disease (Das, 1998; Beura et al., 2008; Udayashankar et al., 2019). Eggplant brown streak was first reported in Nanjing, China in 1932 (Teng, 1932). At present, the disease has spread to most parts of the world (Smith et al., 1988) (Supplementary Figure SEQ Figure * ARABIC 1). In addition to infection of eggplant, Phomopsis comprises more than 100 different species and can live in more than 70 different families of herbaceous and woody plants and cause serious disease in soybean and sunflower oil crops, such as vegetables and fruit trees. These disease include soybean satisfactory stem rot (Jackson et al., 2009), Phomopsis stem cStem anker of sunflower Sunflower (Hulke et al., 2019), asparagus stem blight (Zhang et al., 2012), and die-back disease of neem (Nagendra Prasad et al., 2010), a very important plant pathogenic fungus. Mycoviruses reported in *P. vexans* include only *P. vexans* RNA virus 1 (PvRV1) (Zhang et al., 2015) and *P. vexans* partitivirus 1 (PvPV1) (Zhang et al., 2021). In this study, a number of *P. vexans* strains were isolated 58 eggplant planting areas in eight provinces of China.All *P. vexans* isolated in this study carried mycoviruses, which contained not only rich mycovirus resources but also the possibility of mycoviruses that could be used as plant vaccines.The genome size of the mycovirusesvaried from 1 to 15 kbp, and most of the strains showed mixed infection. Eggplant brown stripe pathogens are rich in mycoviruses resources.

2 Materials and methods

2.1 Fungal strains

The *P. vexans* strains were originally isolated from a typical disease lesion collected from eggplants in China. The isolates were maintained at 25°C on potato dextrose agar and stored at 4°C in the dark. Mycelia were cultured in potato dextrose broth (potato, glucose) liquid medium in an orbital shaker at 25°C for 5 to 7 days for nucleic acid extraction.

2.2 Observation of the spore carrier and spore morphology of *P. vexans* strains

The main basis for identification of the fungi of *P. vexans* strains is to observe the morphology of the two conidia. We attempted to use PDA medium (200 g potato, 20 g glucose, 15 g agar, followed by filtering with gauze and setting the volume to 1000 ml), OMA medium (20 g oat boiled for 1 h, followed by filtering with gauze and setting the volume to 1000 ml) and eggplant tissue culture medium to promote the sporulation of *P. vexans* strains. A large amount of sporulation could be observed on the decomposed eggplant fruit in the field. Fresh mycelial blocks were inoculated on PDA, OMA and eggplant tissue culture media and cultured at 25°C in the dark.

2.3 dsRNA extraction and purification

Mycelia of *P. vexans* strains were cultured in potato dextrose broth at 25°C for 7 days. The mycelia were collected and then finely ground using liquid nitrogen. The cellulose CF-11 method was used to extract the dsRNA. DNA and ssRNA contaminants were eliminated from the dsRNA by digestion with DNase I and S1 nuclease (Thermo). The dsRNA in each extract was dissolved in diethypyrocarbonate-treated water and then visualized by electrophoresis on a 1% (w/v) agarose gel stained with nucleic acid dye. The dsRNA segments extracted from *P. vexans* were purified using a Mini BEST Agarose Gel DNA Extraction Kit.

2.4 cDNA cloning, sequencing, and phylogenetic analysis

Conventional cDNA library construction was performed for viral sequence determination. After denaturation of dsRNA templates at 65°C for 5 min, cDNA was synthesized using Revert Aid M-MuLV with an adapter-tagged primer (5'-CGAT CGATCATGATGCAATGCNNNNNN-3') and amplified with a specific primer (5'- CGATCGATCATGATGCAATGC-3'). To obtain the terminal sequences of mycoviruses, the 5'-end phosphorylated oligonucleotide AdaptorA 5'-TCTCTTCGT GGGCTCTTGCG-(NH2)-3' was used for ligation of dsRNA using T4 RNA ligase at 16 °C for 16 h and was then reverse transcribed using primer B (5'-CGCAAGAGCCC ACGAAGA GA- 3'). The cDNA terminal strands were then used as templates for PCR amplification of the 5'- and 3'- terminal sequences with primer B. All of the amplified DNA fragments were cloned into the pMD18-T vector or pClone007-Blunt cloning vectors and used for the transformation of *Escherichia coli* strain DH51α.

After removing the coupling primer and vector sequences, DNAMAN software was used for splicing and sequencing according to the virus fragments. Primer 5.0 was used to design the primers. The NCBI conserved domain database was used to perform a conservative structure domain search (http://www.ncbi.nlm.nih.gov/Structure/cdd/wrpsb.cgi). The ORFs of the viruses were predicted based on standard genetic codes, and their homologous aa sequences were searched in the NCBI database using ORF finder and the BLASTp programs. Sequence alignment was performed using CLUSTALX. Annotation of the conserved sequences was carried out using GeneDoc. A phylogenetic tree was constructed using MEGA software version 7.0 by the neighbor-joining (NJ) method, with 1000 bootstrap replicates.

3 Results

3.1 Isolation and purification of *P. vexans* strains

From 2017 to 2019, 162 leaf and fruit samples with typical symptoms of eggplant brown streak were collected from 58 eggplant planting areas in Hunan, Hubei, Jiangxi, Sichuan, Zhejiang, Fujian, Guangdong and Anhui Provinces. The location and geographical distribution of the samples in the field are shown in Figure 1, and the symptoms of eggplant brown streak are shown in Figure 2.

A total of 87 P. *vexans* strains were isolated, which included some Colletotrichum and Alternaria, but none of them were our target strains. *P. vexans* colonies were first white and then became yellowish, ultimately resulting in the formation of black pycnidium. By observing the colony morphology, colonies typical of *P. vexans* were selected for purification. The morphology of the isolated *P. vexans* strains is shown in Figure 3.

3.2 Observation of the spore carrier and spore morphology of *P. vexans* strains

The purified strains were identified with ITS4/ITS5 primers. Sequence homology comparison identified 87 strains as *P. vexans*. The pycnidium of *P. vexans* was induced and cultured on three kinds of media. The results showed that the number of pycnidium was greater on OMA medium than on PDA and eggplant decoction medium in the dark at 25 °C. However, the eggplant tissue culture medium was most suitable for spore production; many pycnidia emerged after 5-7 days of cultivation, and the sporulation load of a single pycnidium was the largest (Figures 4A–C). The α-type and β-type conidia of *P. vexans* were observed in the pycnidium (Figures 4D, E), which was consistent with the morphological characteristics of *P. vexans*.

3.3 *P. vexans* contain abundant dsRNAs

A representative *P. vexans* strain was selected from each eggplant planting area, making up all 58 strains, to detect dsRNA viruses (Supplementary Table 1). Nucleic acid extraction resulted in a number of nucleic acid bands (Figure 5) that were resistant to DNase I and S1 nuclease digestion, indicating that the presence of dsRNA-like nucleotides was 100%, and the results showed abundant mycoviral resources in the *P. vexans* strain. The 58 isolated strains all had detectable mycoviruses. The genome size of the mycoviruses varied from 1 to 15 kbp, and most of the strains showed mixed infection. Only 6 strains were infected with a single dsRNA virus (PV_05, PV_06, PV_14, PV_15, PV_25, PV_37), accounting for 10.3% of the tested strains. According to the statistical analysis of dsRNA bands of different sizes, 77.6% of the tested strains were infected with nucleic acid bands of approximately 5.0 kb in size (45/58), demonstrating the highest carrying rate. Nucleic acid bands greater than 10 kb in size (43/58) accounted for 74.1% of the tested strains. There were differences in the detection rate of dsRNA among strains isolated from different provinces. The top three average carrying rates of dsRNA were from Anhui, Sichuan and Hunan, while the lowest was isolated from Guangdong (the number of strains from Jiangxi and Hubei was less than 3, which was not biologically significant and thus was not taken into account (Table 1). Nucleic acid bands of approximately 3.0 kb in size were usually accompanied by other mycoviruses.

3.4 Identification of novel mycoviruses

High-throughput sequencing was carried out using a mixture of 10 strains in 6 batches. In this study, we identified diverse viral segments from *P. vexans* strains using high-throughput transcriptome sequencing. Some viruses discovered in our analysis were nearly full length and included 5 unreported

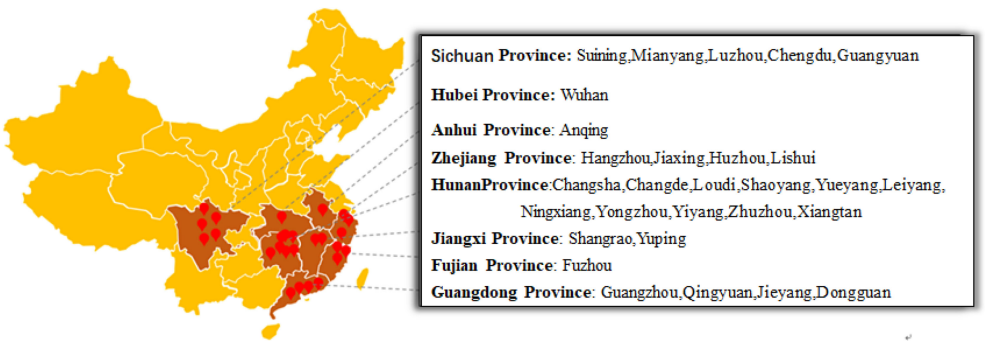

FIGURE 1
Sample collections of Phomopsis blight of eggplant and distribution in China.

10.3389/fpls.2022.996862

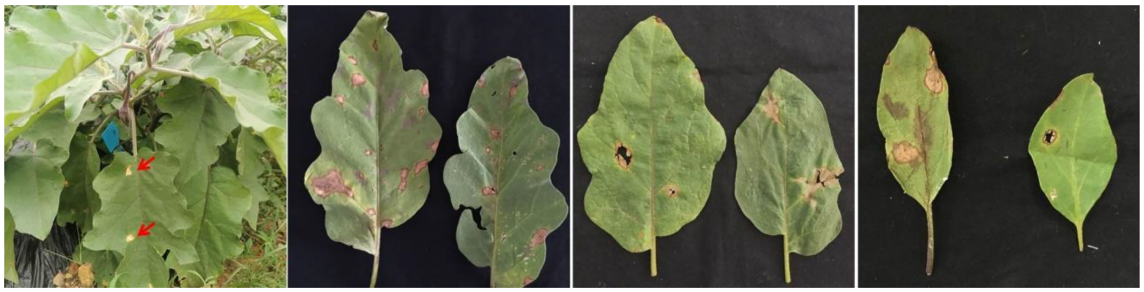

FIGURE 2
Field symptoms of leaf blight of *P. vexans*.

viruses. 5 whole viral genomes were obtained by random primer construction library and ligase-mediated end amplification. Their complete nucleotide sequences were assembled by DNAMAN. The predicted amino acid sequences of the putative viral genomes showed significant sequence identity with described viruses from several distinct lineages, including one novel virus in the family Botourmiaviridae, named *P. vexans* ourmia-like virus 1 (PvOLV1), one novel virus in the family Fusariviridae, named *P. vexans* fusarivirus 1 (PvFV1), one novel virus in the family Endornaviridae, named *P. vexans* endornavirus 2 (PvEV2), one novel virus in the family Partitiviridae, named *P. vexans* partitivirus 1 (PvPV1) and one novel virus in the family Totiviridae in which an unconventional victorivirus consisted of two segments of nucleic acid, named *P. vexans* lexivirus L1 (PvVVL1).

3.4.1 Analysis of the PvOLV1 genome structure

Sequence analysis of the full-length cDNA indicated that the PvOLV1 genome (Figure 6A) was 2452 nt in length and had a C +G content of 54.73%. ORF prediction revealed that PvOLV1 consisted of a unique ORF of 1904 nt (nt positions 68–1972), which encoded a 634-amino-acid (aa)-residue polypeptide with a calculated molecular mass of 72.04 kDa. The 5'-untranslated region (UTR) of PvOLV1 was determined to be 67 nt long. The 3'-UTR was relatively long, at 480 nt. BLASTp alignment of its RdRp indicated that PvOLV1 showed the highest aa identity (E-value: 3e-110; query cover: 95%; identity: 38.7%) with *Plasmopara viticola*-associated ourmia-like virus 52 (PvLaOLV52). A search of the conserved domain database (CDD) and multiple protein alignment confirmed that the predicted RdRp domains contained eight conserved motifs (I

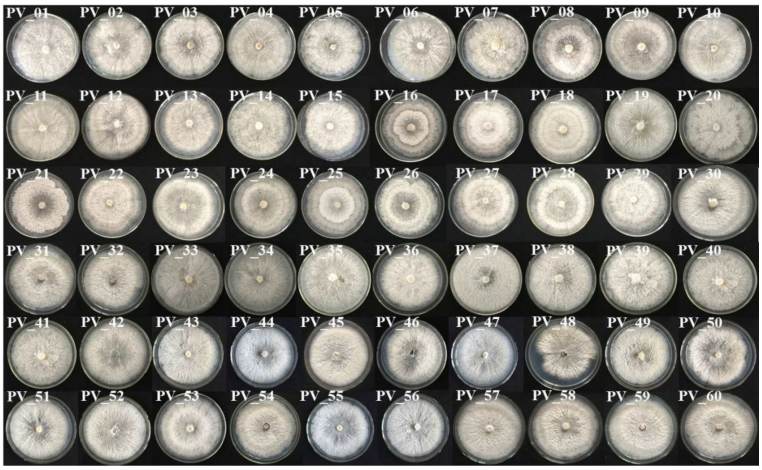

FIGURE 3
Colony morphology of *P. vexans* isolate strains on potato dextrose agar medium after 7 days of incubation at 25°C.

10.3389/fpls.2022.996862

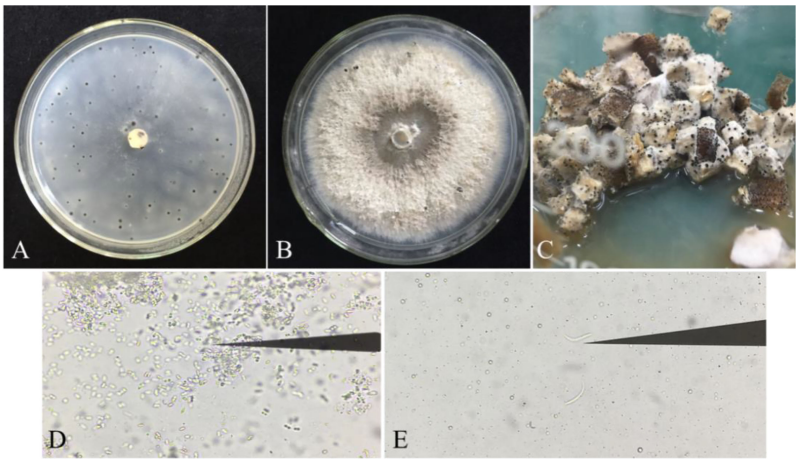

FIGURE 4
Pycnidia of *P. vexans* on different media. **(A)** Colony morphology of *P. vexans* Pycnidia on oatmeal agar medium after 30 days of incubation at 25°C. **(B)** Colony morphology of *P. vexans* Pycnidia on potato dextrose agar medium after 30 days of incubation at 25°C. **(C)** Colony morphology of *P. vexans* Pycnidia on *S. melongena* fruit medium after 5 days of incubation at 25°C. **(D)** α-type conidia under a compound microscope (400 X). **(E)** β-type conidia under a compound microscope (400 X).

to VIII), including the GDD motif, a typical characteristic of mycoviral RdRps (Figure 6B). We have named this novel mycovirus, the first reported in this fungal pathogen, *P. vexans* ourmia-like virus 1 (PvOLV1). The virus sequence has been deposited in GenBank under accession number MZ044287.

A phylogenetic tree was constructed based on the deduced aa sequence of the putative RdRp region encoded by PvOLV1 using the NJ method in MEGA (version 7.0). The results showed that PvOLV1 was clustered with ourmiavirus in the family Botourmiaviridae (Figure 7).

3.4.2 Analysis of the genomic structure of PvFV1

Sequence analysis of the full-length cDNA indicated that the PvFV1 genome (Figure 8A) was 6007 nt in length, excluding the poly(A) structure at the end of the 3' noncoding region, and had a C+G content of 42.86%. The 5' and 3 'noncoding regions were 93 nt and 27 nt long, respectively. Fusariviridae is a new, recently proposed + ssRNA family comprising members that typically have 6 to 8 kbp genomes, with one larger ORF encoding putative polyproteins of replicases and one to three smaller ORFs

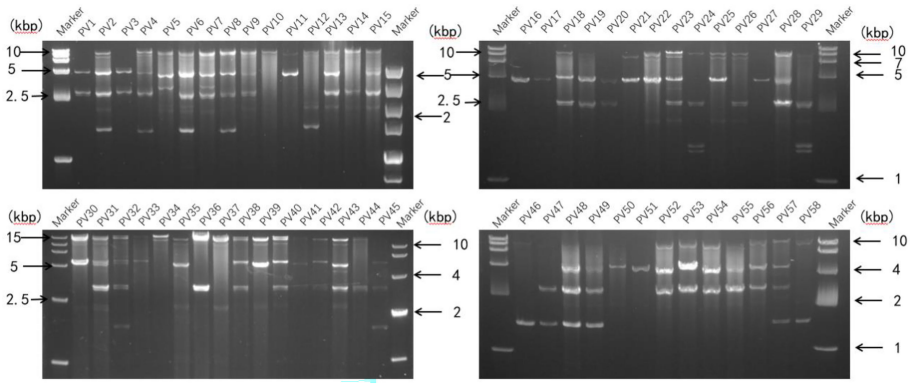

FIGURE 5
Agarose gel electrophoresis analysis of dsRNA extracted from *P. vexans*. Chromatography of cellulose extracts from the *P. vexans* strain showing dsRNA bands indicative of mycovirus infection.

10.3389/fpls.2022.996862

TABLE 1 Table of dsRNA bands in *P. vexans*.

Provinces of strain isolation	Number of strains	Toal number of dsRNA	The average number of dsRNA
Anhui	3	21	7
Sichuan	7	33	4.7
Hunan	27	118	4.37
Zhejiang	6	23	3.83
Fujian	7	25	3.57
Guangdong	5	6	1.2
Jiangxi	2	7	–
Hubei	1	4	–

encoding hypothetical proteins (Zhang et al., 2014). The genome of PvFV1 also contained two ORFs that did not overlap. ORF1 encoded RdRp, which was predicted to encode a protein of 1540 aa with a molecular weight of 174.75 kDa. ORF2 was predicted to encode a 402-aa protein with a molecular weight of 45.78 kDa. CD-Search in NCBI indicated that ORF1 contained a conserved RdRp and an RNA unwinding domain, and ORF2 contained a DUF3084 (e-value, 4.31e-04) domain with unknown function. BLASTp alignment of its ORF1 revealed the highest aa identity (E-value: 0; query cover: 94%; identity: 51.7%) with the RdRp of the Fusariviridae family, *Fusarium graminearum* dsRNA mycovirus-1 (FgV-ch). CD search showed that the ORFs contained eight conserved domains of the Fusariviridae family virus (Figure 8B). The virus sequence was deposited in GenBank under accession number MZ044286.

The phylogenetic tree of PvFV1 encoding RdRp aa was constructed using MEGA7 software, the NJ method and the Poisson model. The results showed that PvFV1 and Fusariviridae were clustered together (Figure 9).

3.4.3 Genomic structure analysis of PvEV2

The sequences showed similarity to members of the family Endornaviridae. Viruses in the Endornaviridae family have linear ssRNA genomes ranging in length from approximately 10 kb to more than 17 kb and containing an ORF encoding a single long polyprotein. The polyprotein encoded by

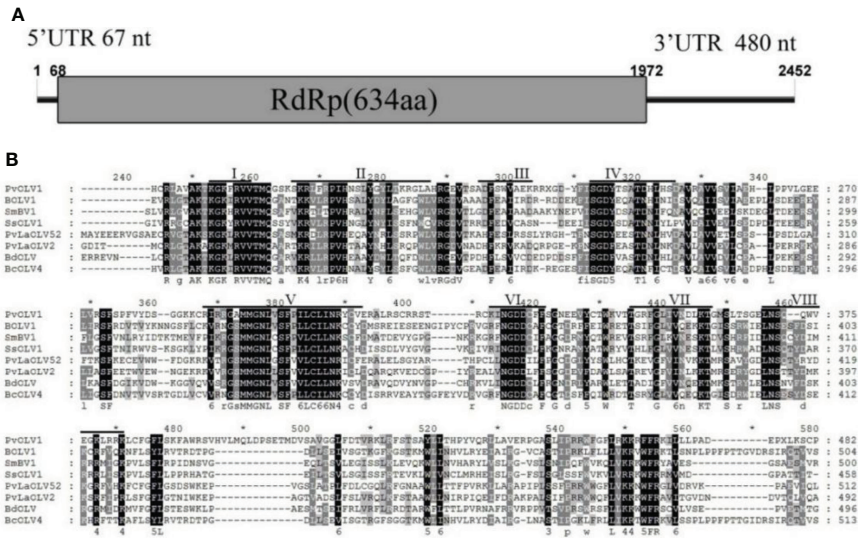

FIGURE 6
Diagrammatic representation of the genome organization and multiple alignment of PvOLV1. **(A)** Schematic representation of the PvOLV1 genome organization, containing a single open reading frame (ORF) encoding a putative RNA-dependent RNA polymerase (RdRp) and 5′ and 3′ untranslated regions (UTRs). **(B)** Multiple alignment of the aa sequences of RdRp domains of PvOLV1 and other similar Botourmiaviridae viruses using the ClustalX program and highlighted using the GeneDoc program. The conserved motifs in these RdRps are indicated by Roman numerals I to VIII. Virus names and accession numbers are as follows: BOLV1, Botrytis ourmia-like virus (QLF49182.1); SmBV1, *Sclerotinia minor* botoulivirus 1 (QHR78948.1); SsOLV1, *Sclerotinia sclerotiorum* ourmia-like virus 1 (ALD89138.1); PvLaOLV52, *Plasmopara viticola* lesion associated ourmia-like virus 52 (QGY72582.1); PvLaOLV2, *Plasmopara viticola* lesion associated ourmia-like virus 2 (QGY72532.1); BdOLV, *Botryosphaeria dothidea* ourmia-like virus (QED22728.1); BcOLV4, *Botrytis cinerea* ourmia-like virus 4 (QJT73670.1).

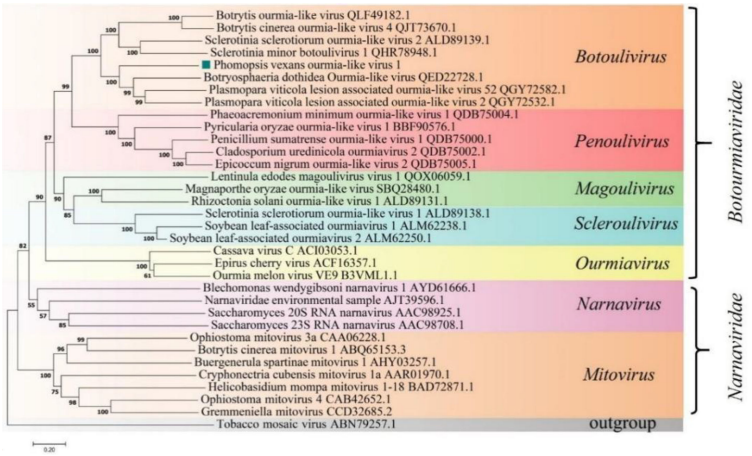

FIGURE 7
Phylogenetic analysis of PvOLV1. Phylogenetic analysis of PvOLV1 based on aa alignments of RdRp and other viruses related to these proteins. A phylogenetic tree was constructed by the neighbor-joining algorithm using MEGA7, with 1000 bootstrap replications. The percentage of bootstrap values supporting the branches in phylogenetic trees are indicated on the nodes. The genetic distance is represented by the scale bar of 0.2 aa substitutions per site. The novel virus PvOLV1 is indicated by a green square. The names and database accession numbers of other related viruses analyzed are indicated in the tree.

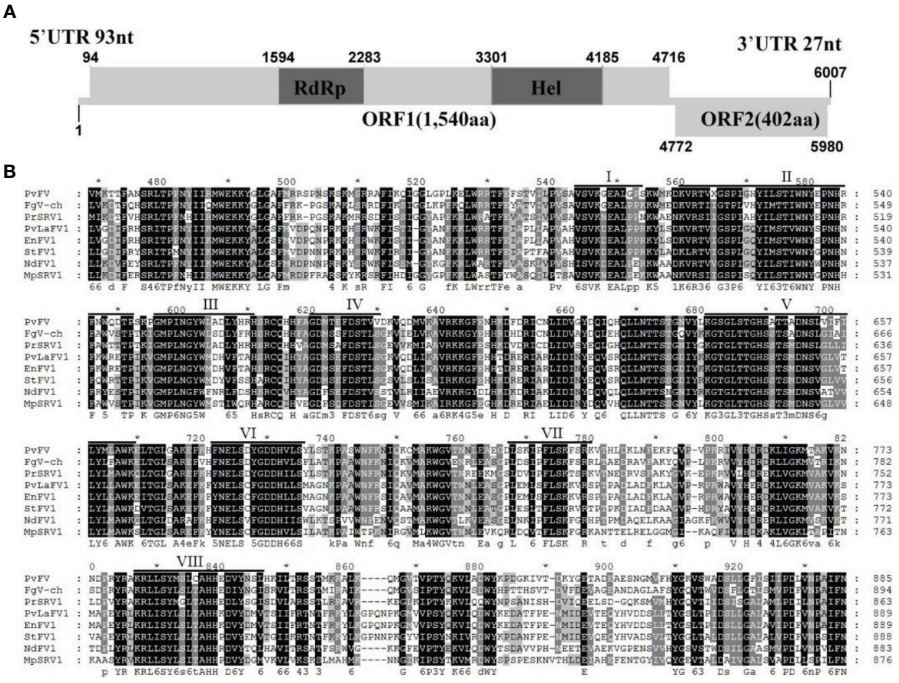

FIGURE 8
Diagrammatic representation of the genome organization and multiple alignment of PvFV1. **(A)** Schematic representation of the PvFV1 genome organization, which contained a single open reading frame (ORF) encoding a putative RNA-dependent RNA polymerase (RdRp) and 5′ and 3′ untranslated regions (UTRs). **(B)** Multiple alignment of the aa sequences of the RdRp domains of PvFV1 and other similar Fusariviruses using the ClustalX program and highlighted using the GeneDoc program. The conserved motifs in these RdRps are indicated by Roman numerals I to VIII. Virus names and accession numbers are as follows: FgV-ch, *Fusarium graminearum* dsRNA mycovirus-1 (AAT07067.2); PrSRV1, *Penicillium roqueforti* ssRNA mycovirus 1 (AII99895.1); PvLaFV1, *Plasmopara viticola* lesion associated fusarivirus 1 (QHD64725.1); EnFV1, *Erysiphe necator*-associated fusarivirus 1 (QHD64833.1); StFV1, *Setosphaeria turcica* fusarivirus 1 (QRI93681.1); NdFV1, *Neurospora discreta* fusarivirus 1 (BCL64192.1); MpSRV1, *Macrophomina phaseolina* single-stranded RNA virus 1 (ALD89094.1).

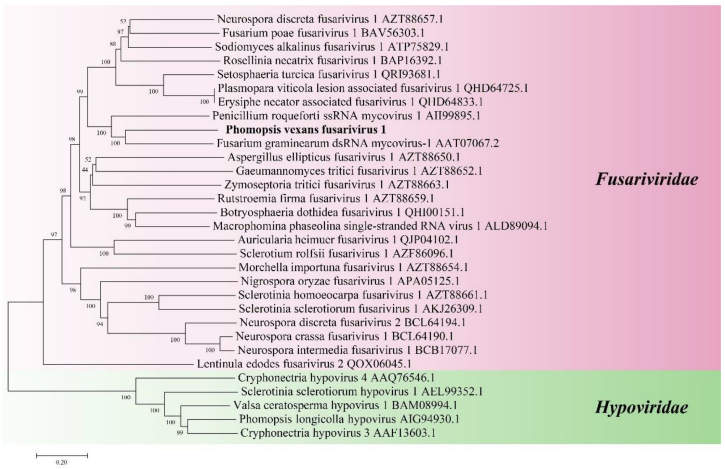

FIGURE 9
Phylogenetic analysis of PvFV1. Phylogenetic analysis illustrating the evolutionary classification of PvFV1 was conducted using the method described in Figure 7. The scale bar represents a genetic distance of 0.2 aa substitutions per site. The black bold font indicates the novel mycoviruses PvFV1 identified in the present study. The names and database accession numbers of other related viruses analyzed are indicated in the tree.

endornaviruses often includes conserved domains, such as viral RNA helicases and RdRps (Ghabrial et al., 2015). We designated the virus *P. vexans* endornavirus 2 (PvEV2). The full-length PvEV2 genome was 11015 nt, excluding the poly(C) structure at the end of the 3' noncoding region, which contained a single ORF encoding a 3597-aa polyprotein with a molecular weight of 397.10 kDa (Figure 10). The BLASTP alignment information of the four conserved domains of PvEV2 with other Endornaviruses are shown in Table 2. Domain searches revealed that this polyprotein contained the conserved domains of viral methyltransferase (Met), putative DEXDc, viral helicase (Hel) and RdRp. Consistent with the homology search, phylogenetic analysis based on the conserved RdRp domain suggested that PvEV2 was a new putative species in the family Endornaviridae. The virus sequence was deposited in GenBank under accession number MZ044288.

A phylogenetic tree was constructed using the neighbor-joining algorithm in MEGA7, with 1000 bootstrap replications (Figure 11). PvEV2 and Betaendornavirus in the family Endornaviridae were clustered together. There was a poly(C) structure at the end of the 3' noncoding region of PvEV2 and a methyltransferase domain rather than a glycosyltransferase domain. It was inferred that PvEV2 was a betaendornavirus.

3.4.4 Structural analysis of the PvPV1 genome

Sequence analysis of *P. vexans* partitivirus 1 (PvPV1) revealed two independent segments (dsRNA1 and dsRNA2), each with a single open reading frame (ORF) (Figure 12A). The

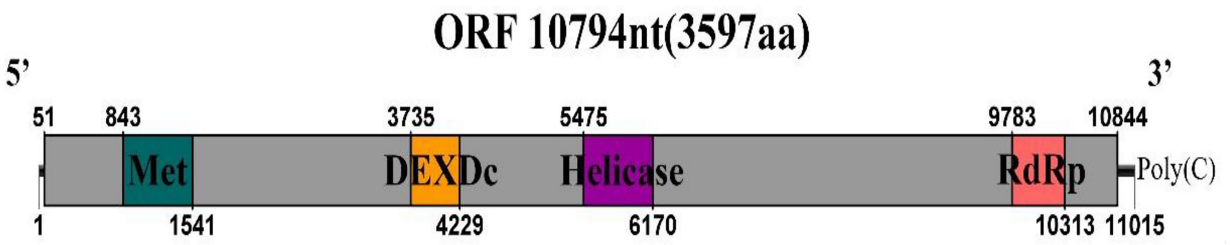

FIGURE 10
Diagrammatic representations of the predicted genomic organization of PvEV2. Comparisons of the genomic organizations of the novel *P. vexans* infecting PvEV2 and the identified member PvEV2 of the Endornaviridae family. PvEV2 was completely sequenced and predicted to harbor a single larger ORF containing domains of viral methyltransferase (MTR), putative DEXDc, viral helicase (Hel) and RdRp, which are indicated in the ORF box.

10.3389/fpls.2022.996862

TABLE 2 Percent aa sequence identity of the 2 conserved domains of *P. vexans* endornavirus compared with those of other endornaviruses.

Protein	Organism name	Accession number	Identify	e-value
RdRp	*Botrytis cinerea* betaendornavirus 1	YP_009315910.1	73.86%	4E-86
	Sclerotinia sclerotiorum endornavirus 2-A	AWY10955.1	74.43%	2E-85
	Gremmeniella abietina type B RNA virus XL1	YP_529670.1	75.57%	6e-85
	Gremmeniella abietina type B RNA virus XL2	ABD73306.1	75%	7E-85
	Sclerotinia sclerotiorum endornavirus 2	AND83000.1	73.86%	2e-84
Hel	*Gremmeniella abietina* type B RNA virus XL1	YP_529670.1	36.36%	1E-37
	Gremmeniella abietina type B RNA virus XL2	ABD73306.1	35.93%	2E-37
	Sclerotinia sclerotiorum endornavirus 2	AND83000.1	33.91%	4E-35
	Sclerotinia sclerotiorum endornavirus 1	AJF94392.1	33.48%	1E-34
	Sclerotinia sclerotiorum betaendornavirus 1	YP_009022070.1	33.91%	3E-34
Met	*Sclerotinia sclerotiorum* endornavirus 2	AND83000.1	54.31%	1E-78
	Sclerotinia sclerotiorum betaendornavirus 1	YP_009022070.1	53.45%	2E-77
	Botrytis cinerea betaendornavirus 1	YP_009315910.1	53.88%	2E-76
	Sclerotinia sclerotiorum endornavirus 1	AJF94392.1	53.02%	3E-76
	Gremmeniella abietina type B RNA virus XL2	ABD73306.1	49.79%	7E-76
DEXDc	*Gremmeniella abietina* type B RNA virus XL2	ABD73306.1	44.79%	4E-32
	Gremmeniella abietina type B RNA virus XL1	YP_529670.1	44.79%	4E-32
	Sclerotinia sclerotiorum endornavirus 1	AJF94392.1	40.65%	4E-32
	Sclerotinia sclerotiorum endornavirus 1	YP_008169851.1	41.29%	5E-32
	Sclerotinia sclerotiorum endornavirus 1	YP_009022070.1	38.71%	1E-29
	Sclerotinia sclerotiorum endornavirus 2	AND83000.1	38.06%	1E-28

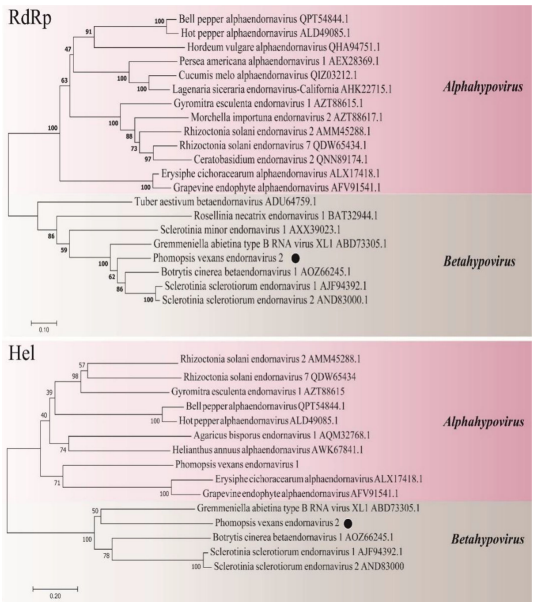

FIGURE 11
Phylogenetic analysis of PvEV2. Phylogenetic analysis illustrating the evolutionary classification of PvEV2 was conducted using the method described in Figure 7. The genetic distance is represented by the scale bar of 0.2 aa substitutions per site. The novel virus PvEV2 is indicated by black dots. The names and database accession numbers of other related viruses analyzed are indicated in the tree.

10.3389/fpls.2022.996862

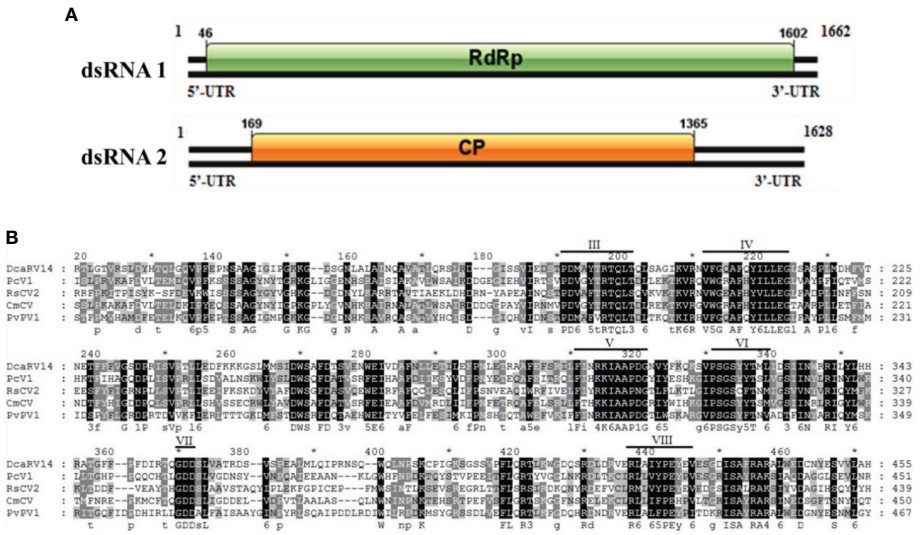

FIGURE 12
Diagrammatic representation of the genome organization of PvPV1. **(A)** Diagram showing the structure of PvPV1. The open reading frame (ORF) and the 5' and 3' untranslated regions (UTRs) are indicated by the colored long rectangular box and solid black lines, respectively. The initiation and termination codons of the ORF are indicated by the numbers under the solid lines. **(B)** Multiple alignment of the aa sequences of RdRp domains of PvPV1 and other similar deltapartitiviruses using the ClustalX program and highlighted using the GeneDoc program. The conserved motifs in these RdRps are indicated by Roman numerals III to VIII. Virus names and accession numbers are as follows: DcaRV14, diatom colony-associated dsRNA virus 14 (AP014906); PcV1, pepper cryptic virus 1 (AVV48358); RsCV2, *Raphanus sativus* cryptic virus 2 (ABB04855); CmCV, *Cucumis melo* cryptic virus (QBC66121).

full-length dsRNA1 was 1662 nt, containing an ORF encoding a 518-aa protein of RDRP with a molecular weight of 59.8 kDa. The 5' and 3' untranslated regions (UTRs) of dsRNA1 were 45 nt and 60 nt, respectively. BLASTp alignment of the ORF encoded by dsRNA1 indicated that the ORF encoded by dsRNA1 was most similar to RdRp in the family Partitiviridae, including diatom colony-associated dsRNA virus 14 (DcaRV14; identity, 48.23%; query cover, 92%; E-value, 4e-148), pepper cryptic virus 1 (PcV1; identity, 36.92%; query cover, 86%; E-value, 6e-93), *Raphanus sativus* cryptic virus 2 (RsCV2; identity, 37.50%; query cover, 86%; E-value, 1e-89), and *Cucumis melo* cryptic virus (CmCV; identity, 36.12%; query cover, 84%; E-value, 37 1e-88). The results of a conservative structure database (CDD) search and multiple alignment (Figure 12B) revealed 6 (III to VIII) conserved domains. The sequence of dsRNA1 was deposited in GenBank under accession number MT711194.

The full-length dsRNA2 was 1628 nts and had a C+G content of 42.86%, and the base numbers of the 5' and 3'-UTRs were 168 nt and 263 nt, respectively. In addition, it contained an ORF (169 nt-1366 nt) encoding a hypothetical protein with a molecular weight of 44.5 kDa. BLASTp alignment of the ORF encoded by dsRNA2 indicated that the ORF of PvPV1 was most closely related to DcaRV14 (identity, 24.10%; query cover, 92%; E-value, 2e-10) in Deltapartitivirus. The sequence of dsRNA2 was deposited in GenBank under accession number MT711195.

A phylogenetic tree based on PvPV1 encoding RdRp was constructed by the neighbor-joining algorithm using MEGA7, with 1000 bootstrap replications (Figure 13). The blue square represents the identified virus in the fungus, and the green triangle represents the identified virus in the plant. Phylogenetic analysis showed that PvPV1 and deltapartitivirus in the family Partitiviridae were clustered together. In addition, it has been reported that the hosts of deltapartitivirus and cryspovirus viruses are plants and protozoa (Nibert et al., 2009; Vainio et al., 2018). This is the first report to describe deltapartitivirus virus in fungi.

3.4.5 Structural analysis of the PvVV L1 genome

Sequence analysis of *P. vexans* partitivirus 1 (PvVVL1) revealed two independent segments (dsRNA1 and dsRNA2), each with a single open reading frame (ORF) (Figure 14). The full-length dsRNA1 was 2996 nts, and the GC content was 56.4%, containing an ORF encoding an 855-aa protein of RDRP with a molecular weight of 95.2 kDa. The 5' and 3' untranslated regions (UTRs) of dsRNA1 were 209 nt and 219 nt, respectively. BLASTp alignment indicated that the ORF encoded by dsRNA1 was most similar to RdRp of victorivirus in the family Totiviridae, including lebolus microspores totivirus 1 (TmTV1; identity, 45.42%; query cover, 76%; E-value, 0.0, *Umbelopsis ramanniana* virus 2 (UmRV2; identity, 41.72%;

10.3389/fpls.2022.996862

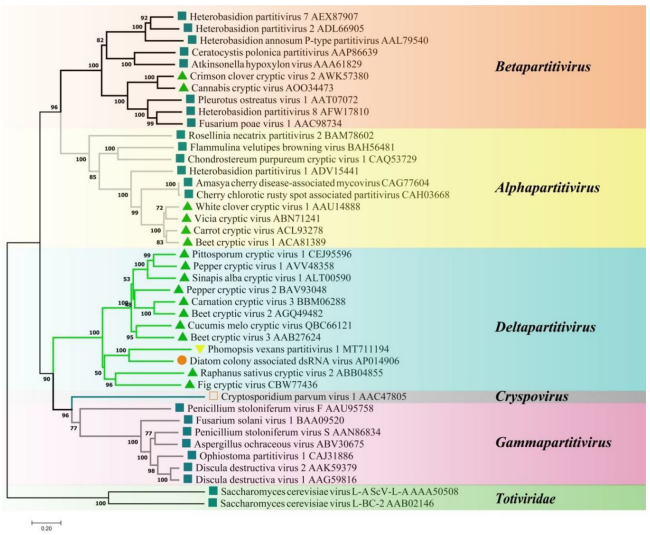

FIGURE 13
Phylogenetic analysis of PvPV1. Phylogenetic analysis illustrating the evolutionary classification of PvPV1 was conducted using the method described in Figure 7. The scale bar represents a genetic distance of 0.2 aa substitutions per site. Yellow triangles indicate the novel mycoviruses PvPV1 identified in the present study. The symbols indicate the viruses isolated from the same group of hosts, such as plants (green triangle), fungi (blue square), and protozoa (orange square). The names and database accession numbers of other related viruses analyzed are indicated in the tree.

query cover, 76%; E-value, 0.0, *Tolypocladium ophioglossoides* totivirus 1 (ToTV1; identity, 41.68%; query cover, 76%; E-value, 0.0, *Ustilaginoidea virens* RNA virus 5(UvRV5; identity, 41.03%; query cover, 76%; E-value, 7e-175, *Sclerotinia nivalis* victorivirus 1 (SnVV1; identity, 37.95%; query cover, 76%; E-value, 6e-158, *Penicillium aurantiogriseum* totivirus 1 (PaTV1; identity, 38.28%; query cover, 76%; e-value, 5e-157. The conservative structure database (CDD) was searched, and multiple aa comparisons were carried out. The results showed that there were 8 (I to VIII) conserved domains of the monotypic Viridae family (Figure 15).

The full-length dsRNA1 was 2901 nts, and the GC content was 59.6%, containing an ORF encoding a 689 aa protein of coat protein (CP) with a molecular weight of 73.5 kDa. The 5' and 3' untranslated regions (UTRs) of dsRNA1 were 540 nt and 291 nt, respectively. BLASTp alignment indicated that the ORF encoded by dsRNA2 was most similar to CP in the family Totiviridae, including *Thelebolus microsporus* totivirus 1(TmTV1, *Tolypocladium ophioglossoides* totivirus 1(ToTV1, *Fusarium asiaticum* victorivirus 1 (FaVV1, *Sclerotinia nivalis* victorivirus 1(SnVV1, *Sphaeropsis sapinea* RNA virus 1(SsRV1.

A phylogenetic tree based on PvVVL1 encoding RdRp and CP aa was constructed by the neighbor-joining algorithm using MEGA7, with 1000 bootstrap replications (Figures 16, 17). The results showed that PvVVL1 and victorivirus of the family Totiviridae were clustered into the same group. Combined

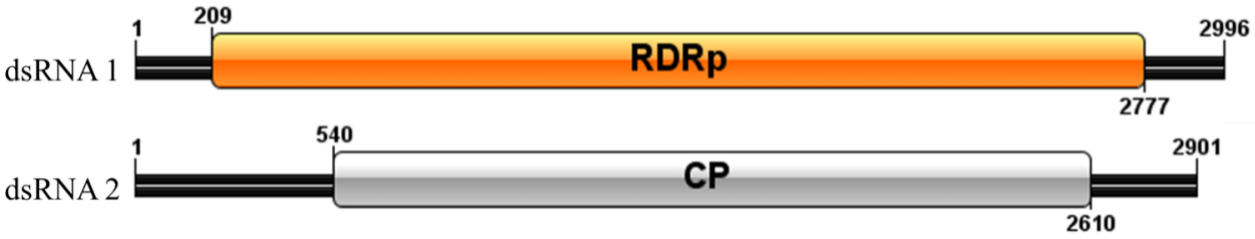

FIGURE 14
Diagrammatic representation of the genome organization of PvVV L1.

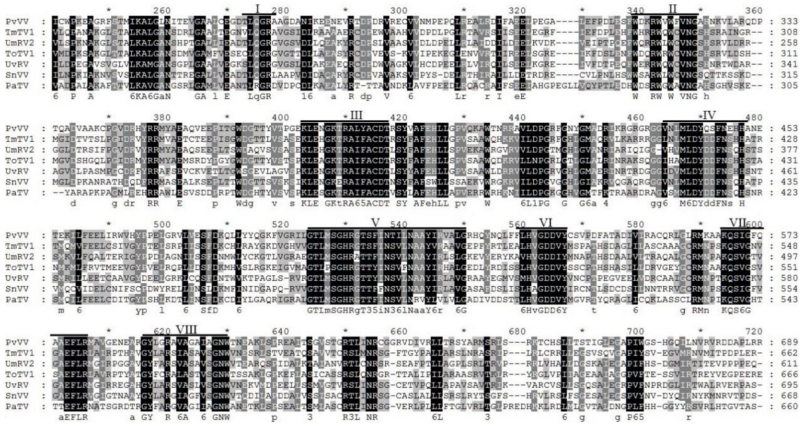

FIGURE 15
Multiple sequence alignment of the aa sequences of the RdRp domains of PvVVL1 and other similar victoriviruses using the ClustalX program and highlighted using the GeneDoc program. The conserved motifs in these RdRps are indicated by Roman numerals I to VIII.

with the results of multiple aa alignment of RdRp, PvVVL1 was found to belong to the victoriviruses based on sequence similarity and phylogenetic analysis.

4 Discussion

The presence of mycoviruses was detected in all 58 P. *vexans* isolates studied, indicating abundant mycovirus resources. This study provides a potential basis for the biological control of *P. vexans* and increases understanding of the diversity of mycoviruses in *P. vexans*. In this study, we characterized five novel mycoviruses (PvFV1, PvOLV1, PvEV2, PvPV1 and PvVVL1) from *P. vexans* strains and identified diverse mycoviruses using high-throughput transcriptome sequencing. The mycoviruses discovered in our analysis were nearly full length. These detected mycoviruses might belong to the families Botourmiaviridae, Fusariviridae, Endornaviridae, Partitiviridae

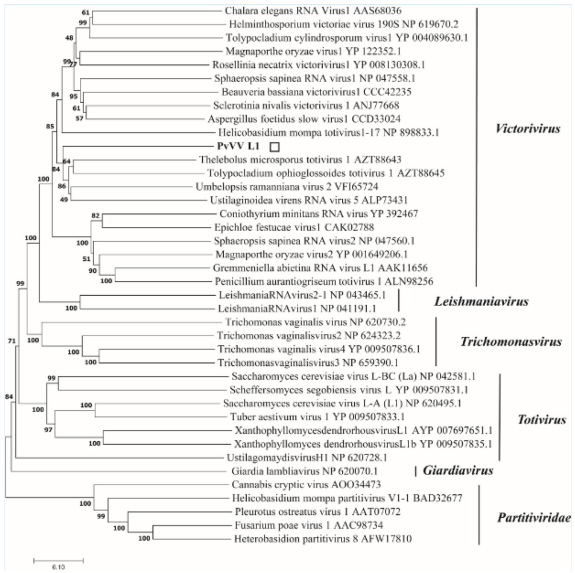

FIGURE 16
Phylogenetic analysis of PvVVL1. Phylogenetic analysis illustrating the evolutionary classification of PvVVL1 was conducted using the method described in Figure 7. The scale bar represents a genetic distance of 0.1 aa substitutions per site. The white square indicates the novel mycovirus PvVVL1 in the present study. The names and database accession numbers of other related viruses analyzed are indicated in the tree.

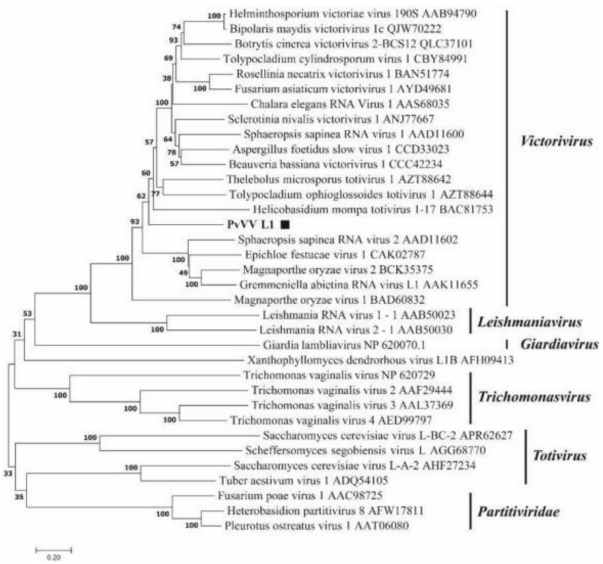

FIGURE 17
Phylogenetic analysis of PvVVL1. The phylogenetic tree was constructed based on the viral CP aa sequences using the neighbor-joining (NJ) method in MEGA 7 and the Poisson model. The scale bar represents a genetic distance of 0.2 aa substitutions per site. Black squares indicate the novel mycoviruses PvVVL1 identified in the present study.

and Totiviridae. We conducted RT–PCR, genomic PCR and Sanger sequencing analyses using specific primers based on the obtained fragments to confirm the origins of our viral sequences. Positive amplicons were produced from only RNAs extracted from the *P. vexans* strain by RT–PCR but not by genomic PCR, confirming that the viral sequences represented nonintegrated RNA virus sequences. To the best of our knowledge, this is the first report of a comprehensive analysis of viral diversity in *P. vexans* strains. Thus, our results represent a step forward in exploring *P. vexans* mycoviruses and provide insight into screening the potential of *P. vexans* controls and understanding the mechanism of *P. vexans* and mycoviruses coexisting with each other. To our knowledge, mycoviruses reported in *P. vexans* include only Phomopsis vexans RNA virus 1 (PvRV1) (Zhang et al., 2015) and Phomopsis vexans partitivirus 1 (PvPV1) (Zhang et al.). There have been no reports of hypovirulence caused by mycoviruses in the pathogenic fungus *P. vexans*. As long as different fungal taxa and strains are screened for the purpose of discovering novel mycoviruses, our insight into the diversity of mycoviruses will by all means largely increase. In this context, this study provides a rich resource of mycoviruses, which may contain a large number of mycoviruses with biocontrol potential. In follow-up research, we will try to obtain virus-free strains using other methods, such as protoplast regeneration technology, to determine the impact of the four Botourmiaviruses investigated herein on host pathogenicity and the interactions among them.

In addition, as an increasing number of atypical mycoviruses were discovered, they provided a reference for the evolution of mycoviruses. There are two hypotheses regarding the origin of mycoviruses (Pearson et al., 2010): the first is that mycoviruses evolve with host fungi; the second is that mycoviruses may be isolated from the natural host plants of pathogenic fungi. Regarding PvPV1, the available information is limited, and it shows the highest homology to diatom colony-associated dsRNA virus14 deriving from marine organisms. PvPV1 is the first deltapartitivirus reported in fungi. Although PvPV1-specific primers were used to detect the virus in eggplant leaves collected in other fields, it is unfortunate that PvPV1 infection of eggplant plants was not detected. It is worth noting that the Partitiviridae genome consists of two separate dsRNA segments, which encode CP and RdRp, and the virion protein has a molecular weight of 37-77 kDa. The genome of Totiviridae is usually a single linear molecule with a size of 4.6-7.0 kbp encompassing two open reading frames. The 5'-terminal ORF encodes the virus capsid protein, the 3'-terminal ORF encodes a dependent RNA polymerase, and the virion protein has a molecular weight of 70-100 kDa. Expression of the downstream open reading frame is the basis of the Totiviridae classification, and the Totiviridae family has a specific translation mechanism. Victorivirus has a ribosomal insertion site (IRES) in the 5' noncoding region for CP translation, while the downstream RdRp translates two independent viral proteins through a cis-trans translation mechanism that enables a stop or restart

mediated by "AUGA" or "UAAUG". Totiviridae forms a fusion protein, and viral translation is mediated by the frameshift structure of "- 1 frameshift". Although atypical victorivirus genomic structures have been reported previously, such as a 98-nt interval between two ORFs in PvRV1 (Zhang et al., 2015) and a 2-nt interval between two ORFs of Magnaporthe oryzae virus 1 in Magnaporthe grisea (Yokoi et al., 2007). It is obvious that there are great differences in the viral genome structure and translation mechanisms between Totiviridae and Partitiviridae. At present, viruses are mainly classified according to their RdRp aa sequences. Through the phylogenetic analysis of PvVVL1, it was found that it was clustered with victoriviruses in the family Totiviridae. Multiple aa alignment analysis showed that the closely related viruses (TmTV1, UmRV2, ToTV1, UvRV5, SnVV1, PaTV1) had eight conserved motifs from the family Totiviridae. The structure of the PvVVL1 genome is composed of two separate dsRNA segments, which is similar to Partitiviridae, indicating a certain evolutionary relationship between the two families of viruses. Ghabrial believes that partitiviruses and totiviruses may share a common ancestor (Ghabrial, 1998). The RdRp of NrVL1 found in N. radicicola has high homology with Partitviridae (Ahn and Lee, 2001), but the genomic structure of the virus is a nondouble segment, and the genome size (6 kbp) is larger than that of Partitviridae, which seems to confirm the view of Ghabrial. At first, the virus may have only RdRp to complete replication in the host, transmission of the virus depends on the transfer of mRNA, and the transmission efficiency of the virus is not high. The virus gradually sequesters the host protein, which is used to encompass and spread RdRp in the form of a virion, forming a multisegmental virus. In recent years, viruses with atypical genomic structures have been reported in fungi. For example, Chiba reported that Narnavirus virus Aspergillus lentulus narnavirus 1 (AleNV1) with a two-segment genome was identified for the first time from Aspergillus (A. fumigatus) using segmented and primer-ligated double stranded RNA sequencing (FLDS) techniques (Chiba et al., 2021). The RdRp of RNA viruses usually encodes an open reading frame, and some viruses of Narnaviridae are often found to lack catalytic domains C and D of RdRp. Chiba found multisegmental Narnavirus viruses, Aspergillus fumigatus narnavirus 2 (AfuNV2) and Magnaporthe oryzae narnavirus 1 (MoNV1), in two different host fungi, Aspergillus and Pyricularia. The missing domains C and D were located at the N-terminus of another RNA segment of the virus. Using SWISS-MODEL software to model the homology of two ORFs, it was found that a functional enzyme could be formed between the two segments, which indicated that the two RNA segments might come from the common segment. In addition, Lin (Lin et al., 2020) and Suvi (Suvi et al., 2020) also described multisegment mycoviruses with mitotic RdRp sequences, indicating that viruses with atypical genomic structures are widely distributed in different host fungi and different countries. The study of multisegment viruses will provide materials for the evolutionary origin of the viruses.

Zhang showed that a dsRNA fragment with a size of approximately 3 kbp and PvRV1 always existed simultaneously and maintained high genetic stability in virus elimination and culture, suggesting that the two dsRNA chains might be related or interact with each other (Zhang et al., 2015). This phenomenon was also observed in 58 tested strains, which confirmed that this phenomenon was not accidental, and it was found in most *P. vexans* strains. Although the electrophoresis results showed that dsRNA of 3 kbp in size and dsRNA of 5 kbp in size did not appear simultaneously, no single dsRNA of 3 kbp in size was observed. According to the electrophoresis results, two dsRNA segments were observed in some strains at the same position, while only one electrophoresis band was observed in some strains, which might be related to the virus type or electrophoresis environment. Therefore, it is speculated that the dsRNA segment at the 3 kbp position might be the defective RNA or satellite RNA segment of a virus. In the long-term experimental process, it was found that the mycoviruses in *P. vexans* could be stably transmitted to progeny through hyphae and spores with high genetic stability. No virus-free wild-type strains were found in the available studies on mycoviruses that infect *P. vexans*, although only 58 strains were isolated and screened, and the probability of carrying the mycoviruses was 100%. These results indicated that the mycoviruses were closely related to the species evolution of *M. aubergine*, and virus transmission occurred frequently among different strains. It was found that eggplant Browning streak was highly genetic conserved (Bhardwaj et al., 2014) and underwent long-distance transmission *via* seeds. Mycoviruses can be transmitted horizontally in homologous strains by mycelial fusion. Some specific mycoviruses can reduce heterologous incompatibility responses and facilitate virus transmission (Wu et al., 2017). There are microbes in nature that can facilitate viral transfer, and CMV has confirmed the existence of transboundary transmission (Andika et al., 2017). Therefore, it is speculated that the mycoviruses carried by the laboratory isolates of *P. vexans* may have a common ancestor. By infecting local *P. vexans*, the virus can be transmitted over a long distance along with the seed circulation of *P. vexans*. After the onset of disease, the virus is transferred to the local population through intermycelial fusion. However, not all viruses can be transmitted by horizontal transfer. Different hosts may have different antiviral mechanisms, and there is also antagonism between viruses. Viruses carried by the host itself will reject the invasion of alien viruses, so viruses need to evolve to complete invasion. Concurrently, there are also types of mutualism between different viruses. Zhang (Zhang et al., 2016) found that through infectious cloning and viral particle transfection, a virus-free ssRNA virus, Yado-Karivirus1 (YkV1), changes its replication pattern by hijacking the viral capsid protein Yado-Nushivirus1 (YnV1). In addition, YkV1 enhances the accumulation of YnV1 in the host. This virus changes its replication mode to suit its own survival to achieve long-term development. The transmissibility of different viruses and the possible different interactions between

them also partly explain the diversity of viral RNA bands in different strains of *P. vexans*.

Data availability statement

The datasets presented in this study can be found in online repositories. The names of the repository/repositories and accession number(s) can be found in the article/Supplementary Material.

Author contributions

HZ, FL,QZ and JZ conceived and designed the experiments. CZ, FX and XZ performed the experiments.FL,HZ and RZ performed the literature search and analyzed the data. FX drafted and revised the manuscript. XZ and CZ contributed equally to writing the manuscript. All authors contributed to the article and approved the submitted version.

Funding

This work was supported by the China Agriculture Research System of MOF and MARA (CARS-24-A-15), Hunan Provincial Natural Science Foundation of China (2021JJ30 356), Hunan Provincial Science and Technology Innovation Platform Construction Fund (20K071) and Innovation and Entrepreneurship Training Program for College Students (XCX2021049).

Conflict of interest

The authors declare that the research was conducted in the absence of any commercial or financial relationships that could be construed as a potential conflict of interest.

Publisher's note

All claims expressed in this article are solely those of the authors and do not necessarily represent those of their affiliated organizations, or those of the publisher, the editors and the reviewers. Any product that may be evaluated in this article, or claim that may be made by its manufacturer, is not guaranteed or endorsed by the publisher.

Supplementary material

The Supplementary Material for this article can be found online at: https://www.frontiersin.org/articles/10.3389/fpls.2022.996862/full#supplementary-material

References

Ahn, I. P., and Lee, Y. H. (2001). A viral double-stranded RNA up regulates the fungal virulence of nectria radicicola. *Mol. Plant Microbe Interact.* 14 (4), 496–507. doi: 10.1094/MPMI.2001.14.4.496

Akhtar, J., and Chaube, H. S. (2006). Variability in phomopsis blight pathogen [*Phomopsis vexans* (Sacc. & syd.) harter] . *Indian Phytopathol.* 59 (4), 439–444.

Andika, I. B., Shuang, W., Cao, C., Salaipeth, L., Kondo, H., and Sun, L.. (2017). Phytopathogenic fungus hosts a plant virus: A naturally occurring cross-kingdom viral infection. *Proc. Natl. Acad. Sci.* 114 (46), 12267–12272. doi: 10.1073/pnas.1714916114

Arjona-López, J. M., and López-Herrera, C. J. (2021). Entoleuca sp. infected by mycoviruses as potential biocontrol agents of avocado white root rot. *Eur. J. Plant Pathol.* 159 (2), 409–420. doi: 10.1007/s10658-020-02171-x

Arjona-Lopez, J. M., Telengech, P., Jamal, A., Hisano, S., Kondo, H., Yelin, M. D., et al. (2018). Novel, diverse RNA viruses from Mediterranean isolates of the phytopathogenic fungus, rosellinia necatrix: insights into evolutionary biology of fungal viruses. *Environ. Microbiol.* 20 (4), 1464–1483. doi: 10.1111/1462-2920.14065

Azhar, A., Mu, F., Huang, H., Cheng, J., Fu, Y., Hamid, M. R., et al. (2019). A novel RNA virus related to sobemoviruses confers hypovirulence on the phytopathogenic fungus *Sclerotinia sclerotiorum*. *Viruses* 11 (8), 759. doi: 10.3390/v11080759

Beura, S. K., Mahanta, I. C., and Mohapatra, K. B.. (2008). Economics and chemical control of phomopsis twig blight and fruit rot of brinjal. *J. Mycopathological Res.* 46 (1), 73–76.

Bhardwaj, N. K., Singh, V., Tiwari, S. K., and Singh, M.. (2014). Phenotyping of recombinant inbred lines for phomopsis blight in Brinjal. *Vegetable Sci.* 41 (2), 195–197.

Chiba, Y., Oiki, S., Yaguchi, T., Urayama, S. I., and Hagiwara, D.. (2021). Discovery of divided RdRp sequences and a hitherto unknown genomic complexity in mycoviruses. *Virus Evol.* 7 (1), veaa101. doi: 10.1093/ve/veab027

Das, B. H. (1998). *Studies on phomopsis fruit rot of brinjal[D]* (Bangladesh Agriculture University).

Ghabrial, S. A. (1998). Origin, adaptation and evolutionary pathways of mycoviruses. *Virus Genes* 16 (1), 119–131. doi: 10.1023/A:1007966229595

Ghabrial, S. A., Castón, J. R., Jiang, D., Nibert, M. L., and Suzuki, N.. (2015). 50-plus years of fungal viruses. *Virology* 479, 356–368. doi: 10.1016/j.virol.2015.02.034

Hao, F., Ding, T., Wu, M., Zhang, J., Yang, L., Chen, W., et al. (2018). Two novel hypovirulence-associated mycoviruses in the phytopathogenic fungus *Botrytis cinerea*: Molecular characterization and suppression of infection cushion formation. *Viruses* 10 (5), 254. doi: 10.3390/v10050254

Hillman, B. I., Annisa, A., and Suzuki, N. (2018). Viruses of plant-interacting fungi. *Adv. Virus Res.* 100, 99–116. doi: 10.1016/bs.aivir.2017.10.003

Hollings, M. (1962). Viruses associated with a die-back disease of cultivated mushroom. *Nature* 196, 962. doi: 10.1038/196962a0

Hulke, B. S., Markell, S. G., Kane, N. C., and Mathew, F. M.. (2019). Phomopsis stem canker of sunflower in north America: Correlation with climate and solutions through breeding and management 26 (13), 19–26. doi: 10.1051/ocl/2019011

Jackson, E. W., Feng, C. A., Fenn, P., and Chen, P.. (2009). Genetic mapping of resistance to phomopsis seed decay in the soybean breeding line MO/PSD-0259 (PI562694) and plant introduction 80837. *J. Heredity* 100 (6), 777–783. doi: 10.1093/jhered/esp042

Jayaramaiah, K. M., Mahadevakumar, S., Raj, A. C., and Janardhana, G. R.. (2013). PCR based detection of *Phomopsis vexans* (Sacc. & syd.) - the causative agent of leaf blight and fruit rot disease of brinjal (Solanum melongena l.) . *Int. J. Life Sci.* 7 (1), 17–20.

Jiang, D., Fu, Y., Guoqing, L., and Ghabrial, S. A.. (2013). Viruses of the plant pathogenic fungus *Sclerotinia sclerotiorum*. *Adv. Virus Res.* 86, 215–248. doi: 10.1016/B978-0-12-394315-6.00008-8

Khan, N. U. (1999). *Studies on epidemiology, seed borne nature and management of phomopsis fruit rot of brinjal[D]* (Bangladesh Agricultural University).

King, A. M., Lefkowitz, E., Adams, M. J., and Carstens, E. B.. (Eds) (2012). *Virus taxonomy: Ninth report of the international committee on taxonomy of Viruses (Vol. 9)* (Elsevier).

Kotta-Loizo, I., and Coutts, R. H. A. (2017). Studies on the virome of the entomopathogenic fungus *Beauveria bassiana* reveal novel dsRNA elements and mild Hypervirulence. *PLoS Pathog.* 13 (1), e1006183. doi: 10.1371/journal.ppat.1006183

Kumar, S., Prasanna, P., and Wankhade, S. (2011). Potential benefits of bt brinjal in India € an economic Assessment. *Agric. Economics Res. Rev.* 24 (1), 83–90.

Lau, S. K., Lo, G. C., Chow, F. W., Fan, R. Y., Cai, J. J., Yuen, K. Y., et al. (2018). Novel partitivirus enhances virulence of and causes aberrant gene expression in talaromyces marneffei. . *MBio* 9 (3), e00947–e00918.

Li, H., Bian, R., Liu, Q., Yang, L., Pang, T., Salaipeth, L., et al. (2019). Identification of a novel hypovirulence-inducing hypovirus from alternaria alternata. *Front. Microbiol.* 10, 1076. doi: 10.3389/fmicb.2019.01076

Lin, Y., Zhou, J., Zhou, X., Shuai, S., Zhou, R., An, H., et al. (2020). A novel narnavirus from the plant-pathogenic fungus magnaporthe oryzae. *Arch. Virol.* 165 (5), 1235–1240. doi: 10.1007/s00705-020-04586-7

Luo, H., Hu, W. C., and Wang, G. P.. (2019). Detection and analysis of the double-stranded rnas diversity from botryosphaeria dothidea strains in hubei province. *Acta Phytopathologica Sinica* 49 (1), 113–123. doi: 10.13926/j.cnki.apps.000366

Marquez, L. M., Redman, R. S., Rodriguez, R. J., et al. (2007). A virus in a fungus in a plant: Three-way symbiosis required for thermal Tolerance. *Science* 315 (5811), 513–515.

Marzano, S. Y. L., and Domier, L. L. (2016). Novel mycoviruses discovered from metatranscriptomics survey of soybean phyllosphere phytobiomes. *Virus Res.* 213, 332–342. doi: 10.1016/j.virusres.2015.11.002

Marzano, S. Y. L., Nelson, B. D., Ajayi-Oyetunde, O., Bradley, C. A., Hughes, T. J., Hartman, G. L., et al. (2016). Identification of diverse mycoviruses through metatranscriptomics characterization of the viromes of five major fungal plant pathogens. *J. Virol.* 90 (15), 6846–6863. doi: 10.1128/JVI.00357-16

Nagendra Prasad, M. N., Bhat, S. S., and Sreenivasa, M. Y. (2010). Antifungal activity of essential oils against phomopsis azadirachtae the causative agent of die-back disease of neem. *J. Agri Tech* 6), 127–133.

Nibert, M. L., Woods, K. M., Upton, S. J., and Ghabrial, S. A.. (2009). Cryspovirus: a new genus of protozoan viruses in the family Partitiviridae. *Arch. Virol.* 154 (12), 1959–1965. doi: 10.1007/s00705-009-0513-7

Niu, Y., Yuan, Y., Mao, J., Yuan, Y., Wang, S., Liu, J., et al. (2018). Characterization of two novel mycoviruses from penicillium digitatum and the related fungicide resistance analysis. *Sci. Rep.* 8 (1), 1–12. doi: 10.1038/s41598-018-23807-3

Nuss, D. L. (1992). Biological control of chestnut blight: an example of virus-mediated attenuation of fungal pathogenesis. *Microbiological Rev.* 56 (4), 561–576. doi: 10.1128/mr.56.4.561-576.1992

Nuss, D. L. (2005). Hypovirulence: mycoviruses at the fungal–plant interface. *Nat. Rev. Microbiol.* 3 (8), 632–642. doi: 10.1038/nrmicro1206

Pandey, A. (2010). Studies on fungal diseases of eggplant in relation to statistical analysis and making of a disease calendar. *Recent Res. ence Technol.* 2 (9), 1–3.

Pearson, M. N., Beever, R. E., Boine, B., and Arthur, K.. (2010). Mycoviruses of filamentous fungi and their relevance to plant pathology. *Mol. Plant Pathol.* 10 (1), 115–128. doi: 10.1111/j.1364-3703.2008.00503.x

Rangaswami, G., and Madevan, A. (1998). *Diseases of crop plants in India [M]* (PHI Learning Pvt. Ltd , introduction), 1–9

Smith, I. M., Dunez, J., Phillips, D. H., Phillips, D. H., and Archer, S. A.. (1988). European Handbook of plant Diseases. *Q. Rev. Biol.*, 1–67. doi: 10.1002/9781444314199

Son, M., Yu, J., Kim, K. H., et al. (2015). Five questions about mycoviruses. *PloS Pathog.* 11 (11), e1005172. doi: 10.1371/journal.ppat.1005172

Sutela, S., Forgia, M., Vainio, E. J., Chiapello, M., Daghino, S., Vallino, M., et al. (2020). The virome from a collection of endomycorrhizal fungi reveals new viral taxa with unprecedented genome organization. *Virus Evol.* 6 (2), veaa076. doi: 10.1093/ve/veaa076

Suvi, S., Marco, F., Vainio, E. J., Chiapello, M., Daghino, S., Vallino, M., et al. (2020). The virome from a collection of endomycorrhizal fungi reveals new viral taxa with unprecedented genome organization . *Virus Evol.* 6 (2).

Teng, S. C. (1932). Fungi of Nanking. *Contribution Biol. Lab.science Soc. Chinabotanical* 8 (1), 5–48.

Thippeswamy, B., Krishnappa, M., and Chakravarthy, C. N.. (2012) Location and transmission of Phomopsis vexans, Alternaria solani in Brinjal. *Indian Phytopathol* 8 (1), 1–12.

Torres-Trenas, A., Prieto, P., Caizares, M. C., García-Pedrajas, M. D., and Pérez-Artés, E.. (2019). Mycovirus fusarium oxysporum f. sp. dianthi virus 1 decreases the colonizing efficiency of its fungal Host. *Front. Cell. Infection Microbiol.* 9, 51. doi: 10.3389/fcimb.2019.00051

Udayashankar, A. C., Nayaka, S. C., Archana, B., Lakshmeesha, T. R., Niranjana, S. R., Lund, O. S., et al. (2019). Specific PCR-based detection of phomopsis vexans the cause of leaf blight and fruit rot pathogen of (Solanum melongena l.) . *Lett. Appl. Microbiol.* 69 (5), 358–365. doi: 10.1111/lam.13214

Vainio, E. J., Chiba, S., Ghabrial, S. A., Maiss, E., Roossinck, M., Sabanadzovic, S., et al. (2018). ICTV virus taxonomy profile: Partitiviridae. *J. Gen. Virol.* 99 (1), 17–18. doi: 10.1099/jgv.0.000985

Wu, S., Cheng, J., Fu, Y., Chen, T., Jiang, D., Ghabrial, S. A., et al. (2017). Virus-mediated suppression of host non-self recognition facilitates horizontal transmission of heterologous viruses. *PLoS Pathog.* 13 (3), e1006234. doi: 10.1371/journal.ppat.1006234

Xiao, X., Cheng, J., Tang, J., Fu, Y., Jiang, D., Baker, T. S., et al. (2014). A novel partitivirus that confers hypovirulence on plant pathogenic fungi. *J. Virol.* 88 (17), 10120–10133. doi: 10.1128/JVI.01036-14

Xie, J., and Jiang, D. (2014). New insights into mycoviruses and exploration for the biological control of crop fungal diseases. *Annu. Rev. Phytopathol.* 52, 45–68. doi: 10.1146/annurev-phyto-102313-050222

Yang, D., Wu, M., Zhang, J., Chen, W., Li, G., Yang, L., et al. (2018). Sclerotinia minor endornavirus 1, a novel pathogenicity debilitation-associated mycovirus with a wide spectrum of horizontal transmissibility. *Viruses* 10 (11), 589. doi: 10.3390/v10110589

Yokoi, T., Yamashita, S., and Hibi, T.. (2007). The nucleotide sequence and genome organization of magnaporthe oryzae virus 1. *Arch. Virol.* 152 (12), 2265–2269. doi: 10.1007/s00705-007-1045-7

Zhai, L., Yang, M., Zhang, M., Hong, N., and Wang, G.. (2019). Characterization of a botybirnavirus conferring hypovirulence in the phytopathogenic fungus *Botryosphaeria dothidea*. *Viruses* 11 (3), 266. doi: 10.3390/v11030266

Zhang, Y., Chen, G., Luo, S., Qu, H., Tang, Y., Xie, Q., et al. (2012). Stress physiology and virulence characterization of phomopsis asparagi (Sacc.) bubák isolated from asparagus in Jiangxi province, China. *Agric. Sci. Technol.* 13 (7), 1502–1508. doi: 10.3969/j.issn.1009-4229-B.2012.07.026

Zhang, R., Hisano, S., Tani, A., Kondo, H., Kanematsu, S., Suzuki, N., et al. (2016). A capsidless ssRNA virus hosted by an unrelated dsRNA virus. *Nat. Microbiol.* 1 (1), 15001. doi: 10.1038/nmicrobiol.2015.1

Zhang, R., Liu, S., Chiba, S., Kondo, H., Kanematsu, S., Suzuki, N., et al. (2014). A novel single-stranded RNA virus isolated from a phytopathogenic filamentous fungus, *Rosellinia necatrix*, with similarity to hypo-like viruses. *Front. Microbiol.* 5, 360. doi: 10.3389/fmicb.2014.00360

Zhang, Y. Z., Shi, M., and Holmes, E. C.. (2018). Using metagenomics to characterize an expanding virosphere. *Cell* 172, 1168–1172. doi: 10.1016/j.cell.2018.02.043

Zhang, H., Xie, J., Fu, Y., Cheng, J., Qu, Z., Zhao, Z., et al. (2020). A 2-kb mycovirus converts a pathogenic fungus into a beneficial endophyte for brassica protection and yield enhancement. *Mol. Plant* 13 (10), 1420–1433. doi: 10.1016/j.molp.2020.08.016

Zhang, R. J., Zhong, J., Shang, H. H., Pan, X. T., Zhu, H. J., Da Gao, B., et al. (2015). The complete nucleotide sequence and genomic organization of a novel victorivirus with two non-overlapping ORFs, identified in the plant-pathogenic fungus *Phomopsis vexans*. *Arch. Virol.* 160 (7), 1805–1809. doi: 10.1007/s00705-015-2420-4

Zhang, C. J., Zhou, X. Y., Zhong, J., Guo, J., Yang, X. P., Zhu, H. J., et al. (2021). Complete nucleotide sequence of a novel partitivirus infecting the plant-pathogenic fungus *Phomopsis vexans*. *Arch. Virol.* 166 (1), 291–294. doi: 10.1007/s00705-020-04835-9

frontiers | Frontiers in Plant Science

TYPE Original Research
PUBLISHED 21 November 2022
DOI 10.3389/fpls.2022.1067723

OPEN ACCESS

EDITED BY
Cunmin Qu,
Southwest University, China

REVIEWED BY
Bingxian Yang,
Zhejiang Sci-Tech University, China
Lunwen Qian,
Hunan Agricultural University, China

*CORRESPONDENCE
Wei Li
weili@cqnu.edu.cn
Tao Zhang
zht2188@126.com

†These authors have contributed equally to this work

SPECIALTY SECTION
This article was submitted to Plant Pathogen Interactions, a section of the journal Frontiers in Plant Science

RECEIVED 12 October 2022
ACCEPTED 03 November 2022
PUBLISHED 21 November 2022

CITATION
Lu J, Yang N, Zhu Y, Chai Z, Zhang T and Li W (2022) Genome-wide survey of Calcium-Dependent Protein Kinases (CPKs) in five *Brassica* species and identification of CPKs induced by *Plasmodiophora brassicae* in *B. rapa, B. oleracea, and B. napus*. *Front. Plant Sci.* 13:1067723. doi: 10.3389/fpls.2022.1067723

Genome-wide survey of Calcium-Dependent Protein Kinases (CPKs) in five *Brassica* species and identification of CPKs induced by *Plasmodiophora brassicae* in *B. rapa, B. oleracea, and B. napus*

Junxing Lu[1†], Nan Yang[2†], Yangyi Zhu[1], Zhongxin Chai[3], Tao Zhang[1*] and Wei Li[1*]

[1]Chongqing Key Laboratory of Molecular Biology of Plant Environmental Adaptations, College of Life Science, Chongqing Normal University, Chongqing, China, [2]Wuxi Fisheries College, Nanjing Agricultural University, Jiangsu, China, [3]Department of Botany, University of British Columbia, Vancouver, BC, Canada

Calcium-dependent protein kinase (CPK) is a class of Ser/Thr protein kinase that exists in plants and some protozoa, possessing Ca^{2+} sensing functions and kinase activity. To better reveal the roles that *Brassica* CPKs played during plant response to stresses, five *Brassica* species, namely *Brassica rapa* (*B. rapa*), *Brassica nigra* (*B. nigra*), *Brassica oleracea* (*B. oleracea*), *Brassica juncea* (*B. juncea*), *and Brassica napus* (*B. napus*) were selected and analyzed. In total, 51 *BraCPK*, 56 *BniCPK*, 56 *BolCPK*, 88 *BjuCPK*, and 107 *BnaCPK* genes were identified genome wide and phylogenetics, chromosomal mapping, collinearity, promoter analysis, and biological stress analysis were conducted. The results showed that a typical *CPK* gene was constituted by a long exon and tandem short exons. They were unevenly distributed on most chromosomes except chromosome A08 in *B. napus* and *B. rapa*, and almost all *CPK* genes were located on regions of high gene density as non-tandem form. The promoter regions of *BraCPKs*, *BolCPKs*, and *BnaCPKs* possessed at least three types of cis-elements, among which the abscisic acid responsive-related accounted for the largest proportion. In the phylogenetic tree, CPKs were clustered into four primary groups, among which group I contained the most *CPK* genes while group IV contained the fewest. Some clades, like *AT5G23580.1*(*CPK12*) and *AT2G31500.1* (*CPK24*) contained much more gene members than others, indicating a possibility that gene expansion occurred during evolution. Furthermore, 4 *BraCPKs*, 14 *BolCPKs*, and 31 *BnaCPKs* involved in the *Plasmodiophora brassicae* (*P. brassicae*) defense response in resistant (R) or susceptible (S) materials were derived from online databases, leading to the discovery that some R-specific induced *CPKs*, such as *BnaC02g08720D*, *BnaA03g03800D*, and *BolC04g018270.2J.m1* might be

ideal candidate genes for *P. brassicae* resistant research. Overall, these results provide valuable information for research on the function and evolution of CDK genes.

KEYWORDS

Brassica* species, calcium-dependent protein kinase, evolution, expression pattern, *Plasmodiophora brassicae

Introduction

Ca^{2+} is a generic form of the second messenger to participate in numerous signaling pathways (Hetherington and Brownlee, 2004; Zhang et al., 2014b). The change of Ca^{2+} concentration in cells can be captured by calcium sensors. Based on whether or not they are adjusted by the combination with Ca^{2+}, calcium sensors are divided into four classes in plants, namely calmodulin (CaM) or CaM-like proteins (CMLs), calcineurin B-like proteins (CBLs), CBL interacting protein kinases (CIPKs), and the calcium-dependent protein kinases (CPKs) and their relatives, CPK-related kinases (CRKs) (Luan et al., 2002; Yang et al., 2021). Among them, CPKs exist in plants and some protozoa, especially in plant extracts. Additionally, rich calcium-stimulated protein kinase activity is found to be related to *CPKs* (Harmon et al., 2000). Typical CPK proteins contain an N-terminal variable domain, a protein kinase domain, an autoinhibitory domain, and a calmodulin-like domain (Cheng et al., 2002). The protein kinase domain is the catalytic domain containing an adenosine triphosphate binding site adjacent to the inhibitory domain, and the successive calmodulin domains always contain a protein kinase domain and EF-hands to determine whether the CPK is calmodulin dependent (Cheng et al., 2002; Hrabak et al., 2003).

Numerous studies have reported that CPKs are involved in plant responses to abiotic stresses. For example, *Arabidopsis CPK1* and *CPK2* were rapidly expressed under drought and high salinity stress, and *CPKs* played a significant role in enhancing abiotic stress tolerance (Urao et al., 1994). In maize, 12 of 40 CPK genes responded to low temperature, drought, salt, ABA, and hydrogen peroxide (Kong et al., 2013). In wheat, 10 of 14 *CPK* genes were responsive to abiotic stress, including drought, NaCl, and ABA. In potatoes, *StCPKs* were responsive to biotic and abiotic stresses as well as hormone stimulation (Bi et al., 2021). Among them, 20 *StCPKs* showed differential expression patterns in drought-tolerant and drought-sensitive potato varieties under drought stress, which allowed for recognition of abiotic stress of potatoes. In grapes, the response of *VpCPKs* to NaCl treatment and transcriptional responses at low and high temperatures has been studied (Zhang et al., 2015). Almost all 19 CPKs were up or down-regulated under at least one abiotic stress, but some genes had a rather mild response, and some grape *CPK* genes, like *VpCPK6, VpCPK9, VpCPK14, VpCPK16*, and *VpCPK19* had positive effects in fighting against powdery mildew. Overall, most CPK-related studies focused on the role in abiotic stress and rarely mentioned biotic stressors.

Brassica is a member of the *Brassicaceae* family, which contains many important vegetables, oil crops, and forage crops and has high economic value. *CPK* gene is a candidate gene for modifying plant stress resistance cations. Although there are some studies on CPKs of *Brassica* plants, such as turnip and canola (Zhang et al., 2014a; Wang et al., 2017), there are few studies on *Brassica* CPKs as a whole. Additionally, most of the studies on *CPKs* are conducted in one type of plant, which cannot be accurately used for comparison between plants. In this study, five *Brassica* Species (*B. rapa, B. nigra, B. oleracea, B. juncea, and B. napus*) *CPKs* (*BraCPKs, BniBCPKs, BolCPKs, BjuCPKs, BnaCPKs*) were identified, for phylogenetic, chromosomal mapping, collinearity, promoter analysis, and biological stress analysis. This study specifically studied the *Brassica* CPK induced by clubroot, which is caused by the obligate biotrophic pathogen *P. brassicae*, one of the most devastating diseases affecting *Brassicae* (Zhang et al., 2016). Our results provide important information on the evolutionary history and biological function of the *Brassica* Species CPKs in biotic stress.

Materials and methods

Identification of *CPK* genes

To identify *CPK* genes in *Brassica*, the whole-genomes of five *Brassica* species were downloaded from the Brassica Database (BRAD) (Chen et al., 2022) (http://brassicadb.cn/). The HMMER profiles of the protein kinase domains (PF00069) and EF-hand domains (PF00036, PF13499, or PF13833) derived from Pfam

(www.ebi.ac.uk/interpro) were used as queries to search for CPKs in the *Brassica* protein database, thereby obtaining the first part of the candidate CPK proteins. Furthermore, all *Arabidopsis* CPK proteins were obtained from TAIR (https://www.arabidopsis.org/) and used as queries to search orthologs in five *Brassica* species using the BLAST search analysis. Subsequently, the two sets of candidates were merged and subjected to NCBI-BLASTP using the UniProtKB/SwissoPrpt database, and their annotations were downloaded for further screening. Then, we excluded the sequences that were CPK-related proteins, calcium/calmodulin-dependent proteins, and calcium and calcium/calmodulin-dependent protein kinases. The remaining proteins were regarded as CPKs. The conserved domains and EF-hand quantity were predicted by SMART (Letunic and Bork, 2018; Letunic et al., 2021) (http://smart.embl-heidelberg.de/). N-terminal myristoylation sites, N-terminal palmitoylation sites, and N-terminal acetylation sites were predicted using NMT (https://mendel.imp.ac.at/myristate/SUPLpredictor.htm), CSS-Palm4.0 (Ren et al., 2008; Chica, 2020) (http://csspalm.biocuckoo.org/index.php), and NetAcet-1.0 (Kiemer et al., 2005) (https://services.healthtech.dtu.dk/service.php?NetAcet-1.0), respectively.

Gene structure, conserved motif, promoter element, and phylogenetic analysis

TBtools (Chen et al., 2020) was used to visualize the exon-intron organization of *CPK* genes according to the annotation information of the *Brassica* genomes in BRAD. MEME suit (https://meme-suite.org/meme/index.html) was used to search for conserved motifs in CPK proteins (Bailey et al., 2015). Approximately 2,000-bp upstream flanking fragments of the CPK genes were derived from the genome, and PlantCARE (http://bioinformatics.psb.ugent.be/webtools/plantcare/html/) was used to predict promoter *cis*-elements (Lescot et al., 2002). Full-length *Brassica* species CPK protein sequences were aligned *via* the MUSCLE program and then used to construct a phylogenic tree *via* the neighbor-joining method of MEGA11.0 software (Tamura et al., 2021). Bootstrap values were estimated to assess the relative support for each branch with 2,000 replicates.

Genomic distribution and synteny analysis

Brassica CPKs were mapped on chromosomes according to genome annotation files from BRAD. The segmental and tandem duplication regions were obtained using the MCscanX software (Wang et al., 2012). For synteny analysis, synteny blocks of the CPK genes were visualized using TBtools (Chen et al., 2020). Nonsynonymous (Ka)/synonymous (Ks) calculation analysis was performed by KaKs_calculator 3.0 (Zhang, 2022).

Expression characteristics of *CPK* genes induced by *Plasmodiophora brassicae*

To study the CPKs induced by *P. brassicae* infection, three RNA-seq datasets of clubroot-resistant (R) and clubroot-susceptible (S) lines of *B.rapa* (PRJNA298858), *B.oleracea* (PRJNA298858), and *B.napus* (PRJNA345072) were downloaded from NCBI (Chen et al., 2015; Zhang et al., 2016; Li et al., 2019). The time points for *B. rapa* dataset were 0, 12, 72, and 96 hours post-inoculation (hpi). The time points for *B.olerascea* were 0, 7, and 14 days post-inoculation (dpi), and for *B.napus* were 0, 12, 24, 60, and 96 hpi. The TPM (Transcripts Per Kilobase Million) value was used to display the gene expression levels, and the heat map was drawn by TBtools (Chen et al., 2020). Correlation analysis was carried out according to their expression levels in the relevant time after *P.brassicae* infection, so as to judge the influence of *P. brassicae* in *Brassica* species.

Results

Identification and characterization of CPKs in *Brassica*

To identify CPKs in *Brassica*, we performed a genome-wide analysis of the *CPK* gene family in the five *Brassica* species through a BLAST search and HMMER analysis. Proteins with protein kinase domain and EF-hand domain were identified, and those that might possess similar domains, such as CPK-related proteins, calcium/calmodulin-dependent proteins, and calcium and calcium/calmodulin-dependent protein kinases were carefully excluded. Altogether, we identified 51 *BraCPKs*, 56 *BniCPKs*, 56 *BolCPKs*, 88 *BjuCPKs*, and 107 *BnaCPKs* from *B. rapa, B. nigra, B. oleracea, B. juncea*, and *B. napus*, respectively. The typical *CPK* genes were constituted by a long exon and tandem short exons (Table S1; Figure S1). Three quarters of *CPK* genes in five species possessed six to eight exons, with detailed proportions of each species possessing this number of exons at 80.39% (*B. rapa*), 78.57% (*B. nigra*), 78.57% (*B. oleracea*), 80.68% (*B. juncea*), and 73.83% (*B. napus*). The exon number ranged from 2 to 21, such as *BjuO012843* having only two short exons and *BraA02g042460.3C* exhibiting 21 exons of varying lengths.

In general, CPK proteins contained one Protein kinase and four EF-hand domains, with some CPKs varying in the number of EF-hand domains, ranging from one to six. (Table S1; Figure S2). Furthermore, the majority of CPK proteins possessed palmitoylation sites at their N-termini (*B. rapa*, 75.44%; *B.*

nigra, 76.79%; *B. oleracea*, 73.21%; *B. juncea*, 69.32%; *B. napus*, 70.09%). This is crucial for regulation, as palmitoylation plays important roles in modulating proteins' trafficking, stability and sorting (Martín and Busconi, 2000; Draper et al., 2007; Greaves and Chamberlain, 2007; Linder and Deschenes, 2007). Moreover, half of CPK proteins contained myristoylation sites, and several contained N-terminal acetylation sites.

Chromosomal localization and gene expansion

To understand the genomic distribution of *CPKs*, gene positions were acquired from the genome database of *Brassica* species (Figure 1). *BraCPK* genes were located on 9 out of 10 chromosomes with an exception of Chromosome A08 (Figure 1A). Chromosome A03 carried 11 evenly distributed *BraCPK* genes, which was the maximum number on one chromosome. Meanwhile, chromosomes A01 and A04 possessed only three *BraCPK* genes. 55 *BniCPK* genes were spread out across eight chromosomes, and among them, 12 *BniCPK* genes were located on Chromosome B08, mostly in cluster manner (Figure 1B). The *BniCPK* gene number on other chromosomes varied, ranging from four to nine. As seen in Figure 1C, *BolCPK* genes distributed on all chromosomes, and most genes clustered on chromosome C03 which was followed by chromosome C07, C09, and C02. As shown in Figure 1D, *BjuCPK* genes were unevenly dispersed on chromosomes excluding A08 and B04 which carried no *BjuCPK* genes. The gene number on different chromosomes varied greatly. For example, there are nine genes on chromosome A03 and only 2 genes on chromosome A01. Similar to the distribution of *BraCPKs* and *BolCPKs*, *BnaCPK* genes were unevenly dispersed on chromosomes. This uneven distribution excluded ChrA08 which was the only one that carried no *BnaCPK* genes (Figure 1E). The quantity of *BnaCPK* genes on different chromosomes ranged from 2 to 10. ChrC09 had 10 *BnaCPK* genes which was the largest number found on a single chromosome, while ChrC06 contained only 2 *BnaCPKs*.

Considering that *B. napus* is derived from the recombination of *B. rapa* and *B. oleracea*, *B. juncea* is derived from *B. rapa* and *B. nigra*, the positions of *BnaCPK* genes on chromosomes ChrAs or ChrCs and *BjuCPK* genes on chromosomes ChrAs or ChrBs showed highly consistent with those of corresponding homologous *BraCPK*, *BolCPK* or *BniCPK* genes. Additionally, almost all *CPK* genes were located on regions of high gene density as non-tandem form. In total, only seven *CPK* gene clusters were found in five species, including one in *B. rapa* (*BraA09g325600.3C* and *BraA09g325610.3C*), two in *B. nigra* (*BniB012674-TA* and *BniB012675-TA*; *BniB003258-TA*, *BniB003259-TA* and *BniB003260-TA*), one in *B. oleracea* (*BolC02g059690.2J.m1*, *BolC02g059700.2J.m1* and *BolC02g059710.2J.m1*), two in *B. juncea* (*BjuA001247* and *BjuA001248*, *BjuA026199* and *BjuA026200*), and one in *B. napus* (*BnaC02g41570*, *BnaC02g41580* and *BnaC02g415790*).

To better reveal the expansion of *CPK* genes in five *Brassica* genomes, the duplication patterns of *CPK* genes were predicted within and between each genome with the *A. thaliana* genome added for comparison (Figure 2). The result showed that there were 15 *CPK* gene pairs in *A. thaliana*, and the gene pair number of *Brassica* species was tripled or even tenfold, namely, 47 pairs in *B. rapa*, 51 pairs in *B. nigra*, 52 pairs in *B. oleracea*, 154 pairs in *B. juncea*, and 200 pairs in *B. napus* (Figure 2A). Moreover, the possible syntenic relationship of *CPK* genes between *Brassica* genomes was also investigated. Subsequently, we obtained 234 orthologous gene pairs between *B. rapa* and *B. napus*, 177 between *B. rapa* and *B. juncea*, 258 between *B. oleracea* and *B. napus*, and 182 between *B. nigra* and *B. juncea*, which are shown in Figure 2B. Chromosome A03/A09, B03/B08, and C03/C07/C09 possessed the higher orthologous regions in *B. rapa, B. nigra* and *B. oleracea*, respectively. Correspondingly, chrA03, chrA09, chrC03, and chrC09 subgenomes were classified as higher orthologous regions in *B.napus*. These higher orthologous regions were not present in chromosome A03, A09, B03, and B08 subgenomes in *B.juncea*, which may be due to the imperfect assembly of the *B.juncea* genome.

Additionally, the nonsynonymous/synonymous mutations (Ka/Ks) analysis was performed on orthologous *CPK* genes between *A. thaliana* and the other five *Brassica species* (Table S2). The Ka/Ks value of the predicted *CPK* paralogs that had average values of 0.087 (*B. rapa*), 0.091 (*B. nigra*), 0.083 (*B. oleracea*), 0.088 (*B. juncea*) and 0.083 (*B. napus*) were less than one, suggesting that all pairs of CPK proteins were under strong purifying selection pressure.

Phylogenetic relationships of *CPK*s

To explore the phylogenetic relationship of *CPK* genes, neighbor-joining trees were constructed by CPK protein sequence from five *Brassica* species (Figure 3). CPKs were clustered into four major groups based on tree topology (group I, group II, group III, group IV), which agreed with the classification of *Arabidopsis* CPKs (Cheng et al., 2002). In the phylogenetic tree of five species, the *CPK* genes of five *Brassica* species and their orthologs in *Arabidopsis* formed distinct clades. Among four groups, group I contained the most *CPK* genes, including 15 *BraCPKs*, 19 *BniCPKs*, 19 *BolCPKs*, 31 *BjuCPKs*, and 37 *BnaCPKs*. A clade including *AT5G23580.1*(*CPK12*) in group I contributed the largest number of orthologs from *Brassica* species, reaching up to 36. The second largest group was group III, including 105 *CPK* genes, in which the top two clades were AT2G31500.1 (CPK24) and AT3G51850.1 (CPK13), possessing 20 and 19 members from five species respectively. There were 99 *CPK* genes in group II, and four clades, namely AT5G12180.1 (CPK17), AT5G19360.1 (CPK34), and

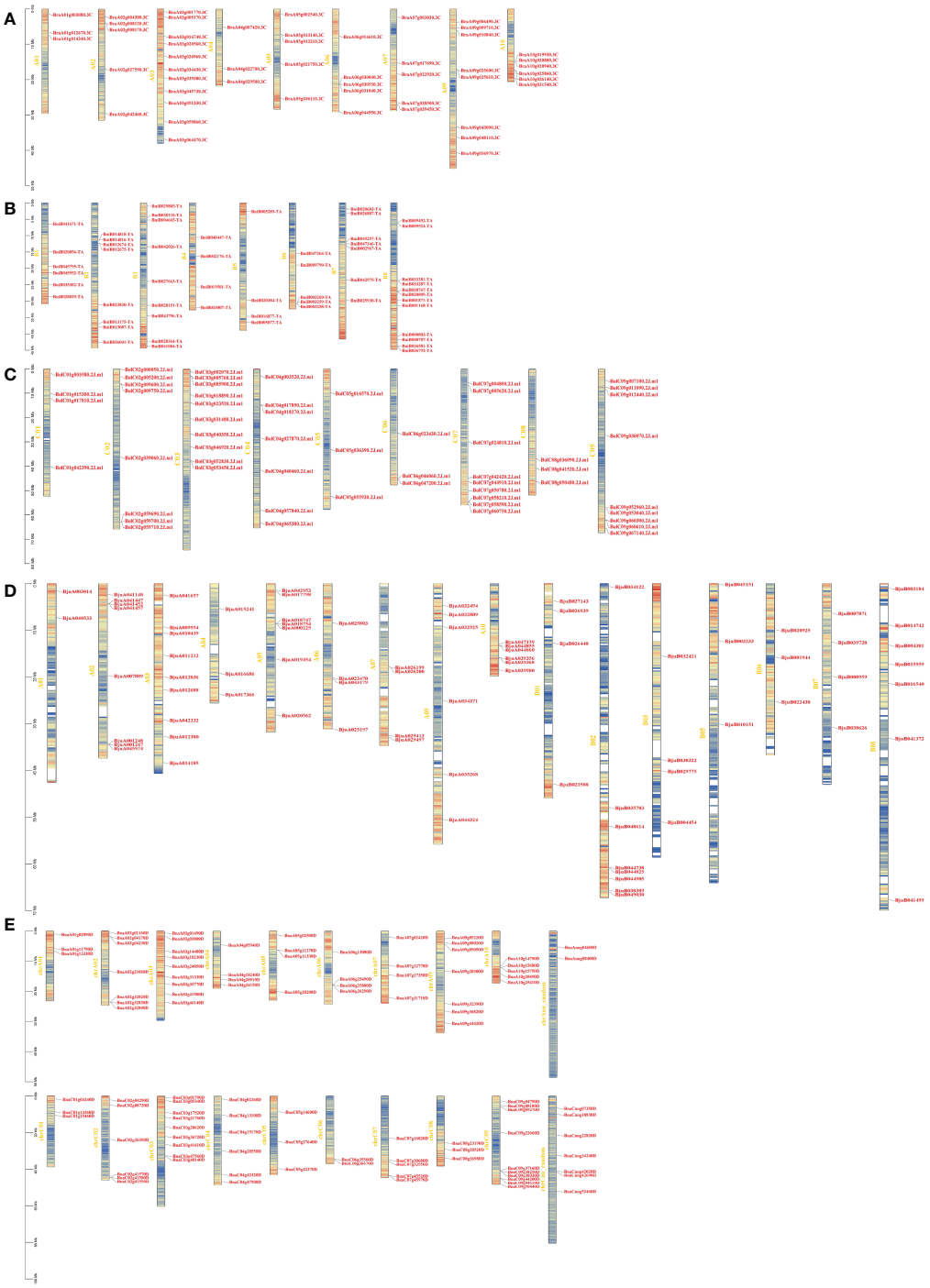

FIGURE 1
Locations of CPK genes on chromosomes in five *Brassica* species. Locations of CPK genes in *B rapa* **(A)**, *B. nigra*. **(B)**, *B. oleracea* **(C)**, *B. juncea* **(D)**, and *B. napus* **(E)**, respectively. A01-A10, B1-B8, C01-C09, A01-B08, and chrA01-chrCnn represent the chromosomes in *B rapa*, *B. nigra*, *B. oleracea*, *B. juncea*, and *B. napus*, respectively. Red indicates high gene density, while blue indicates low.

AT4G04710.1 (CPK22), AT4G23650.1 (CPK3) occupied about 60% of orthologs from *Brassica* species in this group, reaching up to 59 genes. The group with a minimum number of members was group IV, including only three clades with a total of 32 genes. In group IV, clades AT5g66210.2 (CPK28), AT2G17890.1 (CPK16), and AT4G36070.2 (CPK18) possessed 14, 11, and 7 members respectively. In addition, some clades had very few members, such as AT4G04700.1 (CPK27), AT4G04695.1

(CPK31), AT2G35890.1 (CPK25), and AT1G50700.1 (CPK33) merely having one or two orthologs from *Brassica* species.

Analysis of conserved motifs in BraCPK, BolCPK, and BnaCPK

It was found that some CPKs duplicated or lacked certain types of motifs. Most CPKs consisted of 9 to 11 motifs, and covered all motif types (Table S1; Figures S3, S4). As shown in Figure 4, 39 of 51 CPKs in *B. rapa*, 45 of 56 in *B. oleracea*, and 78 of 107 in *B. napus* include ten types of motifs, the proportions of which were up to 76.5%, 80.4%, and 72.90%, respectively. The top three types of motifs were motif 4/1/7 in *B. rapa*, motif 8/6/4 in *B. oleracea*, and motif 8/4/1 in *B. napus*. Further analysis revealed that the composition and the number of conserved motifs or domains varied to a large extent in some CPKs (Figure S3). For example, BnaA02g32830D, BnaA03g46140D, BnaA05g11330D, and BraA09g025610 lacked three to five types of motifs,while BnaC09g22660D had the highest motif

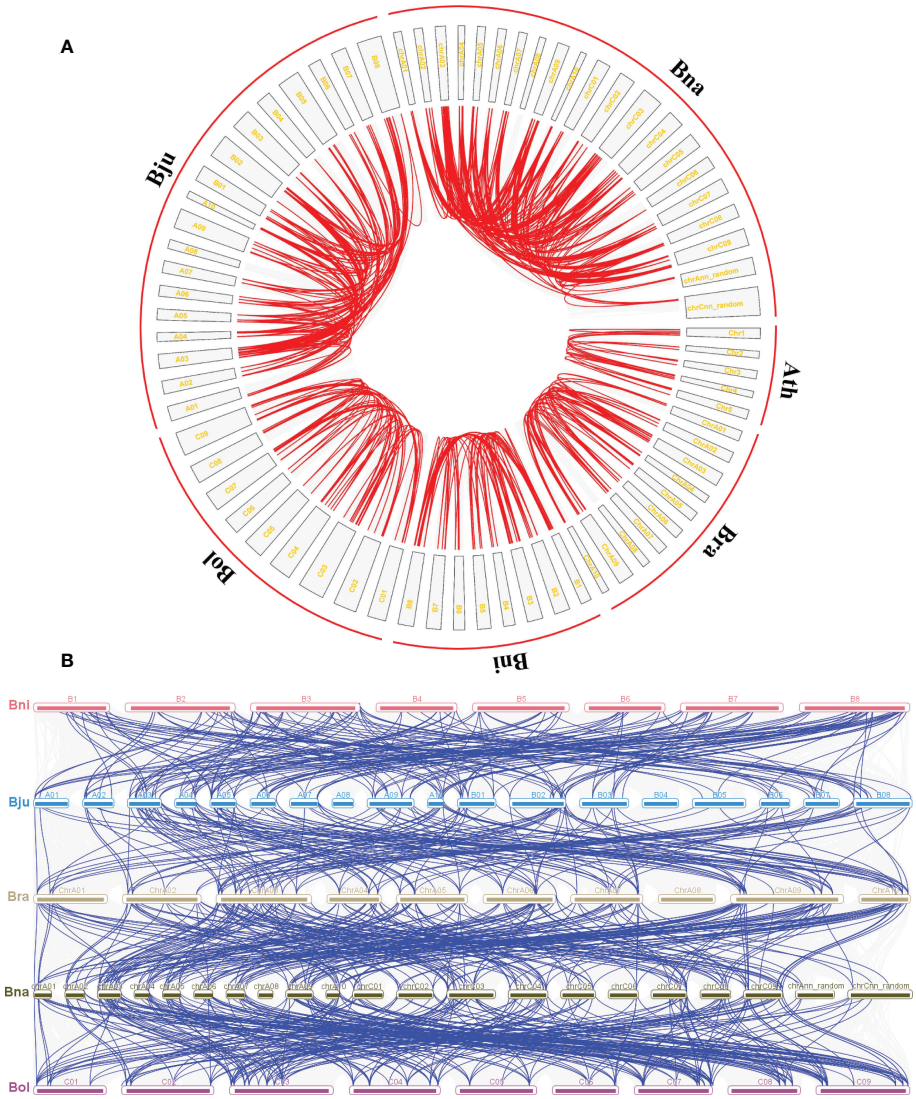

FIGURE 2
Duplication and syntenic relationship of CPK genes in five *Brassica* species. **(A)** Duplication of RLP genes in *A. thaliana, B. rapa, B. nigra, B. oleracea, B. juncea*, and *B. napus*, respectively. The red line represents the gene pairs and the gray box represents the chromosome. **(B)** Syntenic relationship of CPK-encoding genes between *B.rapa, B.nigra, B.oleracea, B.juncea*, and *B.napus*. The blue line represents the gene pairs and the colored box represents the chromosome.

number of 15. In addition, some motif types in BraA02g042460 were tripled. Compared to BraCPKs and BolCPKs, BnaCPK proteins showed more diverse combinations of the motifs.

Analysis of cis-acting elements in the promoter region of *BraCPKs*, *BolCPKs*, and *BnaCPKs*

Cis-acting elements distributed in the promoter region can help predict the function of candidate genes. As most *CPK* genes are related to stress response, we further analyzed the cis-acting elements involved in stress response. Specifically, cis-acting elements are classified as MeJA responsive, gibberellin responsive, abscisic acid responsive, drought inducibility, salicylic acid responsive, and defense and stress responsive related (Table S1; Figure 5 and Figure S5). Among them, *BnaCPKs*, *BraCPKs*, and *BolCPKs* contained the largest number of cis-acting elements related to abscisic acid responsivity, followed by MeJA or gibberellin responsivity (Figure 5). Most genes had three or more promoter elements, but a few genes possessed only one type of cis-acting element, such as six *BnaCPK* genes (*BnaA02g32840D, BnaA03g31330D, BnaA05g11330D, BnaA05g28200D, BnaC05g42370D* and *BnaC09g04790D*), two *BraCPK* genes (*BraA06g030040* and *BraA09g009710*), and three *BolCPK* genes (*BolC03g031480, BolC06g047200* and *BolC07g044910*) (Figure S5), and this presence of single type may give them corresponding functional specificities. In addition, some *CPK* genes contained no promoter elements, which may have a certain impact on gene expressions, such as *BnaA04g24150D, BnaC02g41590D*, and *BolC02g059710*, which may not be involved in plants responding to stress.

Expression pattern of *CPK* genes induced *by Plasmodiophora brassicae*

Plasmodiophora brassicae Wor., an obligate and biotrophic pathogen Rhizaria (Schwelm et al., 2015), can infect over 3,700 species in *Brassicaceae* (Hwang et al., 2012), and lead to club-root, causing significant economic losses every year (Dixon,

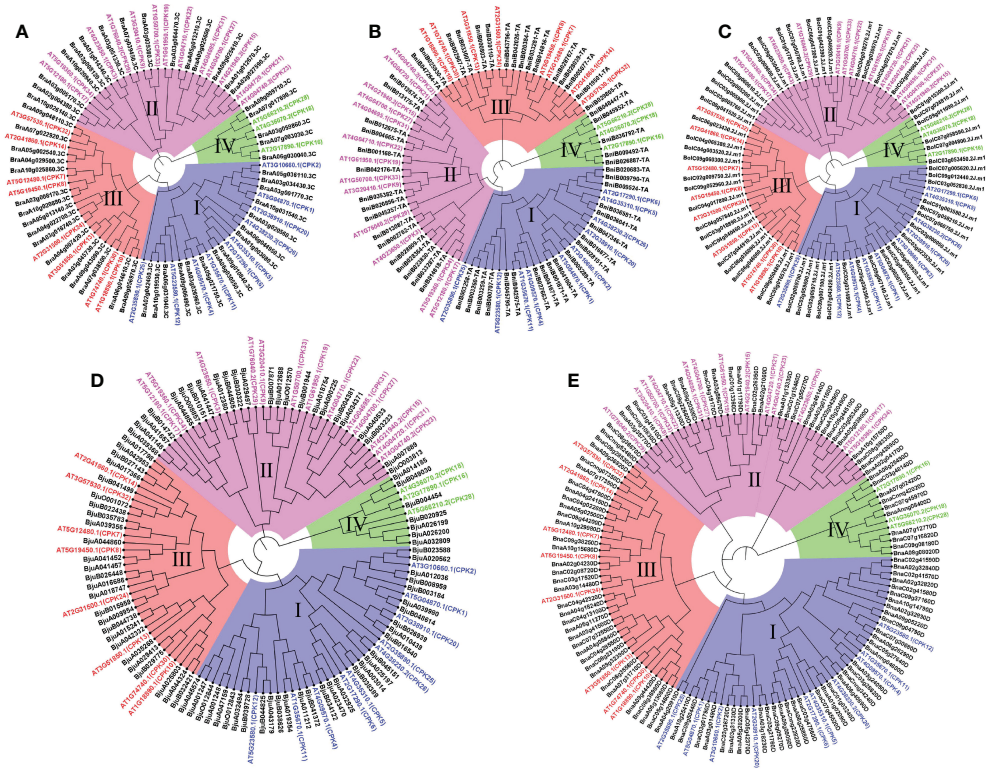

FIGURE 3
Phylogenetic trees of CPK proteins in five *Brassica* species. Phylogenetic trees of CPK proteins in *A. thaliana* and *B. rapa* (A), *B. nigra* **(B)**, *B. oleracea* **(C)**, *B. juncea* **(D)**, *B. napus* **(E)**, respectively. The phylogenetic trees were generated by the NJ method with bootstrap analysis (2,000 bootstrap replicates) using an amino acid sequence alignment of CPK proteins from *A. thaliana* and *Brassica* species by the MEGA 11.0 program. The CPK proteins in each *Brassica* species were clustered into four groups (group I, group I, group III, and group IV).

2009). To further reveal the roles of *CPKs* in *P. brassicae* defense responses, we analyzed the corresponding expression profile data available online. Three RNA-seq datasets were downloaded and analyzed (Chen et al., 2015; Zhang et al., 2016; Li et al., 2019). In total, 43 of 51 *BraCPK*, 49 of 56 *BolCPK*, and 100 of 107 *BnaCPK* genes showed expressional fluctuation after inoculation in resistant (R) and susceptible (S) plants (Figure S6). The expression of most *CPK* genes were down-regulated, and only 4 *BraCPK*, 14 *BolCPK* and 31 *BnaCPK* genes were induced by *P. brassicae* in resistant (R) or susceptible (S) materials at a certain time point (Figure 6). Among them, most *CPKs* presented expression specificity between R and S, such as 18 *CPKs* that were induced merely in R, including 13 *BnaCPKs* (*BnaAnng08400D*, *BnaC03g05340D*, *BnaA03g03800D*, *BnaC04g19170D*, *BnaC03g41610D*, *BnaCnng52460D*, *BnaC03g47900D*, *BnaC02g08720D*, *BnaA09g32390D*, *BnaA06g13080D*, *BnaA02g32830D*, *BnaC07g45520D*, *BnaC09g5044D*), one *BraCPK* (*BraA05g013140.3C*), and four *BolCPKs* (*BolC02g005200.2J.m1*, *BolC04g018270.2J.m1*, *BolC03g018890.2J.m1*, *BolC08g036090.2J.m1*). Additionally, 17 *CPKs* were only induced in S, including eight *BnaCPKs* (*BnaA10g20490D*, *BnaA02g01160D*, *BnaA01g11790D*, *BnaA03g59670D*, *BnaA09g20300D*, *BnaC02g41580D*, *BnaA06g40890D*, *BnaA03g18230D*), one *BraCPK* (*BraA03g020560.3C*), and eight *BolCPKs* (*BolC07g024810.2J.m1*, *BolC09g060610.2J.m1*, *BolC03g005900.2J.m1*, *BolC03g005760.2J.m1*, *BolC01g015300.2J.m1*, *BolC06g047200.2J.m1*, *BolC08g041520.2J.m1*, *BolC05g036390.2J.m1*). Some *CPKs* were highly induced reaching a level of 14.82 (*BnaA03g18230D*, 96 hpi in S), 11.02/10.31 (*BnaC02g08720D*, 12 hpi/60 hpi in R), and 10.31 (*BolC09g060610.2J.m1*, 14 dpi in S) times comparing to their initial concentrations. Apart from *BnaC02g08720D*, other R-specific induced genes, like *BnaA03g03800D* (6.06 folds in 12 hpi, 5.26 folds in 96 hpi) and *BolC04g018270.2J.m1* (5.4 folds in 7 dpi, 5.9 folds in 14 dpi) might also be good candidates for *P. brassicae* resistance research. Moreover, in the phylogenetic tree built by CPKs from *Arabidopsis* and five *Brassica* species, up-regulated genes were distributed in all groups (Figure 7). It is remarkable that the majority of *BraCPK*, *BolCPK*, and *BnaCPK* genes in two families, orthologs of AT5G66210.2 (CPK28) and AT5G12180.1 (CPK17), were up-regulated after *P. brassicae* inoculation, underlining their functional conservation during evolution.

Discussion

B. napus (AACC, 2n = 38) and *B. juncea* (AABB, 2n = 36) are both allopolypoid species formed by the hybridization of two diploid species. *B.napus* is formed through the hybridrization of *B.rapa* (AA = 20) and *B.oleracea* (CC = 18), while the formation of *B. juncea* occurs through the hybridization of *B.rapa* (AA = 20) and *B. nigra* (BB = 16) (Chalhoub et al., 2014; Lu et al., 2019). In our phylogenetic tree, the division of groups was consistent with that of *A. thaliana* (Cheng et al., 2002). The evolution of *CPK* genes was relatively conserved among the five *Brassica* species. In general, the gene number of *BraCPKs* was almost equal to that of *BolCPKs* and *BniCPKs* in the same clade, with duplicated number for *BnaCPKs* and *BjuCPKs*. Nevertheless, in terms of individual branches, the quantity of *BjuCPK* genes was less than two times of that of *BraCPKs* and *BniCPKs*, which might be due to inaccurate assembly occurring during genetic recombination or imperfect sequencing. When selecting *Arabidopsis CPKs* as a reference, there was no doubt that the gene expansion occurred among five species during evolution, especially in some clades, such as Clade AT5G23580.1(CPK12) and AT2G31500.1(CPK24). Of course, the possibility that certain *Arabidopsis CPK* genes have been lost during evolution cannot be ruled out. As the structure of exons/introns and the type and number of introns can account for the evolutionary

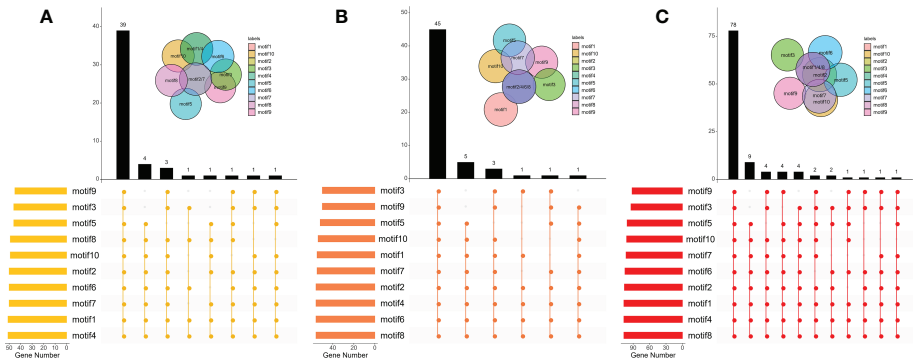

FIGURE 4
Distributions of motifs in BraCPKs **(A)**, BolCPKs **(B)**, and BnaCPKs **(C)**. The Upset plot shows the distribution of motifs in the CPKs. The number chart above represents the number of genes contained in each type of CPK. The bar chart at the bottom left represents the number of genes included in each type of motif. The dotted line shows the types of motifs contained in the group.

10.3389/fpls.2022.1067723

FIGURE 5
Distributions of cis-acting elements in BraCPKs **(A)**, BolCPKs **(B)**, and BnaCPKs **(C)** promoter. The Upset plot shows the distribution of cis-acting elements in CPKs promoter. The bar chart above represents the number of genes contained in each type of CPK. The bar chart at the bottom left represents the number of genes included in each type of cis-acting element. The dotted line shows the types of cis-acting elements contained in the group.

history of organisms, we analyzed the exon/introns substructure of all *CPKs* in this study. Genes in group IV had the most exons, from eleven to thirteen, not including BjuA026200. Most of the *CPK* genes in other groups contained less than ten exons. In general, *CPK* genes clustered in the same subfamily showed similar exon/intron structures, indicating a close evolutionary relationship between them.

At present, *CPK* genes have been identified in *Arabidopsis* (Cheng et al., 2002), rice (Asano et al., 2005), soybean (Liu et al., 2016), maize (Kong et al., 2013; Ma et al., 2013), cucumber (Xu et al., 2015), tomato (Hu et al., 2016) and many other plants (Yang et al., 2017; Wen et al., 2020; Zhang et al., 2020; Zhao et al., 2021), and their roles in biotic and abiotic stresses have been understood to some extent (Asano et al., 2012; Boudsocq and Sheen, 2013; Ranty et al., 2016; Bredow and Monaghan, 2019). Previous studies found that plant CPKs are involved in abscisic acid signaling pathways (Liu et al., 2006, 1; Yu et al., 2006; Zhu et al., 2007; Jiang et al., 2013; Chen et al., 2019), jasmonic acid signaling pathway (Ulloa et al., 2002; Hettenhausen et al., 2013; Matschi et al., 2015), gibberellin signaling pathway (Abo-el-Saad and Wu, 1995; Abbasi et al., 2004; Ishida et al., 2008; Nakata et al., 2009), and also response to drought stress (Ma and Wu, 2007; Cieśla et al., 2016, 2; Bundó and Coca, 2017; Huang et al., 2018). In line with these results, a large number of cis-acting elements related to abscisic acid, jasmonic acid, gibberellin, and drought stress response were found in the promoter region of *Brassica CPK* genes in this study.

Plasmodiophora, as one class of obligate biotrophic pathogens (Ludwig-Müller et al., 2009), is highly destructive to many *Brassica* plants and exerts negative effect on their quality and yield (Dixon, 2009), which seriously hinders the development of agricultural industry. In this study, utilizing the expression data from the resistant (R) and susceptible (S) lines in three *Brassica* species (*B. rapa*, *B. oleracea*, and *B. napus*), we found 49 up-regulated genes induced by *P. brassicae*. These up-regulated genes would be helpful to identify positive regulators in the process of response to *P. brassicae* (Figure 6). Interestingly, the distribution of these 49 genes was extremely uneven among the three *Brassica* species. Among them, 31 genes were found in *B. napus*, accounting for 29% of *BnaCPKs*, while only 4 genes were found in *B. rapa*, with a proportion of 8%, suggesting that BnaCPKs played an important role in *B. napus* taking charge in response to *P. brassicae* infection, while BraCPKs might be mainly involved in other stresses. Moreover, of the 49 up-regulated genes, 18 genes were specifically up-regulated in R, and those genes identified from incompatible interactions might be good candidates for further functional assignment of *CPK* genes against *P.brassicae* infection. The up-regulated genes of the three species were distributed in the four groups in varying amounts (Figure 7). There were 9 *CPK* genes in group I, 23 in group I, 11 in group III,

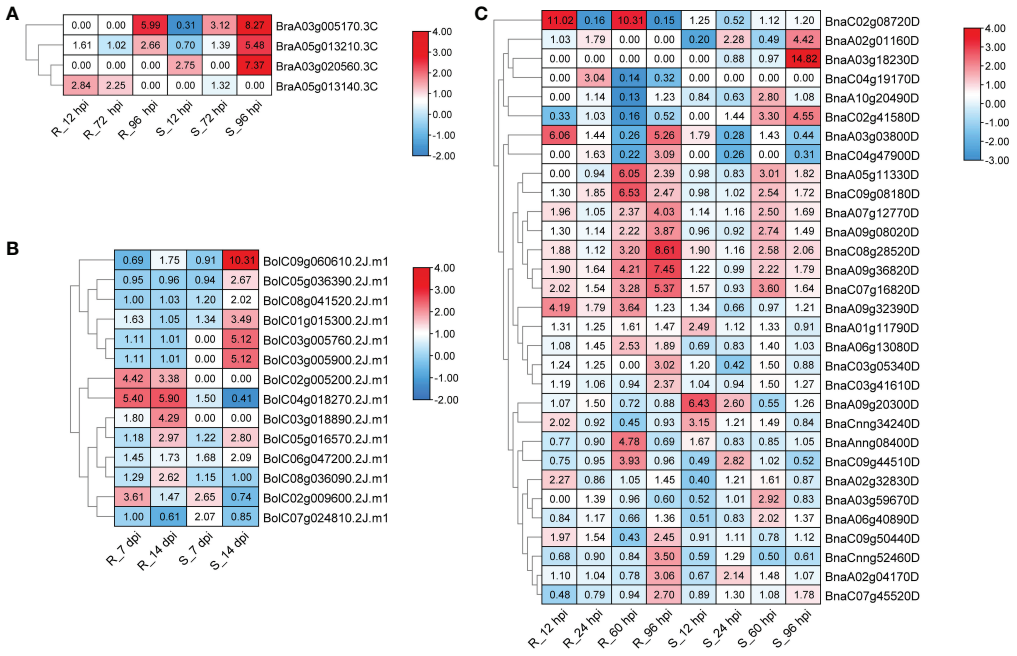

FIGURE 6
Heat maps of upregulated *BraCPKs* **(A)**, *BolCPKs* **(B)**, and *BnaCPKs* **(C)** elicited by *P. brassicae*. R and S, resistant and susceptible genotype, respectively. hpi: hours post-inoculation, dpi: days post-inoculation. The red color indicates up-regulated, and numbers in boxes indicate fold change. The legends show $\log_2$ fold-change. TPM value was used for heat map construction.

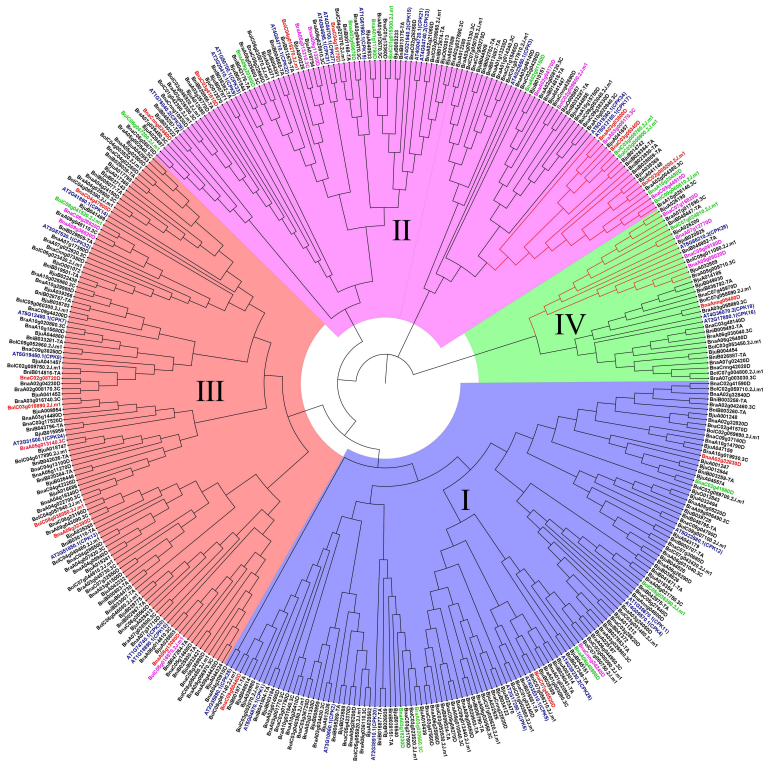

FIGURE 7
Phylogenetic tree of CPK proteins of *A. thaliana* and five *Brassica* species. The phylogenetic tree was generated by the NJ method with bootstrap analysis (2,000 bootstrap replicates) by the MEGA 11.0. The CPK proteins were clustered into four groups (group I, group I, group III, and group IV). Blue mark *AthCPK* genes, red mark upregulated-CPKs in resistance (R) genotype only, green mark upregulated-CPKs in susceptible (S) genotype only, pink mark upregulated-CPKs both resistance (R) and susceptible (S) genotypes. Red lines mark At5G12180.1 (CPK17) and AT5G66210.3 (CPK28) clades.

and only 6 in group IV, suggesting that *CPK* genes involved in *P.brassicae* response evolved independently in four groups along with the functional divergence in *Brassica* species. However, the genes in group I may play a broader role in response to *P.brassicae* infection. It is worth noting that more genes in clade AT5G12180.1 (CPK17) and clade AT5G6621.2 (CPK28) were up-regulated by *P.brassicae* induction. Evolutionarily, these two clades of genes were functionally conserved, and most likely to be active gene clusters during response to *P.brassicae* infection in *Brassica* species.

Conclusion

The gene and protein characterization, localization, evolution, and expression analysis of highly conserved *CPK* genes in *Brassica* showed that most of the *CPK* gene families in this study were relatively conserved during evolution. Genome-wide identification and expression analysis of *CPK* family members can provide an alternative strategy for enhancing resistance to *P. brassicae* in *Brassica* species. These identified genes may be good candidates for further identification of *CPK* genes of *P. brassicae* infection and provide theoretical basis and preliminary guidance for prevention of *P. brassicae* pathogen damage to *Brassica* plants.

Data availability statement

The original contributions presented in the study are included in the article/Supplementary Material. Further inquiries can be directed to the corresponding authors.

Author contributions

JL: formal analysis, writing the original draft, data curation, and validation. NY: investigation, resources, and visualization.

YZ: data curation. ZC: data validation. TZ: writing-review and editing, and supervision. WL: conceptualization, writing-review and editing, and supervision. All authors contributed to the article and approved the submitted version. All authors have read and agreed to the published version of the manuscript.

Funding

This work was supported by grants from the Chongqing Municipal Education Commission (KJQN201900533) to JL, the National Natural Science Foundation of China (31171588) and the Chongqing Municipal Education Commission (KJZD-K202200508) to TZ, and Chongqing Bureau of Human Resources and Social Security Postdoctoral Funding (0019) to WL. JL and WL were partly supported by fellowships from China Scholarship Council (CSC).

Acknowledgments

We sincerely thank Athena Li from the University of British Columbia for the critical reading of the manuscript.

Conflict of interest

The authors declare that the research was conducted in the absence of any commercial or financial relationships that could be construed as a potential conflict of interest.

Publisher's note

Supplementary material

The Supplementary Material for this article can be found online at: https://www.frontiersin.org/articles/10.3389/fpls.2022.1067723/full#supplementary-material

SUPPLEMENTARY FIGURE 1
Gene structures of CPK genes in five *Brassica* species: (A) *BraCPK*, (B) *BniCPK*, (C)*BolCPK*, (D)*BjuCPK*, (E)*BnaCPK* genes. The green bars represent CDS, the black lines represent intron, and the yellow bar represents UTR.

SUPPLEMENTARY FIGURE 2
The conserved domains of CPK proteins in five *Brassica* species. **(A)** BraCPKs, **(B)**BniCPKs, **(C)** BolCPKs, **(D)**BjuCPKs, **(E)**BnaCPKs. The green bar represents protein kinase domain (Pkinase), and the yellow bar represents EF-hand domain (EFh).

SUPPLEMENTARY FIGURE 3
The motifs in CPK proteins of *B. rapa* **(A)**, *B. oleracea* **(B)**, and *B. napus* **(C)**. Motif labeled as motif 1 - motif 10.

SUPPLEMENTARY FIGURE 4
The sequence of motif 1 - motif 10 of *B. rapa, B. oleracea*, and *B. napus*.

SUPPLEMENTARY FIGURE 5
The cis-acting elements in CPKs promoter of *B. rapa* (A), *B. oleracea* (B), and *B. napus* (C). Approximately 2,000-bp upstream flanking fragments of the CPK genes were derived, and PlantCARE was used to predict promoter cis-elements.

SUPPLEMENTARY FIGURE 6
The expression heat map of CPK genes in *B. rapa* **(A)**, *B. oleracea* **(B)**, and *B. napus* **(C)** elicited by *P. brassicae*. R and S, resistant and susceptible genotypes, respectively. hpi: hours post-inoculation, dpi: days post-inoculation. The red color indicates up-regulated, and blue color indicates down-regulated. The legends show $\log_2$ fold-change. TPM value was used for heat map construction.

References

Abbasi, F., Onodera, H., Toki, S., Tanaka, H., and Komatsu, S. (2004). OsCDPK13, a calcium-dependent protein kinase gene from rice, is induced by cold and gibberellin in rice leaf sheath. *Plant Mol. Biol.* 55, 541–552. doi: 10.1007/s11103-004-1178-y

Abo-el-Saad, M., and Wu, R. (1995). A rice membrane calcium-dependent protein kinase is induced by gibberellin. *Plant Physiol.* 108, 787–793. doi: 10.1104/pp.108.2.787

Asano, T., Hayashi, N., Kikuchi, S., and Ohsugi, R. (2012). CDPK-mediated abiotic stress signaling. *Plant Signal Behav.* 7, 817–821. doi: 10.4161/psb.20351

Asano, T., Tanaka, N., Yang, G., Hayashi, N., and Komatsu, S. (2005). Genome-wide identification of the rice calcium-dependent protein kinase and its closely related kinase gene families: Comprehensive analysis of the CDPKs gene family in rice. *Plant Cell Physiol.* 46, 356–366. doi: 10.1093/pcp/pci035

Bailey, T. L., Johnson, J., Grant, C. E., and Noble, W. S. (2015). The MEME suite. *Nucleic Acids Res.* 43, W39–W49. doi: 10.1093/nar/gkv416

Bi, Z., Wang, Y., Li, P., Sun, C., Qin, T., and Bai, J. (2021). Evolution and expression analysis of CDPK genes under drought stress in two varieties of potato. *Biotechnol. Lett.* 43, 511–521. doi: 10.1007/s10529-020-03037-2

Boudsocq, M., and Sheen, J. (2013). CDPKs in immune and stress signaling. *Trends Plant Sci.* 18, 30–40. doi: 10.1016/j.tplants.2012.08.008

Bredow, M., and Monaghan, J. (2019). Regulation of plant immune signaling by calcium-dependent protein kinases. *Mol. Plant Microbe Interact.* 32, 6–19. doi: 10.1094/MPMI-09-18-0267-FI

Bundó, M., and Coca, M. (2017). Calcium-dependent protein kinase OsCPK10 mediates both drought tolerance and blast disease resistance in rice plants. *J. Exp. Bot.* 68, 2963–2975. doi: 10.1093/jxb/erx145

Chalhoub, B., Denoeud, F., Liu, S., Parkin, I. A. P., Tang, H., Wang, X., et al. (2014). Early allopolyploid evolution in the post-neolithic brassica napus oilseed genome. *Science* 345, 950–953. doi: 10.1126/science.1253435

Chen, C., Chen, H., Zhang, Y., Thomas, H. R., Frank, M. H., He, Y., et al. (2020). TBtools: An integrative toolkit developed for interactive analyses of big biological data. *Mol. Plant* 13, 1194–1202. doi: 10.1016/j.molp.2020.06.009

Cheng, S.-H., Willmann, M. R., Chen, H.-C., and Sheen, J. (2002). Calcium signaling through protein kinases. the arabidopsis calcium-dependent protein kinase gene family. *Plant Physiol.* 129, 469–485. doi: 10.1104/pp.005645

Chen, D.-H., Liu, H.-P., and Li, C.-L. (2019). Calcium-dependent protein kinase CPK9 negatively functions in stomatal abscisic acid signaling by regulating ion channel activity in arabidopsis. *Plant Mol. Biol.* 99, 113–122. doi: 10.1007/s11103-018-0805-y

Chen, J., Pang, W., Chen, B., Zhang, C., and Piao, Z. (2015). Transcriptome analysis of brassica rapa near-isogenic lines carrying clubroot-resistant and -susceptible alleles in response to plasmodiophora brassicae during early infection. *Front. Plant Sci.* 6 1183. doi: 10.3389/fpls.2015.01183

Chen, H., Wang, T., He, X., Cai, X., Lin, R., Liang, J., et al. (2022). BRAD V3.0: an upgraded brassicaceae database. *Nucleic Acids Res.* 50, D1432–D1441. doi: 10.1093/nar/gkab1057

Chica, R. A. (2020). Protein engineering, design and selection. *Protein Engineering Design Selection* 33, gzaa024. doi: 10.1093/protein/gzaa024

Cieśla, A., Mituła, F., Misztal, L., Fedorowicz-Strońska, O., Janicka, S., Tajdel-Zielińska, M., et al. (2016). A role for barley calcium-dependent protein kinase CPK2a in the response to drought. *Front. Plant Sci.* 7 1550. doi: 10.3389/fpls.2016.01550

Dixon, G. R. (2009). The occurrence and economic impact of plasmodiophora brassicae and clubroot disease. *J. Plant Growth Regul.* 28, 194–202. doi: 10.1007/s00344-009-9090-y

Draper, J. M., Xia, Z., and Smith, C. D. (2007). Cellular palmitoylation and trafficking of lipidated peptides. *J. Lipid Res.* 48, 1873–1884. doi: 10.1194/jlr.M700179-JLR200

Greaves, J., and Chamberlain, L. H. (2007). Palmitoylation-dependent protein sorting. *J. Cell Biol.* 176, 249–254. doi: 10.1083/jcb.200610151

Harmon, A. C., Gribskov, M., and Harper, J. F. (2000). CDPKs – a kinase for every Ca2+ signal? *Trends Plant Sci.* 5, 154–159. doi: 10.1016/S1360-1385(00)01577-6

Hetherington, A. M., and Brownlee, C. (2004). THE GENERATION OF Ca2+ SIGNALS IN PLANTS. *Annu. Rev. Plant Biol.* 55, 401–427. doi: 10.1146/annurev.arplant.55.031903.141624

Hettenhausen, C., Yang, D.-H., Baldwin, I. T., and Wu, J. (2013). Calcium-dependent protein kinases, CDPK4 and CDPK5, affect early steps of jasmonic acid biosynthesis in nicotiana attenuata. *Plant Signal Behav.* 8, e22784. doi: 10.4161/psb.22784

Hrabak, E. M., Chan, C. W. M., Gribskov, M., Harper, J. F., Choi, J. H., Halford, N., et al. (2003). The arabidopsis CDPK-SnRK superfamily of protein kinases. *Plant Physiol.* 132, 666–680. doi: 10.1104/pp.102.011999

Huang, K., Peng, L., Liu, Y., Yao, R., Liu, Z., Li, X., et al. (2018). Arabidopsis calcium-dependent protein kinase AtCPK1 plays a positive role in salt/drought-stress response. *Biochem. Biophys. Res. Commun.* 498, 92–98. doi: 10.1016/j.bbrc.2017.11.175

Hu, Z., Lv, X., Xia, X., Zhou, J., Shi, K., Yu, J., et al. (2016). Genome-wide identification and expression analysis of calcium-dependent protein kinase in tomato. *Front. Plant Sci.* 7, 469. doi: 10.3389/fpls.2016.00469

Hwang, S.-F., Strelkov, S. E., Feng, J., Gossen, B. D., and Howard, R. J. (2012). Plasmodiophora brassicae: A review of an emerging pathogen of the Canadian canola (Brassica napus) crop. *Mol. Plant Pathol.* 13, 105–113. doi: 10.1111/j.1364-3703.2011.00729.x

Ishida, S., Yuasa, T., Nakata, M., and Takahashi, Y. (2008). A tobacco calcium-dependent protein kinase, CDPK1, regulates the transcription factor REPRESSION OF SHOOT GROWTH in response to gibberellins. *Plant Cell* 20, 3273–3288. doi: 10.1105/tpc.107.057489

Jiang, S., Zhang, D., Wang, L., Pan, J., Liu, Y., Kong, X., et al. (2013). A maize calcium-dependent protein kinase gene, ZmCPK4, positively regulated abscisic acid signaling and enhanced drought stress tolerance in transgenic arabidopsis. *Plant Physiol. Biochem.* 71, 112–120. doi: 10.1016/j.plaphy.2013.07.004

Kiemer, L., Bendtsen, J. D., and Blom, N. (2005). NetAcet: Prediction of n-terminal acetylation sites. *Bioinformatics* 21, 1269–1270. doi: 10.1093/bioinformatics/bti130

Kong, X., Lv, W., Jiang, S., Zhang, D., Cai, G., Pan, J., et al. (2013). Genome-wide identification and expression analysis of calcium-dependent protein kinase in maize. *BMC Genomics* 14, 433. doi: 10.1186/1471-2164-14-433

Lescot, M., Déhais, P., Thijs, G., Marchal, K., Moreau, Y., Van de Peer, Y., et al. (2002). PlantCARE, a database of plant cis-acting regulatory elements and a portal to tools for in silico analysis of promoter sequences. *Nucleic Acids Res.* 30, 325–327. doi: 10.1093/nar/30.1.325

Letunic, I., and Bork, P. (2018). 20 years of the SMART protein domain annotation resource. *Nucleic Acids Res.* 46, D493–D496. doi: 10.1093/nar/gkx922

Letunic, I., Khedkar, S., and Bork, P. (2021). SMART: recent updates, new developments and status in 2020. *Nucleic Acids Res.* 49, D458–D460. doi: 10.1093/nar/gkaa937

Li, L., Long, Y., Li, H., and Wu, X. (2019). Comparative transcriptome analysis reveals key pathways and hub genes in rapeseed during the early stage of plasmodiophora brassicae infection. *Front. Genet.* 10, 1075. doi: 10.3389/fgene.2019.01275

Linder, M. E., and Deschenes, R. J. (2007). Palmitoylation: policing protein stability and traffic. *Nat. Rev. Mol. Cell Biol.* 8, 74–84. doi: 10.1038/nrm2084

Liu, G., Chen, J., and Wang, X. (2006). VfCPK1, a gene encoding calcium-dependent protein kinase from vicia faba, is induced by drought and abscisic acid. *Plant Cell Environ.* 29, 2091–2099. doi: 10.1111/j.1365-3040.2006.01582.x

Liu, H., Che, Z., Zeng, X., Zhou, X., Sitoe, H. M., Wang, H., et al. (2016). Genome-wide analysis of calcium-dependent protein kinases and their expression patterns in response to herbivore and wounding stresses in soybean. *Funct. Integr. Genomics* 16, 481–493. doi: 10.1007/s10142-016-0498-8

Luan, S., Kudla, J., Rodriguez-Concepcion, M., Yalovsky, S., and Gruissem, W. (2002). Calmodulins and calcineurin b-like proteins: calcium sensors for specific signal response coupling in plants. *Plant Cell* 14 Suppl, S389–S400. doi: 10.1105/tpc.001115

Ludwig-Müller, J., Prinsen, E., Rolfe, S. A., and Scholes, J. (2009). Metabolism and plant hormone action during clubroot disease. *D. J. Plant Growth Regul.* 28, 229–244. doi: 10.1007/s00344-009-9089-4

Lu, K., Wei, L., Li, X., Wang, Y., Wu, J., Liu, M., et al. (2019). Whole-genome resequencing reveals brassica napus origin and genetic loci involved in its improvement. *Nat. Commun.* 10, 1154. doi: 10.1038/s41467-019-09134-9

Ma, P., Liu, J., Yang, X., and Ma, R. (2013). Genome-wide identification of the maize calcium-dependent protein kinase gene family. *Appl. Biochem. Biotechnol.* 169, 2111–2125. doi: 10.1007/s12010-013-0125-2

Martín, M. L., and Busconi, L. (2000). Membrane localization of a rice calcium-dependent protein kinase (CDPK) is mediated by myristoylation and palmitoylation. *Plant J.* 24, 429–435. doi: 10.1046/j.1365-313x.2000.00889.x

Matschi, S., Hake, K., Herde, M., Hause, B., and Romeis, T. (2015). The calcium-dependent protein kinase CPK28 regulates development by inducing growth phase-specific, spatially restricted alterations in jasmonic acid levels independent of defense responses in arabidopsis. *Plant Cell* 27, 591–606. doi: 10.1105/tpc.15.00024

Ma, S.-Y., and Wu, W.-H. (2007). AtCPK23 functions in arabidopsis responses to drought and salt stresses. *Plant Mol. Biol.* 65, 511–518. doi: 10.1007/s11103-007-9187-2

Nakata, M., Yuasa, T., Takahashi, Y., and Ishida, S. (2009). CDPK1, a calcium-dependent protein kinase, regulates transcriptional activator RSG in response to gibberellins. *Plant Signal Behav.* 4, 372–374. doi: 10.4161/psb.4.5.8229

Ranty, B., Aldon, D., Cotelle, V., Galaud, J.-P., Thuleau, P., and Mazars, C. (2016). Calcium sensors as key hubs in plant responses to biotic and abiotic stresses. *Front. Plant Sci.* 7, 327. doi: 10.3389/fpls.2016.00327

Ren, J., Wen, L., Gao, X., Jin, C., Xue, Y., and Yao, X. (2008). CSS-Palm 2.0: an updated software for palmitoylation sites prediction. *Protein Eng. Des. Sel* 21, 639–644. doi: 10.1093/protein/gzn039

Schwelm, A., Fogelqvist, J., Knaust, A., Jülke, S., Lilja, T., Bonilla-Rosso, G., et al. (2015). The plasmodiophora brassicae genome reveals insights in its life cycle and ancestry of chitin synthases. *Sci. Rep.* 5, 11153. doi: 10.1038/srep11153

Tamura, K., Stecher, G., and Kumar, S. (2021). MEGA11: Molecular evolutionary genetics analysis version 11. *Mol. Biol. Evol.* 38, 3022–3027. doi: 10.1093/molbev/msab120

Ulloa, R. M., Raíces, M., MacIntosh, G. C., Maldonado, S., and Téllez-Iñón, M. T. (2002). Jasmonic acid affects plant morphology and calcium-dependent protein kinase expression and activity in solanum tuberosum. *Physiol. Plant* 115, 417–427. doi: 10.1034/j.1399-3054.2002.1150312.x

Urao, T., Katagiri, T., Mizoguchi, T., Yamaguchi-Shinozaki, K., Hayashida, N., and Shinozaki, K. (1994). Two genes that encode Ca2+-dependent protein kinases are induced by drought and high-salt stresses in arabidopsis thaliana. *Molec. Gen. Genet.* 244, 331–340. doi: 10.1007/BF00286684

Wang, Y., Tang, H., Debarry, J. D., Tan, X., Li, J., Wang, X., et al. (2012). MCScanX: a toolkit for detection and evolutionary analysis of gene synteny and collinearity. *Nucleic Acids Res.* 40, e49. doi: 10.1093/nar/gkr1293

Wang, Q., Yin, X., Chen, Q., Xiang, N., Sun, X., Yang, Y., et al. (2017). Genome-wide survey indicates diverse physiological roles of the turnip (Brassica rapa var. rapa) calcium-dependent protein kinase genes. *Sci. Rep.* 7, 15803. doi: 10.1038/s41598-017-16102-0

Wen, F., Ye, F., Xiao, Z., Liao, L., Li, T., Jia, M., et al. (2020). Genome-wide survey and expression analysis of calcium-dependent protein kinase (CDPK) in grass brachypodium distachyon. *BMC Genomics* 21, 53. doi: 10.1186/s12864-020-6475-6

Xu, X., Liu, M., Lu, L., He, M., Qu, W., Xu, Q., et al. (2015). Genome-wide analysis and expression of the calcium-dependent protein kinase gene family in cucumber. *Mol. Genet. Genomics* 290, 1403–1414. doi: 10.1007/s00438-015-1002-1

Yang, Y., Wang, Q., Chen, Q., Yin, X., Qian, M., Sun, X., et al. (2017). Genome-wide survey indicates diverse physiological roles of the barley (Hordeum vulgare l.) calcium-dependent protein kinase genes. *Sci. Rep.* 7, 5306. doi: 10.1038/s41598-017-05646-w

Yang, H., You, C., Yang, S., Zhang, Y., Yang, F., Li, X., et al. (2021). The role of Calcium/Calcium-dependent protein kinases signal pathway in pollen tube growth. *Front. Plant Sci.* 12, 633293. doi: 10.3389/fpls.2021.633293

Yu, X.-C., Li, M.-J., Gao, G.-F., Feng, H.-Z., Geng, X.-Q., Peng, C.-C., et al. (2006). Abscisic acid stimulates a calcium-dependent protein kinase in grape berry. *Plant Physiol.* 140, 558–579. doi: 10.1104/pp.105.074971

Zhang, Z. (2022). KaKs_calculator 3.0: Calculating selective pressure on coding and non-coding sequences. *Genomics Proteomics Bioinf.* S1672-0229 (21), 00259–0025X. doi: 10.1016/j.gpb.2021.12.002

Zhang, L., Du, L., and Poovaiah, B. W. (2014b). Calcium signaling and biotic defense responses in plants. *Plant Signal Behav.* 9, e973818. doi: 10.4161/15592324.2014.973818

Zhang, K., Han, Y.-T., Zhao, F.-L., Hu, Y., Gao, Y.-R., Ma, Y.-F., et al. (2015). Genome-wide identification and expression analysis of the CDPK gene family in grape, vitis spp. *BMC Plant Biol.* 15, 164. doi: 10.1186/s12870-015-0552-z

Zhang, X., Liu, Y., Fang, Z., Li, Z., Yang, L., Zhuang, M., et al. (2016). Comparative transcriptome analysis between broccoli (Brassica oleracea var. italica) and wild cabbage (Brassica macrocarpa guss.) in response to plasmodiophora brassicae during different infection stages. *Front. Plant Sci.* 7, 1929. doi: 10.3389/fpls.2016.01929

Zhang, M., Liu, Y., He, Q., Chai, M., Huang, Y., Chen, F., et al. (2020). Genome-wide investigation of calcium-dependent protein kinase gene family in pineapple: evolution and expression profiles during development and stress. *BMC Genomics* 21, 72. doi: 10.1186/s12864-020-6501-8

Zhang, H., Liu, W.-Z., Zhang, Y., Deng, M., Niu, F., Yang, B., et al. (2014a). Identification, expression and interaction analyses of calcium-dependent protein kinase (CPK) genes in canola (Brassica napus l.). *BMC Genomics* 15, 211. doi: 10.1186/1471-2164-15-211

Zhao, P., Liu, Y., Kong, W., Ji, J., Cai, T., and Guo, Z. (2021). Genome-wide identification and characterization of calcium-dependent protein kinase (CDPK) and CDPK-related kinase (CRK) gene families in medicago truncatula. *Int. J. Mol. Sci.* 22, 1044 doi: 10.3390/ijms22031044

Zhu, S.-Y., Yu, X.-C., Wang, X.-J., Zhao, R., Li, Y., Fan, R.-C., et al. (2007). Two calcium-dependent protein kinases, CPK4 and CPK11, regulate abscisic acid signal transduction in arabidopsis. *Plant Cell* 19, 3019–3036. doi: 10.1105/tpc.107.050666

frontiers | Frontiers in Plant Science

TYPE Original Research
PUBLISHED 05 June 2023
DOI 10.3389/fpls.2023.1096831

OPEN ACCESS

EDITED BY
Qi Peng,
Jiangsu Academy of Agricultural Sciences (JAAS), China

REVIEWED BY
Wenjun Zhu,
Wuhan Polytechnic University, China
Jiatao Xie,
Huazhong Agricultural University, China
Duan Yabing,
Nanjing Agricultural University, China

*CORRESPONDENCE
Guogen Yang
yangguogen@ahau.edu.cn
Yuemin Pan
panyuemin2008@163.com

†These authors have contributed equally to this work

RECEIVED 12 November 2022
ACCEPTED 02 May 2023
PUBLISHED 05 June 2023

CITATION
Wei J, Yao C, Zhu Z, Gao Z, Yang G and Pan Y (2023) Nitrate reductase is required for sclerotial development and virulence of *Sclerotinia sclerotiorum*. *Front. Plant Sci.* 14:1096831. doi: 10.3389/fpls.2023.1096831

Nitrate reductase is required for sclerotial development and virulence of *Sclerotinia sclerotiorum*

Junjun Wei[1†], Chuanchun Yao[1†], Zonghe Zhu[2], Zhimou Gao[1], Guogen Yang[1*] and Yuemin Pan[1*]

[1]Anhui Province Key Laboratory of Integrated Pest Management on Crops, Key Laboratory of Biology and Sustainable Management of Plant Diseases and Pests of Anhui Higher Education Institutes, School of Plant Protection, Anhui Agricultural University, Hefei, China, [2]College of Agronomy, Anhui Agricultural University, Hefei, China

Sclerotinia sclerotiorum, the causal agent of Sclerotinia stem rot (SSR) on more than 450 plant species, is a notorious fungal pathogen. Nitrate reductase (NR) is required for nitrate assimilation that mediates the reduction of nitrate to nitrite and is the major enzymatic source for NO production in fungi. To explore the possible effects of nitrate reductase SsNR on the development, stress response, and virulence of *S. sclerotiorum*, RNA interference (RNAi) of *SsNR* was performed. The results showed that *SsNR*-silenced mutants showed abnormity in mycelia growth, sclerotia formation, infection cushion formation, reduced virulence on rapeseed and soybean with decreased oxalic acid production. Furthermore *SsNR*-silenced mutants are more sensitive to abiotic stresses such as Congo Red, SDS, H_2O_2, and NaCl. Importantly, the expression levels of pathogenicity-related genes *SsGgt1*, *SsSac1*, and *SsSmk3* are down-regulated in *SsNR*-silenced mutants, while *SsCyp* is up-regulated. In summary, phenotypic changes in the gene silenced mutants indicate that SsNR plays important roles in the mycelia growth, sclerotia development, stress response and fungal virulence of *S. sclerotiorum*.

KEYWORDS

***Sclerotinia sclerotiorum*, nitrate reductase, SsNR, sclerotial development, infection cushion, virulence**

Introduction

Sclerotinia sclerotiorum (Lib.) de Bary is a necrotrophic pathogen that causes white mold disease on many crops, including rapeseed, soybean, sunflower, peanut, and other economically important crops (Bolton et al., 2006). *Sclerotinia* stem rot (SSR) is one of the most important diseases on rapeseed in China, which causes significant yield losses and economic damage. SSR accounts for an estimated 10–30% of yield losses and may reach 80% in certain years. This fungus produces black sclerotia to overcome cold

winters and survival in the field for many years (Adams and Ayers, 1979). When the average temperature is cool (8–14°C) during the flowering period of rapeseed, the prolonged humid or wet conditions are conducive to carpogenic germination of sclerotia-producing apothecia to release ascospores for infection and favor disease development. Under the new policy guidelines and the increasingly negative effects of traditional chemical control, elucidating the molecular mechanism of pathogenesis of *S. sclerotiorum* may provide important information for the effective control SSR of oilseed.

Currently, most studies mainly focus on the mechanism of action of pathogenic factors, such as hydrolase and oxalic acid (OA) secreted by *S. sclerotiorum* during infection. Cutinases secreted by *S. sclerotiorum* degrade the cuticle of host plants, promoting penetrating the epidermis cells. SsCut, a cutinase produced by *S. sclerotiorum*, could cause plant cell necrosis and induce host plant resistance (Zhang et al., 2014). Many plant cell wall degradation enzymes (PCWDEs) and proteases, including cellulases, hemicellulose, pectinases, xylanases, and aspartyl protease secreted by *S. sclerotiorum* to degrade host cell wall, and pectinases have received attention, especially polygalacturonases (PGs).

S. sclerotiorum has 183 PCWDEs (including lignase), among which 33 are pectin degradation enzymes (Amselem et al., 2011; Lyu et al., 2015; Seifbarghi et al., 2017). In addition, SsXyl1 (endo-onosine-1, 4-xylanase) is involved in the pathogenesis (Yu et al., 2016). Aspartate protease SsAp1 was significantly expressed during the early stage of infection on *Brassica napus* and *Phaseolus vulgaris* (Oliveira et al., 2015; Seifbarghi et al., 2017). OA plays an important role in the process of infecting host plants; the oxaloacetic acid hydrolase (OAH1, EC 3.7.1.1) deletion mutant, although able to infect the host plants, only causes smaller necrotic leaf lesions (Liang et al., 2015b; Xu et al., 2015).

Besides, many genes also participate in the pathogenesis of *S. sclerotiorum*, such as NADPH oxidase (SsNox1 & SsNox2) related to ROS production and the accumulation of oxalic acid (Kim et al., 2011). *Ss-Ggt1* (γ-glutamyl transpeptidase) is involved in the formation of infection cushions (Li et al., 2012), Cu/Zn superoxide dismutase SsSOD1 deficient resulting in significantly decreased virulence (Veluchamy et al., 2012; Xu and Chen, 2013). Forkhead-box transcription factor SsFKH1 regulates the development of the infection cushion, and silenced mutants produce small disease spots on tomatoes (Fan et al., 2017; Cong et al., 2022). However, elicitor SsPemG1 negatively regulated the pathogenicity of *S. sclerotiorum* (Pan et al., 2015). Moreover, secreted proteins play important roles in the penetration and regulation of plant immunity response, including SsCm1, *ssv263*, SSITL, Ss-Caf1, SsCVNH, SsSSVP1, Ss-Rhs1, SsCP1, and SsCut1 (Djamei et al., 2011; Liang et al., 2013; Zhu et al., 2013; Xiao et al., 2014; Lyu et al., 2015; Lyu et al., 2016a; Yu et al., 2017; Pan et al., 2018; Yang et al., 2018; Gong et al., 2022). Furthermore, SsSSVP1 and SsCP1 have been identified as effectors and target host QCR8 and PR1, respectively (Lyu et al., 2016a; Yang et al., 2018).

Nitrogen metabolism in fungi is a strictly regulated process that allows fungi to have the ability to utilize other nitrogen sources when the desired substrate is insufficient (Bolton and Thomma, 2008). Nitrate reductase (NR) is required for nitrate assimilation in fungi that mediates the reduction of nitrate to nitrite and have been confirmed in *Aspergillus nidulans*, *Neurospora crassa*, and *Aspergillus fumigatus* (Johnstone et al., 1990; Okamoto et al., 1991; Amaar and Moore, 1998). NR is widely distributed in ectomycorrhizal (ECM) fungi to utilize nitrate as an N source even though the nitrate supply is very low (Nygren et al., 2008). While NR-silenced in mycorrhizal fungus *Laccaria bicolor* resulted in the inhibition of symbiosis with *Populus* (Kemppainen et al., 2009). The nitrate reductase (NR) gene (niaD) is required for nitric oxide (NO) production in *A. nidulans* during conidiation (Marcos et al., 2016; Franco-Cano et al., 2021), while nitrate reductase NIA1 is essential for nitrate assimilation and dispensable for pathogenicity in *Magnaporthe oryzae* (Samalova et al., 2013).

Here, we characterized an NR gene in *S. sclerotiorum* and applied RNAi technology to reveal the function of SsNR in *S. sclerotiorum*. We show that SsNR is associated with mycelium growth and pathogenesis and that SsNR knockdown results in defective infection cushion formation.

Materials and methods

Fungal strains and culture conditions

The *Sclerotinia sclerotiorum* wild-type strain FXGD2, preserved at the Fungus Laboratory of Anhui Agricultural University, was cultured on PDA. *SsNR*-silenced mutants were cultured on PDA containing 180 μg/mL hygromycin B at 25°C in the dark. *S. sclerotiorum* strains were cultured on PDA at 25°C for 3–5 days in the dark, and mycelium was collected to extract genomic DNA and RNA. The extraction procedure of total RNA of *S. sclerotiorum* was based on the instruction of E.Z.N.A.TM Total RNA Kit I from (Omega Bio-Tek, Atlanta, USA), and the extracted RNA was treated with RNAse-free DNAse I (TaKaRa Biotechnology, Dalian, China).

Gene cloning and bioinformatics analysis

BLASTp searches were performed from the *S. sclerotiorum* genome database at National Center for Biotechnology Information (NCBI). A homolog of nitrate reductase (NR) was retrieved from the *S. sclerotiorum* genome and was named SsNR (SS1G_01885). The ORF of SsNR was amplified using primer *SsNR*-F/*SsNR*-R (Table S1), then cloned into pMD19-T for sequencing. ClustalX 2.1 (Larkin et al., 2007) was used for multiple sequence alignment of the SsNR and its homologs, and the phylogenetic tree was reconstructed by MEGA11 using maximum likelihood method (Tamura et al., 2021). The conserved motifs of the nitrate reductase family were analyzed at a web resource SMART (Letunic et al., 2021).

Nucleotide acid extraction and quantitative reverse transcription-PCR

Total RNA was extracted from *S. sclerotiorum* strains according to the instruction of E.Z.N.A.TM Total RNA Kit I (Omega Bio-Tek,

USA), and contaminant genomic DNA was removed with RNAse-free DNAse I (TaKaRa, Dalian, China). qRT-PCR was performed using SYBR Green RT-PCR Kit (TaKaRa, Dalian, China) to analyze the expression level of *SsNR* during mycelium growth and sclerotia formation and to confirm the *SsNR*-silenced mutants with house-keeping gene *β-tubulin* (*SsTub*, SS1G_04652) as reference gene. For gene expression of pathogenicity-related genes *SsGgt1* (SS1G_14127), *SsSmk3* (SS1G_05445), *SsSac1* (SS1G_07715) and *SsCyp* (SS1G_06284) in *SsNR*-silenced mutants, total RNA was extracted from strains and transcribed into cDNA for qRT-PCR using CFX96 thermal cycler (Bio-Rad, CA, USA). For each gene, qRT-PCR was repeated at least twice with three biological replicates.

Construction of RNAi vector and transformation of *S. sclerotiorum*

pSilent-1, which carries a hygromycin resistance cassette, was used for hairpin RNA expression of *SsNR* (Nakayashiki et al., 2005). Two fragments amplified from cDNA using *SsNR-H-L*/SsNR-*X-R* and *SsNR-K-L*/*SsNR-S-R* (Table S1) were ligated into pSilent-1 respectively, to generate pSilent-*SsNR*. Plasmids of pSilent-*SsNR* were transferred into protoplasts of FXGD2 with polyethylene glycol (PEG)-mediated transformation (Rollins, 2003). Hygromycin-resistant colonies on RM were transferred to new PDA plates containing 45 μg/mL hygromycin B, and transformants of pSilent-1 were used as control. To confirm all putative transformants, Primers Hyg-F and Hyg-R were used to amplify the partial sequence of the hygromycin resistance gene.

Mycelia growth, sclerotia, and formation of infection cushions

For mycelia growth and sclerotia formation, wild-type, *SsNR*-silenced transformants and mock strains were inoculated on PDA plates at 25°C for 2 d or 15 d. For infection cushion formation, agar plugs of all strains were inoculated onto the surfaces of glass slides and incubated at 25°C with 100% relative humidity, the number of infection cushion were counted at 24 h. All experiments were repeated three times independently.

Determination of stress tolerance

For stress tolerance assay, fresh mycelium plugs of wild-type, *SsNR*-silenced transformants and mock strains were cultured on MM medium containing Congo Red (2 mg/mL), SDS (0.01%), sorbitol (1.2 M), NaCl (1 M), and H_2O_2 (4 mM), respectively. Colony diameters were measured every 12 h, and sclerotia formation was observed at 7 days. Experiments were repeated three times with three biological replicates.

Quantification of oxalic acid

Strains were cultured on MM medium containing 0.01% bromophenol blue for qualitative analysis of oxalic acid production. For quantification of oxalic acid, mycelium plugs of different strains were cultured in 100 mL YSPU medium at 25°C for 5 days, and the content of oxalic acid secreted in YSPU was measured by $KMnO_4$ titration method (Baker, 1952). This experiment was repeated three times.

Pathogenicity assay

Rapeseed and soybean plants were used for the pathogenicity assay of *S. slcerotiorum* wild-type, *SsNR*-silenced and mock strains. Detached leaves were inoculated with mycelia plugs (Φ=5 mm) from the margins of actively growing colonies on PDA in an incubator at 18°C and 100% relative humidity. Disease severity was calculated by lesion percentage of leaf and lesion size. These experiments were repeated three times, and each replicate was performed with three leaves.

Statistical analysis

All experiments were repeated three times. Microsoft Office 365 and SPSS v22.0 were used for statistical analysis. Statistical analysis was performed using Student's t-test and one-way analysis of variance (ANOVA).

Results

SsNR is a putative nitrate reductase

A nitrate reductase SsNR was identified from the *S. scelrotiorum* genome, and the ORF of *SsNR* is 2733 bp in length, encoding 910 amino acids. SsNR, like other nitrate reductases, has five functional domains: Oxidored_molyb structural domain (122-298 aa), Mo-co_dimer structural domain (326-475 aa), Cyt-b5 structural domain (541- 613 aa), FAD_binding_6 structural domain (645-751 aa) and NAD_binding_1 structural domain (771-895 aa) (Figure 1A). Phylogenetic analysis indicated that orthologs of SsNR are widely distributed in fungi and plant (Figure 1B).

SsNR is essential for mycelium growth and sclerotial development

qRT-PCR was used for *SsNR* expression analysis during hyphal growth and six stages of sclerotial formation: (S1) initiation, (S2) condensation, (S3) enlargement, (S4) consolidation, (S5) pigmentation, and (S6) maturation (Li and Rollins, 2009). Our qRT-PCR results showed that *SsNR* is highly expressed from S1 to S6. The transcript level increased by 1060%, 1124%, 717%, 96%, 98%, and 1888%, respectively, indicating that SsNR might be involved in the sclerotial development of *S. sclerotiorum* (Figure 2). We performed PEG-mediated transformation. We obtained 82 transformants that could grow on PDA-containing hygromycin. *SsNR*-silenced mutants were confirmed by qRT-PCR, and two mutants (NR12 and NR66) were chosen for analysis in which the expression of *SsNR* decreased by

10.3389/fpls.2023.1096831

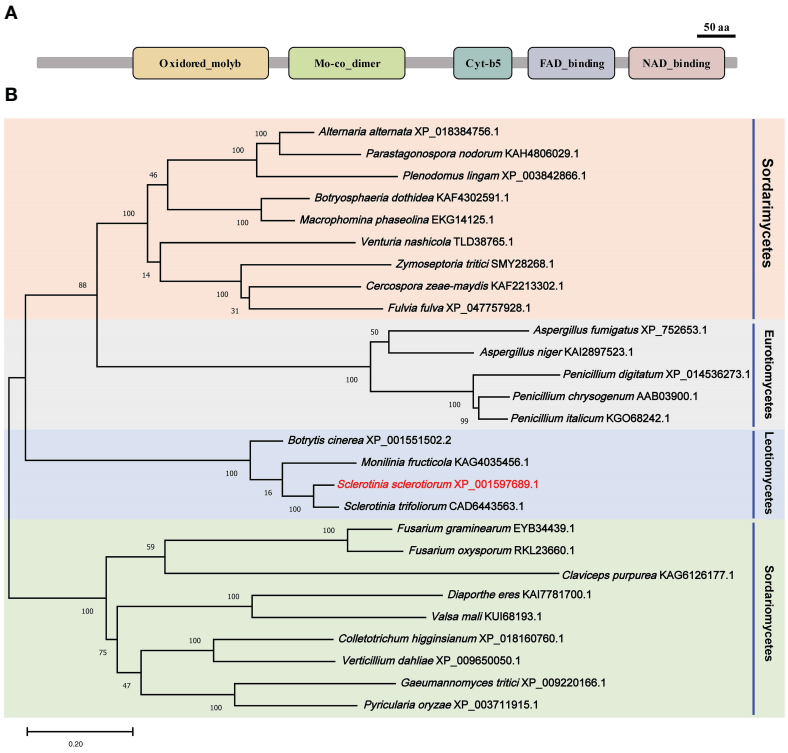

FIGURE 1
Functional domain identification and phylogenetic tree reconstruction. **(A)** Functional domains of SsNR were identified by searching SMART containing an Oxidored_molyb, Mo-co_dimer, Cyt-b5 domain, FAD_binding_6 domain, and NAD_binding_1. **(B)** Phylogenetic tree reconstructed using the maximum likelihood (ML) method with 1,000 bootstraps.

76.5% and 66.3%, respectively (Figure 3A). *SsNR*-silenced mutants exhibited slower mycelial growth compared to wild-type and mock strain (Figure 3B). The wild-type and mock strain produced sclerotia in 6 days post-inoculation, but *SsNR*-silenced mutants produced few sclerotia or did not form scerotia, indicating that SsNR was involved in mycelium growth and sclerotial development (Figure 3B).

SsNR is involved in response to Congo red, SDS, NaCl, and H_2O_2

To check the potential role of nitrate reductase in the cell wall and membrane integrity of *S. sclerotiorum*, *SsNR*-silenced mutants were cultured on MM containing Congo Red (2 mg/mL) and SDS

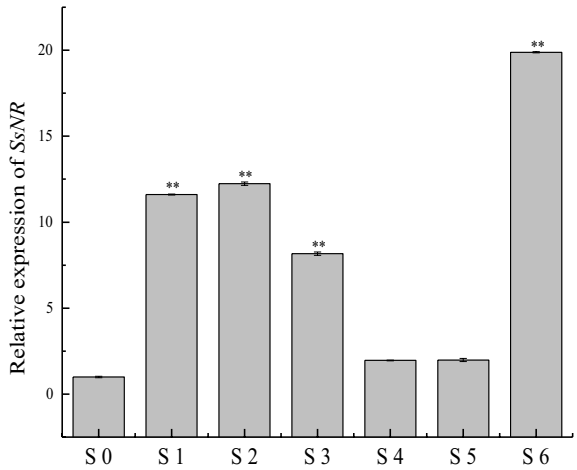

FIGURE 2
qRT-PCR analysis of the expression of *SsNR* in different stages of *S. sclerotiorum*. S0 = the hyphal stage of *S. sclerotiorum*; S1 = the initiation stage of sclerotial development; S2 = condensation stage; S3 = enlargement stage; S4 = consolidation stage; S5 = pigmentation stage; S6 = maturation stage. The expression level of SsNR cDNA measured by qRT-PCR was standardized with the housekeeping gene *S. sclerotiorum β-tubulin*. The abundance of cDNA from S0 samples was assigned a value of 1. Bars indicate standard error. Statistical significance is indicated: **, $P < 0.01$.

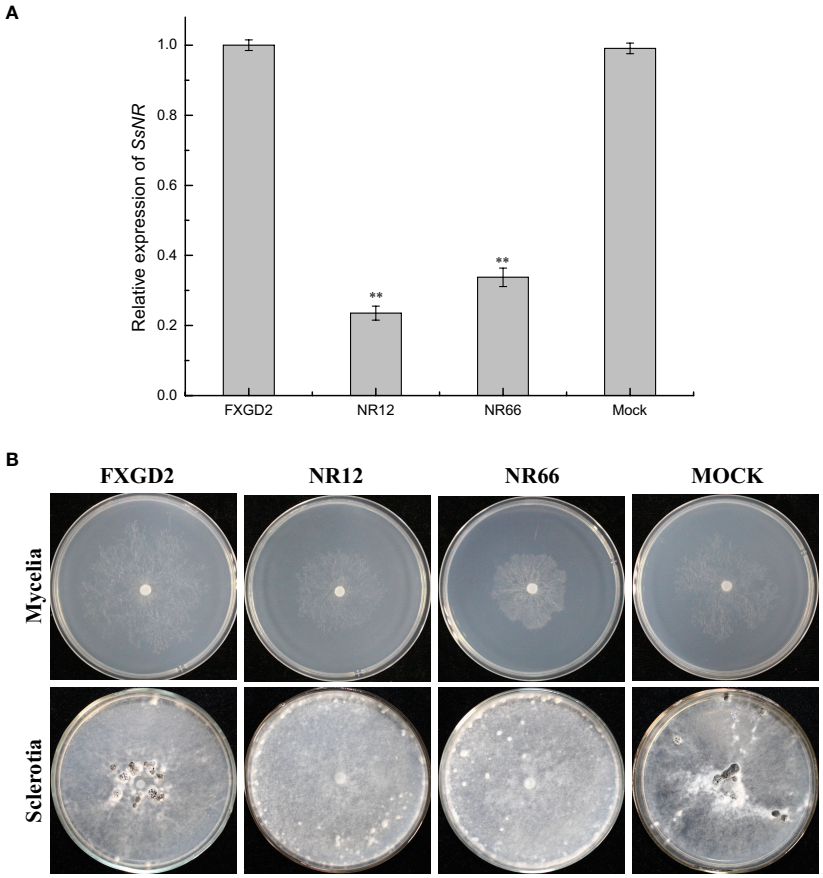

FIGURE 3
SsNR-silenced impaired hyphae growth and sclerotia development. **(A)** qRT-PCR analysis of the expression of *SsNR* in WT, *SsNR*-silenced mutants and mock. Statistical significance is indicated: **, $P < 0.01$. **(B)** Colony morphology of WT, *SsNR*-silenced mutants and mock cultured on PDA at 25°C. Photos were taken at 2 dpi, and the sclerotia of WT, *SsNR*-silenced mutants and mock cultured on PDA at 25°C. Photos were taken at 10 dpi.

(0.01%), respectively. Under Congo Red treatment, the colony diameter of *SsNR*-silenced mutants is about 1.85 and 2.72 cm, much smaller than the wild-type (4.93 cm) and mock strain (4.67 cm). Similarly, *SsNR*-silenced mutants grew much slower than wild-type and mock strain on an SDS-amended medium. The colony diameters of wild-type, mock strain and *SsNR*-silenced mutants (NR12 and NR66) were 5.75, 5.45, 3.3, and 4.1, respectively (Figure 4). These results showed that SsNR is required for cell wall integrity.

We also detect the response of different strains to other stress -including chemicals, such as sorbitol, NaCl, and H_2O_2. The results showed that colony morphology of *SsNR*-silenced mutants did not change on MM containing sorbitol and that the mycelium growth and sclerotial development were not affected, indicating that SsNR is not associated with osmotic pressure (Figure 4). NaCl at 1 M could significantly inhibit mycelium growth of *SsNR*-silenced mutants compared to wild-type and mock. Likewise, in *SsNR*-silenced mutants grown on MM containing H_2O_2, the diameter of the colony was much smaller (3.1 and 4.6 cm) compared to wild-type (6.0 cm), indicating that SsNR has the function of tolerance to H_2O_2 (Figure 4).

SsNR is associated with hyphal branching and infection cushion development

For *SsNR*-silenced mutants that exhibited abnormal colony morphology, we detected the hyphal tip under a microscope to determine whether SsNR affects hyphal growth (Figure 5A). The result showed that the hyphal branching of *SsNR*-silenced mutants increased in the number of tips, and the hyphal diaphragm was shortened compared to the wild-type. The infection cushions played important roles during penetration of *S. sclerotiorum*; we detected the number of infection cushions produced by different strains on hydrophobic surfaces that the *SsNR*-silenced mutants produce less and smaller infection cushions compared to WT (Figures 5B, C). These results indicated that SsNR plays an important role in infection cushions formation.

SsNR is required for virulence and oxalic acid accumulation

For SsNR is associated with mycelium growth, we also performed a pathogenicity assay on detached leaves of rapeseed

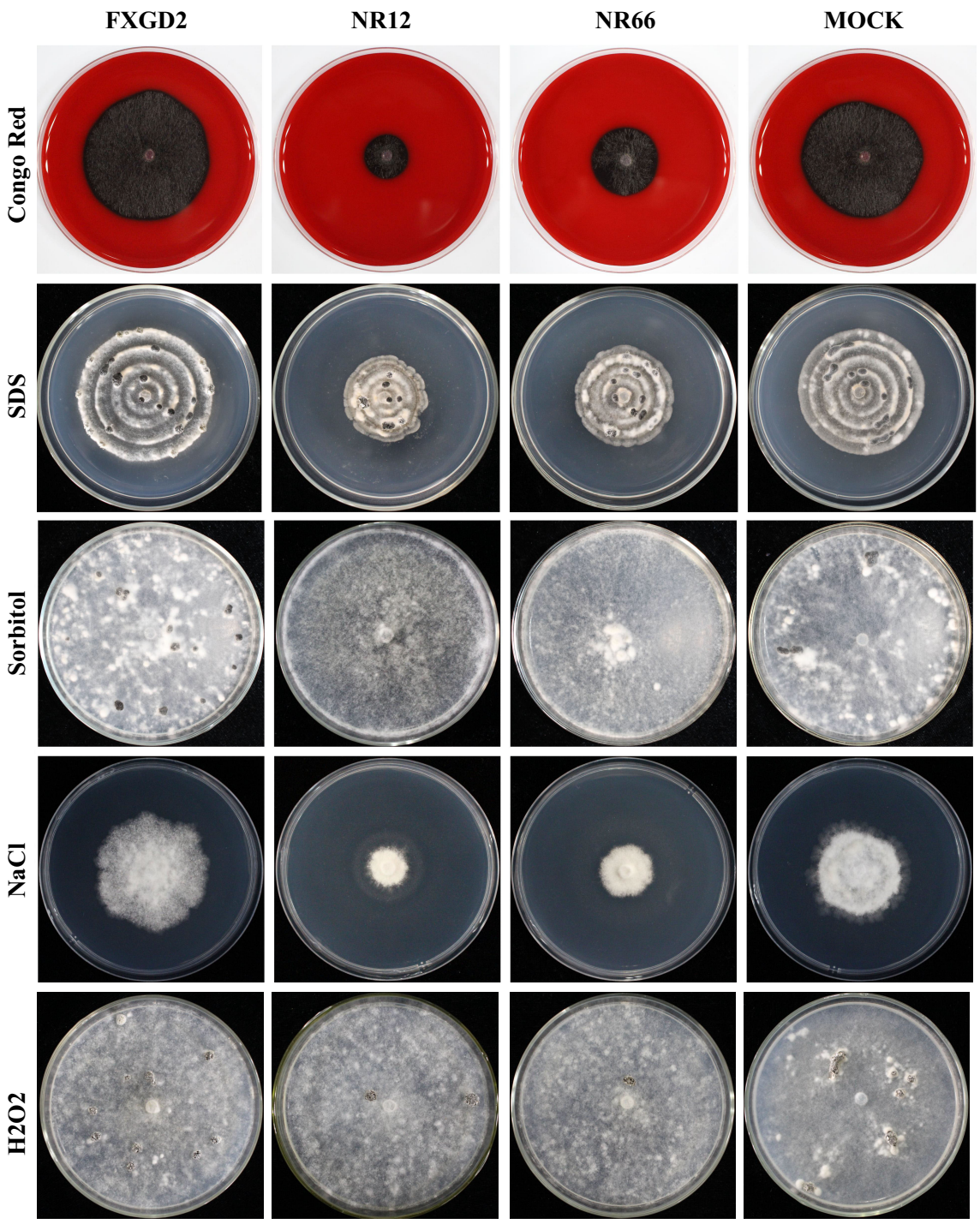

FIGURE 4
Tolerance of WT, *SsNR*-silenced mutants and mock to different chemicals. The phenotype of WT, *SsNR*-silenced mutants and mock grown on MM supplemented with 2 mg/mL Congo Red, 0.01% SDS, 1.2 M Sorbitol and 1 M NaCl and 4 mM H_2O_2. Photos were taken at 1 dpi, 5 dpi, 7 dpi, 2 dpi, and 7 dpi, respectively.

and soybean plants. The results showed that SsNR-silenced mutants could produce lesions on leaves of both rapeseed and soybean (12.64%~13.12% and 44.36%~56.50%), but the lesion size of mutants was much smaller (3.28%~4.73% and 14.39%~15.72%) than wild-type and mock strains, indicating that SsNR is required for infection of *S. sclerotiorum* (Figure 6).

Oxalic acid plays an important role in pathogenicity during infection. All strains were cultured on a medium containing bromophenol to determine the OA in wild-type and SsNR-silenced mutants. The diameters of the yellow zone produced by silenced transformants NR12 and NR66 were about 2.3 and 4.1 cm, respectively, which were significantly smaller than those of the wild-

10.3389/fpls.2023.1096831

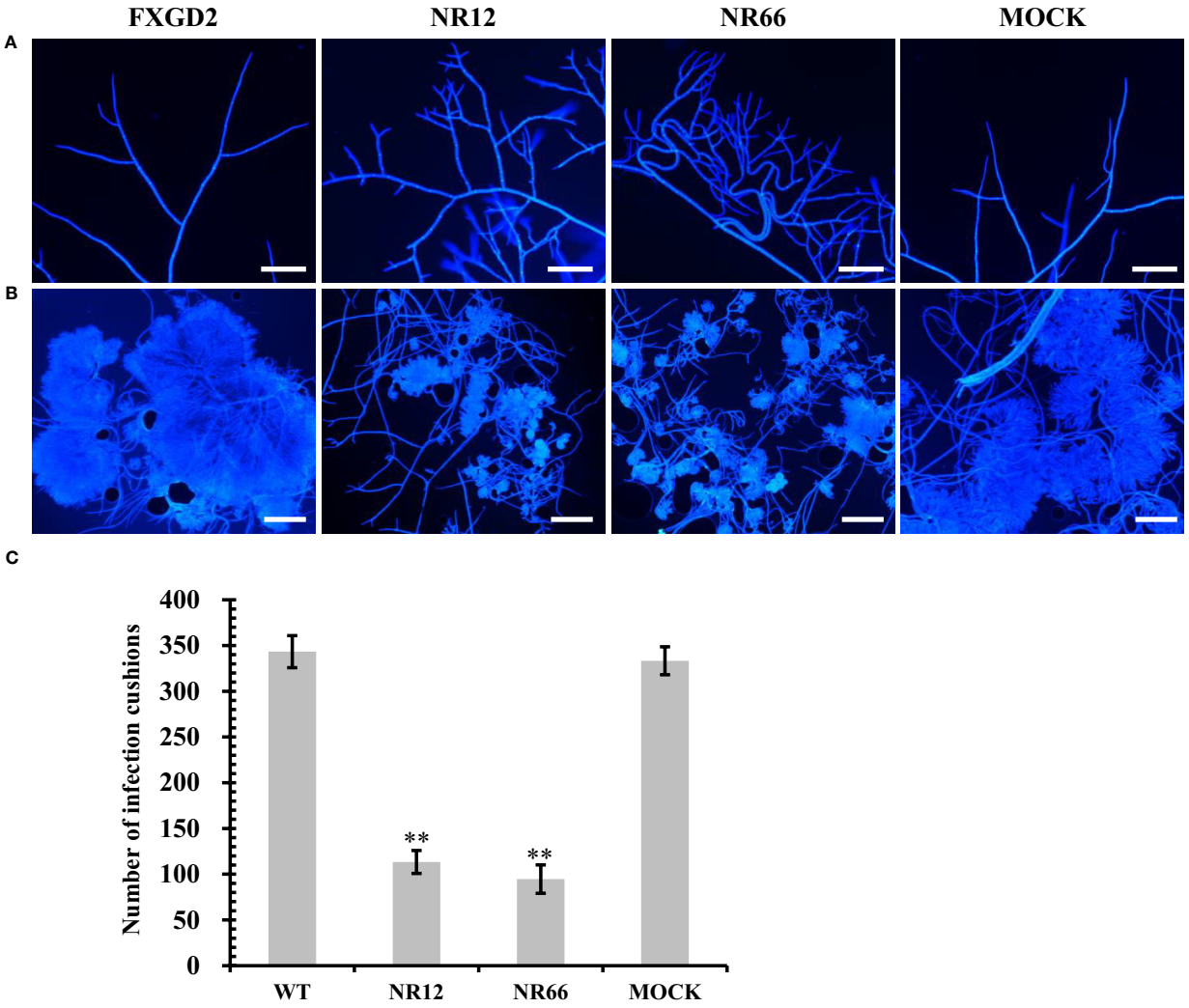

FIGURE 5
Mycelial growth and infection cushion formation of *SsNR*-silenced mutants. **(A)** Hyphal branching and tips stained of all strains were observed under a light microscope. **(B)** Infection cushions stained of all strains were observed under a light microscope. **(C)** Number of infection cushion produced by all strains. Bar = 100 µm, hyphae and infection cushions were by Calcofluor white (CFW) (10 µg/mL). Statistical significance is indicated: **, $P < 0.01$.

type (5.7 cm) and mock control (5.6 cm) (Figure 6). Also, the concentration OA of all strains were determined by $KmnO_4$ titration, results showed that OA concentration of NR12 and NR66 were 16.65 mg and 36.9 mg in 100 ml medium, respectively, while those of wild-type and mock strain were 97.35 mg and 97.05 mg, respectively (Figure 6). These results showed that SsNR is important for OA production.

Regulation of the expression of pathogenicity-related genes of *S. sclerotiorum*

To investigate whether *SsNR*-silencing affects the transcriptional expression levels of other pathogenicity-related genes, *Ggt1*, *Sac1*, *Smk3*, and *CYP*, were analyzed by qRT-PCR. The results showed that the expression levels of *Ggt1*, *Sac1*, and *Smk3* in *SsNR*-silenced mutants were decreased by 96%~98%, 65%~74%, and 56%~72%, respectively. At the same time, the expression level of *CYP* was increased by 230%~440% (Figure 7).

Discussion

Nitrate reductase is an enzyme that catalyzes the reduction of nitrate to nitrite and is the major enzymatic source for NO production in fungi (Cánovas et al., 2016). The nitrate reductase SsNR of *S. sclerotiorum* was studied using sequence analysis and RNAi technology which could be a good approach for gene function analysis in this fungus (Lyu et al., 2016a; Rana et al., 2021). *SsNR*-silenced mutants exhibited altered phenotypes, including hyphal growth and sclerotia development. We performed a pathogenicity assay on detached leaves of rapeseed and soybean plants; although the *SsNR*-silenced mutants could penetrate the host cell, they produced smaller lesions than WT.

SsNR-silenced mutants exhibited increased hyphal branching tips and shortened hyphal diaphragm, and diminished sclerotia

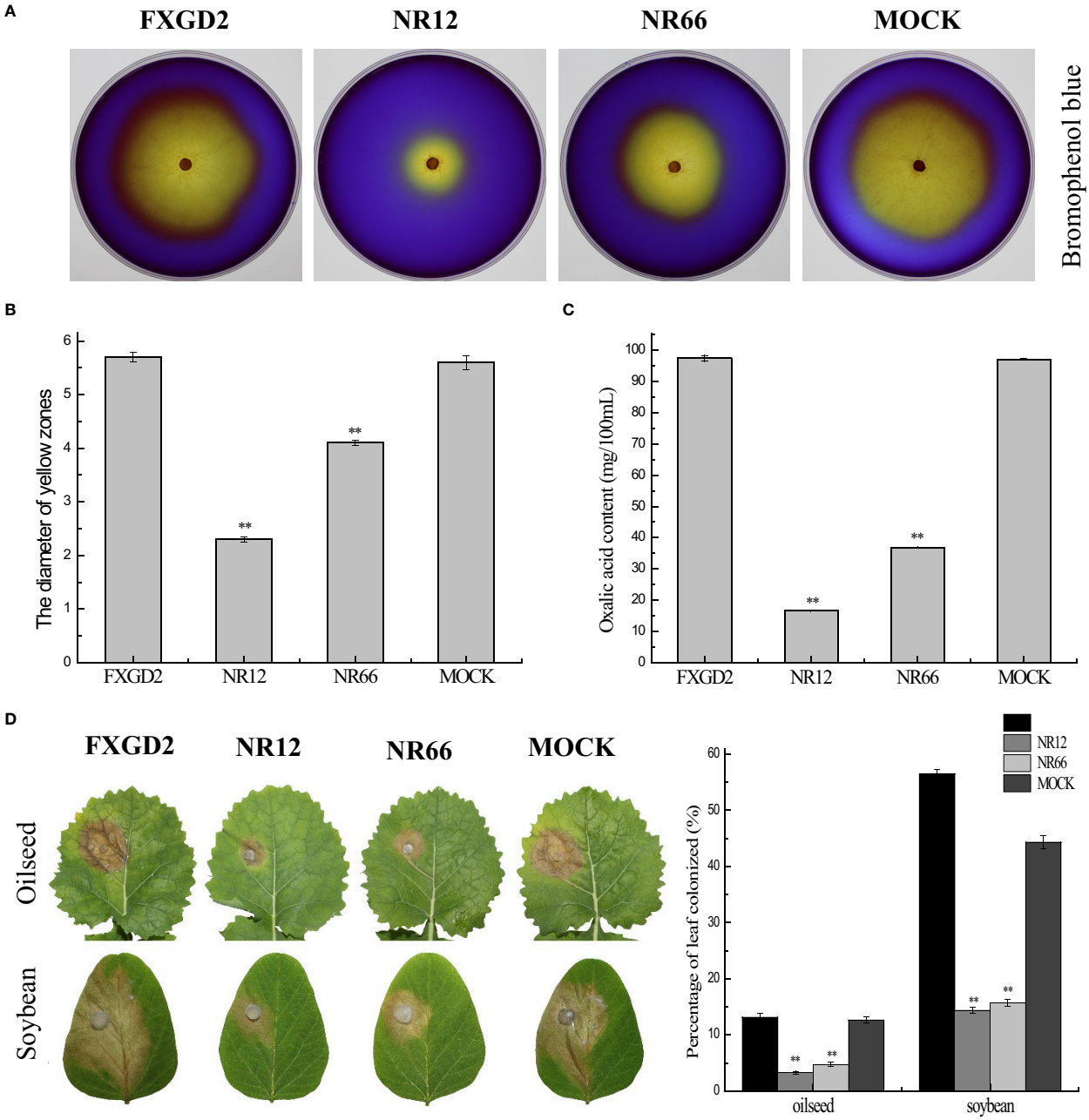

FIGURE 6
SsNR is required for virulence and accumulation of oxalic acid in *S. sclerotiorum*. **(A)** Morphology of WT, *SsNR*-silenced mutants and mock grown on MM supplemented with 0.01% bromophenol blue. Photos were taken at 2 dpi. **(B)** The diameters of the yellow zone produced by WT, *SsNR*-silenced mutants and mock (2 dpi). **(C)** Oxalic acid concentration of WT, *SsNR*-silenced mutants and mock cultured in liquid medium 5 days. **(D)** The percentages of lesion area produced by WT, *SsNR*-silenced mutants and mock-inoculated on detached leaves of oilseed rape and soybean (48 hpi). Statistical significance is indicated: **, P < 0.01.

development (Figure 3). These results indicated that mycelium growth might be related to sclerotia development, and these phenomena are also observed in knockout or knock down mutants of other genes, such as *Sop1*, *Ss-Sl2*, *SsFkh1*, *SCD1*, and *THR1* (Yu et al., 2012; Lyu et al., 2016b; Fan et al., 2017; Yue et al., 2018). Also, endogenous small RNAs may regulate genes controlling sclerotial development (Xia et al., 2020). Nitrate reductase *SsNR*-silenced mutants may affect nitrogen metabolism and protein synthesis, which might cause abnormal hyphal growth and sclerotia formation. An infection cushion (or compound appressorium) is required for infection, which is the primary means of infection initiation by *S. sclerotiorum* to breach the cuticle layer of the host epidermal cell (Huang et al., 2008). *SsNR*-silenced mutants produced less infection cushion on parafilm. SsNR could regulate the development of infection cushion accomplished with decreased virulence (Figure 5). Several genes have been reported in regulating infection cushion development, such as *Sac1*, *Ss-caf1*, *Ss-oah1*, *Ss-odc2*, and *Smk3* (Jurick and Rollins, 2007; Li et al., 2012; Xiao et al., 2014; Liang et al., 2015a; Liang et al., 2015b; Bashi et al., 2016),

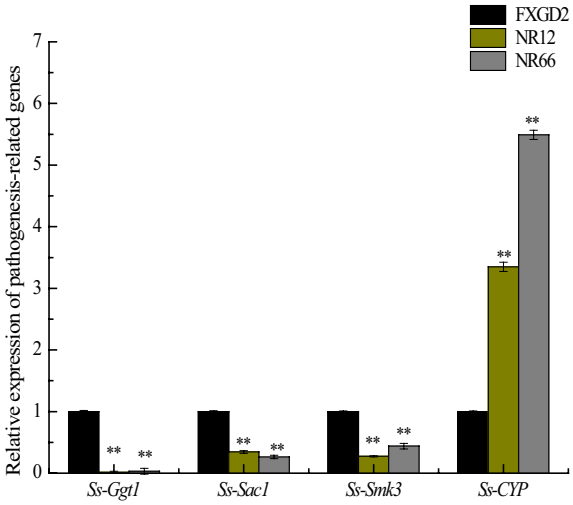

FIGURE 7
The expression of *SsGgt1*, *SsSac1*, *SsSmk3*, and *SsCYP* in different strains using *β-tubulin* as a reference gene. Statistical significance is indicated: **, P < 0.01.

meanwhile *Ggt1*, *Sac1*, and *Smk3* are downregulated in *SsNR*-silenced mutants, indicating that SsNR is involved in the expression of infection cushion development-related genes in fine-tuning the infection cushion formation process during penetration of *S. sclerotiorum*.

OA is important for infection of *S. sclerotiorum* primarily in acidifying the microenvironment in infection (Xu et al., 2018), in addition to other roles, including chelation with Ca^{2+}, regulation stomatal closure, inhibition of reactive oxygen species (ROS) bursting, promotion of apoptosis, and repression autophagy of plant cell (Rollins and Dickman, 2001; Guimaraes and Stotz, 2004; Williams et al., 2011; Kabbage et al., 2013; Uloth et al., 2015; Derbyshire et al., 2022). OA production of *SsNR*-silenced mutants decreased compared to WT; we proposed that SsNR may play an important role in OA accumulation, implying that SsNR regulated the pathogenicity of *S. sclerotiorum* through oxalic acid secretion. For decreased OA concentration, *SsNR*-silenced mutants produced fewer infection cushions and impaired function of OA during plant-*Sclerotinia* interaction, causing debilitation in virulence. Moreover, cell wall integrity (CWI) is required in fungi to adapt to perturbing conditions, including osmotic pressure, heat, oxidative stress, and antifungals (Dichtl et al., 2016). *SsNR*-silenced mutants were more sensitive to Congo Red, SDS, and NaCl than the wild type, indicating impaired CWI. Reactive oxygen species (ROS) played important roles in plant immunity (Qi et al., 2017), while *SsNR*-silenced mutants showed more sensitivity to H_2O_2 compared to WT resulting in decreased virulence in plants (soybean and rapeseed). Similar results were obtained in the tea leaf spot which is caused by *Didymella segeticola*, the antimicrobial kasugamycin inhibits the pathogen by binding to NR, disturbing fungal metabolism with changes in hyphal growth and development (Jiang et al., 2022).

Conclusion

SsNR is essential for normal mycelium growth, sclerotia development, and virulence by regulating OA production and expression of pathogenesis-related genes involved in the infection of *S. sclerotiorum*.

Data availability statement

The original contributions presented in the study are included in the article/Supplementary Material. Further inquiries can be directed to the corresponding authors.

Author contributions

ZG, GY, and YP designed the research. JW and CY conducted the experiments and data analysis. JW, CY, ZZ, ZG, GY, and YP wrote and revised the manuscript. All authors scrutinized and corrected the manuscript. All authors contributed to the article and approved the submitted version.

Funding

This research was supported by Anhui Provincial Natural Science Foundation (2008085MC76), the National Natural Science Foundation of China (31801676), the Natural Science Foundation of Anhui Higher Education Institutions of China (KJ2016A229), and The Research and Development Program of China (2018YFD0200900).

Acknowledgments

We thank Prof. Zhengguang Zhang of the Department of Plant Pathology, Nanjing Agricultural University, Nanjing, China, for the gift of the vector pSilent-1.

Conflict of interest

The authors declare that the research was conducted in the absence of any commercial or financial relationships that could be construed as a potential conflict of interest.

Publisher's note

All claims expressed in this article are solely those of the authors and do not necessarily represent those of their affiliated organizations, or those of the publisher, the editors and the reviewers. Any product that may be evaluated in this article, or claim that may be made by its manufacturer, is not guaranteed or endorsed by the publisher.

Supplementary material

The Supplementary Material for this article can be found online at: https://www.frontiersin.org/articles/10.3389/fpls.2023.1096831/full#supplementary-material

References

Adams, P. B., and Ayers, W. A. (1979). Ecology of *Sclerotinia* species. *Phytopathology* 69 (8), 896–899. doi: 10.1094/Phyto-69-896

Amaar, Y. G., and Moore, M. M. (1998). Mapping of the nitrate-assimilation gene cluster (crnA-niiA-niaD) and characterization of the nitrite reductase gene (niiA) in the opportunistic fungal pathogen *Aspergillus fumigatus*. *Curr. Genet.* 33 (3), 206–215. doi: 10.1007/s002940050328

Amselem, J., Cuomo, C. A., van Kan, J. A., Viaud, M., Benito, E. P., Couloux, A., et al. (2011). Genomic analysis of the necrotrophic fungal pathogens *Sclerotinia sclerotiorum* and *Botrytis cinerea*. *PLoS Genet.* 7 (8), e1002230. doi: 10.1371/journal.pgen.1002230

Baker, C. J. L. (1952). The determination of oxalates in fresh plant material. *Analyst* 77 (916), 340–344. doi: 10.1039/AN9527700340

Bashi, Z. D., Gyawali, S., Bekkaoui, D., Coutu, C., Lee, L., Poon, J., et al. (2016). The *Sclerotinia sclerotiorum Slt2* mitogen-activated protein kinase ortholog, *SMK3*, is required for infection initiation but not lesion expansion. *Can. J. Microbiol.* 62 (10), 836–850. doi: 10.1139/cjm-2016-0091

Bolton, M. D., and Thomma, B. P. H. J. (2008). The complexity of nitrogen metabolism and nitrogen-regulated gene expression in plant pathogenic fungi. *Physiol. Mol. Plant Pathol.* 72 (4), 104–110. doi: 10.1016/j.pmpp.2008.07.001

Bolton, M. D., Thomma, B. P. H. J., and Nelson, B. D. (2006). *Sclerotinia sclerotiorum* (Lib.) de bary: biology and molecular traits of a cosmopolitan pathogen. *Mol. Plant Pathol.* 7 (1), 1–16. doi: 10.1111/j.1364-3703.2005.00316.x

Cánovas, D., Marcos, J. F., Marcos, A. T., and Strauss, J. (2016). Nitric oxide in fungi: is there NO light at the end of the tunnel? *Curr. Genet.* 62 (3), 513–518. doi: 10.1007/s00294-016-0574-6

Cong, J., Xiao, K., Jiao, W., Zhang, C., Zhang, X., Liu, J., et al. (2022). The coupling between cell wall integrity mediated by MAPK kinases and SsFkh1 is involved in sclerotia formation and pathogenicity of *Sclerotinia sclerotiorum*. *Front. Microbiol.* 13. doi: 10.3389/fmicb.2022.816091

Derbyshire, M. C., Newman, T. E., Khentry, Y., and Taiwo, A. O. (2022). The evolutionary and molecular features of the broad-host-range plant pathogen sclerotinia sclerotiorum. *Mol. Plant Pathol.* 23 (8), 1075–1090. doi: 10.1111/mpp.13221

Dichtl, K., Samantaray, S., and Wagener, J. (2016). Cell wall integrity signalling in human pathogenic fungi. *Cell. Microbiol.* 18 (9), 1228–1238. doi: 10.1111/cmi.12612

Djamei, A., Schipper, K., Rabe, F., Ghosh, A., Vincon, V., Kahnt, J., et al. (2011). Metabolic priming by a secreted fungal effector. *Nature* 478 (7369), 395–398. doi: 10.1038/nature10454

Fan, H., Yu, G., Liu, Y., Zhang, X., Liu, J., Zhang, Y., et al. (2017). An atypical forkhead-containing transcription factor SsFKH1 is involved in sclerotial formation and is essential for pathogenicity in *Sclerotinia sclerotiorum*. *Mol. Plant Pathol.* 18 (7), 963–975. doi: 10.1111/mpp.12453

Franco-Cano, A., Marcos, A. T., Strauss, J., and Cánovas, D. (2021). Evidence for an arginine-dependent route for the synthesis of NO in the model filamentous fungus *Aspergillus nidulans*. *Environ. Microbiol.* 23 (11), 6924–6939. doi: 10.1111/1462-2920.15733

Gong, Y., Fu, Y., Xie, J., Li, B., Chen, T., Lin, Y., et al. (2022). *Sclerotinia sclerotiorum* SsCut1 modulates virulence and cutinase activity. *J. Fungi* 8 (5), 526. doi: 10.3390/jof8050526

Guimaraes, R. L., and Stotz, H. U. (2004). Oxalate production by *Sclerotinia sclerotiorum* deregulates guard cells during infection. *Plant Physiol.* 136 (3), 3703–3711. doi: 10.1104/pp.104.049650

Huang, L., Buchenauer, H., Han, Q., Zhang, X., and Kang, Z. (2008). Ultrastructural and cytochemical studies on the infection process of *Sclerotinia sclerotiorum* in oilseed rape. *J. Plant Dis. Prot.* 115 (1), 9–16. doi: 10.1007/BF03356233

Jiang, X., Jiang, S., Huang, H., Li, D., Yang, R., Yang, Y., et al. (2022). Multi-omics analysis reveals that the antimicrobial kasugamycin potential targets nitrate reductase in *Didymella segeticola* to achieve control of tea leaf spot. *Phytopathology* 112 (9), 1894–1906. doi: 10.1094/PHYTO-11-21-0457-R

Johnstone, I. L., McCabe, P. C., Greaves, P., Gurr, S. J., Cole, G. E., Brow, M. A. D., et al. (1990). Isolation and characterisation of the crnA-niiA-niaD gene cluster for nitrate assimilation in *Aspergillus nidulans*. *Gene* 90 (2), 181–192. doi: 10.1016/0378-1119(90)90178-T

Jurick, W. M.II, and Rollins, J. A. (2007). Deletion of the adenylate cyclase (*sac1*) gene affects multiple developmental pathways and pathogenicity in *Sclerotinia sclerotiorum*. *Fungal Genet. Biol.* 44 (6), 521–530. doi: 10.1016/j.fgb.2006.11.005

Kabbage, M., Williams, B., and Dickman, M. B. (2013). Cell death control: the interplay of apoptosis and autophagy in the pathogenicity of *Sclerotinia sclerotiorum*. *PLoS Pathog.* 9 (4), e1003287. doi: 10.1371/journal.ppat.1003287

Kemppainen, M., Duplessis, S., Martin, F., and Pardo, A. G. (2009). RNA Silencing in the model mycorrhizal fungus *Laccaria bicolor*: gene knock-down of nitrate reductase results in inhibition of symbiosis with *Populus*. *Environ. Microbiol.* 11 (7), 1878–1896. doi: 10.1111/j.1462-2920.2009.01912.x

Kim, H.-j., Chen, C., Kabbage, M., and Dickman, M. B. (2011). Identification and characterization of *Sclerotinia sclerotiorum* NADPH oxidases. *Appl. Environ. Microbiol.* 77 (21), 7721–7729. doi: 10.1128/aem.05472-11

Larkin, M. A., Blackshields, G., Brown, N. P., Chenna, R., McGettigan, P. A., McWilliam, H., et al. (2007). Clustal W and clustal X version 2.0. *Bioinformatics* 23 (21), 2947–2948. doi: 10.1093/bioinformatics/btm404

Letunic, I., Khedkar, S., and Bork, P. (2021). SMART: recent updates, new developments and status in 2020. *Nucleic Acids Res.* 49 (D1), D458–D460. doi: 10.1093/nar/gkaa937

Li, M., Liang, X., and Rollins, J. A. (2012). *Sclerotinia sclerotiorum* γ-glutamyl transpeptidase (Ss-Ggt1) is required for regulating glutathione accumulation and development of sclerotia and compound appressoria. *Mol. Plant-Microbe Interact.* 25 (3), 412–420. doi: 10.1094/mpmi-06-11-0159

Li, M., and Rollins, J. A. (2009). The development-specific protein (Ssp1) from *Sclerotinia sclerotiorum* is encoded by a novel gene expressed exclusively in sclerotium tissues. *Mycologia* 101 (1), 34–43. doi: 10.3852/08-114

Liang, X., Liberti, D., Li, M., Kim, Y.-T., Hutchens, A., Wilson, R., et al. (2015b). Oxaloacetate acetylhydrolase gene mutants of *Sclerotinia sclerotiorum* do not accumulate oxalic acid, but do produce limited lesions on host plants. *Mol. Plant Pathol.* 16 (6), 559–571. doi: 10.1111/mpp.12211

Liang, X., Moomaw, E. W., and Rollins, J. A. (2015a). Fungal oxalate decarboxylase activity contributes to *Sclerotinia sclerotiorum* early infection by affecting both compound appressoria development and function. *Mol. Plant Pathol.* 16 (8), 825–836. doi: 10.1111/mpp.12239

Liang, Y., Yajima, W., Davis, M. R., Kav, N. N. V., and Strelkov, S. E. (2013). Disruption of a gene encoding a hypothetical secreted protein from *Sclerotinia sclerotiorum* reduces its virulence on canola (*Brassica napus*). *Can. J. Plant Pathol.* 35 (1), 46–55. doi: 10.1080/07060661.2012.745904

Lyu, X., Shen, C., Fu, Y., Xie, J., Jiang, D., Li, G., et al. (2015). Comparative genomic and transcriptional analyses of the carbohydrate-active enzymes and secretomes of phytopathogenic fungi reveal their significant roles during infection and development. *Sci. Rep.* 5, 15565. doi: 10.1038/srep15565

Lyu, X., Shen, C., Fu, Y., Xie, J., Jiang, D., Li, G., et al. (2016a). A small secreted virulence-related protein is essential for the necrotrophic interactions of *Sclerotinia sclerotiorum* with its host plants. *PLoS Pathog.* 12 (2), e1005435. doi: 10.1371/journal.ppat.1005435

Lyu, X., Shen, C., Fu, Y., Xie, J., Jiang, D., Li, G., et al. (2016b). The microbial opsin homolog *Sop1* is involved in *Sclerotinia sclerotiorum* development and environmental stress response. *Front. Microbiol.* 6 (1504). doi: 10.3389/fmicb.2015.01504

Marcos, A. T., Ramos, M. S., Marcos, J. F., Carmona, L., Strauss, J., and Cánovas, D. (2016). Nitric oxide synthesis by nitrate reductase is regulated during development in *Aspergillus*. *Mol. Microbiol.* 99 (1), 15–33. doi: 10.1111/mmi.13211

Nakayashiki, H., Hanada, S., Quoc, N. B., Kadotani, N., Tosa, Y., and Mayama, S. (2005). RNA Silencing as a tool for exploring gene function in ascomycete fungi. *Fungal Genet. Biol.* 42 (4), 275–283. doi: 10.1016/j.fgb.2005.01.002

Nygren, C. M. R., Eberhardt, U., Karlsson, M., Parrent, J. L., Lindahl, B. D., and Taylor, A. F. S. (2008). Growth on nitrate and occurrence of nitrate reductase-encoding genes in a phylogenetically diverse range of ectomycorrhizal fungi. *New Phytol.* 180 (4), 875–889. doi: 10.1111/j.1469-8137.2008.02618.x

Okamoto, P. M., Fu, Y.-H., and Marzluf, G. A. (1991). Nit-3, the structural gene of nitrate reductase in *Neurospora crassa*: nucleotide sequence and regulation of mRNA synthesis and turnover. *Mol. Gen. Genet.* 227 (2), 213–223. doi: 10.1007/bf00259673

Oliveira, M. B., de Andrade, R. V., Grossi-de-Sá, M. F., and Petrofeza, S. (2015). Analysis of genes that are differentially expressed during the *Sclerotinia sclerotiorum*–*Phaseolus vulgaris* interaction. *Front. Microbiol.* 6. doi: 10.3389/fmicb.2015.01162

Pan, Y., Wei, J., Yao, C., Reng, H., and Gao, Z. (2018). SsSm1, a cerato-platanin family protein, is involved in the hyphal development and pathogenic process of *Sclerotinia sclerotiorum*. *Plant Sci.* 270, 37–46. doi: 10.1016/j.plantsci.2018.02.001

Pan, Y., Xu, Y., Li, X., Yao, C., and Gao, Z. (2015). SsPemG1 encodes an elicitor-homologous protein and regulates pathogenicity in *Sclerotinia sclerotiorum*. *Physiol. Mol. Plant Pathol.* 92, 70–78. doi: 10.1016/j.pmpp.2015.08.010

Qi, J., Wang, J., Gong, Z., and Zhou, J.-M. (2017). Apoplastic ROS signaling in plant immunity. *Curr. Opin. Plant Biol.* 38, 92–100. doi: 10.1016/j.pbi.2017.04.022

Rana, K., Ding, Y., Banga, S. S., Liao, H., Zhao, S., Yu, Y., et al. (2021). *Sclerotinia sclerotiorum* Thioredoxin1 (SsTrx1) is required for pathogenicity and oxidative stress tolerance. *Mol. Plant Pathol.* 22 (11), 1413–1426. doi: 10.1111/mpp.13127

Rollins, J. A. (2003). The *Sclerotinia sclerotiorum pac1* gene is required for sclerotial development and virulence. *Mol. Plant-Microbe Interact.* 16 (9), 785–795. doi: 10.1094/Mpmi.2003.16.9.785

Rollins, J. A., and Dickman, M. B. (2001). pH signaling in *Sclerotinia sclerotiorum*: identification of a *pacC/RIM1* homolog. *Appl. Environ. Microbiol.* 67 (1), 75–81. doi: 10.1128/aem.67.1.75-81.2001

Samalova, M., Johnson, J., Illes, M., Kelly, S., Fricker, M., and Gurr, S. (2013). Nitric oxide generated by the rice blast fungus *Magnaporthe oryzae* drives plant infection. *New Phytol.* 197 (1), 207–222. doi: 10.1111/j.1469-8137.2012.04368.x

Seifbarghi, S., Borhan, M. H., Wei, Y., Coutu, C., Robinson, S. J., and Hegedus, D. D. (2017). Changes in the *Sclerotinia sclerotiorum* transcriptome during infection of *Brassica napus*. *BMC Genomics* 18 (1), 266. doi: 10.1186/s12864-017-3642-5

Tamura, K., Stecher, G., and Kumar, S. (2021). MEGA11: molecular evolutionary genetics analysis version 11. *Mol. Biol. Evol.* 38 (7), 3022–3027. doi: 10.1093/molbev/msab120

Uloth, M. B., Clode, P. L., You, M. P., and Barbetti, M. J. (2015). Calcium oxalate crystals: an integral component of the *Sclerotinia sclerotiorum*/*Brassica carinata* pathosystem. *PLoS One* 10 (3), e0122362. doi: 10.1371/journal.pone.0122362

Veluchamy, S., Williams, B., Kim, K., and Dickman, M. B. (2012). The CuZn superoxide dismutase from *Sclerotinia sclerotiorum* is involved with oxidative stress tolerance, virulence, and oxalate production. *Physiol. Mol. Plant Pathol.* 78, 14–23. doi: 10.1016/j.pmpp.2011.12.005

Williams, B., Kabbage, M., Kim, H.-J., Britt, R., and Dickman, M. B. (2011). Tipping the balance: *Sclerotinia sclerotiorum* secreted oxalic acid suppresses host defenses by manipulating the host redox environment. *PLoS Pathog.* 7 (6), e1002107. doi: 10.1371/journal.ppat.1002107

Xia, Z., Wang, Z., Kav, N. N. V., Ding, C., and Liang, Y. (2020). Characterization of microRNA-like RNAs associated with sclerotial development in *Sclerotinia sclerotiorum*. *Fungal Genet. Biol.* 144, 103471. doi: 10.1016/j.fgb.2020.103471

Xiao, X., Xie, J., Cheng, J., Li, G., Yi, X., Jiang, D., et al. (2014). Novel secretory protein ss-Caf1 of the plant-pathogenic fungus *Sclerotinia sclerotiorum* is required for host penetration and normal sclerotial development. *Mol. Plant-Microbe Interact.* 27 (1), 40–55. doi: 10.1094/MPMI-05-13-0145-R

Xu, L., and Chen, W. (2013). Random T-DNA mutagenesis identifies a Cu/Zn superoxide dismutase gene as a virulence factor of *Sclerotinia sclerotiorum*. *Mol. Plant-Microbe Interact.* 26 (4), 431–441. doi: 10.1094/MPMI-07-12-0177-R

Xu, L., Liu, G., Jiang, D., and Chen, W. (2018). Sclerotinia sclerotiorum: an evaluation of virulence theories. *Annu. Rev. Phytopathol.* 56 (1), 311–318. doi: 10.1146/annurev-phyto-080417-050052

Xu, L., Xiang, M., White, D., and Chen, W. (2015). pH dependency of sclerotial development and pathogenicity revealed by using genetically defined oxalate-minus mutants of *Sclerotinia sclerotiorum*. *Environ. Microbiol.* 17 (8), 2896–2909. doi: 10.1111/1462-2920.12818

Yang, G., Tang, L., Gong, Y., Xie, J., Fu, Y., Jiang, D., et al. (2018). A cerato-platanin protein SsCP1 targets plant PR1 and contributes to virulence of *Sclerotinia sclerotiorum*. *New Phytol.* 217 (2), 739–755. doi: 10.1111/nph.14842

Yu, Y., Jiang, D., Xie, J., Cheng, J., Li, G., Yi, X., et al. (2012). Ss-Sl2, a novel cell wall protein with PAN modules, is essential for sclerotial development and cellular integrity of *Sclerotinia sclerotiorum*. *PLoS One* 7 (4), e34962. doi: 10.1371/journal.pone.0034962

Yu, Y., Xiao, J., Du, J., Yang, Y., Bi, C., and Qing, L. (2016). Disruption of the gene encoding endo-β-1, 4-xylanase affects the growth and virulence of *Sclerotinia sclerotiorum*. *Front. Microbiol.* 7. doi: 10.3389/fmicb.2016.01787

Yu, Y., Xiao, J., Zhu, W., Yang, Y., Mei, J., Bi, C., et al. (2017). Ss-Rhs1, a secretory rhs repeat-containing protein, is required for the virulence of *Sclerotinia sclerotiorum*. *Mol. Plant Pathol.* 18 (8), 1052–1061. doi: 10.1111/mpp.12459

Yue, L., Wei, X., Siegrid, S., and Jie, F. (2018). Deficiency of the melanin biosynthesis genes *SCD1* and *THR1* affects sclerotial development and vegetative growth, but not pathogenicity, in *Sclerotinia sclerotiorum*. *Mol. Plant Pathol.* 19 (6), 1444–1453. doi: 10.1111/mpp.12627

Zhang, H., Wu, Q., Cao, S., Zhao, T., Chen, L., Zhuang, P., et al. (2014). A novel protein elicitor (SsCut) from *Sclerotinia sclerotiorum* induces multiple defense responses in plants. *Plant Mol. Biol.* 86 (4-5), 495–511. doi: 10.1007/s11103-014-0244-3

Zhu, W., Wei, W., Fu, Y., Cheng, J., Xie, J., Li, G., et al. (2013). A secretory protein of necrotrophic fungus *Sclerotinia sclerotiorum* that suppresses host resistance. *PLoS One* 8 (1), e53901. doi: 10.1371/journal.pone.0053901

Frontiers in
Plant Science

Cultivates the science of plant biology and its applications

The most cited plant science journal, which advances our understanding of plant biology for sustainable food security, functional ecosystems and human health.

Discover the latest Research Topics

See more →

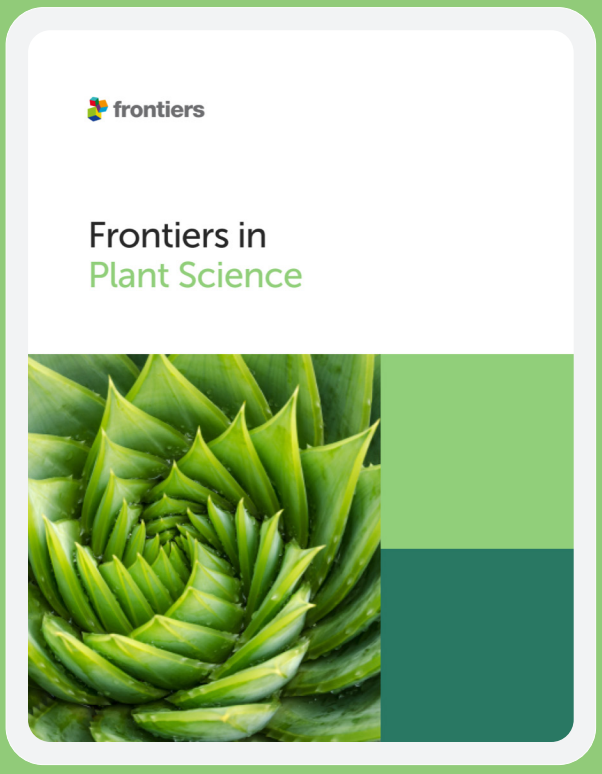

Frontiers

Avenue du Tribunal-Fédéral 34
1005 Lausanne, Switzerland
frontiersin.org

Contact us

+41 (0)21 510 17 00
frontiersin.org/about/contact